ABSTRACT

COLLOIDAL BEHAVIOR OF NANOBUBBLES AND THEIR APPLICATION IN ENHANCING PLANT GROWTH: MECHANISMS OF NANOBUBBLE INTERACTIONS WITH MICROBIAL AND SOIL SPECIES

By

Shan Xue

Climate change has resulted in increasing uncertainties of water resources and disturbance on agricultural activities. For example, the shortage of water resources, land erosion and pollution from runoff significantly affect agricultural sustainability. This dissertation research focuses on the fundamental studies of nanobubble (NB) water and explores the benefits for irrigation to enhance plant germination and growth. Unlike bulk bubbles, NBs exhibit prolonged stability in water and possess large surface areas that facilitate efficient mass transfer and potential tailored reactions (e.g., disinfection). However, the enhancement mechanisms for NBs on seed germination and plant growth remain elusive.

This research first evaluated the membrane bubbling method to produce NBs in water and provided insights into the optimization of bubble water with desirable quality such as high bubble concentrations and small bubble sizes. The results demonstrate that the ceramic membranes with a hydrophilic surface and hydrophobic pores produced greater levels of NBs with small sizes compared to the pristine or surface hydrophobized membranes. Additionally, this study discovered that dissolution kinetics of oxygen NBs are strongly influenced by the initial bubble size and the dissolution could lead to shrinkage or

expansion of bubbles in water. Smaller NBs exhibit a faster increase in DO, while larger NBs can result in higher equilibrium dissolved oxygen (DO) levels. Oxygen NBs significantly enhanced the oxygen transfer efficiency compared to microbubble aeration, exhibiting a remarkable increase of up to 300%, as well as a mass transfer coefficient of 21.05 h^{-1}. Lastly, this study provides compelling evidence that NBs have a positive impact on seed germination and plant growth through changing various soil properties such as soil pH, oxygen content, redox potential and nutrient release, enzymatic activities and microbial communities. For example, oxygen NBs significantly boosted peroxidase activity in tomato leaves, with an impressive increase of 100%-1000%. The composition and structure of rhizosphere microbial communities in early tomato plants were found to be influenced by irrigation frequency, NB concentration, and the specific types of NBs used. Through discovering and characterizing these intriguing nanoscale phenomena and processes, this research aims to deliver new insight into novel sustainable agricultural practices using NB water that may increase agricultural production and reduce water and chemical fertilizer uses.

COLLOIDAL BEHAVIOR OF NANOBUBBLES AND THEIR APPLICATION IN ENHANCING PLANT GROWTH: MECHANISMS OF NANOBUBBLE INTERACTIONS WITH MICROBIAL AND SOIL SPECIES

by
Shan Xue

A Dissertation
Submitted to the Faculty of
New Jersey Institute of Technology
in Partial Fulfillment of the Requirements for the Degree of
Doctor of Philosophy in Environmental Engineering

John A. Reif, Jr. Department of Civil and Environmental Engineering

August 2023

COLLOIDAL BEHAVIOR OF NANOBUBBLES AND THEIR APPLICATION IN ENHANCING PLANT GROWTH: MECHANISMS OF NANOBUBBLE INTERACTIONS WITH MICROBIAL AND SOIL SPECIES

Shan Xue

Dr. Wen Zhang, Dissertation Advisor .... Date
Professor of Civil and Environmental Engineering, NJIT
Affiliated Faculty of Chemical and Materials Engineering, NJIT

Dr. Taha F. Marhaba, Committee Member .... Date
Professor and Chair of Civil and Environmental Engineering, NJIT

Changqing Liu, Committee Member .... Date
Professor of Environmental and Municipal Engineering,
Qingdao University of Technology, Qingdao, Shandong, China

Dr. Lucia Rodrigues-Freire, Committee Member .... Date
Assistant Professor of School of Engineering, Newcastle University,
Newcastle upon Tyne, Tyne and Wear, United Kingdom

Dr. James F. White, Committee Member .... Date
Professor of Department of Plant Biology,
School of Environmental and Biological Sciences,
Rutgers, New Brunswick, NJ

BIOGRAPHICAL SKETCH

Author: Shan Xue

Degree: Doctor of Philosophy

Date: August 2023

Undergraduate and Graduate Education:

- Doctor of Philosophy in Environmental Engineering,
  New Jersey Institute of Technology, Newark, NJ, 2023

- Master of Environmental Science and Engineering,
  Qingdao University of Technology, Shangdong, P. R. China, 2019

- Bachelor of Water Supply and Sewerage Engineering,
  Qingdao University of Technology, Shangdong, P. R. China, 2016

Major: Environmental Engineering

Presentations and Publications:

Journal Publications:

Shan Xue, Taha Marhaba, and Wen Zhang. Nanobubble Watering Affects Nutrient Release and Soil Characteristics. *ACS Agricultural Science and Technology,* 2, 3 (2022): 453-461.

Shan Xue, Yihan Zhang, Taha Marhaba, and Wen Zhang. Aeration and Dissolution Behavior of Oxygen Nanobubbles in Water. *Journal of Colloid and Interface Science*, 609 (2022): 584-591.

Shan Xue, Shaobin Sun, Weihua Qing, Taobo Huang, Wen Liu, Changqing Liua, Hong Yao, Wen Zhang. Experimental and Computational Assessment of 1,4-Dioxane Degradation in a Photo-Fenton Reactive Ceramic Membrane Filtration Process. *Frontiers of Environmental Science and Engineering*, 15,5 (2021):1-13.

Yan, Dajiang, Shan Xue, Zhibin Zhang, Guodong Xu, Yanhao Zhang, Yanfeng Shi, Menglong Xing, and Wen Zhang. Physiological Changes and Antioxidative Mechanisms of Alternanthera Philoxeroides in Phytoremediation of Cadmium. *ACS Environment and Health* (2023).

Xiaonan Shi, Shan Xue, Taha Marhaba, and Wen Zhang. "Probing Internal Pressures and Long-Term Stability of Nanobubbles in Water." *Langmuir,* 37, 7 (2021): 2514-2522.

Shaobin Sun, Hong Yao, Wanyi Fu, Shan Xue, Wen Zhang. Enhanced Degradation of Antibiotics by Photo-fenton Reactive Membrane Filtration, *Journal of Hazardous Materials*, 386 (2020): 121955.

Book Publications:

Wen Zhang, Shan Xue, Xiaonan Shi, and Taha Marhaba. Nanobubble Technology: Generation, Properties and Applications. *In Emerging Nanotechnologies for Water Treatment*, London, United Kingdom, Royal Society of Chemistry, pp. 447-506. 2021.

Wen Zhang, Shan Xue, Qingquan Ma, Fangzhou Liu, Weihua Qing, Shaobin Sun, Hong Yao. Catalytically Reactive Membrane Filtration for Water Treatment. *In The World Scientific Reference of Water Science: Volume 2 Nanotechnology for Water Treatment and Water Interfaces*, Singapore, World Scientific, pp. 221-301. 2023.

Oral Presentations:

Shan Xue, Thu Le, Chuanwu Xi, Taha Marhaba, Wen Zhang. Mechanisms of Nanobubbles and Soil Interactions in Enhanced Plant Growth, Nanobubble 2022, Magdeburg, Germany, 09/2022

Shan Xue, Xiaonan Shi, Taha Marhaba, Wen Zhang. Formation Detection and Stability Assessment of Nanobubble in Water, 2021 Eastern Analytical Symposium and Exposition, Princeton, NJ, 11/2021

Shan Xue, Xiaonan Shi, Taha Marhaba, Wen Zhang. Probing Internal Pressures and Long-term Stability of Nanobubbles in Water, ACS Fall 2021 National Meeting and Expo, Atlanta, GA, 08/2021

Shan Xue, Xiaonan Shi, Taha Marhaba, Wen Zhang. The Effect of Nanobubbles on Plant Growth and Soil Nutrient Release, ACS Spring 2021 National Meeting and Expo, Atlanta, GA, 08/2021

Shan Xue, Taha Marhaba, Wen Zhang. Electrochemical analysis of soil after treatment by nanobubble water, 2020 Eastern Analytical Symposium and Exposition, Online，11/2020

Shan Xue, Shaobin Sun, Changqing Liu, Wen Zhang. Enhanced Degradation of 1,4-dioxane by Photo-Fenton Reactive Ceramic Membrane, ACS Spring 2020 National Meeting and Expo, Online, 03/202

Poster presentations:

Shan Xue, Thu Le, Chuanwu Xi, Taha Marhaba, Wen Zhang. Use of Novel Nanobubble Watering Processes for Enhanced Plant Growth, AEESP, NJIT, Newark, NJ, 04/2023

Shan Xue, Thu Le, Chuanwu Xi, Taha Marhaba, Wen Zhang. Use of Novel Nanobubble Watering Processes for Enhanced Plant Growth and Pathogen Control, Convergence of Nanotechnology with Food and Agriculture, Southern New Hampshire University, Manchester, NH, 06/2022

Shan Xue, Taha Marhaba, Wen Zhang. Mechanisms of Nanobubbles and Soil Interactions in Enhanced Plant Growth, 2022 Dana Knox Student Research Showcase, NJIT, Newark, NJ, 04/2022

Shan Xue, Xiaonan Shi, Taha Marhaba, Wen Zhang. Nanobubble Watering for Enhanced Plant: Mechanisms of Nanobubbles and Soil Species Interactions, 2021 10th Nano Conference, Online, 07/2021

Shan Xue, Taha Marhaba, Wen Zhang. Nanobubble Watering for Enhanced Plant: Mechanisms of Nanobubbles and Soil Species Interactions, 2021 CAPEES Student E-Poster Competition, Online, 07/2021

Shan Xue, Taha Marhaba, Wen Zhang. Nanobubble Technology for Soil Remediation and Pollutant Removal, New Jersey Site Remediation Conference, Online, 02/2021

Shan Xue, Wen Zhang. Enhanced Degradation of 1,4-dioxane by Photo-Fenton Reactive Ceramic Membrane, 2019 NJIT Graduate Research Day, NJIT, Newark, NJ, 11/2019

Shan Xue, Changqing Liu, Shaobin Sun, Wen Zhang. Photo-Fenton ceramic membrane for 1,4-dioxane treatment, Environmental Nanotechnology and Biotechnology Workshop, Tongji University, China, 07/2019

To the experiences never expected,

and the paths that were never redirected.

To the friends and family who accompanied me throughout the journey.

ACKNOWLEDGMENTS

This journey would not have been possible without the support of my family, professors, and friends. I am grateful and appreciative of all the help and support I've received along the way.

First and foremost, I would like to express my sincere thanks to my advisor, Dr. Wen Zhang, for giving me the opportunity to join his group and his unwavering support throughout my academic journey. I am truly thankful for his patience when the results were not always positive. Of course, I must also extend my thanks for his invaluable time and effort in reading and correcting my manuscripts. His constant and precious guidance has been an essential compass throughout my academic pursuits, providing me with the knowledge and experience to grow and excel. I feel incredibly fortunate to have been involved in multiple research projects and to have attended various international and regional conferences, thanks to his guidance and mentorship. Moreover, his encouragement allowed me to participate in proposal writing and mentoring students, broadening my horizons and helping me achieve my academic and professional goals. Dr. Zhang's mentorship and advice have not only contributed to my academic success but also have had a profound impact on my personal growth. I am deeply grateful for his dedication and unwavering commitment to my success. I am fortunate to have had such a dedicated and supportive advisor who has helped me to become the person I am today. In addition, I

would like to extend my gratitude to my co-adviser, Dr. Taha F. Marhaba. His continuous support and willingness to write recommendation letters have been crucial in helping me seize opportunities and accomplish my goals. I truly appreciate his unwavering encouragement throughout my academic journey.

I would like to give special thanks to the esteemed members of my dissertation committee. Drs. James F. White, Lucia Rodrigues-Freire, and Changqing Liu, for graciously dedicating their valuable time amidst their busy schedules to review this dissertation and provide invaluable guidance, considerate advice, and constructive feedback. I want to take a moment to express my deepest gratitude and admiration for Dr. Changqing Liu. His unwavering support has been a constant source of courage as I embarked on this significant journey of academic and personal growth. Moreover, his invaluable insights and advice on studying abroad have truly enriched my experience, making it an unforgettable and transformative chapter in my life.

I am deeply grateful for the immense support and assistance I received from the

industrial mentors, Ms. Yuhong Jiang (BRISEA International Inc.), Dr. Likun Hua (BRISEA International Inc.) and Dr. Guangyu Guo (BRISEA International Inc.), who not only promote commercialization of nanobubble generator but also provided invaluable guidance and advice throughout my research. I would like to extend a special appreciation to Ms. Yuhong Jiang for her invaluable insights on career development. Furthermore, I would like to express my gratitude to the engineers, Dr. Jeffrey Bodycomb and Faizan Masood, from Horiba for their support on the use of the NTA instrument.

I also thank my current and former group members: Xiaonan Shi, Qingquan Ma, Yihan Zhang, Jianan Gao, and Weihua Qing, whose invaluable assistance and unwavering support have greatly contributed to the progress and success of my research. Their dedication and collaboration have been instrumental in shaping my journey. To my dear friends in China, I want to express my sincerest appreciation for their constant presence and support. Their thoughts, well-wishes, prayers, video calls, e-mails, and texts have meant the world to me.

To my beloved family, it's hard to put into words just how deeply grateful and appreciative I am for the unwavering support and boundless love they have showered upon me throughout my life's journey. Their presence has been a constant source of strength and inspiration, propelling me forward even in the face of challenges. To my extraordinary parents, Shaoxiang Song and Yongcai Xue, they are my pillars of strength and my ultimate role models. Their guidance, unwavering belief in me, and selfless sacrifices have played

TABLE OF CONTENTS

LIST OF TABLES

LIST OF TABLES
(Continued)

LIST OF FIGURES

LIST OF FIGURES
(Continued)

CHAPTER 1

INTRODUCTION

1.1 Background and Challenges

Water scarcity poses a significant threat to sustainable development due to its limited availability. Currently, approximately 70% of global water demand is attributed to irrigation (Knox, Kay, & Weatherhead, 2012). Projections for 2050 suggest that the global population will exceed 9 billion, with nearly 45% people people residing in countries grappling with water scarcity. Despite temporary market disruptions and the COVID-19 pandemic, the agricultural sector is anticipated to grow by an average of 3% annually in the coming decade. This growth is primarily driven by megatrends such as population expansion and the mounting pressure on crop yields due to climate change. Failure to enhance irrigation efficiency would necessitate a 20% increase in irrigation demand to ensure food security, potentially leading to significant reductions in soil productivity and crop output. Thus, the sustainability of irrigation has emerged as a critical concern amid the threat of water scarcity to sustainable development.

The adoption of effective irrigation methods therefore is of utmost importance in

agricultural water management practices. Additionally, the choice of irrigation methods has substantial consequences, including land erosion, pollution, and depletion of water resources (Islam & Tanaka, 2004; Newton et al., 2014). Over-irrigation poses risks such as surface runoff, deep percolation, and leaching of nitrates and nutrients, while under-irrigation leads to reduced crop yields, lower quality, and inefficient use of fertilizers and other inputs for crop production. It is reported that only half of the total freshwater volume abstracted globally for irrigation reaches the intended crops(Hedley, Knox, Raine, & Smith, 2014). The degradation of 38% of crop land worldwide can be attributed to inadequate water management and improper fertilizer application (Yost et al., 2017). Given the escalating costs of fertilizers and concerns regarding environmental impacts, there is an urgent need for innovative technologies in agriculture to improve efficiency and mitigate the detrimental environmental effects of farming activities (D. L. Corwin & S. M. Lesch, 2005).

Nanobubbles (NBs) have become a revolutionary technology with diverse applications in agriculture, aquaculture, food engineering, and sterilization (Dzubiella, 2010; Tsuge, 2014). The utilization of oxygen NBs resulted in a significant increase in oxygen concentration, elevating it from 7.7 mg·L^{-1} in regular distilled water to 31.7 mg·L^{-1} within a span of 30 minutes (Ebina et al., 2013b). As a result, NBs are commonly employed in aquaculture to enhance water quality and boost dissolved oxygen levels, thereby improving fish productivity even in confined spaces (Kurita, Chiba, & Kijima,

2017). Additionally, NBs have been successfully integrated into agricultural practices to enhance seed germination, plant growth, and crop yield (Ebina et al., 2013b; S. Liu, Oshita, Kawabata, Makino, & Yoshimoto, 2016; S. Liu, Oshita, Kawabata, & Thuyet, 2017; S. Liu et al., 2015). For instance, barley seeds submerged in NB-infused water (comprising bubbles formed from a mixture of nitrogen and pure air) exhibited germination rates 15-25% higher than seeds submerged in distilled water with an equivalent level of dissolved oxygen (S. Liu, Kawagoe, Makino, & Oshita, 2013). Furthermore, the use of water containing air MNBs resulted in fresh lettuce leaf weights 2.1 times greater and dry leaf weights 1.7 times greater compared to plants treated with macro-bubbles (J.-S. Park & Kurata, 2009).

Despite the above proof-of-concept studies on agricultural applications of NBs, the enhancement mechanisms for NBs on seed germination and plant growth remain elusive. For example, the roles of reactive oxygen species (ROS) generated in the presence of NBs during germination and growth processes are still not fully comprehended. Bailly et al. proposed the concept of the "oxidative window for germination" (Bailly, El-Maarouf-Bouteau, & Corbineau, 2008), which defines the optimal range of ROS levels for the occurrence of cellular events associated with germination. Moreover, NBs have the potential to enhance nutrient delivery, such as nitrogen or oxygen, to plants. Nitrogen and carbon, essential elements for biomass growth, significantly impact germination rates, plant growth, and grain quality (Bénard et al., 2009; Tavarini, Sgherri, Ranieri, & Angelini,

2015). Introducing a solution of nitrogen NBs could improve nitrogen accessibility and enhance molecular nitrogen fixation by diazotrophs or nitrogen-fixing organisms (Rodrigues, Ladeira, & Arrobas, 2018), facilitating seed germination and plant growth through the conversion of N_2 to ammonia via nitrogenase.(Havlin, Beaton, Tisdale, & Nelson, 2005; Marschner & Rengel, 2012). Additionally, oxygen plays a crucial role in nutrient absorption by facilitating the transport of nutrients across cell walls and into the plant roots. Increased oxygen uptake by the roots improves nutrient absorption and supports the overall growth of the plant (Shahzad et al., 2016). Thus, employing NBs technologies holds promise in enhancing plant nutrient absorption and utilization efficiency while minimizing secondary pollution.

Furthermore, the intriguing interactions between NBs and soil and rhizosphere-associated microbes influence the characteristics and functionality of microbial communities, which remain largely unexplored. For instance, oxygen NBs have the potential to activate root bacterial metabolisms and enhance the absorption of soil nutrients by plants. A better understanding of changes of microbial community upon exposure to extended exposure to diverse NBs is critical for developing effective NB irrigation strategies and tuning properties that are needed to synergize the growth of plants and beneficial microbial systems in soil and/or in rhizosphere.

1.2 Definition of NBs

Since the 21st century, the emergence of gaseous nanotechnology has enabled research on oxygenation techniques. Recently, there is a growing interest in NBs technologies because of their unique properties. The concept of the NBs was first introduced by Parker et al (Parker, Claesson, & Attard, 1994), when researching the hydrophobic long-range self-gravity of two solid surfaces. Microbubbles (MBs) are generally defined as gaseous bubbles with diameter less than 100 μm and larger than 10 μm (Temesgen, Bui, Han, Kim, & Park, 2017). NBs are normally reported to have a size less than 1 μm in diameter, which are also called ultrafine bubbles (Alheshibri, Qian, Jehannin, & Craig, 2016; Kobayashi, Maeda, Kashiwa, & Fujita, 2014a, 2014b; Maeda et al., 2014; T Tuziuti, Yasui, & Kanematsu, 2014).

1.3 Bubble Properties and Behavior in Aquatic Environment

Figure 1.1 shows the key differences in aquatic properties among macro-bubbles, MBs and NBs. For instance, large bubbles such as macro-bubbles and microbubbles rise quickly due to buoyance. Meanwhile, some bubbles may decrease in size due to dissolution and collapse. By contrast, due to the dominant Brownian motion, NBs remains suspended and stay in liquid for much longer times (a few hours to weeks) and do not burst (Ohgaki, Khanh, Joden, Tsuji, & Nakagawa, 2010; Takahashi, 2009; Ushikubo et al., 2010). NBs have a higher efficiency of mass transfer compared to bulk scale bubbles due to the high

specific surface areas (Agarwal, Ng, & Liu, 2011; Bowley & Hammond, 1978; Uchida et al., 2011). The high specific surface areas also increase physical adsorption and chemical reactions at the gas liquid interface. The collapse of NBs creates shock waves, localized heating and even sonochemical processes that could generate reactive hydroxyl radicals (•OH) (Agarwal et al., 2011; Bowley & Hammond, 1978; Uchida et al., 2011). NB also has the characteristics of having a surface charge (Ushikubo et al., 2010), a strong hydrogen bond in the gas-liquid interface (Agarwal et al., 2011; Ohgaki et al., 2010) and a high internal density (X. H. Zhang, Quinn, & Ducker, 2008). These unique properties lead to a massive range of current and expected applications of NBs, including, but not limited to, ecological restoration (Agarwal et al., 2011; H. Li, Hu, Song, & Lin, 2014; S. Liu et al., 2013), sewage treatment (Agarwal et al., 2011; H. Li et al., 2014; S. Liu et al., 2013; Marui, 2010; Qiu et al., 2017; O. C. Thomas, Cavicchi, & Tarlov, 2003; Żbik & Horn, 2003), biomedicine (Alheshibri et al., 2016; Modi, Jana, Ghosh, Watson, & Pahan, 2014) aquaculture,(Ebina et al., 2013a; S. Liu et al., 2013) plant cultivation, the cleaning industry (G. Liu, Wu, & Craig, 2008; Ngai, Xing, & Jin, 2008; Qiu et al., 2017; Wu et al., 2008), the food and beverage industry (Miyashita, Yasuda, Ota, & Suzuki, 1999; Safonov & Khitrin, 2013), interface slip (Bhushan, Pan, & Daniels, 2013; Yuliang Wang & Bhushan, 2010) mineral flotation(Calgaroto, Wilberg, & Rubio, 2014; Hampton & Nguyen, 2009) and enhanced chemical reactions (Kononov, 2015).
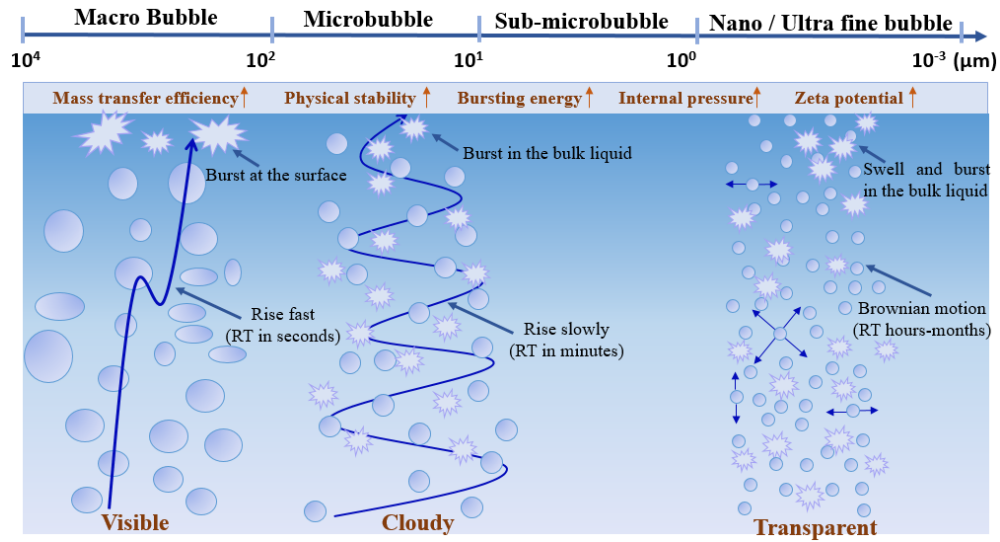
Figure 1.1 Rising behavior of different bubbles and other major aquatic properties.
Source: (Temesgen et al., 2017).

1.3.1 Colloidal behavior and interactions of ultrafine bubbles

NBs may undergo many dynamic processes, such as dissolution, coalescence and collapse (Agarwal et al., 2011). These processes are influenced by the types of NBs (e.g., air, oxygen and nitrogen) and environmental factors such as pH, ionic strength, and organic matters (Khaled Abdella Ahmed et al., 2018). **Figure 1.2** shows that three different types of NBs exhibited different stable bubble size distribution and zeta potentials. Furthermore, membrane pores size, surface energy, and the injected gas pressures were shown to affect the bubble size and zeta potential (Ahmed, Sun, et al., 2018) when using membrane method to generate NBs. For example, increasing the injection air pressure reduces the bubble size, which is explained by the Laplace-Young Equation (Attard, 2013; Oguz & Prosperetti, 1993). The bubble size distribution of oxygen NBs in water in sealed containers was

measured under different temperatures for 15 hours, which shows that the size of ONBs

reduced from 255±30 nm under 6℃ to 147±11nm under 40℃. The decreased NBs' size

under higher temperature may due to the decreased surface tension of water at high

temperatures and removal of large sized NBs (Behkish, Lemoine, Sehabiague, Oukaci, &

Morsi, 2007; Y. Liu et al., 2018).
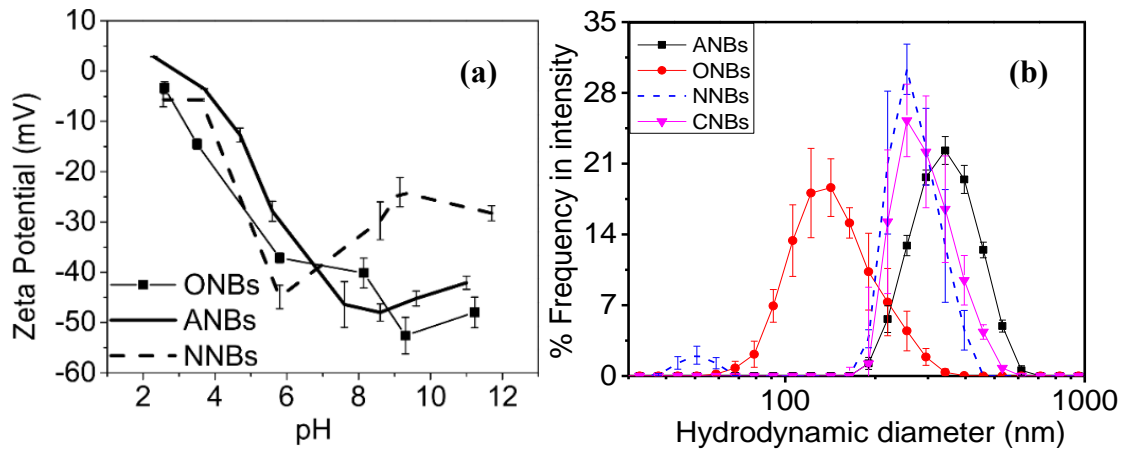
Figure 1.2 (a) Zeta potential for ANBs, ONBs, and NNBs at different pHs; (b) Hydrodynamic diameter of air NBs (ANBs), oxygen NBs (ONBs), nitrogen NBs (NNBs), and carbon dioxide NBs (CNBs).
Source: (Khaled Abdella Ahmed et al., 2018).

Similar to aqueous thin-liquid films (Karraker & Radke, 2002; Wan & Wilson,

1994; Yaminsky, Ohnishi, Vogler, & Horn, 2010) and due to the softness and deformation

potential, the bubble-bubble interaction energy may be studied by the soft-particle

extended Derjaguin-Landau-Verwey-Overbeek (EDLVO) theory (Ge et al., 2014; Ge,

Agbakpe, Zhang, & Kuang, 2015; Karraker & Radke, 2002; LaFrance & Grasso, 1995;

Wan & Wilson, 1994; Yaminsky et al., 2010). Soft-particle EDLVO calculation is used to

simplify the quantification of surface interaction energies of two identical soft particles

such as bacterial cells (before attachment, coalescence or deformation occurs). Here the sphere-sphere geometry was adopted in the application of EDLVO equations. This hypothesis is made because NBs, due to the high internal pressure, are believed to have taut inflexible surfaces (like high pressure balloons) that limit distortion (Cancelos et al., 2016).

NBs often carry electric charges when they are dispersed in electrolyte due to the surface sorption of counter ions. The cloud of counter ions surrounding the charged bubbles results in an electrical repulsion or attraction between them depending on the net interaction energy. The zeta potential is the potential difference between the bulk fluid and the layer of counter ions that remain associated with the charged NBs. When zeta potential is high in magnitude (positive or negative), electrical repulsion between colloidal bubbles is strong and would stabilize the bubble suspension. When zeta potential is close to zero, colloidal bubbles may coalesce due to the Van der Waals forces or attraction. When that happens, colloidal bubbles will coalesce or aggregate.

In general, a two-step mechanism (adsorption and attachment) could mediate bubbles coalescence (if existed) (Ong, Razatos, Georgiou, & Sharma, 1999). Both steps are influenced by the chemical properties of interacting surfaces and the electrolytic environment (Hammer & Tirrell, 1996; Vandamme, Foubert, & Muylaert, 2013; W. Zhang, Rittmann, & Chen, 2011). As the bubbles approach each other they will experience short-range forces such as Lifshitz-van der Waals and electrostatic forces, as usually described

by the DLVO theory (Van Oss, 2006; Verwey & Overbeek, 1948), which however is preferably used for monovalent salts at relatively low concentrations. Although the dominating factors involved in NBs interactions remain elusive, quantitative information on the nonspecific interaction force between NBs can be directly obtained with the extended DLVO theory assuming that Lifshitz-van der Waals, Lewis acid-base (AB) interaction, and electrostatic forces are the dominant forces. The electrostatic forces obtained for each condition investigated were modeled using the Ohshima's soft particle electrophoresis modeling (Ohshima, 1995).

The total interaction energies, $U_{Total\text{-}EDLVO}$, between the interacting NBs are calculated by:

$$U_{Total-EDLVO} = U_{vdW} + U_{EL} + U_{AB} \tag{1.1}$$

where U_{vdW} is the van der Waals interaction energy, U_{EL} is the electrostatic interaction energy, and U_{AB} is the Lewis acid-base interaction energy. Besides these three forces, other non-DLVO forces, such as hydration force (Butt, 1991; Chang & Chang, 2002), hydrophobic force (Ong et al., 1999), oscillatory force (Bostrom, Williams, & Ninham, 2001), osmotic force,(Marenduzzo, Finan, & Cook, 2006; Yodh et al., 2001) and steric and Helfrich repulsion force (an entropy effect) (Rijnaarts, Norde, Lyklema, & Zehnder, 1999), may play a role under different scenarios of bubble-bubble or bubble-surface interactions.

1.3.2 Internal pressures and dependence on bubble sizes

Stability of NBs against collapse or rapid dissolution may originate from the selective adsorption of anions at their interface, surface zeta potentials and the construction of a hydrogen bonding network at the gas-water interface (Agarwal et al., 2011; Ohgaki et al., 2010). The diffusivity of gaseous molecules through the gas/water interface may thus be reduced by these surface charge accumulation and hydrogen bonding network. Recently, NBs are shown to be kinetically stable against high internal pressures due to the diffusive resistance at the gas-water interface (S. Wang, Liu, & Dong, 2013). According to a previous study (Khaled Abdella Ahmed et al., 2017), the bulk NBs in water could be stabilized by the outbound and inbound pressures from a number of interfacial forces. The hypothesis is that (1) The outbound pressure (P_{out}) is ascribed to surface charge repulsion, and internal gas pressure (P_{int}) as shown in **Equation (1.2)**; particularly, the electric double layer formed at the liquid/gas interface of NBs may also produce repulsion between the surface charges of NBs and thus cause an outbound pressure to the interface of NBs (Khaled Abdella Ahmed et al., 2017; Srinivas & Ghosh, 2011)**.** (2) The inbound pressure (P_{in}) is contributed by the surface tension pressure of NBs (P_r) exerted from the surrounding water molecules, the atmospheric pressure (P_0), and the water head pressure (P_h) as shown in **Equation (1.3)**. For NBs that are at a quasi-steady state (i.e., $P_{in} = P_{out}$), we can derive a relationship between the radius of NBs and the internal pressure.

$$P_{out} = \frac{\sigma^2}{2 \cdot D \cdot \varepsilon_0} + P_{int} \tag{1.2}$$

$$P_{in} = \frac{2 \cdot \gamma}{r} + P_0 + \rho \cdot g \cdot h \tag{1.3}$$

$$P_{int} = \frac{2 \cdot \gamma}{r} + (P_0 + \rho \cdot g \cdot h) - \frac{\sigma^2}{2 \cdot D \cdot \varepsilon_0} \tag{1.4}$$

where D is the relative dielectric constant of the gas bubbles (assumed unity), ε_0 is the dielectric permittivity of a vacuum, 8.854×10^{-12} (C·V^{-1}·m^{-1}), γ is the water surface tension (71.99 mN·m^{-1} for pure water at 20 °C) (Ulatowski, Sobieszuk, Mróz, & Ciach, 2019), r is the radius of NBs (m), ρ is the density of water (kg·m^{-3}), g is the gravity acceleration (9.80 m·s^{-2}), and h is the height of water (m). By measuring the colloidal properties of NBs, such as bubble diameter and zeta potential, the internal pressures of NBs can be estimated or predicted using **Equation (1.4)**, which further permits the assessment of the dependence of bubble radius on internal pressures if NBs are at a quasi-steady state without significant dissolution or other forms of action that destabilize their sizes or internal pressures. **Equation (1.4)** predicts that increasing salinity compresses the electric double layer and reduces the net surface charge of colloidal particles (H. Li, Hu, & Xia, 2013; Millare & Basilia, 2018; Oh & Kim, 2017), which will reduce the outbound force and potentially reduce bubble size as the inbound force outweighs the outbound force. Moreover, water temperatures affect water surface tension, density and dielectric constant as well as solubility of gases, which may indirectly change the stability of NBs in water (Behkish et al., 2007; Y. Liu et al., 2018). Some studies that reported high internal gas

pressures of more than 1000 psi (~68 atm) (Suleymani, Ghotbi, Ashoori, Moghadasi, & Kharrat, 2020), whereas the colloidal force balance model predicted lower internal pressures (2-10 atm) as shown in **Figure 1.3** so that the gas NBs could still remain in a dense gas phase.
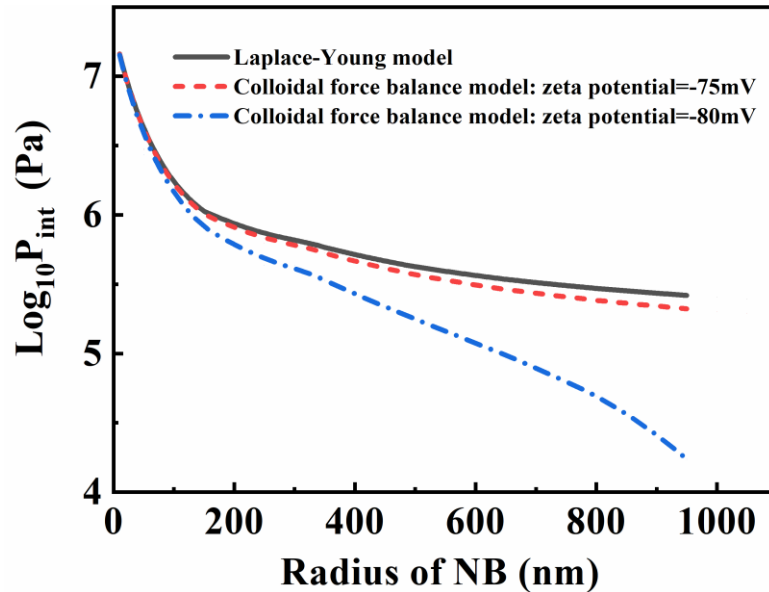
Figure 1.3 Prediction of internal pressures of oxygen NBs of different bubble radius.

Besides the colloidal characterization method as shown in **Figure 1.3**, some studies also measured the internal pressures of NBs using atomic force microscope (AFM) and theories of contact mechanics. There are two major contact mechanics models, JKR or DMT, to assess mechanical properties such as Young's modules and hardness of soft particles such as bacteria, viruses and bubbles (Y.-S. Chu, Dufour, Thiery, Perez, & Pincet, 2005; Jasevičius, Baronas, & Kruggel-Emden, 2015; Korayem, Rastegar, & Taheri, 2012; Korayem & Taheri, 2014; W. Zhang, Stack, & Chen, 2011). In this method, a sharp AFM probe is used to compress a local sample surface to induce the indentation or deformation

(δ) as illustrated in **Figure 1.4** (Touhami et al., 2002).
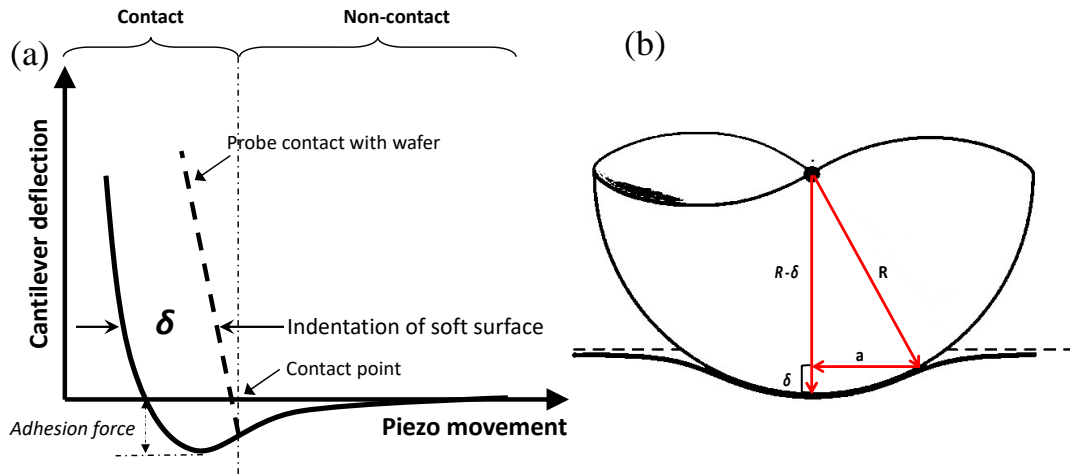
Figure 1.4 (a) Force-distance curve showing the indentation (δ) of the AFM probe in contact with a bubble surface. (b) Illustration of the geometry of the AFM tip on the deformed surface of NBs.

Source: (X. Shi, Xue, Marhaba, & Zhang, 2021).

This contact mechanics model provides an alternative way to experimentally evaluate the internal pressures of NBs, and, further, the mechanical hardness of NBs, which will be compared with the internal pressures obtained from the colloidal force balance model. Unlike the colloidal modeling method, this contact mechanics model primarily relies on direct AFM measurements of the interfacial force-distance curves with fewer unknown model parameters. Some uncertainties may evolve from the reading of indentation values and adhesion force due to the difficulty in the determination of the tip contact on soft samples that may deform as the tip approaches. The tip-bubble contact is currently defined as the point when the tip experiences a significant attractive force that usually causes a jump-in peak in the force-distance curve (Butt, Cappella, & Kappl, 2005).

Additionally, the AFM probe radius may differ slightly from batch to batch. To ensure the reproducibility and accuracy of the experimental results (e.g., the force-distance curves obtained from the tip-NBs contact), morphological mapping of surface NBs should be repeated on each sample. Force measurements should be conducted on the center of one discrete surface NB to produce stable and reproducible values of indentation, adhesion force and Young's modulus and stiffness.

1.3.3 Radical formation and plausible mechanisms of NBs in liquid

Generation of free radicals such as •OH through the collapse of MBs or NBs was widely reported or experimentally observed (S. Liu, S. Oshita, S. Kawabata, et al., 2016; Tada et al., 2014; Takahashi, Chiba, & Li, 2007b; Yasui, Tuziuti, & Kanematsu, 2018). Highly reactive radical formation may open many valuable opportunities for engineering applications such as water disinfection and cleaning/defouling of solid surface (Takahashi et al., 2007b). Radical generation in water suspension of NBs is usually detected by electron spin resonance spectroscopy (Takahashi et al., 2007b) and other radical-scavenger indicator (Fan, Zhang, Liu, Li, & Li, 2020; S. Liu, Oshita, Thuyet, Saito, & Yoshimoto, 2018; L. Xiao et al., 2020). Liu et al. experimentally reported that OH radicals were detected using a fluorescent reagent APF (3′-p-(aminophenyl) fluorescein) from liquid water containing oxygen NBs without dynamic stimuli (S. Liu et al., 2013). They estimated the concentration of •OH radicals produced from oxygen NBs with a concentration of about

10^8 per ml as about 0.25 µM or on an order of 10^{14} per ml. As the typical lifetime of •OH radicals is in the order of 20 ns (Henglin, 1998; JohnáElliot, 1990; Yasui, 2018), the detected •OH radicals are considered to be produced from bulk NBs especially under a dynamic stimulus. Takahashi et al. were detected radicals in a bulk NB solution after ceasing the NBs generation to avoid the influence of the external dynamic energy (i.e., hydrodynamic cavitation) (Takahashi et al., 2007b). It is widely known that during hydrodynamic cavitation many •OH radicals are produced by cavitation bubbles as temperature and pressure inside bubbles increase dramatically at their collapses (Gogate et al., 2001; Krishnan, Dwivedi, & Moholkar, 2006). Similarly, sonochemical production of •OH radicals in liquid water is attributed to the sonication cavitation effect and energy transfer to break up water molecules and transform them to •OH radicals (Yasui, Tuziuti, Kozuka, Towata, & Iida, 2007).

Despite the research findings in the last paragraph, some studies reported negative detection of radicals in similar experimental conditions. For instance, Tada et al. and Yasui et al. showed the opposite, no •OH radical generation from air NBs self-collapse in water (Tada et al., 2014). The discrepancy could rise from the subtle differences in experimental parameters as the physical or mechanical stimulus or agitation (e.g., sonication, laser or light irradiation) as well as the type of gases could significantly affect the quantity or quality of free radicals that could be generated in water (Izawa, Inoue, & Kimura, 1995; M. Kim, Song, Kim, & Han, 2020; P. Li, Takahashi, & Chiba, 2009; L. Wang et al., 2020;

Yasui, Tuziuti, & Kanematsu, 2016). For example, oxygen MBs favored the formation of

•OH radical compared to nitrogen MBs (P. Li et al., 2009). Izawa et al. reported that

reactive oxygen species such as superoxide anion radical, H_2O_2 and radical •OH radicals

are generated during the reduction of molecular oxygen to water through acceptance of

four electrons (Izawa et al., 1995). The radical formation inside a bubble is negligible

because the probability of nitrogen dissociation is only on the order of 10^{-15} (Yasui et al.,

2016). Furthermore, adding acid to alter the circumstance of the adsorbed ions around the

gas–water interface of the microbubble can increase •OH radicals generation (Takahashi et

al., 2007b). Some researchers also reported that microbubbles could accelerate the

formation of radical •OH radicals during an ozonation process (Bando et al., 2008; L.-B.

Chu et al., 2007; L.-B. Chu et al., 2008; Takahashi, Chiba, & Li, 2007a; Yasui, Tuziuti, &

Kanematsu, 2019b).

1.3.4 Potential redox chemistry in water suspension of NBs

In a hydrogen or oxygen NB water, the H_2/H_2O or O_2/H_2O redox couples result in a redox

potential that is governed by this reaction.

$$H_2O + e^- \rightarrow \frac{1}{2} H_2 + OH^- \quad (\text{E}^0=0.83 \text{ V}) \tag{1.5}$$

$$O_2 + 4H^+ + 4e^- \rightleftharpoons 2H_2O \quad (\text{E}^0=1.229 \text{ V}) \tag{1.6}$$
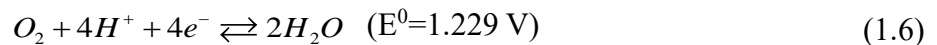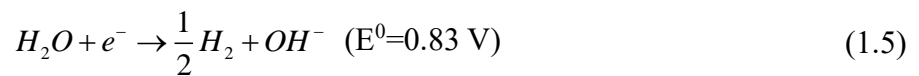
The redox potential can be calculated by the Nernst Equation:

$$E_H = E^0 - \frac{1}{2}\frac{1}{16.9}\log(P_{H_2}) + \frac{1}{16.9}(14 - pH) \tag{1.7}$$

$$E = E_h^{\;0} + \frac{0.059}{4} \log P_{O_2} + 0.059 \log(H^+) \tag{1.8}$$

1.4 Generation Methods of MBs and NBs

Different generation methods have been reported and investigated for ultrafine bubbles, mainly including membrane bubbling (Ahmed, Sun, et al., 2018; Khaled Abdella Ahmed et al., 2018), hydrodynamic cavitation (Agarwal et al., 2011), acoustic cavitation or sonication (Agarwal et al., 2011; T. Kim & Han, 2010; Q. Xu, Nakajima, Ichikawa, Nakamura, & Shiina, 2008), electrochemical cavitation (Wu et al., 2008) and mechanical agitation (Q. Xu et al., 2008). For example, injection of pressured gases through membrane pores is reported to produce NBs in liquid as shown in **Figure 1.5(a)** (Ahmed, Sun, et al., 2018; Khaled Abdella Ahmed et al., 2018). Different from other generation techniques (e.g., hydrodynamic cavitation, electrochemical production, laser ablation or sonication), the membrane bubbling method enables precise control of bubble sizes and internal pressures.[109] The bubble size varies with the surface tension of the membrane, pore size, injection pressure, gas flow and pressure, fluid viscosity and temperature.

Cavitation is another method to generate NBs which is a rapid process of forming vapor cavities in liquid, because of a sudden pressure drop or depressurization (hydrodynamic cavitation) or due to a passage of ultrasonic waves (acoustic cavitation). For example, hydrodynamic cavitation achieves pressure variation due to the flow velocity variation. As shown in **Figure 1.5(b)**, the spiral liquid-flow type (H. Li et al., 2013), venturi

type (Nazari et al., 2020) and orifice plate (Z. Wu et al., 2019) follow a hydrodynamic-cavitation mechanism (Gogate & Pandit, 2005). Besides, hydrodynamic cavitation involves other possible physical or mechanical agitation such as bubble shearing and splitting (Ebina et al., 2013b; H. Kim, 2014; T. Kim & Han, 2010; S. Liu et al., 2010; Ohgaki et al., 2010; Terasaka, Hirabayashi, Nishino, Fujioka, & Kobayashi, 2011; Ushikubo et al., 2010; J. Zhu et al., 2016). Moreover, an ultrasonic probe inside the bulk liquid (Q. Xu et al., 2008) or external ultrasonic wave generator (T. Kim & Han, 2010) induce the ultrasonic waves and cause cavitation when there is a high negative pressure exceeding the ambient hydrostatic pressure (Besancon, 2013). Two possible mechanisms are proposed to explain the cavitation: (1) homogeneous nucleation, where the liquid molecules rupture when the tensile stress or stretch from the acoustic wave exceeds the intermolecular cohesion forces; (2) heterogeneous nucleation, where nucleation starts from surface cracks as the cracks are filled with gas ("gas pockets"). The gas molecules are agitated to detach and form bubbles (Zijlstra, 2011). Similar to acoustic cavitation, optical cavitation is also reported to generate cavitation by passing high intensity particles (e.g., laser, proton and neutrinos) into the liquid (Agarwal et al., 2011; Manickam & Ashokkumar, 2014; Maoming, Daniel, HONAKER, & Zhenfu, 2010). However, the major drawback of this cavitation-based generation is the lack of a control of bubble sizes and generation of essentially a mixture of MBs and NBs.

The formation of surface and bulk NBs in an electrochemical system has

increasingly been studied (German, Edwards, et al., 2016; Perez Sirkin, Gadea, Scherlis, & Molinero, 2019; L. Zhang et al., 2006). For example, when an electrical current runs through the electrode surface that is immersed into a given solution (Wu et al., 2008), surface electrochemical reactions will generate surface nuclei of gaseous molecules and they merge and grow into NBs that eventually detach from the electrode surface. Water electrolysis, for example, splits water into hydrogen and oxygen gases as shown **Figure 1.5(c)**. Typically, an electrolyzer consists of an anode and a cathode separated by an ion exchange membrane. A direct current (DC) is applied to run currents through anode, electrolyte and cathode, where anodic reactions involve electron sequestration from electrolyte (e.g., water) and cathodic reactions donate electrons to electrolyte and achieve reductive reactions such as hydrogen evolution.
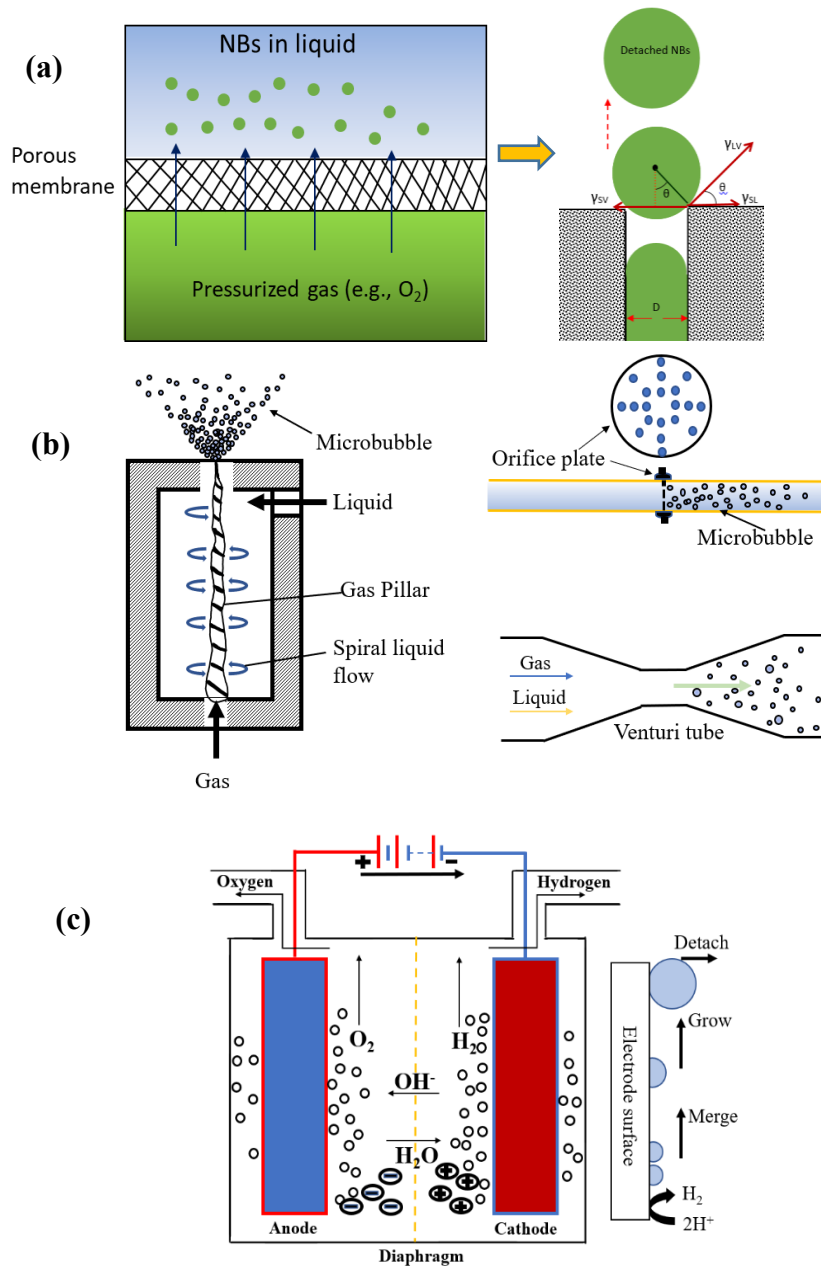
Figure 1.5 (a) Schematics of membrane bubbling and the interfacial process of bubble detachment at one single membrane pore. (b) The spiral liquid flow type, orifice plate and Venturi type. (c) The formation of surface NBs in an electrochemical system.
Source: (W. Zhang, Xue, Shi, & Marhaba, 2021).

1.5 Reported Engineered Applications of MBs and NBs

Engineering applications of MBs and NBs have widely been demonstrated (T. Kim & Han,

2010), ranging from aeration, enhanced ozonation, disinfection, surface cleaning, ecological restoration such as harmful algal bloom (HAB) mitigation (Agarwal et al., 2011; Ghadimkhani, Zhang, & Marhaba, 2016; Jyoti & Pandit, 2003; Jyoti & Pandit, 2001; T. Kim & Han, 2010; Mezule, Tsyfansky, Yakushevich, & Juhna, 2009; Sumikura, Hidaka, Murakami, Nobutomo, & Murakami, 2007; Takahashi, 2009).This section summarizes and discusses the state of art knowledge with focuses on environmental and agricultural applications.

1.5.1 Aeration with enhanced mass transfer

The efficiency of gas-liquid phase operations is typically determined by the rate of gas to liquid transfer, making mass transfer a crucial factor (P. Khan, Zhu, Huang, Gao, & Khan, 2020; Wilkinson & Dierendonck, 1990). Mass transfer efficiency depends on various factors such as the bubbles' size distribution, rising velocity, gas–liquid hydrodynamics, coalescence, and break-up surface-to-volume ratio, and physical properties (Bouaifi, Hebrard, Bastoul, & Roustan, 2001). According to the two-film theory of gas absorption, the mass transfer rate between two phases is influenced by the coefficient of liquid-gas mass transfer, surface area to volume ratio, and concentration gradient within the phases (Bouaifi et al., 2001). Unlike larger bubbles that rise quickly and collapse, MBs and NBs possess high internal pressure (several times higher than atmospheric pressure) and long-term stability. This allows them to concentrate dissolved gases in the aqueous phase beyond

the saturation point, thereby enhancing gas dissolution and gas-liquid mass transfer (A. K. Patel et al., 2021; Xue, Zhang, Marhaba, & Zhang, 2022). Furthermore, NBs, in particular, continue to dissolve oxygen until they collapse, making them more efficient than larger bubbles in terms of oxygen transfer (W. Xiao & Xu, 2020; S. Zhou, Liu, Chen, Sun, & Lu, 2022). For instance, research conducted by (H. Li et al., 2014) demonstrated that using MB- and NB-aeration in deionized water resulted in dissolved oxygen (DO) levels of 10.4 and 34.2 mg·L^{-1}, respectively, compared to 9.9 and 19.1 mg·L^{-1} achieved by macro-bubble-aeration using air and oxygen, respectively. This improved oxygen mass transfer under MB- and NB-aeration suggests lower aeration rate requirements and reduced energy consumption compared to conventional aeration systems in the current activated sludge process (Sander, Behnisch, & Wagner, 2017). Furthermore, NBs have been found to enhance oxygen supply to biofilms, leading to a 1.5-fold increase in oxygen transfer efficiency compared to control group. This acceleration in biofilm growth results in improved removal efficiencies of chemical oxygen demand and ammonia (W. Xiao & Xu, 2020; Z. Xiao, Aftab, & Li, 2019). Moreover, MNBs show promise in groundwater remediation by significantly enhancing the mass transfer efficiency of ozone and maintaining stability to continuously supply ozone (L. Hu & Xia, 2018; Z. Xiao et al., 2019).

While NBs offer advantages in enhancing mass transfer during aeration, it is crucial to consider the cost implications associated with their generation. The specialized

equipment and techniques required for NB production can lead to higher production and maintenance costs compared to conventional aeration methods (A. K. Patel et al., 2021). Furthermore, the use of NBs is limited in larger-scale applications such as microbial fermentation, extraction and separation, product refining, medical imaging, and nanoparticle generation (A. K. Patel et al., 2021). However, when it comes to energy efficiency and the mass removal of pollutants in relation to electricity consumption, NB aeration outperforms conventional methods (S. Zhou et al., 2022).

1.5.2 Surface cleaning and biofoulant prevention and removal

1.5.2.1 Surface cleaning mechanisms of NBs NBs are also found to remove organic contaminants from pyrolytic graphite (Wu et al., 2008; Wu et al., 2006), gold surfaces (G. Liu et al., 2008) and stainless steel surface (K.-K. Chen, 2009). Similar to MBs, when NBs collapse they may also produce radicals and wave shocks that contributes to surface foulant removal (Ahmed, Shi, et al., 2018; Ghadimkhani et al., 2016; S. Liu, S. Oshita, S. Kawabata, et al., 2016; S. Liu, S. Oshita, Y. Makino, et al., 2016; Magaletti, Marino, & Casciola, 2015; Ushikubo et al., 2010; Wu et al., 2006; Wu et al., 2007; Yasui et al., 2018). Unlike bulk bubbles, NBs behave like colloids and have much less mechanical impacts (e.g., physical scouring) than MBs do. Therefore, besides mechanical shocks and radicals, there are two additional mechanisms that could lead to efficient surface cleaning (G. Liu & Craig, 2009; G. Liu et al., 2008; Wu et al., 2008) (1) Foulant repulsion or surface

masking. As NBs form under microwave irradiation or electrochemical reactions at the interface of the solid surface and surface foulants (e.g., BSA proteins as illustrated in **Figure 1.6(a)**), NBs could mechanically lift and remove the foulants from the solid surface (H. Chen et al., 2009; Wu et al., 2008). The coating layer of negatively charged NBs may also establish a physical barrier or surface mask that prevents the adsorption or deposition of contaminants on the surface (Mukumoto et al., 2012; Wu et al., 2008; Wu et al., 2007). (2) Hydrophobic interactions. NBs are hydrophobic in nature and thus, due to the strong hydrophobic or electrostatic interactions, NBs are able to sequester hydrophobic contaminants or foulants via adsorption or partitioning as shown in **Figure 1.6(b)** (Wu et al., 2007; J. Zhu et al., 2016). Some studies employed NBs or MBs or a mixture of them for filtration membrane fouling mitigation (H. Chen et al., 2009; Wu et al., 2008). Thus, incorporating MBs for membrane defouling may reduce chemical cleaning that involves the use of detergents, surfactants and chelants.
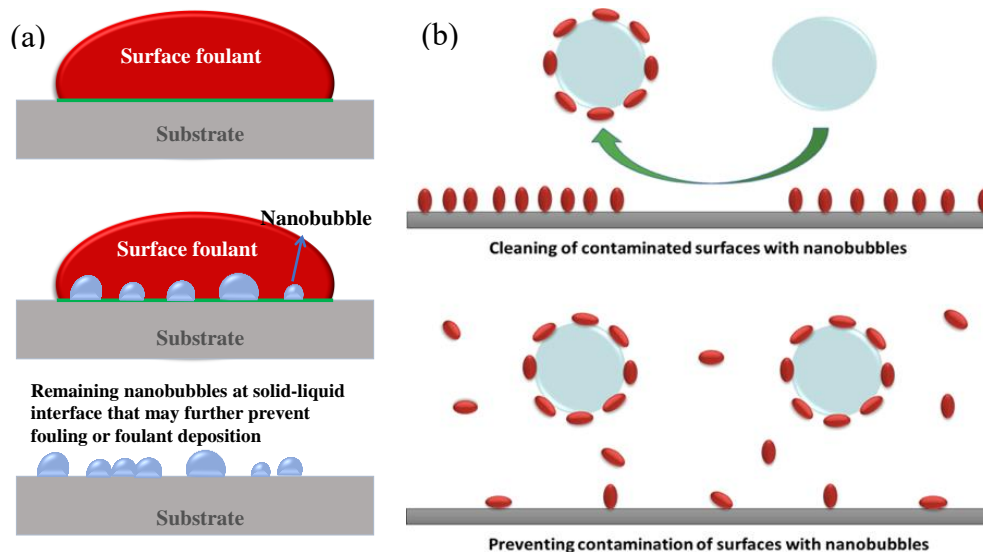
Figure 1.6 (a) Proposed mechanisms of defouling and fouling prevention due to the formation of surface NBs under electrochemical reactions, where the fouling materials may be repelled by the surface NBs, which may further prevent foulant deposition due to electrostatic repulsion or steric repulsion. (b) The modes of surface foulant removal by hydrophobic intearctions of NBs with surface foulants (red particles).

1.5.2.2 Antimicrobial activity of NBs and biofilm mitigation Microbial contamination in drinking water distribution system (DWDS) negatively affects public health as well as pertinent infrastructure's integrity via biocorrosion. Particularly, biofilm formation reduces the drinking water quality and harm human health. Biofilms may act a vector and habitat or reservoir for many microorganisms (bacteria, fungi, protozoa, and/or viruses) to survive from disinfection, antibiotics and biocides (Farkas, Bocos, Dragan-Bularda, & Crăciunaş, 2014). Biofilms foul many surfaces including food processing systems, interior pipe works, storage tanks, and cooling towers, causing material corrosion and failure. Pathogenic bacteria in biofilm negatively affect water quality and human health (W.-J. Lee et al., 2017), causing disease such as typhoid fever, Salmonellosis, Bacillary

dysentery, Cholera, and Gastroenteritis (Ingraham, 2017).

Despite regulated use of residual disinfectants in the United States and other countries to limit the biofilm growth in DWDS, there are well-known drawbacks in traditional disinfection such as disinfection by production (DBP) formation. Chlorine, for example, effectively inactive a wide spectrum of waterborne pathogens (Alexander, Knopp, Dötsch, Wieland, & Schwartz, 2016), though oxidation or denaturation of enzymes, nucleic acid and damage polysaccharide macromolecular polymers (e.g., depolymerization of carbon-nitrogen bonds of proteins) and thus the metabolic and reproductive capabilities of bacteria are reduced (Buhmann et al., 2018; J. Zheng et al., 2017). During disinfection or water storage/delivery, toxic chlorite (ClO_2^-) and chlorate (ClO_3^-) are potentially produced. Moreover, chlorination renders the rise of more than 600 different potentially carcinogenic DBPs (e.g., trichloromethane, brominedichloromethane, dibromomethane and tribromomethane) (Daiber et al., 2016; Jeong et al., 2015; Krasner et al., 2006; Lavonen, Gonsior, Tranvik, Schmitt-Kopplin, & Köhler, 2013; Zhai, Zhang, Zhu, Liu, & Ji, 2014) and NDMA (N-nitrosodimethylamine) during the chlorine disinfection of water containing dimethylamine (Nihemaiti, Le Roux, & Croué, 2015).

As opposed to chlorine, ozone has high oxidation potential and more reactive at comparable doses (Somerlot & Davis, 2015). Moreover, ozone leaves far less chemical residuals in ozonation and disinfection treatment (Verma, Gupta, & Gupta, 2016). However, ozone has limited water solubility and unstable with rapid decay in water, which often

reduces the effective exposure dose and disinfection efficacy. A feasibility study investigated the use of ozone MNBs as a disinfectant to prevent airborne disease (He, Zheng, Li, & Song, 2015). The results showed that ozone MNBs achieved (5.2 to 3.3) and (5.0 to 3.7) log reduction in *Alternaria solani Sorauer conidia*, a fungal pathogen and *Cladosporium fulvum conidia*, a genus of fungi respectively. Ozone MBs also achieved 99.99% inactivation of *E. coli* cells with a lower ozone dose and a smaller volume of the water disinfection systems (Sumikura et al., 2007). Another study showed that ozone MBs achieved 75% reduction of *E. coli* through 3 min of continuous injection of MBs. In addition, ozone MBs are effective against other types of bacteria such as *Bacillus subtilis* spores and *Cryptosporidium parvum*. Bacteria inactivation and removal by ozone NBs is largely attributed to the formation of hydroxyl radicals or other reactive species especially during collapse or burst (Temesgen et al., 2017). Bacterial removal can be improved by the burst of high intensity number and smaller size of bubbles (K.-K. Chen, 2009). Combinations of NBs with UV irradiation or ultrasonication usually boost up radical formation and improve disinfection power of NBs (Agarwal et al., 2011; Ikeda-Dantsuji et al., 2011; T. Zheng et al., 2015).

1.5.3 Harmful algal bloom mitigation and ecological restoration and remediation

Excess nutrients can cause eutrophication and harmful algal blooms (HABs) in natural waters, which may negatively affect water quality, landscape aesthetics, human health and

economic development (Conley et al., 2009). HABs cause direct economic losses of several million pounds in the UK (Berdalet et al., 2016) and >$2 billion in the USA (DODDS et al., 2009) in the fish industry. Owing to rapid population growth and economic development, various human activities, industrial, agricultural and transportation have intensified water eutrophication (Horppila, 2019; Huisman et al., 2018). Despite of the control of external nutrient loading from anthropogenic discharges, the existing N and P loads from contaminated sediment are expected to prolong eutrophication episodes (Breitburg et al., 2018). The main cause of internal nutrient loading would be hypoxia/anoxia (dissolved oxygen < 2 mg/L) induced biochemical reactions at the sediment-water interface. Therefore, measures for the reduction of nutrient internal loadings and for mediating hypoxia/anoxia have attracted increasing attention for eutrophication control. Many recent ecological engineering practices and technologies (e.g., aeration, nutrient fixation and algicide use) have been developed and tested for water quality restoration. However, traditional bottom water oxygenation methods, such as deep-water aeration, have been reported to be hindered due to excessive costs, high energy consumption and hydrologic disturbance of the benthos (Conley* et al., 2009).

Recently, NB technologies have demonstrated promising potentials in sustainable control and abatement of eutrophication and HABs. NBs have been directly introduced into eutrophic/polluted waters to remove aerobically-degradable pollutants, such as BOD and ammonium (Y. Sun, Wang, & Niu, 2018; Yifei Wu et al., 2019). Previous studies have also

shown that NBs can improve the lysis of harmful algal cells and the detoxification of cyanotoxins, and companies in Asia, the US and Europe have become increasingly involved in projects that use NB technology for mitigation of HABs (Gunther; P. Li, Song, & Yu, 2014; ltd.). Alongside the use of the bulk NBs, a novel refinement of the technology, which involves interfacial NBs, was developed in 2018, using natural minerals loaded with oxygen to deliver oxygenated NBs onto sediment surfaces (L. Wang, Miao, Lyu, & Pan, 2018; Honggang Zhang et al., 2018).This approach successfully reversed sediment hypoxia and reduced N and P fluxes from the sediment for over four months. Nevertheless, the underlying mechanisms of NBs' stability and aquatic behavior such as gas diffusion dynamics remain elusive. Currently, the emerging NB technology for water restoration has been mainly tested in freshwaters or inland lakes. However, HABs and hypoxia problems also occur in coastal areas (D et al., 2018), where high salinity and high dissolved organic matter (DOM) may inevitably reduce the longevity of NBs (Cui, Shi, Xie, Liu, & Zeng, 2016). More importantly, temperature increases and acidification of water bodies may also affect the stability and gas dissolution properties of NBs. Thus, a fundamental understanding of physicochemical properties and behavior of NBs are worthy of further elucidation to support the engineering applications of NBs.

1.5.4 Agricultural applications

MNBs and NBs have rapidly transformed many practices in agriculture, aquaculture, food engineering, and sterilization (Dzubiella, 2010; KURATA, TANIGUCHI, FUKUNAGA, MATSUDA, & HIGAKI, 2007; Tsuge, 2014).

Many studies recently demonstrated proper irrigation with NBwater could promote germination and plant growth with improved productivity (Ahmed, Shi, et al., 2018; Ebina et al., 2013b; S. Liu, S. Oshita, Y. Makino, et al., 2016; Yuncheng Wu et al., 2019). Ozone MBs could effectively remove and degrade fenitrothion and pathogens in food and vegetables in such as lettuce, cherry tomatoes, and strawberries (Ikeura, Kobayashi, & Tamaki, 2011). For instance, seed germination rates increased in mixed nitrogen and air NBs water compared to that in distilled water, because of the generation of exogenous ROS and increased the mobility of the water molecules (S. Liu, S. Oshita, S. Kawabata, et al., 2016; S. Liu et al., 2017). MNBs improved the growth of plants such as lettuce (J.-S. Park & Kurata, 2009; J. Park, Ohashi, Kurata, & Lee, 2010) and rice (Minamikawa, Takahashi, Makino, Tago, & Hayatsu, 2015). Moreover, the influences of air, oxygen, nitrogen, and carbon dioxide NBsmay be different as the soil chemistry (e.g., pH or dissolved oxygen) will be changed upon exposure to different NB water. **Figure 1.7a** and **b** compare the hypocotyl growth process of lettuce and fava bean (*Vicia faba*) that differed with the types of NB waters. The tap water-treated ones had no leaf sprouting during the same initial growth period. **Figure 1.7c** reveals nitrogen NBs promoted most plants (especially tomato)

in terms of leave numbers. **Figure 1.7d** illustrates the generation of exogenous ROS by

NBs that could activate the cell wall loosening and cell elongation (S. Liu et al., 2017; S.

Liu, S. Oshita, Y. Makino, et al., 2016). The positive impacts on germination or plant

growth may also be attributed to the effective delivery of nitrogen or CO_2 elements and

other possible factors such as release of soil nutrients (Bowley & Hammond, 1978; Uchida

et al., 2011). Moreover, different plants including lettuce, carrot, fava bean, and tomato

may have different responses to NBs not only because they have physiological differences

but also have different rhizosphere bacteria or other microorganisms that grow near the

plant roots and play critical roles in the plant's nutrient absorption and growth.
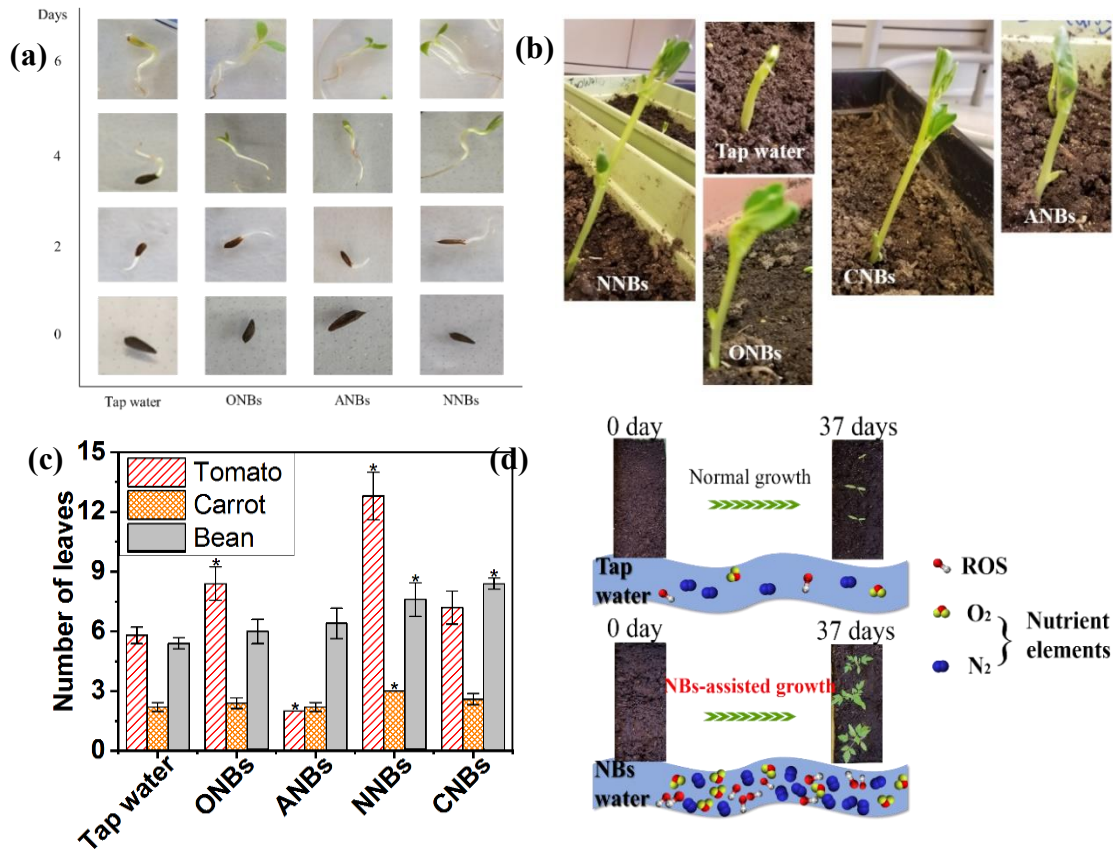
Figure 1.7 (a) Photos of hypocotyl growth process of lettuce seeds at different submersion days. (b) Growth of fava bean (*Vicia faba*) taken after the first week of incubation. (c) Influence of water type on number of leaves of tomato, carrot, and bean after 37 days. (d) Summary of the promoting effect by NBs and potential mechanisms of promotion. Source: (Ahmed, Shi, et al., 2018).

1.6 Research Objective

Currently, stable NBs have been experimentally confirmed, but a consistent theoretical framework to elucidate their behavior in water is yet to be established. Therefore, it is imperative to establish a consistent theoretical foundation for comprehending the properties and behaviors of these bubbles, ensuring their practical and functional utilization. Additionally, despite the aforementioned confirmation of NBs' viability in

agricultural applications, the mechanisms by which they enhance seed germination and plant growth remain elusive. Furthermore, the intriguing interactions between NBs and soil and rhizosphere-associated microbes influences the characteristics and functionality of microbial communities, which remain largely unexplored. Lastly, we are actively engaged in commercializing our NB technology, aiming to address various practical challenges in the realms of agriculture and the environment. There are four main objectives of this dissertation:

1. The ceramic membrane was used in this study. Among the various methods for producing NBs in water, the membrane-bubbling process stands out due to its many appealing features in the control of the gas type or bubble size. However, the underlying mechanisms of the bubble evolution and release at the interface of the membrane surface and water layer are fully understood. My first objective is to exam the influences of the injection gas flow, the overlying water flow, and the interfacial surface tension on the produced NBs in water. These investigations uncovered valuable insights into the formation mechanisms and characteristics of NBs in water and laid the foundation for novel engineering applications.

2. NBs in water elicit unique physicochemical and colloidal properties (e.g., high stability and longevity). Aeration kinetics and dissolution behavior of oxygen (O_2) NBs are assumed to be bubble size dependent. Thus, my second objective is to exam the bubble aeration and dissolution behavior using both modeling and experimental approaches.

3. To reveal the impacts of NBs nutrient release from soil, my third objective is to compare soil chemical properties and the release of soil elements elements (e.g., NH_4^+, K^+ and Mg^{2+}) before and after immersion with different gaseous NBs (e.g., oxygen(O_2), nitrogen(N_2), hydrogen(H_2), carbon dioxide(CO_2) and air). Spiking different types of gaseous NBs into soil induced complex interactions with soil substances and various impacts on soil characteristics. The changes of these soil properties may yield tremendous impacts or implications on soil fertility and plant growth, which deserves further investigations.

4. To further unravel the promotion mechanism of NBs on plant growth, my fourth objective is to investigate the characterization of NBs in tap water and their impacts on tomato's early growth, enzymatic activity, microbial communities and electrochemical properties of plant roots. This study provides valuable insights into the potential effects of NBs on plant growth and soil properties, contributing to our understanding of the environmental implications of NB technology in agriculture.

CHAPTER 2

EVALUATING MECHANISMS OF NANOBUBBLE FORMATION VIA CERAMIC MEMBRANE

2.1 Introduction

Nanobubbles (NBs) hold tremendous potential across various fields, including energy production (L. Qin, Alam, & Wang, 2019), environmental remediation (Han, Yang, Yan, Li, & Liu, 2020), chemical engineering (Han et al., 2020) and aquaculture (Roy, Machavaram, Pareek, & Mal, 2021). In the water aeration process, the bubble size plays a critical role in gas/liquid mass transfer and overall aeration efficiency. Ultrafine bubbles, such as NBs, clearly enhance the gas/liquid mass transfer due to their increased gas/liquid contact area and prolonged residence time in solutions. Moreover, many chemical reaction kinetics could be improved by fine bubbles (Tomisaki, Natsui, Fujioka, Terasaka, & Einaga, 2021; Z. Xiao, Li, Wang, Sun, & Lin, 2020; Z. Xiao, Li, Zhu, & Sun, 2020). For example, the NBs of CO_2 reduced the overpotential of the electrochemical CO_2 reduction on boron-doped diamond (BDD) electrodes with improved production of carbon monoxide (CO) (Tomisaki et al., 2021). (Z. Xiao, D. Li, F. Wang, et al., 2020; Z. Xiao, D. Li, Q. Zhu, et al., 2020) reported that the conversion efficiency of NO_x to N_2 was improved with the assistance of micro-nano bubble (MNB) because of the oxidation of radical ·OH generated by MNBs and high mass transfer efficiency. Consequently, the acquisition and control of the bubble size have become pivotal in these applications.

There are various reported methods to produce nanobubbles in liquid, including orifices (Mohseni, Chiamulera, Reinecke, & Hampel, 2022), nozzles (C. Wang, Li, Huang, & Weng, 2022), porous plates (J. K. Lee et al., 2020), cavitation (Favvas, Kyzas, Efthimiadou, & Mitropoulos, 2021) and electrolysis (Postnikov, Uvarov, Penkov, & Svetovoy, 2018). For example, (J.-Y. Kim, Song, & Kim, 2000) successfully generated stable NBs in water with average diameters of 300-500 nm using ultrasonication and a palladium electrode. Similarly, (Seo & Lee, 2023) demonstrated the production of high-density bulk NBs (2.25×10^9 #·mL^{-1}) with average diameters of 150 -200 nm through megasonic cavitation and atomization. To achieve tunable sizes of NBs, many studies also reported the use of porous membranes as a platform to produce bulk NBs by changing the operating parameters such as pore size and gas flow rate (Kukizaki & Goto, 2006; J. Tang et al., 2021). For example, (Ahmed, Sun, et al., 2018) reported that the size of NBs are dependent on the membrane pore size and the injected gas pressure. However, the bubble formation encounters the complex impacts of hydraulic sheer and interfacial surface tension at the water/membrane pores. The size of the ejected bubbles is primarily influenced by the gas/solid adhesion rather than the pore size of the membrane. Thus, the membrane surface wettability plays a crucial role in bubble release (Ahmadi & Okawa, 2015) and a gas-repelling surface is usually desirable to facilitate bubble detachment from the membrane surface (Yang, Hou, Wan, Chen, & Xu, 2016).

Recently, hydrophobic membranes have emerged as a promising method for

enhancing gas transfer efficiency, whether for extraction or supply purposes. For example, membrane distillation (MD) processes or membrane reactors usually employ hydrophobic membranes such as polytetrafluoroethylene (PTFE), polypropylene (PP), polyvinylidene fluoride (PVDF), and polydimethylsiloxane (PDMS) to transfer or dispense gases (e.g., H_2, CH_4, and CO_2) from or to the reaction fluids (Hou, Jassby, Nerenberg, & Ren, 2019). Moreover, hydrophobic membranes can also be prepared through surface modifications with hydrophobic chemicals such as steric acid (Ahmed, Sun, et al., 2018), PTFE (K. Wang et al., 2018) and PVA (M. J. Park, Gonzales, Abdel-Wahab, Phuntsho, & Shon, 2018). These modifications are reported to improve the recovery of gaseous products (e.g., volatile organic compounds, methane and H_2) at the membrane/solution interface (Hou et al., 2019; Rongwong & Goh, 2020). Reducing the triple phase contact line (TPCL) is shown to decrease air adhesion on the membrane surface during the bubbling process, leading to improved bubbling efficiency (J. Tang et al., 2021). Additionally, the strong interaction between the solid surface and gas on hydrophobic surfaces allows liquid atoms to break free from the surface, resulting in the accumulation of gaseous atoms and the formation of NBs (Ryan & Hemmingsen, 1993; D. Zhang, Guan, Shen, Tang, & Zhou, 2022). Thus, a hydrophilic surface is preferred for the membrane. Nevertheless, directly using a hydrophilic membrane is not ideal as water may permeate into the membrane pores, causing significant membrane wetting and a higher gas transfer resistance. Therefore, the effects of the membrane surface wettability and pore functionalization must be addressed

to understand the formation mechanism of NBs and the control strategies of bubble sizes.

The primary objective of this study is to examine the impact of surface wettability and operating conditions, including transmembrane pressure and water phase flow velocity, on the size and concentration of the NBs generated by ceramic membrane. Ceramic membrane is inherently hydrophilic due to the presence of hydroxyl groups, such as silanol groups, on their surface. Thus, in this research, we modified the ceramic membrane with PTFE to impart hydrophobicity and examined the influences of different hydrophobic coating procedures on NB generation in water. To assess the mass transfer performance, we also calculated the enhanced oxygen transfer efficiency (OTE) and a mass transfer coefficient of the NB generation system. Additionally, we further studied the impact of other critical factors such as ambient temperature, air exposure and surfactants on the stability of aqueous NBs during storage.

2.2 Materials and Methods

2.2.1 The generation of NBs using ceramic tubular membranes with different coating

The generation of bulk NBs in water was achieved by the reported membrane bubbling method (Ahmed, Sun, et al., 2018). Specifically, the tubular ceramic membranes (Sterlitech, USA) that had a nominal pore diameter of 140 nm or 1400 nm with 250 mm in length and inner/outer diameters of 5.4 mm and 10 mm respectively were used for producing NBs in

water. The modified membranes were achieved by coating PTFE as illustrated in **Figure 2.1**. Briefly, the PTFE solution was prepared by diluting the 60 wt% PTFE emulsion (Teflon™ PTFE DISP 30 Fluoropolymer Dispersion) with Milli-Q deionized (DI) water. To coat the outer surface of the ceramic membrane to achieve a surface hydrophobic membrane (HM), a PTFE solution (2.5 wt%) was prepared and spray-coated on the ceramic membrane with the pore size of 1400 nm with an air brush to reach a density of 2.5±0.3 mg·cm^{-2} as determined by the dry weight change of the membrane before and after coating. To only coat the internal pore surface of the ceramic membrane to form a Janus membrane (JM), the tubular membrane was immersed in 300 mL of 10 wt% PTFE solution and sonicated for 30 min (40 kHZ). Then, the tubular ceramic membrane was carefully rinsed the outside and inside of the tube with 50 mL DI water in a vertical orientation. After coating with PTFE, the above two types of PTFE-coated membranes were dried at room temperature for 12 h and sintered at 340 °C with a heat rate of 10 °C·min^{-1} for 30 min (X. Chen et al., 2022; P. Xu et al., 2021). The morphology of surface and cross section of the obtained membranes were characterized by scanning electron microscopy (SEM) (JSM-7900F, JEOL Ltd., USA) and water contact angles to indicate the surface wettability.
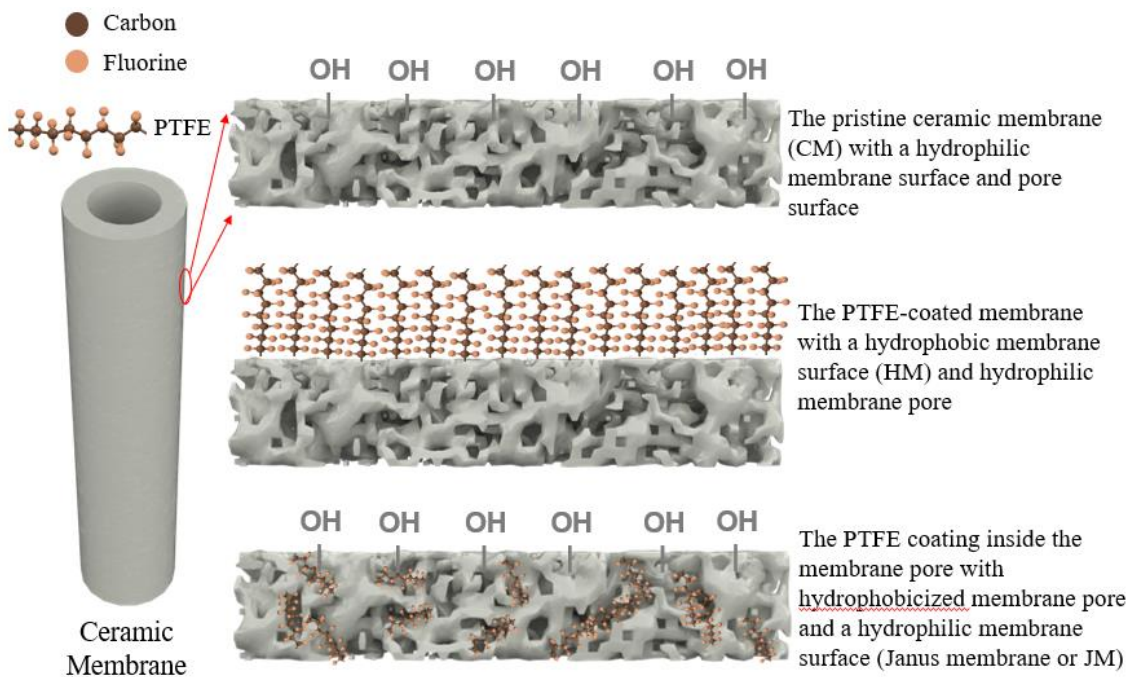
Figure 2.1. The tubular ceramic membrane before and after modification by PTFE.

2.2.2 Evaluation of the produced NBs in water under different conditions

As **Figure 2.2** shows, a high-purity oxygen gas cylinder was used to provide the compressed oxygen gas that passed through the membrane module and dispersed into the flowing water outside the tubular membrane. The flow water was either recirculated between a 500-mL water reservoir tank and the membrane module (**Figure 2.2a)** or directly stored in the tank without recirculation or single-pass (**Figure 2.2b**). Unless indicated otherwise, the water flow rate of 1 L·min^{-1} or a cross-flow velocity of 0.17 m·s^{-1} and a gas flow of 0.5 L·min^{-1} or gas flux of 1.36 m^3·m^{-2}·min^{-1} under an injection pressure of 114 kPa were used in both the recirculation and single-pass modes.

When evaluating the production of NBs using the four types of membranes, the

single-pass mode was employed with the water flow rate of 0.05 $L \cdot min^{-1}$ or a cross-flow velocity of 0.08 $m \cdot s^{-1}$ and the injection gas flow of 0.5 $L \cdot min^{-1}$ (114 kPa). When the water flow rate varied from 0.033, 0.05, 0.1, 0.5, 1, 2, 3.33 $L \cdot min^{-1}$, the gas flow rate was fixed at 0.5 $L \cdot min^{-1}$ (114 kPa). When varying the gas flow rate (e.g., 0.5, 2, 4 and 6 $L \cdot min^{-1}$) by changing the gas pressure accordingly to 114, 133, 155 and 175 kPa, the water flow rate was kept at 1 $L \cdot min^{-1}$. The response surface methodology (RSM) with the central composite design (CCD) were applied to optimize the NBs concentration via adjusting water flow rate and gas flow rate using the Design Expert Software (version 7.0).

In the recirculation operation, 2 mL of the bubble water was sampled from the reservoir tank at different times (1, 10, 30, 60, and 90 min). When operated in single pass mode, the NB water was sampled from the water pipe outlet immediately after the water flew out of the membrane module. All the above comparative studies were repeated at least three times to yield average and standard deviation for the presented data. The bubble size distribution and concentration in the water samples were analyzed using a Horiba ViewSizer 3000 nanoparticle tracking analysis (NTA) instrument (Horiba, USA). Meanwhile, the dissolved oxygen (DO) concentration in the reservoir water was recorded by a DO sensor (PS-2196, PASCO, USA) with an Xplorer GLX datalogger (PS 2002, PASCO, USA) with a reporting range of 0–40 $mg \cdot L^{-1}$ and an accuracy level of ± 0.6 $mg \cdot L^{-1}$. The DO data were then analyzed to estimate the apparent volumetric mass transfer coefficient, $K_L a$ (h^{-1}) using the method reported elsewhere (Xue, Zhang, et al., 2022).
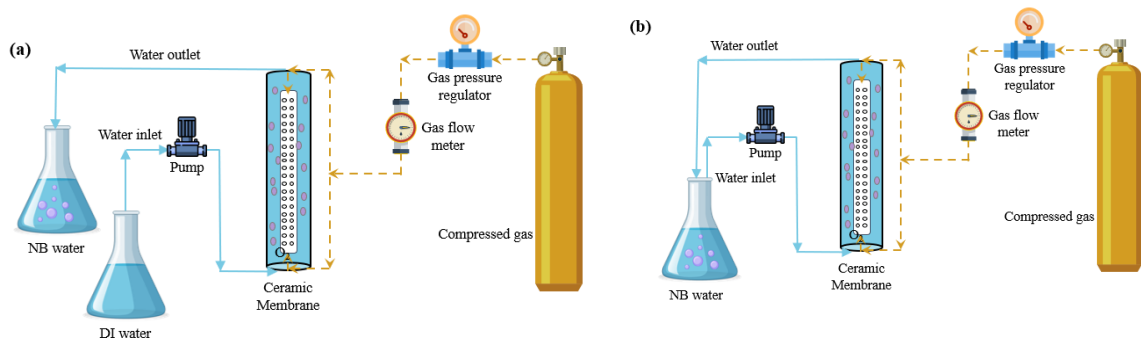
Figure 2.2 Schematic diagrams of the NB generation system in (a) a single-pass mode and (b) a recirculation mode.

2.2.3 Assessment of oxygen transfer efficiency

In this method, oxygen gas (114 kPa and 0.5 LPM) was pressed through the membrane into flowing continuous water (1 $L \cdot min^{-1}$). 500 mL DI water is circulated in this system. 2 mL of NB water was sampled at different times (1, 10, 30, 60, 90 min) to characterize the concentration of the NBs via PAT (ViewSizer3000, HORIBA). Meanwhile, the DO concentration change was recorded by a real time monitor DO sensor (PS-2196, PASCO, USA) with Xplorer GLX datalogger (PS 2002, PASCO, USA) with a reporting range of 0–40 $mg \cdot L^{-1}$ and an accuracy level of ±0.6 $mg \cdot L^{-1}$. The concentration of particle detected with PTA in DI water is 6-8×10^6 particles·mL^{-1}.

The DO data obtained at each determination point were then analysed by a simplified mass transfer model to estimate the apparent volumetric mass transfer coefficient, K_La (h^{-1}) and the steady-state DO saturation concentration, C_s ($mol \cdot L^{-1}$). The basic model is:

$$OTE(\%) = \frac{(C_{DO} + \frac{4}{3}\pi r^3 \times C_{NB} \times \rho_{NB} \times N) \times Q_{water}}{Q_{gas} \times \rho_{gas}} \times 100 \qquad (2.1)$$

$$\frac{\rho_{NB}}{\rho_{gas}} = \frac{P_{NB}}{P_{gas}} \qquad (2.2)$$

where C_{DO} is the DO in water (kg·L⁻¹), r is the radius of NBs (m), C_{NB} is the concentration of NBs in water (#·L⁻¹), ρ_{NB} is the oxygen density in NBs (4.5 kg·m⁻³), which is estimated by **Equation (2.3)** by assuming the internal bubble pressure of 342 kPa which is 3 times higher than the inject pressure (X. Shi et al., 2021), ρ_{gas} is the oxygen density of the inject gas (1.5 kg·m⁻³) under 114 kPa and temperature of 20°C, Q_{water} is the water flow rate (L·min⁻¹), Q_{gas} is the oxygen flow rate (0.5 L·min⁻¹), and N is the concentration of NBs (#·mL⁻¹).

2.2.4 Calculation of the hydraulic shear stress on the interfacial bubbles

The shear stress at the membrane wall, σ, was calculated using:

$$\sigma = \frac{\lambda \rho_c u^2}{8} \qquad (2.3)$$

where ρ is the flow water density (1 kg·m⁻³) and u is the cross-flow velocity or water flux (m·s⁻¹), which is calculated by **Equation (2.4)** and shown in **Table 2.1**:

$$u = \frac{Q_{water}}{A} \qquad (2.4)$$

where Q$_{water}$ is the cross-flow water flow rate and A is the cross-sectional area of the membrane module (0.98 cm²). λ is the Moody friction factor and calculated by

Equation (5a) or **Equation (5b)** (Plascencia, Díaz–Damacillo, & Robles-Agudo, 2020):

$$\lambda = \frac{64}{Re} \quad (\text{ Laminar flow when Re} <2500) \tag{2.5a}$$

$$\lambda = 0.3164\,Re^{-0.25}\,(\text{ Reynolds number when Re} >2500) \tag{2.5b}$$

$$Re = \frac{\rho u D_h}{\mu} \tag{2.6}$$

where μ is the dynamic viscosity of water (1×10^{-3} N·s·m^{-2}) and D_h is the inner diameter of the tubular membrane channel (5 mm).

Table 2.1 The Velocity and Re of Water Flow Under Different Water Flow Rate

low rate (L·min^{-1})	0.033	0.05	0.1	0.5	1	2	3.33
Velocity (m·s^{-1})	0.006	0.008	0.017	0.085	0.17	0.34	0.51
Re	53	81	161	807	1614	3228	4842

2.3 Results and Discussion

2.3.1 Characterization of the membrane properties

SEM images in **Figure 2.3** revealed the morphology of the top membrane surface and cross-sectional structure of the pristine ceramic membrane and two PTFE-coated membranes. Compared to the top surface of the pristine ceramic membrane (CM), hydrophobic membrane (HM) and Janus membrane (JM) both had apparent surface deposits of PTFE, which blocked the surface pores. However, JM appeared to have less PTFE surface coating than HM and exhibited more porous. The cross-section images also

reveal that the PTFE was successfully coated on the pore surface of JM. And the PTFE

didn't appear in the pores of CM and HM.
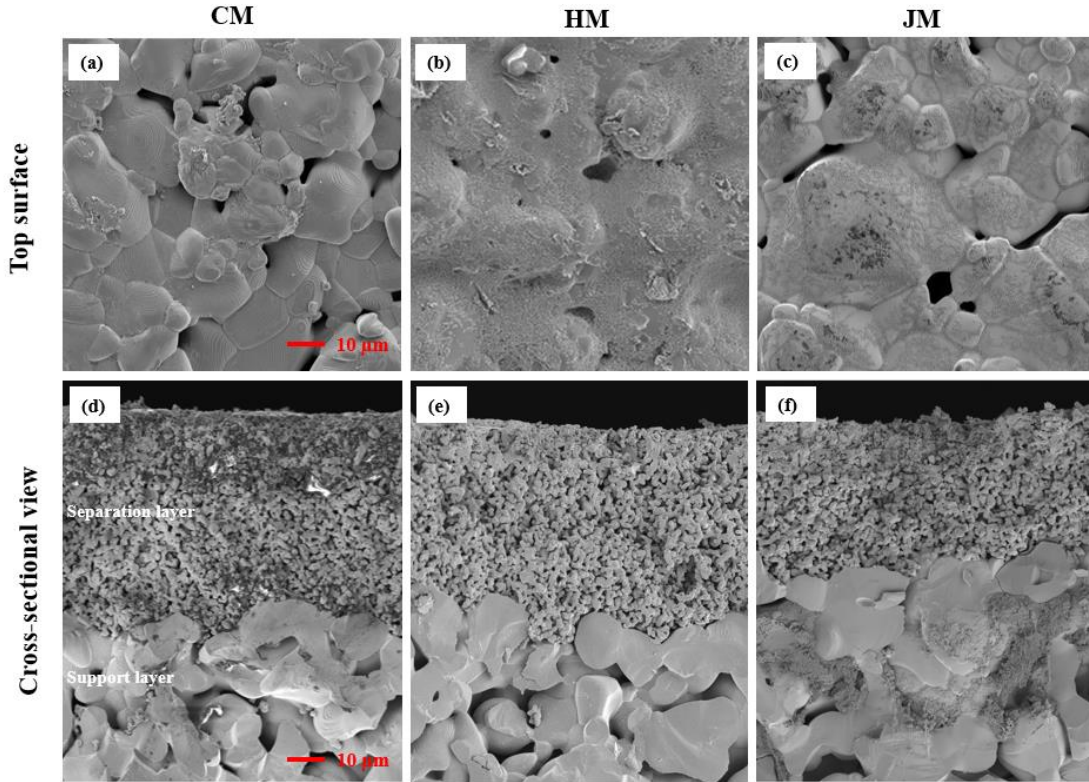
Figure 2.3 SEM images of (a-c) the top membrane surface and (d-f) the cross-sectional view of the CM, HM and JM samples.

Figure 2.4 shows that the water contact angle on the membrane with the surface

coating of PTFE was around 122°, whereas the pristine ceramic membranes yielded an

initial water contact angle of 49° that quickly spread over the surface within 2 s, indicative

of the hydrophilic nature. In contrast, the water droplet onto the Janus membrane surface

yielded a contact angle of 57°, which gradually decreased over a duration of 23 s. This

delayed water droplet spread is attributed to the hydrophobicized membrane pores that

prevented the entry and permeation of the water droplet.
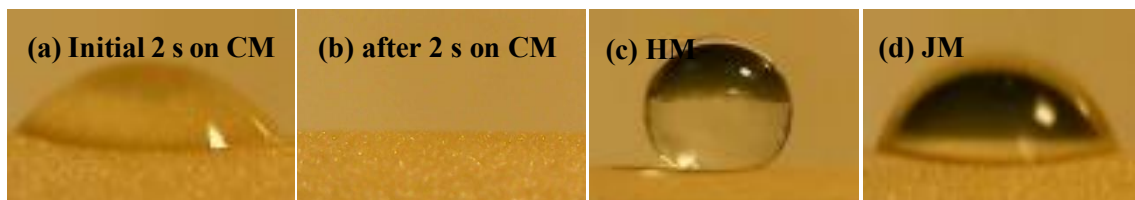
Figure 2.4 Water contact angles on the different membrane surfaces.

2.3.2 Comparison of the NB formation on four types of membranes

Figure 2.5 compares the bubble concentrations and diameters of the produced NBs with

the pristine membranes with pore diameters of 140 nm and 1400 nm and two other PTFE-

coated membranes (HM and JM). The influences of the pore size and PTFE coating on the

bubble concentration and bubble size are complex. For example, for the same pore size of

1400 nm, CM and JM achieved smaller bubble sizes (c.a., 63 nm in diameter) and higher

bubble concentrations (e.g., $2\text{-}4\times10^8$ particle·ml^{-1}) than HM, which yielded an average

bubble diameter of 70 nm and an average concentation of 1×10^8 particle·ml^{-1}. According

to the above characterization, the surface hydrophobicized membrane had reduced surface

pore sizes that affected the bubble formation. Moreover, according to the triple phase

contact line (TPCL) theory, the contact line of gas bubbles on the hydrophilic membrane

was considerably smaller with the bubble contact angle large than 90$^\text{o}$ compared to that on

the hydrophobic membrane with the contact angle less than 90$^\text{o}$ as shown in **Figure 2.9b**

and **1c**, resulting in a decreased surface tension force for gas bubbles and thus enhanced

detachment of fine bubbles from the membrane surface (Kukizaki & Wada, 2008). For

example, a mean bubble diameter of 360–720 nm was produced from hydrophilic shirasu-

porous-glass (SPG) membranes with mean pore diameters of 43–85 nm.(Kukizaki & Goto, 2006)   A "gas film" is believed to form on the hydrophobic membrane surface, where the gas/liquid contact area is much larger than the pore size, preventing further reduction in bubble size (Yang et al., 2016). Therefore, the hydrophilic surface of CM or JM enhances the dissolution of gas into the surrounding liquid, ensuring a continuous supply of gas to sustain bubble formation (Yang et al., 2016). Unlike CM, the hydrophobicity of the inside pores of JM may prevent water from entering or permeating through the membrane pores, which thus facilitates the formation of a stable air layer and the nucleation and growth of NBs.

Additionally, the data comparison for the two CM membranes with pore diameters of 140 nm and 1400 nm indicate the small membrane pore increased the bubble concentration to 5.6×10^8 bubble·mL^{-1} quite significantly, as compared to 2×10^8 bubble·mL^{-1} obtained by the large pore membrane. This means that the high gas permeability on large-pore membrane is critical for achieving high bubble fluxes in the membrane bubbling process. However, the average bubble diameter on the large pore membrane decreased slightly to 62 nm compared to the average diameter of 67 nm on the small pore membrane.
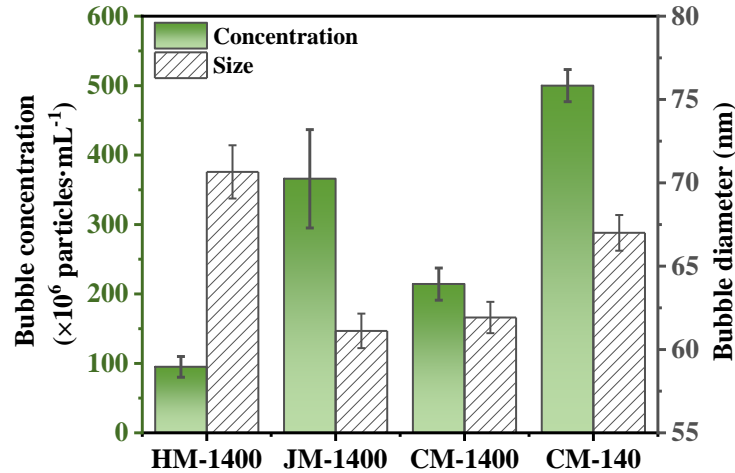
Figure 2.5 The bubble concentrations and diameters of NBs produced by different membranes in the single-pass mode with the gas flow rate of 0.5 L·min⁻¹ (114 kPa) and the water flow rate of 0.05 L·min⁻¹.

2.3.3 Effect of the water circulation time on the production of NBs

Most commercial generators of NBs require the produced water to circulate and increase the bubble concentration in the produced water. **Figure 2.6(a)** indicates that the bubble concentration increased slightly from 5.7×10^7 particles·mL⁻¹ to 7×10^7 particles·mL⁻¹ after the 90-min circulation. The hydraulic retention time under the water flow rate of 1 L·min⁻¹ is approximately 1.2 s, which means the 90 min circulation resulted in 4500 times of the water/membrane contact or the single pass. **Figure 2.6(b)** demonstrates that DO levels increased with circulation time with a peak level at approximately 31 mg·L⁻¹ after 12 min. The $K_L \cdot a$ value for NB was 21.05 h⁻¹, which is 5-8 times greater that of the oxygen macrobubbles we reported previously (Xue, Zhang, et al., 2022). The enhanced mass transfer coefficient for the present water suspension of O_2 NBs primarily results from their

higher specific surface area and internal pressure (Xue, Zhang, et al., 2022). Our previous

study employed a model to predict the change of DO during the aeration using O_2 NBs,

which assumes spherical bubbles were well dispersed in a closed water tank without any

DO loss due to evaporation or bubble exit from liquid to air (Xue, Zhang, et al., 2022). The

equilibrium levels of DO for 100-nm and 400-nm NBs are 650 and 100 mg·L^{-1}, respectively,

due to the differences in the internal pressures that are assumed to dictate the mass transfer

equilibrium. In most studies, NBs are stored and dispersed in water that is open to the air,

which probably results in rapid depressurization and release of DO. Thus, it is uncommon

to observe high DO levels (e.g., above 50 mg·L^{-1}) and instead, the reported DO

concentrations of O_2 NBs in water usually ranged from 25–42 mg·L^{-1} (Tekile, Kim, & Lee,

2016).
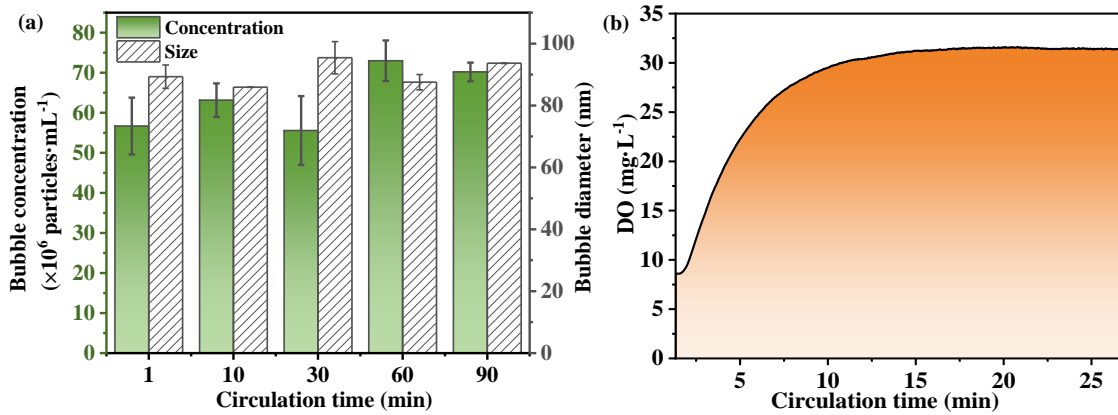
Figure 2.6 (a) The changes of the bubble concentration and diameter produced by the HM over recirculation time under the water flow rate of 1 L·min^{-1} and the gas flow rate of 0.5 L·min^{-1}. (b) The DO level changes over the recirculation time.

2.3.4 Effect of water flow rate on the production of NBs and oxygen transfer

Besides the recirculation time, the water flow over the membrane surface also affects the bubble formation as the detachment of bubbles formed on the membrane surface may influenced by the shear stress imposed by the water flow (Schröder & Schubert, 1999). As the water flow rate increases, the shear force imposed on the evolving bubbles on the membrane surface will increase and affect the bubble detachment (rate) and perhaps the bubble sizes. According to section **Equation (2.3)**, the shear stress could increase up to 1.2 Pa as the water flow rate increased to 3 $L\cdot min^{-1}$ with the corresponding increase of the cross-flow velocity as shown in **Figure 2.7(a)**. Accordingly, the concentration of NBs in the produced water gradually decreased (**Figure 2.7(b)**), with the highest bubble concentration of 1.95×10^8 $bubble\cdot mL^{-1}$ when the cross-flow velocity was 0.006 $m\cdot s^{-1}$. Clearly, reducing the water flow rate permits a longer contact time between the gas and water on the membrane surface and promotes the bubble dispensing into the flowing water. However, the bubble size within the experimental range of flow rate remained almost constant near 100 nm in diameter. It is reported that the diameter of NBs decreased from 500 nm to 400 nm as the liquid crossflow velocity increased from 0.5 $m\cdot s^{-1}$ to 3.7 $m\cdot s^{-1}$ over the Shirasu-porous-glass (SPG) membrane with a pore size of 55 nm until the bubble diameter became stable at around 400 nm and independent of the flow velocity (Kukizaki & Goto, 2006). Thus, increasing the flowing water rate primarily affects the bubble concentration but not the bubble size, which also indicates that the bubble detachment rate

is more controlled by the gas flow and membrane pores instead of the flowing water.

Furthermore, the DO concentration in the produced bubble suspension was monitored to examine the flow rate effect on oxygen delivery or transfer efficiency. **Figure 2.7(c)** shows that DO progressively declined as the flow velocity increased. To assess the effectiveness of aeration, OTE was calculated and shown to increase the water flow velocity from 0.15% to 5.8%. Typical aeration systems achieve OTE of approximately 20-30% using air microbubbles (Atkinson, Apul, Schneider, Garcia-Segura, & Westerhoff, 2019). OTEs of 80-90% or even higher were reported for aeration systems using air NBs. Once the oxygen is replaced with air, the OTEs of our NB generator are expected to rise to 80%-300% according to according to the **Equation (2.1)**. Reducing bubble size to the nanometer scale, compared to microbubbles, significantly enhances the efficiency of oxygen mass transfer (Terasaka et al., 2011). The small size and higher surface tension of NBs result in an increased interfacial gas-liquid surface area, thereby promoting mass transfer (Atkinson et al., 2019).
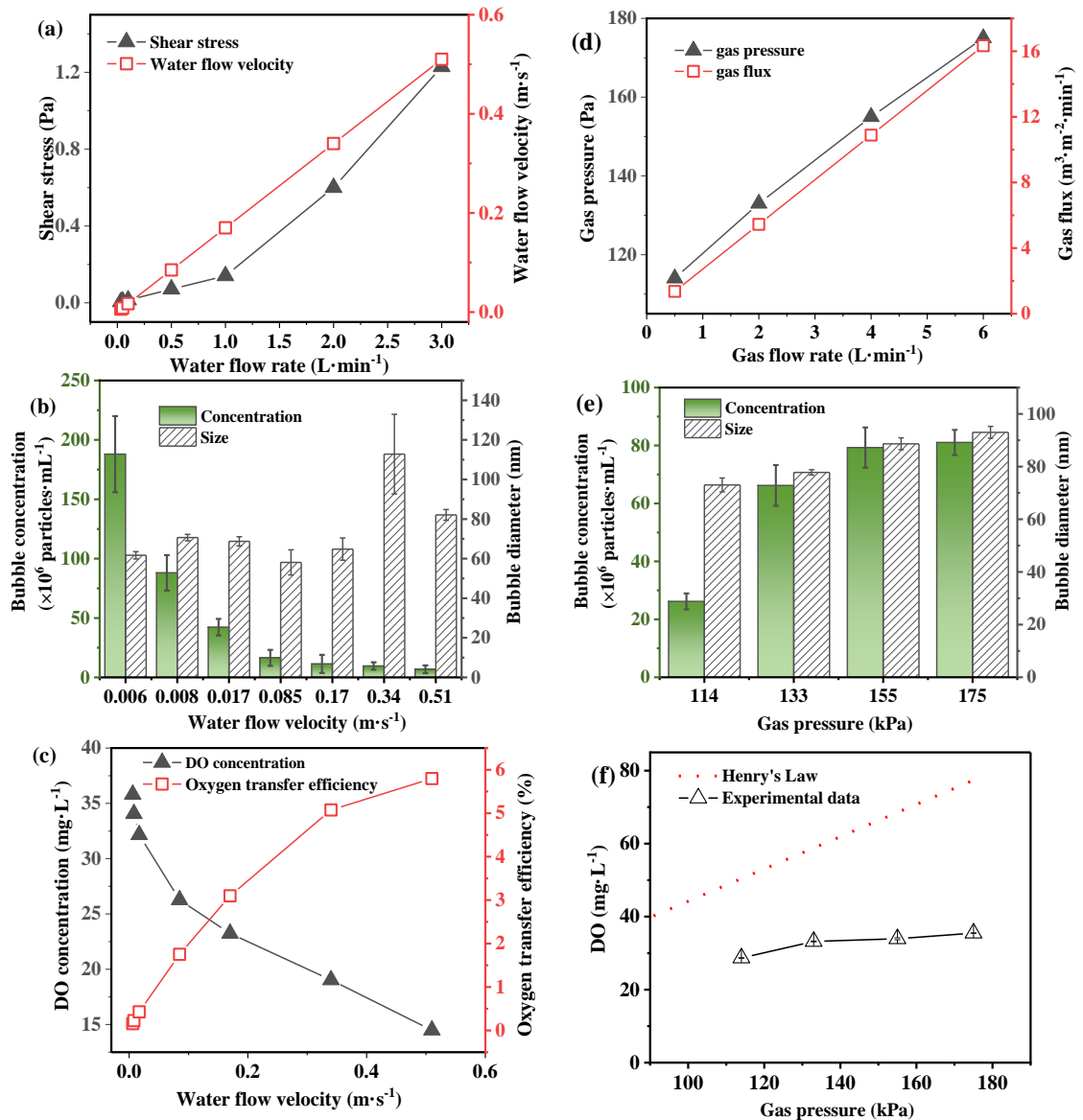
Figure 2.7 (a) The shear stress and cross-flow velocity at the membrane surface under different flow rates, (b) The produced bubble concentration and diameter under different water flow rates, (c) The DO and OTE changes under different water flow rates and a constant gas flow rate of 0.5 L·min^{-1}, (d) The injection gas pressures and gas fluxes at different gas flow rates, (e) The produced bubble concentration and diameter under different gas pressure, and (f) The DO levels in the produced bubble water under different injection gas pressures and a constant water flow rate of 1 L·min^{-1}.

2.3.5 Effect of the injection gas flow rate

Similar to the water flow rate, the gas flow or gas pressure may also affect the bubble formation processes. **Figure 2.7(d)** shows the linear relationships of the gas pressures, gas flow rate and gas flux under the temperature ($20^{\circ}C$) and a constant water flow rate of 1 $L \cdot min^{-1}$ (the corresponding hydraulic retention time of 1.2 s). **Figure 2.7(e)** indicates that the bubble concentration increased appreciably with the increase of the injection gas pressure, whereas the bubble size was not sensitive to the gas pressure changes. However, higher gas pressures or gas flow rates are shown to yield smaller NBs due to the increased diffusion rates of the gas through the membrane and reduced bubble coalescence (Kukizaki & Goto, 2006). According to the RSM analysis (**Figure 2.8**) and our experimental data (**Figure 2.7(e)**), the highest bubble concentration was achieved at a low water flow rate of 0.03 $L \cdot min^{-1}$ and a high gas flow rate of 6 $L \cdot min^{-1}$. **Figure 2.7(f)** indicates the resulting DO in the produced water increased with the increasing injection gas pressure. However, the measured DO levels were lower than the predicted DO levels according to the Henry's law, probably due to the reported depressurization of O_2 NBs in water (X. Shi et al., 2021). Moreover, the NBs released oxygen into the water, leading to a temporary surge in DO levels. However, this influx of oxygen was not sustained due to a rapid loss of dissolved oxygen from the process of air/water transfer.
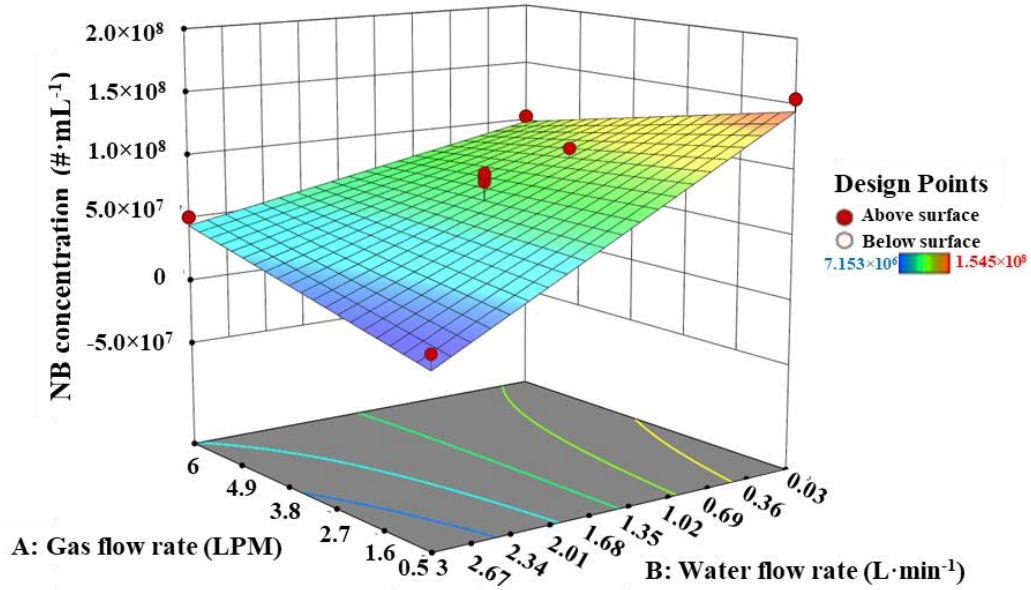
Figure 2.8 The concentration of NB as a function of water flow rate and gas flow rate.

2.3.6 Analysis of the bubble detachment mechanisms and factors

To determine the relative contributions of air pressure and cross-flow velocity to the bubble detachment from the hydrophilic membrane surface and hydrophobic membrane pore of JM, we conducted an interfacial force balance analysis as shown in **Figure 2.9(c)**. The force pushing the bubble to rise upward and detach from the membrane pore is the internal gas pressure force (F_p), whereas the force that drags and prevents the bubble from detachment is the surface tension force (F_s) in the vertical direction. These two forces are expressed in **Equations (2.7) and (2.8)**:

$$F_p = \pi \left(\frac{D}{2} \right)^2 P_{inj} = \pi \left(\frac{2r\sin\theta}{2} \right)^2 P_{inj} = \pi r^2 P_{inj} (\sin\theta)^2 \tag{2.7}$$

$$F_s = F_{lg} \sin\theta = \left(\gamma_{lg} \pi D \right) \sin\theta = \gamma_{lg} \pi \left(2r\sin\theta \right) \sin\theta = 2\gamma_{lg} \pi r (\sin\theta)^2 \tag{2.8}$$

$$D = 2r\sin(\pi - \theta) = 2r\sin\theta \qquad (2.9)$$

where P_{inj} is the injected gas pressure (Pa), D is the membrane pore diameter (nm), which is related to the radius of the bubble (nm), r, in **Equation (2.3)**, and the contact angle (θ) as shown in **Figure 2.9(c)**, F_{lg} is the liquid–gas surface tension force (N), γ_{lg} is the liquid–gas surface tension (72 mN·m^{-1}) and the perimeter of the pore (πD), Thus, if this ratio of F_p/F_s in **Equation (2.10)** is greater than 1, then the bubble will be able to detach, which means the product of rP_{inj} must be greater than $2\gamma_{lg}$ and the membrane surface hydrophobicity (e.g., θ) doesn't affect the detachment. For our experimental conditions (e.g., r=70 nm and P_{inj}=2×10^6 pa), the product of rP_{inj} is greater than $2\gamma_{lg}$ (144 mN·m^{-1}).

$$\frac{F_p}{F_s} = \frac{rP_{inj}}{2\gamma_{lg}} \qquad (2.10)$$

Thus, the bubble detachment process for the Janus membrane follows the same Equation (10), meaning that in the vertical direction, the bubble detachment is independent on the membrane hydrophobicity and is only governed by the ratio of the injection gas pressure and the liquid–gas surface tension.

For a hydrophobic surface, the force balance is slightly different as illustrated in **Figure 2.9(b)**, where the gas bubble may spread out as a thin gas layer and become large sized bubbles when detached. This agrees with the observation in **Figure 2.5**. For a hydrophilic membrane surface and pore surface, the water will enter the inside of the membrane pore, the bubble may produce as shown in **Figure 2.9a**.

Though the experimental results in **Figure 2.7(b)** show that the flow rate significantly affected the bubble production rate, the bubble formation and detachment may also be affected by interfacial forces in the horizontal direction, especially for large sized bubbles under a high crossflow velocity that may exert a high stress against the membrane surface or the emerging bubbles as shown in **Figure 2.9(d)**. For example, the water shear force (F_w), calculated in **Equation (2.11)**, may influence the bubble detachment more significantly on a hydrophilic surface than on a hydrophobic surface. For example, the shear force should lead to bubble deformation and drag the bubble to detach from the membrane pore. The resisting force to prevent the bubble's detachment is the surface tension force that is exerted along the contact line of the bubble with the pore edge. For a bubble under a non-steady state, the net surface tension force ($F_{S'}$) is contributed by the component of the liquid–gas surface tension force (F_{lg}) in the horizon direction, the solid–gas surface tension force (F_{sg}) and the solid–liquid surface tension force (F_{sl}). According to Young's equation, $F_{S'}$ can be written by **Equation (2.12)**, where the value of (γ_{sl}- γ_{sg}) should be positive but ignored to simplify the analysis. Similarly, to determine the significance of the horizontal shear impact on bubble detachment, the ratio of $F_w/F_{s'}$ is derived in **Equation (2.13)**, which indicates that the ratio increases with the shear stress and the bubble size, implying that large bubbles may experience strong influences from a horizontal shear flow and tend to deform or detach.

$$F_w = \sigma \pi r^2 \qquad (2.11)$$

$$F_{s'} = \left[\gamma_{sl} + \gamma_{lg} \cos\left(\pi - \theta\right) - \gamma_{sg} \right] \pi D \approx -2\pi r \gamma_{lg} \sin\theta \cos\theta \qquad (2.12)$$

$$\frac{F_w}{F_{s'}} = \frac{\sigma \pi r^2}{-2\pi r \gamma_{lg} \sin\theta \cos\theta} = \frac{\sigma r}{-2\gamma_{lg} \sin\theta \cos\theta} \qquad (2.13)$$
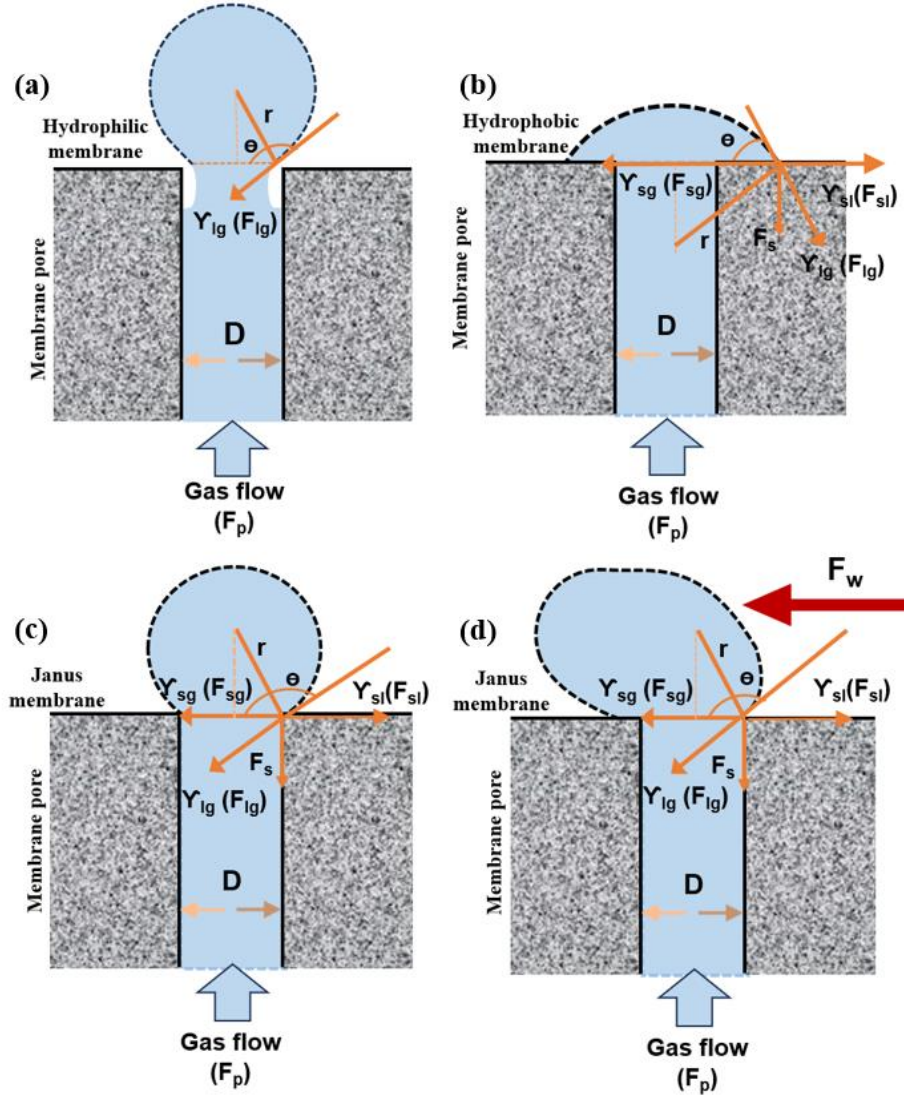
Figure 2.9 The potential bubble formation and interfacial forces (a) on a hydrophilic surface of CM, (b) on a hydrophobic surface of HM, (c) on a hydrophilic surface of JM and (d) on the same hydrophilic surface of JM under a horizontal water flow.

In our experiments, the highest water flow velocity of 0.51 m·s^{-1} or the flow rate of 3 L·min^{-1} resulted in a shear stress of 1.2 Pa according to **Equation (2.3)**. It is worth noting that the results of F_w/F_s, in **Figure 10(a)** and **10(b)** are overestimated as we ignored the term (γ_{sl}- γ_{sg}). Despite of this overestimation, it is clear that only after the water flow rate over the membrane surface is large enough (e.g., greater than 4-6×10^5 L·min^{-1} for bubbles with radius of 500-1000 nm respectively), the ratio could be greater than 1, where the horizontal flow will start to affect the detachment of NBs from membrane pores, which is a major difference from the bulk large sized bubbles produced from a porous surface. **Figure 10(c)** suggests that for the observed bubble sizes (< 6 cm in radius), this ratio will always be far less than 1 when the water flow rate is less than 3 L·min^{-1} and thus, the horizontal water flow is not likely to affect the NB detachment as it is less significant than the interfacial surface tension. Moreover, as the membrane surface becomes more hydrophilic, the contact angle (θ) would increase, which further reduces this ratio as indicated by **Figure 10(d)** and thus reduces the influence of the water flow rate on bubble detachment.
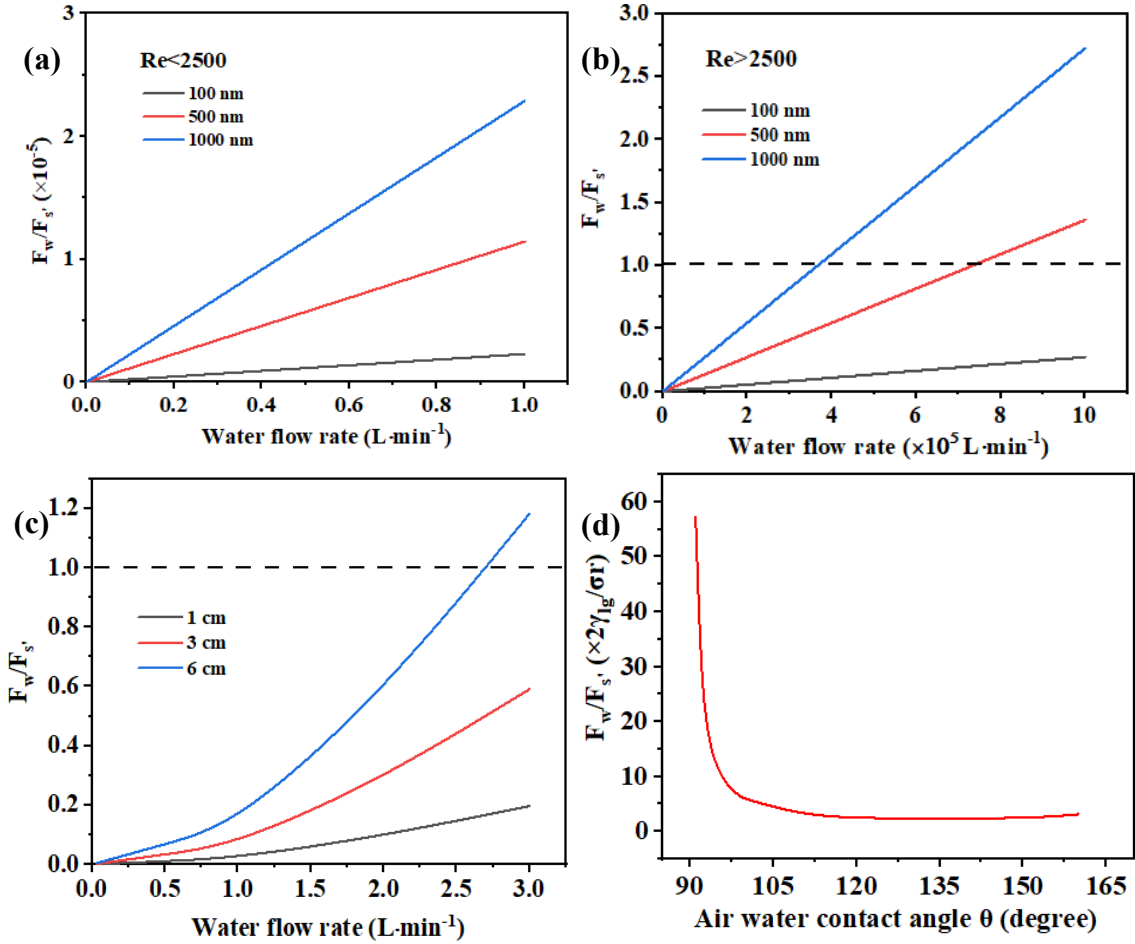
Figure 2.10 The value of $F_w/F_{s'}$ of bubble with radius of 100 nm, 500 nm and 1000 nm when the (a) Re< 2500 and (b) Re> 2500 at air water contact angle θ of 120°, (c) the value of $F_w/F_{s'}$ of bubble with radius of 1 cm, 5 cm and 6 cm at θ of 120° and (d) the value of

$F_w/F_{s'} \times \dfrac{2\gamma_{lg}}{\sigma r}$ at θ.

2.4 Conclusion

This study holistically examined the influences of the injection gas flow, the overlying water flow, and the interfacial surface tension on the produced NBs in water. The results indicate that the combination of a high injection gas flux (> 1.36 m³·min⁻¹·m⁻²) and a low water cross flow velocity (< 0.17 m·s⁻¹) resulted in a high NB concentration (> 1.6×10⁷

bubble·mL^{-1}). Moreover, using ceramic membranes with a hydrophilic surface and hydrophobic pores, the NB concentration reached the highest level (3.6 ×10^8 bubble·mL^{-1}), compared to other membrane coating conditions (e.g., hydrophobic surface coating). To assess the mass transfer performance, we measured the dissolved oxygen (DO) concentration in the produced water suspension of oxygen NBs, which revealed enhanced oxygen transfer efficiency (OTE) and a mass transfer coefficient of up to 300 % and 21.05 h^{-1}, respectively. These investigations uncovered valuable insights into the formation mechanisms and characteristics of NBs in water and laid foundation for novel engineering applications.

CHAPTER 3

AERATION AND DISSOLUTION BEHAVIOR OF OXYGEN NANOBUBBLES IN WATER

Work of this chapter is related to the publication:

Xue, Shan, Yihan Zhang, Taha Marhaba, and Wen Zhang. "Aeration and dissolution behavior of oxygen nanobubbles in water." *Journal of Colloid and Interface Science*, 609 (2022): 584-591.

3.1 Introduction

Nanobubbles (NBs) are nanoscale air pockets residing in liquid, which elicit intriguing physical and thermodynamic properties during formation and dissolution (Alheshibri et al., 2016; N. Nirmalkar, A. Pacek, & M. Barigou, 2018). For instance, NBs may possess a long retention time in liquid with a scale of hours (Atkinson et al., 2019), days (Rak, Ovadová, & Sedlák, 2019) and even weeks (L. Hu & Xia, 2018) or months (X. Shi et al., 2021). However, bubbles with a small size have a large internal pressure (e.g., Laplace pressure of NBs with radius of 100 nm is about 14 atm) according to the Young−Laplace equation, which presumably leads to a short lifetime of microseconds to nanoseconds (N. Bunkin et al., 2012; X. Shi et al., 2021). Therefore, the observed high colloidal stability of bulk or surface NBs in many prior studies may be attributed to the unknown mechanisms such as selective adsorption of ions on their interface resulting in high surface zeta potentials, the rise of surface tension and inter-bubble repulsion (N. F. Bunkin et al., 2021; Craig, Ninham, & Pashley, 1993). Moreover, a hydrogen bonding network in ice and gas hydrates was reported to form at the gas-water interface, which provides additional cohesion to prevent

bubble from instant burst or dissolution (Michailidi et al., 2020). The local oversaturation of the gas molecules surrounding NBs (Favvas et al., 2021; X. Zhang, Chan, Wang, & Maeda, 2013) and other unknown features of bulk NBs may also increase the residence time and yield controllable gas supply or delivery as demonstrated in sediment or soil aeration to remediate hypoxia issues (W. Shi et al., 2018; Honggang Zhang et al., 2018).

Most previous studies focused on the aqueous stability of surface NBs (e.g., collapse or coalescence) (Boshenyatov, Kosharidze, & Levin, 2019; Chan, Arora, & Ohl, 2015; Choi, Li, & Peterson, 2021). By contrast, the dissolution behavior and mechanisms of bulk NBs in liquid remain elusive because of the limited detection tools and relevant theories for bubble properties at nanoscale (Michelin, Guérin, & Lauga, 2018; Peñas-López et al., 2017; Solano-Altamirano, Malcolm, & Goldman, 2015). For example, the numerical simulations revealed that air NBs with the initial radius of 100 nm would shrink within 75.36 μs during dissolution (Yasui et al., 2016). However, (German, Chen, Edwards, & White, 2016) measured the lifetimes of hydrogen (H_2) and nitrogen (N_2) NBs using fast-scan electrochemical technique indicated that the dissolution rates of NBs are 1000 times slower than predictions of diffusion/kinetic theories due to the limitation of mass transfer on the gas/water interface. (Tanaka, Kastens, Fujioka, Schlüter, & Terasaka, 2020) observed a single air microbubble using high-speed imaging techniques and found that microbubbles larger than about 30 μm in diameter shrunk at a constant rate and the rate of shrinkage increased gradually when microbubbles became smaller than 30 μm in diameter.

Despite of the observed controversy, it is common to describe the growth and dissolution process of a single spherical gas bubble in liquid using the classical Epstein-Plesset (EP) model. This theory predicts the bubble will shrink or grow unboundedly during the diffusion depending on whether the liquid is undersaturated or oversaturated (Duncan & Needham, 2004; Tan, An, & Ohl, 2020). Moreover, this theory assumes a stationary bubble with the concentration of the dissolved gas at the gas–liquid interface following the Henry's law. (Kapodistrias & Dahl, 2012) used acoustic scattering to measure the microbubble size change during the dissolution process, which took over 1 h for a 140-µm bubble to dissolve completely while an 885 µm bubble required over 20 h. This dissolution result agreed with the EP theory model prediction. As opposed to microbubbles, the dissolution behavior of NBs has not been extensively studied or predicted by the EP theory. Only one study so far predicted that NBs with radius of 100 nm may completely dissolve within about 80 µs (Yasui, 2018; Yasui et al., 2018). Clearly, more research is still needed to verify this modeling approach for the dissolution behavior of NBs.

Furthermore, understanding the gas bubble aeration is also critical to guide many engineering applications such as wastewater treatment (Temesgen et al., 2017), ozonation for disinfection (Saijai, Thonglek, & Yoshikawa, 2019), hydroponics (Abu-Shahba, Mansour, Mohamed, & Sofy, 2021), cultured fishery (Budhijanto, Darlianto, Pradana, & Hartono, 2017) and rapid oxygen (O_2) delivery in therapeutics (L. Song et al., 2020). For example, small-sized gas bubbles yield larger Laplace pressures and longer residence time

in water (Ranaweera & Luo, 2020), which could dramatically increase the O_2 transfer rate in aeration compared to microbubbles and macrobubbles (e.g., 500 μm in diameter or greater). The microbubble aeration is reported to achieve 25-44 times enhanced O_2 utilization rate compared to macrobubble aeration (B. Thomas et al., 2021).

The present study leveraged our previous research on the aqueous bulk NBs that are generated by a pressurized membrane bubbling process (Ahmed, Sun, et al., 2018; Khaled Abdella Ahmed et al., 2018; X. Shi et al., 2021), and further examined the bubble aeration and dissolution behavior using both modeling and experimental approaches. First, we experimentally assessed the volumetric mass transfer coefficient ($K_L \cdot a$) of O_2 NBs with different sizes. The mass transfer coefficient (K_L) of O_2 NBs was estimated by correlation analysis to compare with the experimental results. The dissolved oxygen (DO) level during the aeration with O_2 NBs was simulated to analyze the dependence on various factors such as mass transfer coefficient and bubble size. Then, we further employed the modified EP model to predict the dissolution behavior of O_2 NBs such as the changes of DO level and bubble sizes. Finally, the modeling result of dissolution process of NB was verified experimentally.

3.2 Materials and Methods

3.2.1 Generation and characterization of bulk O_2 NBs in water

Bulk O_2 NBs with a diameter of 200 nm-700 nm were generated in deionized (DI) water by direct injection of compressed O_2 (purity of 99.999%, Airgas, Inc.) through a membrane as reported previously. The DI water we used is produced from a Milli-Q water machine (Direct – Q 3UV, Millipore) that produces ultrapure water with resistivity of 18.2 MΩ•cm at 25 °C and a surface tension of 72.2 dynes·cm^{-1}. Briefly, the pure O_2 gas was supplied from a cylinder with the outlet pressure of 30-60 psi as controlled by a gas pressure regulator. A ceramic tubular membrane (model WFA 0.1-Refractron, USA) with a mean pore size of 100 nm, the inner and outer diameters of 8 and 13 mm, and a length of 51 mm was connected to the gas cylinder by air-tight polyvinyl chloride (PVC) tubes. The tubular membrane surface was hydrophobized by coating with a steric acid monolayer (Ahmed, Sun, et al., 2018; Khaled Abdella Ahmed et al., 2018). The compressed O_2 gas was injected into 500-ml water through the membrane at a flow rate (0.45 L·min^{-1}) for 90 min to reach a stable bubble number and a saturated DO in water. The stability and colloidal properties (e.g., zeta potentials and hydrodynamic diameters) of the produced NBs in DI water were also analyzed previously (Ahmed, Sun, et al., 2018; Khaled Abdella Ahmed et al., 2018; X. Shi et al., 2021). The aqueous suspension of O_2 NBs was used for the following experiments. The size of NBs was measured immediately after preparation on a Zetasizer

instrument (Nano ZS, Malvern Instruments, USA). Furthermore, Nanosight nanoparticle tracking analysis (NTA) instrument (NS300, NanoSight, USA) was used to measure the mean concentration of NBs with a laser light source of 532-nm. The standard deviations of the 5 different measurements for each sample were given as error bars on the NTA graphs. The size distributions and number densities or concentrations of O$_2$ NBs are shown in **Figure 3.1**.
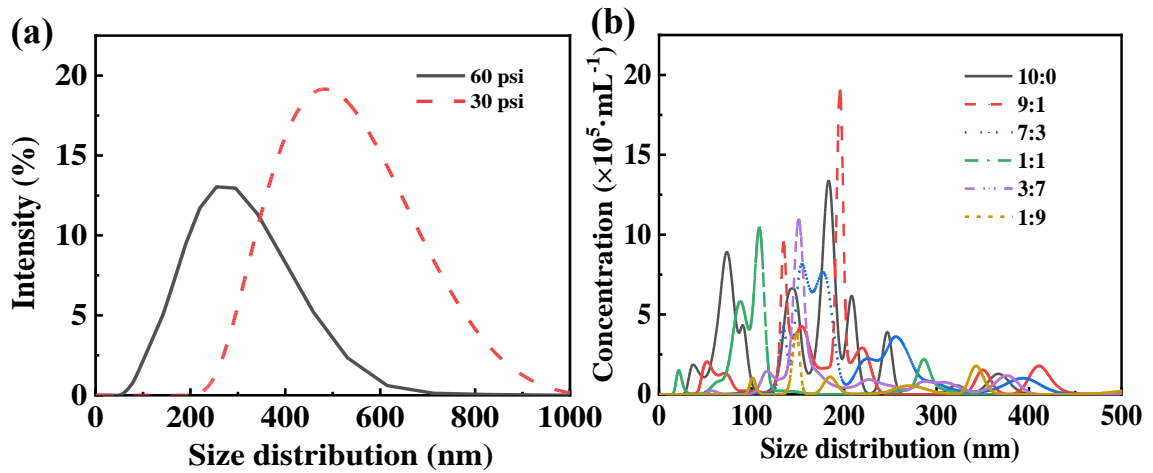
Figure 3.1 (a) O$_2$ NBs' size distribution produced under 30 psi and 60 psi and (b) O$_2$ NBs' size distribution produced under 60 psi at different dilution ratios.

3.2.2 Experimental assessment of the volumetric mass transfer coefficient (K$_L$·a) of O$_2$ NB

The bulk mass transfer efficiency in aeration is often described by **Equation (3.1)**:

$$V \frac{dC}{dt} = K \cdot A \cdot (\frac{P_a}{K_H} - C) \tag{3.1}$$

where V is the volume of the solution (m^3), C is the O$_2$ concentration in the water (mol·L^{-1}), t is the aeration time (h), K is the bulk transfer coefficient (m·h^{-1}), A is the air-

water surface area (m^2), P_a is the partial pressure of O_2 that governs the DO following the Henry's Law, K_H is the Henry's law constant (770 L·atm·mol^{-1}, in water at 298.15 K), and P_a/K_H is the saturation concentration of O_2 in water (C_s, mol·L^{-1}). The integration of **Equation (3.1)** with boundaries of $C=C_0$ and $C=C_t$ at $t=0$ and $t=t$ leads to:

$$In(\frac{C_s - C_t}{C_s - C_0}) = -(K_L \cdot a) \cdot t \tag{3.2}$$

where a (A/V) is the specific surface area of bubbles in liquid ($m^2 \cdot m^{-3}$), C_s is the saturation DO concentration (mol·L^{-1}), C_0 and C_t are the DO concentrations in the water at the aeration time start 0 and time t (mol·L^{-1}), and $K_L \cdot a$ is the volumetric mass transfer coefficient (h^{-1}). The bulk transfer coefficient (K_L) equals the inverse sum of resistances to transfer on the two sides of the air/water interface as shown in **Equation (3.3)** and is replaced by the bulk liquid film coefficient (K_L) because for the gases with low solubility in water, mass transfer of oxygen is water-side controlled or has a greater resistance on the water side than that on the air side ($K_L << K_H \cdot K_a$).

$$\frac{1}{K} = \frac{1}{K_L} + \frac{1}{K_H K_a} \tag{3.3}$$

where K_a is the bulk gas film coefficient (m·h^{-1}).

To determine K_L of O_2 NBs in water, the DO concentration was measured by purging O_2 gas into the deoxygenated water through the hydrophobized tubular membrane as mentioned above. As depicted in **Figure 3.2a**, the tubular membrane was placed in water to purge O_2 gas with an immediate measurement of DO. The produced bubble size was controlled by applying different injection pressures. According to our previous work, bulk

NBs of approximately 400-700 nm and 200-400 nm in diameter were generated at the injection gas pressure of 30 and 60 psi. The measured DO levels at different aeration time (t) were incorporated into **Equation (3.2)** to determine the value of $K_L \cdot a$.
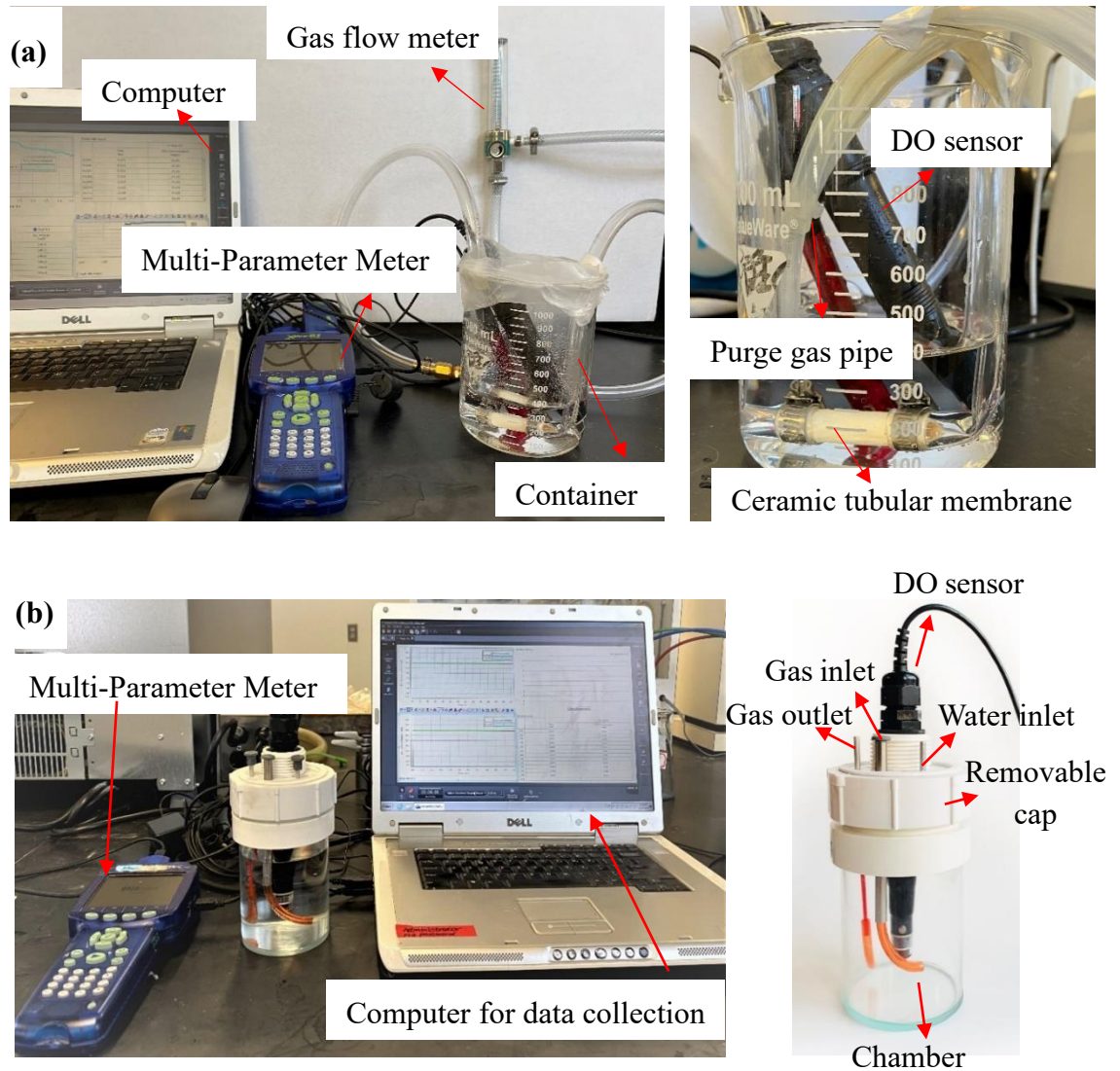
Figure 3.2 (a) The DO measurement system consists of data logging PC, DO sensor, gas flow regulator, ceramic tubular membrane for dispensing oxygen gas. (b) The air-tight setup for the measurement of the dissolved oxygen concentration in the NBs-containing water.

3.2.3 Correlation analysis of K_L for O_2 NBs

In a typical process of aeration, there are numerous dissolving gas bubbles, and consequently, the total surface area for the mass transfer of O_2 is incalculable. Thus, K_L was estimated by the correlation of mass transfer coefficients using Schmidt Number (Sc) and Sherwood Number (Sh) by **Equation (3.4)**.

$$K_L = Sh \cdot D' / (2 \cdot r) \tag{3.4}$$

where D' is the diffusion coefficient of dissolved gas in water (2×10^{-9} m$^2 \cdot$s^{-1}) and r is the radius of bubbles (nm).

For small bubbles (less than 0.6 mm diameter) under mild agitation, the following correlation in **Equation (3.5)** may be used to estimate the Sherwood Number (Sh):

$$Sh = 2 + 0.31 \left[\frac{(\rho - \rho_g) \cdot \rho \cdot g \cdot (2 \cdot r)^3}{\mu_L^2} \right]^{1/3} Sc^{1/3} \tag{3.5}$$

$$\rho_g = \frac{P_{int}}{RT} \tag{3.6}$$

where ρ_g is the gas density in NBs, T is the solution temperature (298 K), R is ideal gas constant (8134.50 L$\cdot$Pa$\cdot$mol$^{-1}\cdot$K^{-1}), P_{int} the internal pressure of NB (Pa), μ_L is dynamic viscosity of water (8.90×10^{-4} Pa$\cdot$s at 25 °C).

The outbound pressure (P_{out}) is ascribed to the surface charge repulsion and the internal gas pressure (P_{int}) as calculated by the Laplace-Young equation (Brennen, 2013; Israelachvili, 2011) :

$$P_{out} = \frac{\sigma^2}{2 \cdot D \cdot \varepsilon_0} + P_{int} \tag{3.7}$$

where D is the relative dielectric constant of the gas bubbles (1.004), ε_0 is the dielectric permittivity of a vacuum ($8.854\times10^{-12}\,C^2\cdot N^{-1}\cdot m^{-2}$), σ is the surface charge density ($C\cdot m^{-2}$) and is calculated by the Gouy–Chapman equation in **Equation (3.8)** modified for spherical particles by (Hunter, 1981) when the zeta potential is less than 80 mV (Antonietti & Vorwerg, 1997; Y.-R. Shi, Ye, Du, & Weng, 2018).

$$\sigma = \varepsilon_0 \cdot D \frac{k_B \cdot T}{z_1 \cdot e \cdot \lambda_D} \cdot \left[2\sinh\left(\frac{z_1 \cdot e \cdot \psi}{2k_B \cdot T}\right) + \frac{2\lambda_D}{r} \tanh\left(\frac{z_1 \cdot e \cdot \psi}{4k_B \cdot T}\right) \right] \tag{3.8}$$

The zeta potential (ξ) can be calculated from the surface potential (Ψ) using **Equation (3.9)**, which is derived from the Gouy-Chapman theory for flat plates:

$$\tanh(\frac{z_1 \cdot e \cdot \xi}{k_B \cdot T}) = \tanh(\frac{z_1 \cdot e \cdot \xi}{4k_B \cdot T})\exp(-\frac{x}{\lambda_D}) \tag{3.9}$$

where λ_D is the Debye length that is calculated by:

$$\lambda_D = (\frac{\varepsilon_0 \varepsilon k_B T}{N_A e^2 \sum_i c_i z_i^2})^{0.5} \tag{3.10}$$

where ε is the dielectric constant of water, z_1 is the distance from the particle's surface to the slipping plane, r is the bubble radius (m), k_B is Boltzmann constant ($1.38\times10^{-23}\,J\cdot K^{-1}$), x is distance at the plane of shear from the particle surface (3.00×10^{-10} m), z_i is the valence of the i ion (for NaCl or H^+), c_i is concentration of the I ion ($mol\cdot m^{-3}$), N_A is Avogadro's number ($6.02\times10^{23}\,mol^{-1}$), and e is unit charge ($1.602\times10^{-19}\,C$).

The inbound pressure (P_{in}, Pa) is contributed by the surface tension pressure of NBs (P_r, Pa) exerted from the surrounding water molecules, the atmospheric pressure (P_0,

Pa), and the water head pressure (*Ph*, *Pa*):

$$P_{in} = P_r + P_0 + P_h \tag{3.11}$$

$$P_r = \frac{2 \cdot \gamma}{r} \tag{3.12}$$

$$P_h = \rho \cdot g \cdot h \tag{3.13}$$

where γ is the water surface tension (0.07 N·m^{-1}), g is the gravity acceleration (9.81

N·kg^{-1}), ρ is the density of water (998.19 kg·m^{-3}), and h is the height of water (0.1 m).

If $P_{in} = P_{out}$, P_{int} of NBs can be estimated by:

$$P_{int} = \frac{2\gamma}{r} + P_0 + \rho g h - \frac{\sigma^2}{2 \cdot D \cdot \varepsilon_0} \tag{3.14}$$

For bubbles of 2.5 mm in diameter, the following correlation may be used:

$$Sh = 0.42 \left[\frac{(\rho - \rho_g) \cdot \rho \cdot g \cdot (2 \cdot r)^3}{\mu_L^2} \right]^{1/3} Sc^{1/2} \tag{3.15}$$

where Sherwood Number (*Sh*) is calculated by:

$$Sc = \frac{\mu_L}{\rho \cdot D} \tag{3.16}$$

3.2.4 Modeling analysis of the DO change during the aeration using O$_2$ NBs

To predict the DO concentration using **Equation (3.2)**, we need to make three basic

assumptions: (1) the aerated solution is closed to the ambient air such that no O$_2$ transfer

occurs from the solution to the air; and (2) the saturation level of DO in water (C_s) follows

the Henry's law in **Equation (3.17)** with the internal gas pressure of O$_2$ NBs (P_{int}) to drive

the dissolution equilibrium

$$C_s = \frac{P_{int}}{K_H}$$
(3.17)

Thirdly, all NBs are treated as spheres with a same radius (r), which permits the calculation of a by **Equation (3.18)**:

$$a = \frac{N}{V} \cdot 4\pi \cdot r^2 = \frac{1}{V} \cdot \frac{3}{r} \cdot \frac{Q \cdot t \cdot P_{inj}}{P_{int}}$$
(3.18)

where a is time dependent because both the bubble number (N) in the solution and r can change with aeration time. The aeration process in our experiments was obtained by purging a pressurized O_2 gas into water at a flowrate of Q ($m^3 \cdot s^{-1}$) under the specific injection pressure (P_{inj}). The conversion of **Equation (3.18)** was conducted with the ideal gas law that replaced N with the flowrate and the aeration time. Integration of **Equation (3.17)** and **Equation (3.18)** into **Equation (3.2)** allowed us to numerically predict the DO level during the initial stage of aeration without consideration of the loss of the purged bubbles due to the transfer from the liquid to the air phase as mentioned above. The model prediction was used to analyze influences of the bulk liquid film coefficient (K_L), available specific surface area (a), the bubble size (r) as well as internal bubble pressure (P_{int}) on saturation concentration of oxygen in water (C_s).

3.2.5 Modeling analysis of DO and bubble radius changes during O_2 NBs dissolution in water

This study modified the widely reported Epstein-Plesset (EP) theory in **Equation (3.19)** that incorporates the internal pressure of NBs.

$$\frac{dr}{dt} = -\frac{D'\Delta c}{\rho_g}(\frac{1}{r} + \frac{1}{\sqrt{\pi D't}})$$

(3.19)

where $\Delta c=(c_b - c)$ is the difference between the DO concentration (c_b) near the interface of NBs and the one that is far from NBs in the bulk liquid (c) that increases with the dissolution time t (mol·L^{-1}). C_b is calculated by the Henry's law as shown in **Equation (3.17)**, in which the internal pressure of NBs (P_{int}) could be time-dependent during dissolution. This speculation is supported by **Equation (3.10)** from taking derivative of **Equation (3.14)** on both sides.

$$\frac{dP_{int}}{dt} = -\frac{2\gamma}{r^2}\frac{dr}{dt}$$

(3.20)

If we ignore the loss of oxygen, the increase of the dissolved gas concentration (c) will be proportional to the dissolution of the gas molecules from NBs, which yields the following equation.

$$\frac{dc}{dt} = \frac{N}{V}\frac{dn}{dt} = \frac{N}{V}\frac{d(P_{int}V')}{RTdt} = \frac{1}{RT}\frac{N}{V}(\frac{V'dP_{int}}{dt} + \frac{P_{int}dV'}{dt}) = \frac{1}{RT}\frac{N}{V}(-\frac{2\gamma V'}{r^2} + 4\pi r^2 P_{int})\frac{dr}{dt}$$

(3.21)

where n is the moles of gas molecules within one single NB that dissolve within time t. According to the ideal gas law, n can be expressed by P_{int}, the volume of single NBs (V'), and the ideal gas constant (R=8134.5 L·Pa·mol^{-1}·K^{-1}). Since we assume a spherical shape of NBs with a radius of r (thus, V'=4/3·π·r^3), **Equation (3.21)** is further simplified

by replacing dV'/dt. Similarly, the term of dP_{int}/dt can be replaced by **Equation (3.20)**.

Numerical solutions of **Eqs. (3.19)** and **(3.21)** were achieved using MATLAB, which

determined the DO concentration and the radius (r) of NBs at different dissolution time t

under specific parameters such as P_{int} and N or the initial bubble concentration. In this

model calculation, the initial bubble number density (N/V) was 10^{14} #·m^{-3} unless indicated

otherwise, and the dissolution process of bubbles with initial sizes of 100 and 400 nm were

predicted.

3.2.6 Experimental assessment of DO changes during O₂ NBs dissolution in water

The DO concentration change was measured during the dissolution process of O₂ NBs using

an air-tight container with the total volume of 660 mL as shown in **Figure 3.2b**, where a

real time monitor DO sensor (PS-2196, PASCO, USA) with Xplorer GLX datalogger (PS

2002, PASCO, USA) was inserted to measure the DO change with a reporting range of 0–

40 mg·L^{-1} and an accuracy level of ±0.6 mg·L^{-1}. DO levels were assessed with and without

sealing the container (or open to ambient air) for comparisons. Removal of DO from water

was obtained by rigorously purging the DI water with N₂ gas (purity of 99.999%, Airgas,

Inc). Then, the NBs water suspension was spiked with the deoxygenated water at different

dilution ratios (from 0:10 to 10:0 v/v) to reach a total volume of water at 400 ml. The

concentration was measured by NTA immediately after diluting the water suspension of O₂

NBs. Additionally, another control aeration was conducted by producing O₂ macrobubbles

(35-85 mm in diameter) in water through the injection of O_2 gas into a PVC pipe (ID: 10 mm) at a pressure of 50 kPa (Xs. Shen, & Li, 2008). Each experiment was repeated twice to obtain the mean and standard deviation of the DO concentration.

The pH of the purged DI water was found to increase slightly from 6.3±0.11 to 6.5±0.12, primarily because of the removal of the dissolved CO_2. The solution conductivity did not significantly change, indicative of no contamination by ionic species or others during nitrogen purging. Such a small pH change does not affect the stability of NBs according to the previous studies (Khaled Abdella Ahmed et al., 2018; Neelkanth Nirmalkar et al., 2018). There are other methods for the removal of O_2 from water such as the addition of reducing reagents (e.g., sodium dithionite) into the solution. However, chemical additions will change the ionic strength and induce unknown NBs-electrolyte interactions. Freeze-thaw cycling is common and effective for small volume liquid such as expensive solvents. Argon (Ar) or N_2 are both widely used to remove DO or keep low DO levels for bulk water. We chose N_2 to produce deoxygenated water as it has been repeatedly proven cost effective as compared to Ar.

3.3 Results and Discussions

3.3.1 Evaluation of $K_L \cdot a$ for aeration with O2 NBs of different sizes

To explore the distinguished features of aeration using O_2 NBs, we compared the DO levels

when delivering O_2 NBs of different sizes into water. **Figure 3.3a** shows the aeration

experimental data fitting which is used to determine the $K_L \cdot a$ for bubbles of different sizes.

The $K_L \cdot a$ values for bubbles with diameters of 200-400 nm and 400-700 nm reached 23.99

h^{-1} and 15.59 h^{-1}, which are almost 5-8 times that for the O_2 macrobubbles of 35-85 mm in

diameter. This result agrees with the size dependence of $K_L \cdot a$ for air microbubbles

(Suwartha, Syamzida, Priadi, Moersidik, & Ali, 2020). The increased $K_L \cdot a$ for small

bubbles mainly results from a higher specific surface area and a longer retention time in

water (or low rising velocity).

K_L for O_2 NBs was further estimated using **Equation (3.4)**. **Figure 3.3b** reveals

that K_L is also highly dependent on bubble size, where K_L for O_2 NBs of 100 nm in radius

is about 3 times that for those of 200 nm in radius. This size dependence becomes less

significant when the bubble radius exceeds 300-400 nm. The dotted line separates the

general understanding or definition of NBs and microbubbles according to their size and

colloidal behavior (rise vs random motion) (Khaled Abdella Ahmed et al., 2018).

According to the Laplace-Young equation, the bubble size affects the internal pressure of

NBs and thus the gas density (ρ_g), which also influences the mass transfer coefficient. The

NTA measurement indicates that the O_2 NB concentration ranged from 1×10^8 to 3×10^8

bubbles·mL^{-1} under room temperature. Thus, for a spherical shape for O_2 NBs with radii

of 200-700 nm, we can estimate that the liquid-side mass transfer coefficient K_L of O_2 NBs

in water is about 9.6×10^{-6}–5.3×10^{-4} m·s^{-1}, which is significantly lower than the prediction

in **Figure 3.3b** as the prediction does not consider the loss of O_2 in aeration. However, our

calculated results of K_L are in a similar order of magnitude with the previous studies, which

also reported the bubble size dependence of K_L for O_2 microbubbles or macrobubbles

(Sardeing, Painmanakul, & Hébrard, 2006; Z. Wang et al., 2020).
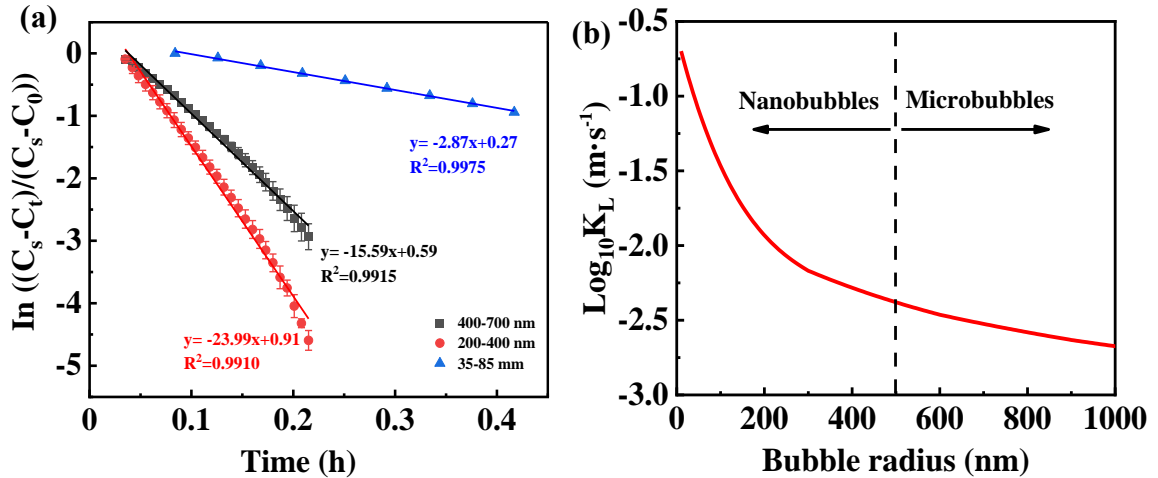
Figure 3.3 (a) The aeration experimental data fitting to determine the $K_L \cdot a$ for bubbles of different size. (b) The estimated K_L for O_2 NBs with different initial sizes in water.

3.3.2 Analysis of the change of DO during the aeration using O_2 NBs

Figure 3.4 shows that the comparison of the time-resolved concentrations of DO when

injecting O_2 NBs with radii of 100–1000 nm in water with an initial DO of 9 mg·L^{-1}. This

result is predicted with **Equations (3.2), (3.17)** and **(3.18)**, which assumes spherical

bubbles were well dispersed in a closed water tank without any DO loss due to evaporation

or bubble exit from liquid to air. Though this assumption does not match the realistic

situation, the model prediction is mainly intended to unravel the differences in aeration

when purging different sized NBs in the initial stage of aeration (within a few

microseconds), where the DO loss could largely be ignored. Moreover, K_L is treated as a constant in the model calculation, which has been shown above to depend on bubble sizes or internal bubble pressures. Clearly, smaller NBs exhibit higher surface areas for mass transfer than large ones, which affects the value of a in **Equation (3.18)**. Thus, the rate of DO increase for 100-nm NBs is almost 4 times that of 1000-nm NBs.

Furthermore, the equilibrium levels of DO for 100-nm and 400-nm NBs are 650 and 100 mg·L^{-1}, respectively, due to the differences in the internal pressures that are assumed to dictate the mass transfer equilibrium. In most studies, NBs are stored and dispersed in water that is open to the air, which probably results in rapid depressurization and release of DO. Thus, it is uncommon to observe high DO levels (e.g., above 50 mg·L^{-1}) and instead, the reported DO concentrations of O$_2$ NBs in water usually ranged from 25–42 mg·L^{-1} (Tekile et al., 2016).
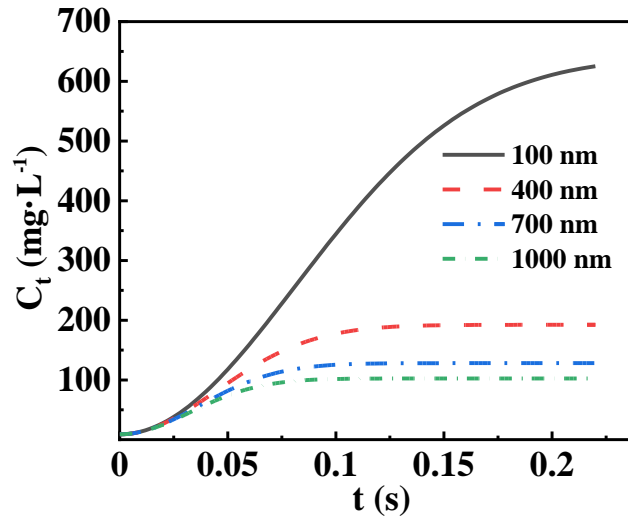
Figure 3.4 The prediction of DO concentration at time t in water when purging O_2 NBs with different sizes (100-1000 nm in radius) under K_L=0.0005 m·s^{-1} and P_{inj}= 414 kPa.

Figure 3.5(a) shows that for the same size of NBs (400 nm in radius), if K_L for O_2 NBs is increased, the rate of DO growth could also be appreciably enhanced. The level of K_L could increase with the increasing mixing intensity or the internal bubble pressures according to **Equations (3.4)-(3.16)**. For instance, **Figure 3.5(b)** confirms that increasing the inject pressure can promote the DO rise kinetics due to the enhanced driving force for mass transfer or diffusion.
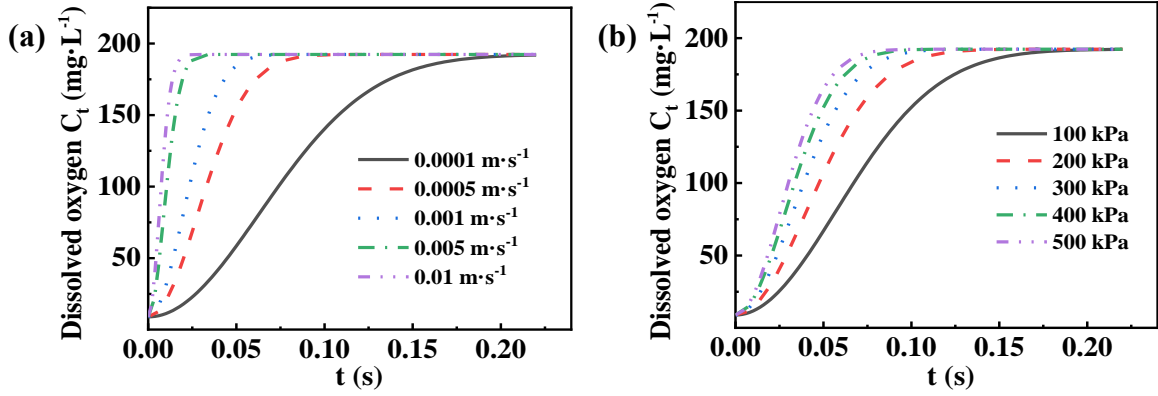
Figure 3.5 (a) when purging O_2 NBs (400 nm) with different K_L (0.0001-0.01 m·s^{-1}) under P_{inj}= 414 kPa and (b) when purging O_2 NBs (400 nm) with different inject pressures (100-500 kPa). Other important parameters used in the calculation include: the O_2 gas flow, Q=7.5×10^{-6} m^3·s^{-1}, the volume of NB water, V=4×10^{-4} m^3, DO concentrations in the water at time 0, C_0=9 mg·L^{-1}.

3.3.3 Model prediction of DO and bubble size changes during dissolution of O_2 NBs in water

The model calculation with **Equations (3.19)** and **(3.21)** reveals the DO and bubble size changes with time. In this simulation, we varied the initial number density (N/V) of NBs. **Figure 3.6(a)** indicates that the dissolution of O_2 NBs in water will progressively increase the DO level that gradually reaches a plateau. Moreover, the DO increase rate also depends on the initial radius of O_2 NB as well as many other factors such as solution surface tension and surface charge density of NB as discussed below. For instance, the dissolution rate of O_2 NBs with an initial radius of 100 nm is higher than NBs with an initial radius of 400 nm. In addition, the maximum DO level reached over 45 mg·L^{-1} for 400-nm O_2 NBs, which is greater than that obtained in the suspension of O_2 NBs with an initial radius of 100 nm. This difference results from the same initial number density (10^{14} #·m^{-3}) we used in the

model calculation. Clearly, large bubbles contain greater O_2 content than small bubbles and thus cause higher DO after complete dissolution.

Many previous studies experimentally revealed that the dissolution of NBs resulted in bubble size increase due to coalescence (German, Chen, et al., 2016; Koshoridze, 2020; Meegoda, Aluthgun Hewage, & Batagoda, 2018; Tanaka et al., 2020; Toru Tuziuti, Yasui, & Kanematsu, 2018; Yasui et al., 2016). **Figure 3.6(b)** shows that during the dissolution, NBs grew rapidly in size that eventually level off after approximately 1 hour. In the simulation, the bubble is assumed to be spherical in shape during the diffusion process. The bubble grew during dissolution because the bubble may swell or expand as its internal pressure decreases according to the Laplace-Young equation. Moreover, the coalescence of NBs was found to be a reshaping process into dumbbell-like and spherical morphology after rupture and fusion of their interface. O_2 NBs with an initial radius of 400 nm grew into a stable radius of 3.5 μm, which was much smaller than that (60 μm) reached by O_2 NBs with an initial radius of 100 nm. This remarkable difference could be ascribed to the coalescence rate, which might be much faster for small NBs as they may undergo more stochastic collisions with each other. Smaller NBs were reported to be prone to disappear around the surface of the growing larger bubbles (Shin et al., 2015), perhaps due to the Ostwald ripening phenomenon in which smaller particles dissolve in solution followed by depositing on larger particles, which minimizes the surface to area ratio to achieve a more thermodynamically stable state (Tcholakova et al., 2017). By contrast, large NBs (e.g., 400

nm in diameter) may be dominated by dissolution rather than coalescence.
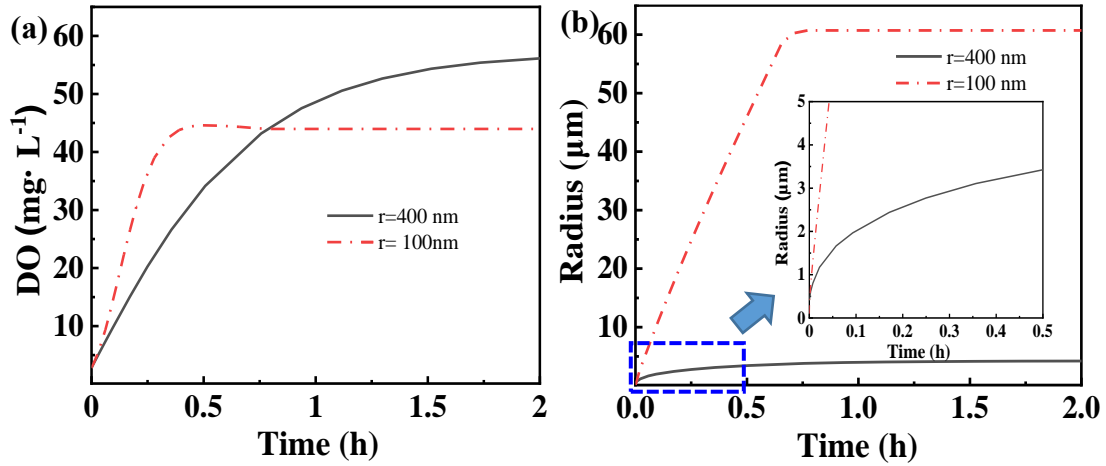
Figure 3.6 (a) The predicted DO levels during the dissolution of O_2 NBs in water (NBs were prepared with the initial radii of 100 and 400 nm). (b) The predicted bubble radius changes during the dissolution. The N/V of 10^{14} #·m^{-3} was used in the model calculation.

On the other hand, our model prediction indicates that the dissolution may also result in the bubble size decrease, which agrees with experimental findings (M. Li et al., 2021; X. Zhang et al., 2013). **Figure 3.7(a)** shows that the DO concentration increases during the dissolution process of O_2 NBs in water, which is similar to **Figure 3.6(a)**. **Figure 3.7(b)** indicates that the bubble radius could also decrease from the initial radius (100 or 400 nm) to zero and then negative values when we adjusted the initial bubble number density (e.g., 1.1×10^{14} #·m^{-3}). Clearly, the model solution with **Equations (3.19)** and **(3.21)** could also reveal the bubble radius shrinkage during the dissolution. Negative radii are unrealistic and could indicate that NBs have completely dissolved and disappeared. In addition, NB with a radius of 100 nm shrinks faster than NB with radius of 400 nm.
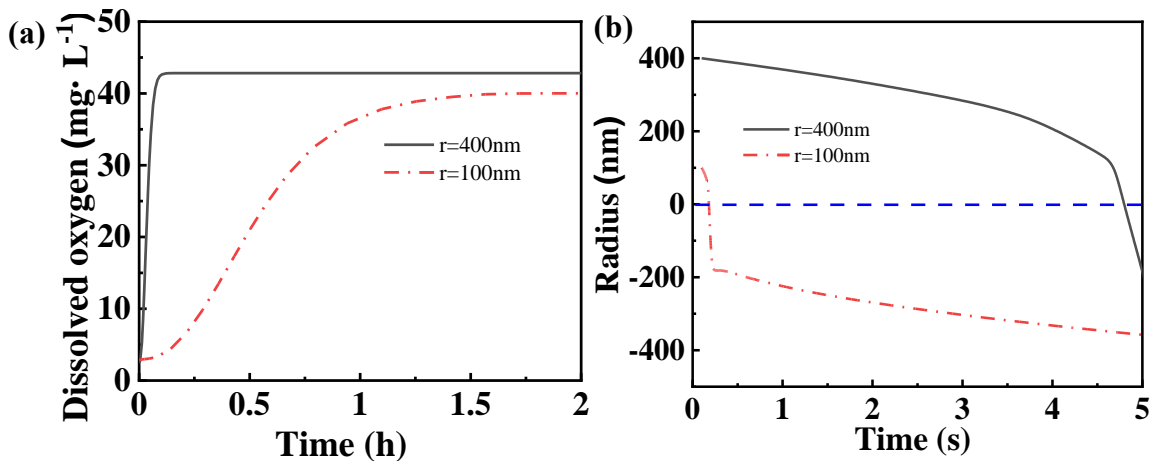
Figure 3.7 (a) The predicted DO levels during the dissolution of O_2 NBs in water (NBs were prepared with the initial radii of 100 and 400 nm). (b) The predicted bubble radius changes during the dissolution. The N/V of 1.1×10^{14} #·m^{-3} was used in the model calculation.

Water chemistry and other environmental conditions as temperature clearly affect dissolution kinetics of NBs. For instance, water surface tension, density, and dielectric constant as well as pH/temperature incorporated in the model **Equations (3.19)** and **(3.21)** indicate their influences on dissolution and size changes of NBs in liquid. Higher temperatures correspond to lower water surface tension, which reduces the size of NBs according to our model and has been verified by our previous work (X. Shi et al., 2021). The dissolution rate of NBs could increase at high temperatures due to the increased internal pressures of NBs and the reduced solubility of O_2 (Berkelaar, Seddon, Zandvliet, & Lohse, 2012). In addition to temperature, the impact of salinity on NB dissolution kinetics in water may also be evident. Generally, increasing salinity compresses the electric double layer and reduces the net surface charge of colloidal particles. However, many

previous studies found zeta potentials of NBs do not vary sensitively with salinity, and the

NBs exhibit superior stability against coalescence (Khaled Abdella Ahmed et al., 2018; Oh

& Kim, 2017).

3.3.4 Observations of DO levels after the dilution of the water suspension of O_2 NBs

The dissolution of O_2 NBs is primarily driven by the concentration gradient of dissolved

gas in the liquid and the surface tension of bubble due to Laplace overpressure (Duncan &

Needham, 2004). **Figure 3.8(a)** shows the DO levels versus the dissolution time after the

O_2 NB suspension was diluted using deoxygenated water. The DO level in the original

spiked NBs (10^{14} #·m^{-3}) without any dilution dropped from the peak level of 37 mg·L^{-1} to

a quasi-steady level of 18 mg·L^{-1}. Conversely, the deoxygenated water without addition of

any O_2 NBs had a stable DO level near 0 mg·L^{-1}. As the O_2 NB suspension was diluted

with more deoxygenated water, the initial DO levels (C_i) declined proportionally as

expected and all dropped to different stable levels (C'). To analyze the DO changes before

and after dilution, we performed a mass balance analysis as below.

Equation (3.22) shows that the total amount of DO comes from the storage of O_2

NBs and the initial DO in the water phase. After dilution with water in a volume of V_{H2O},

there is an additional term or contribution from the overhead space (V_{air}), where the initial

O_2 content is ignored. Moreover, the number concentration of NBs was reduced due to

dilution and expressed in **Equation (3.24)**, which ignores the collapse or any other forms

of loss of NBs. This simplification treatment is supported by a study that reported the presence of stable bulk O_2 NBs in water undersaturated with oxygen (Toru Tuziuti et al., 2018). **Figure 3.8(c)** shows that the average number concentrations of O_2 NBs in water was proportionally reduced when varying the dilution ratio (10:0, 7:3, 3:7, 1:9) with deoxygenated water, which justifies the assumption for **Equation (3.24)**. C' is the quasi-steady state or equilibrium DO concentration in the diluted NB water that were monitored and presented in **Figure 3.8(a)**. According to the ideal gas law and Henry's law, the partial pressure of oxygen in the overhead space is related to C', which allows us to rearrange **Equation (3.22)** into **Equation (3.23)**. Combining **Equations (3.23)** and **(3.24)** leads to **Equation (3.25)**, which reveals that the ratio (C_i/C') of the initial DO and the equilibrium DO in the NB water is highly dependent on the dilution ratio (V_{H2O}/V_{NB}). **Equation (3.25)** indicates that increasing the dilution ratio (V_{H2O}/V_{NB}) will increase the ratio of C_i/C', which supports our experimental data in **Figure 3.8b**.

$$V_{NB} \times (f \times N + C_i) = (V_{NB} + V_{H_2O}) \times (f \times N' + C') + \frac{P_{O_2,NB} V_{air}}{RT} \times M_{O_2} \tag{3.22}$$

$$f \times N + C_i = (1 + \frac{V_{H_2O}}{V_{NB}}) \times (f \times N' + C') + \frac{C'}{K_H} \frac{V_{air}}{RT} \times M_{O_2} \tag{3.23}$$

$$N' \approx N \times \frac{V_{NB}}{V_{NB} + V_{H_2O}} \tag{3.24}$$

$$\frac{C_i}{C'} \approx 1 + \frac{V_{H_2O}}{V_{NB}} + \frac{M_{O_2} V_{air}}{K_H RT} \tag{3.25}$$

where V_{NB} is the total volume of the water suspension of O_2 NBs (L), V_{H2O} is the

added volume of deoxygenated water (L), V_{air} is the volume of air in the overhead space in the container (L), N is the NB concentration in NB water ($\#\cdot L^{-1}$), N' is the NB concentration in diluted NB water ($\#\cdot L^{-1}$), f is a factor that indicates the DO concentration produced by one single O_2 NB in water ($mg\cdot L^{-1}\cdot\#^{-1}$), C_i is the initial DO concentration in the water suspension of O_2 NBs, M_{O2} is the molar mass of O_2 ($32\ g\cdot mol^{-1}$).

Figure 3.8(b) shows that increasing the dilution ratio (the volume of the spiked deoxygenated water divided by the volume of the NB suspension, V_{H2O}/V_{NB}) will increase the ratio of C_i/C' significantly, which supports our experimental data in **Figure 3.8(a)**. Moreover, the rate of decline also decreased with the dilution ratio increased. Particularly, the DO drop became less significant when the dilution ratio was more than 1:1, due to a lower degree of O_2 saturation. The DO level decline in the dissolution process could primarily result from the DO transfer from the liquid mixture (400 ml) to the air in the overhead space (approximately 260 ml). In addition, the average number concentration of O_2 NBs in water (**Figure 3.8(d)**) was proportionally reduced when varying the dilution ratio (0:10, 3:7, 7:3, 9:1) with deoxygenated water, which justifies our assumption. Furthermore, we conducted the same dissolution experiments by either completely filling up the container with the liquid mixture or completely opening the container to the ambient air. **Figure 3.8(c)** shows that when the liquid mixture was completely open to the air, the DO declined much faster ($1.80\ mg\cdot L^{-1}\cdot h^{-1}$) than that obtained ($0.38\ mg\cdot L^{-1}\cdot h^{-1}$) when the liquid mixture fully occupied the overhead space. It is quite odd that the DO level still

dropped slightly even when the container was fully filled up with water, where DO should have remained constant due to the absence of liquid/air phase transfer. We suspect that the presence of O_2 NBs could potentially interfere with the accuracy of the DO probe due to the blockage of the active electrochemical reaction sites.
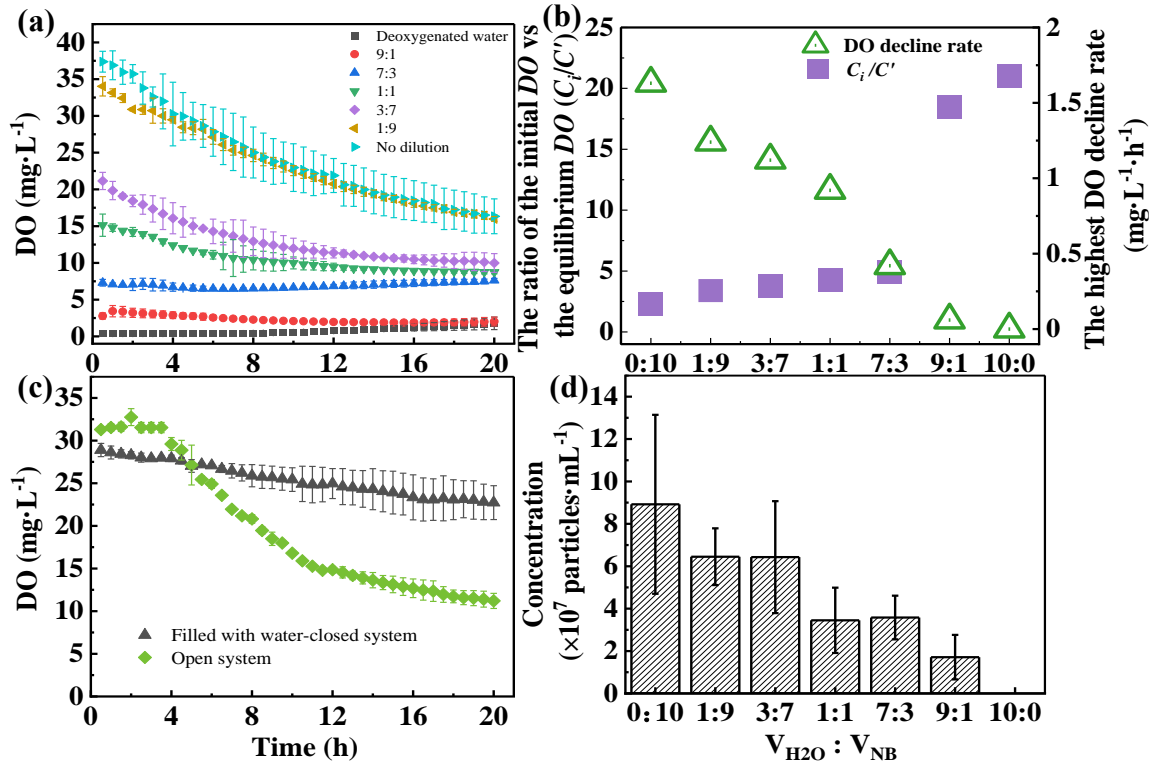
Figure 3.8 (a) DO levels versus the dissolution time under different dilution ratios (V_{H2O}/V_{NBs}) in an air-tight container, (b) The ratio of the initial DO vs the equilibrium DO (C_i/C') and the decline rate of DO under different dilution ratio, (c) DO levels versus the dissolution time of O_2 NBs in the container fully filled up and open to the ambient air, and (d) The influence of dilution ratios on the average concentration of O_2 NBs.

3.3.5 Effects of the presence of O2 NBs on the DO levels

To verify the above speculation, O_2 NBs were removed from water by Amicon ultrafiltration centrifugal filters (Amicon Ultracel 3K, Millipore, USA), which is reported

to remove substances greater than 1 nm (W. Zhang, Yao, Sullivan, & Chen, 2011). After filtration, the DO level in the filtered water is reduced from 34.4 ± 2 to 8.6 ± 0.5 mg·L^{-1} (a saturation DO level under one atmosphere at room temperature) as shown in **Figure 3.9**. By contrast, applying centrifugation only without filtration reduced the DO in the supernatant to 12.4 ± 0.5 mg·L^{-1}, suggesting that high-speed centrifugation can remove a few large sized O_2 NBs in water as reported elsewhere (J. Zhang et al., 2019). As a negative control, the DO level of 20.0 ± 1.3 mg·L^{-1} was measured for the same NB suspension without filtration or centrifugation after 10 min. An evident drop was also observed and the reduced DO level is likely due to the dissolution of NBs and escape of DO from water to air. Another negative control experiment was conducted on deoxygenated water with a low initial DO of 0.8 ± 0.2 mg·L^{-1}. After going through the same filtration and centrifugation procedure, the DO level bounced up to around 8.4 mg·L^{-1}, the same level we obtained from the NB water. This result indicates that the deoxygenated water can quickly replenish the DO level once in contact with the air during the filtration/centrifugation processes which are completed in 10 min.

The above results suggest that the presence of O_2 NBs strongly dictates the DO level and follows Henry's law. For instance, according to our previous modeling prediction and experimental measurement (X. Shi et al., 2021), the internal pressure of O_2 NBs should be close to the gas injection pressure (60 psi or 4 atm). Thus, the vapor pressure of O_2 inside O_2 NBs supersedes the partial pressure of O_2 in the ambient air and directly influence

the DO in water. Once O_2 NBs are removed by filtration (or partially by natural dissolution), the DO level is shown to progressively reduce and eventually reach the equilibrium level $(8.6\pm0.5 \text{ mg·L}^{-1})$ with the ambient air.
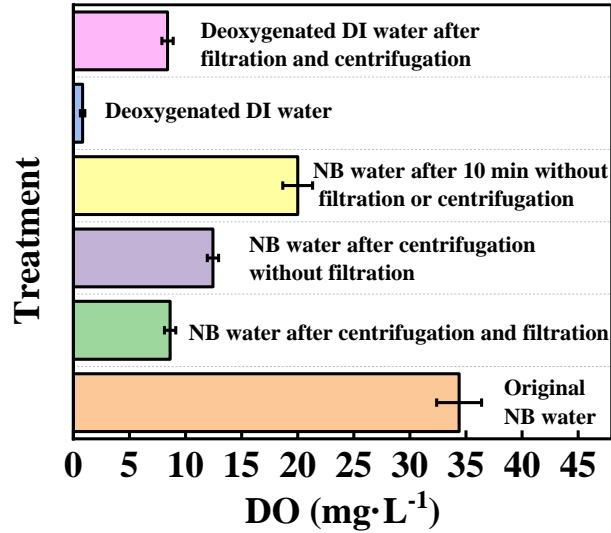
Figure 3.9 DO levels in different conditions. The centrifugal speed and time were $5300\times g$ and 10 min.

3.4 Conclusion

The presented study aims to unravel the aeration and dissolution behavior of O_2 NBs in water and guide the design of engineering applications of NBs. For the aeration behavior of O_2 NBs, we found that mass transfer efficiency ($K_L \cdot a$ or K_L) increases as the size of bubble decreases. Specifically, smaller O_2 NBs could raise up DO faster than larger O_2 NBs. Moreover, increasing the internal pressure and the supply rate of O_2 NBs can also substantially enhance the aeration kinetics. Thus, NBs with higher internal pressures and smaller sizes hold great potential to enhance the gas delivery in many engineering

processes such as wastewater treatment (Temesgen et al., 2017), ozonation (Saijai et al., 2019) and aeration of hypoxia water (Honggang Zhang et al., 2018). For the dissolution behavior of O_2 NBs, most studies only reported the shrinking process of NBs (German, Chen, et al., 2016; Kapodistrias & Dahl, 2012; Michelin et al., 2018; Peñas-López et al., 2017; Solano-Altamirano et al., 2015; Tanaka et al., 2020; Yasui et al., 2016). However, our model reveals that O_2 NBs may either increase or decrease (swelling or shrinking) during the dissolution process. Moreover, the changes of DO were also predicted with the dissolution time according to the EP theory (Duncan & Needham, 2004; Tan et al., 2020). Furthermore, the changes of DO and the bubble size are both affected by the initial size of NBs. In addition, the dilution slowed down the dissolution process of O_2 NBs as indicated by the decrease of the DO decline rate. Our experiments also confirm that O_2 NBs are a major source of O_2 governing the DO level instead of the ambient air that only dictates the DO dynamics in bubble-free water. Yet a simpler experiment involving the dissolution of NBs than we have reported is difficult to conceive. Further research is under way to understand the bubble effects on DO detection and potential artifacts from the presence of NBs that could potentially interfere the electrochemical sensing or reactions on DO probes. Moreover, novel nanoscale imaging is deserved to explore which would largely verify the model prediction of bubble swelling or shrinkage during dissolution that is difficult to observe.

CHAPTER 4

NANOBUBBLE WATERING AFFECTS NUTRIENT RELEASE AND SOIL CHARACTERISTICS

4.1 Introduction

Recently, nanobubbles (NBs) are attracting increasing attention in agriculture due to the intriguing characteristics such as high stability (Neelkanth Nirmalkar et al., 2018), enhanced gas solubility (Yasui, Tuziuti, & Kanematsu, 2019a) and the generation of reactive oxygen species (ROS) (S. Liu, S. Oshita, S. Kawabata, et al., 2016). Irrigation with water containing NBs has proven effective to promote diverse seed germination (S. Liu, S. Oshita, Y. Makino, et al., 2016; M. Zhu, Wang, Sun, & Zhang, 2021), plant growth (Ahmed, Shi, et al., 2018; Yuncheng Wu et al., 2019) and crop yield (Y. Zhou et al., 2020; Y. Zhou, Li, Liu, Wang, & Muhammad, 2019b). Such promotion effects were repeatedly reported for different plants (e.g., tomato, cucumber, and maize) with different types of NBs such as O_2, air, and nitrogen (N_2) in irrigation (Ahmed, Shi, et al., 2018; Yuncheng Wu et al., 2019; Y. Zhou, Li, et al., 2019b; Y. Zhou, Zhou, Xu, Muhammad, & Li, 2019). However, the effect of the NBs on the plant promotion still remains unclear.

Previous studies primarily indicated that appropriate levels of ROS generated by NBs can serve as signal molecules and promote plant growth(Ahmed, Shi, et al., 2018; S.

Liu et al., 2017; Y. Zhou, Li, Liu, Wang, & Muhammad, 2019a; Y. Zhou, Li, et al., 2019b). For example, Liu et.al showed both low concentrations of H_2O_2 and the air NB water can stimulate the germination of barley seeds (S. Liu et al., 2017). NBs could produce the exogenous hydroxyl radicals ($\bullet$OH) that may directly regulate the expression of genes for peroxidase and promote cell proliferation and survival (S. Liu, S. Oshita, S. Kawabata, et al., 2016). Other studies have largely attributed the boost in plant growth to dissolved oxygen (DO) supplied by NBs (Ebina et al., 2013b; S. Liu et al., 2015). For example, NBs used for oxygenation in drip irrigation systems have proved to promote the maize or corn growth and enhance the root development (Y. Zhou, Li, et al., 2019b). O_2 supplied by air NBs could effectively reach to the zone of root and alleviate soil hypoxia, which consequently enhance plant growth, crop yield and quality (Ying Wang, Wang, Sun, Dai, Zhang, Xiang, Hu, Hu, et al., 2021). Moreover, high O_2 content in soil can boosts up the activity of some rhizosphere bacteria (Yuncheng Wu et al., 2019; Y. Zhou, Li, et al., 2019b; Y. Zhou, Zhou, et al., 2019). Besides the reported changes of ROS, DO and microbial activity, there is still a lack of systematic investigations of the impacts of NBs on the major soil chemical characteristics, which may unravel the promotion mechanisms. The soil chemistry could be significantly affected by NBs due to their high surface areas and negative electrical charges that may attach to the soil surface, the root of plant and attract cations (e.g., Ca^{2+} and Na^+) (Bui, Nguyen, & Han, 2019). For example, O_2 NBs were shown to significantly enhance the release of NH_4^+-N from sediment to water by mitigating

hypoxia/anoxia at the sediment-water interfaces (Honggang Zhang et al., 2018).

To explore the mechanisms of plant growth promotion and promote applications of NBs in agricultural applications, this study explored the influences of different NBs made of O_2, N_2, hydrogen (H_2), air and carbon dioxide (CO_2) gases on the soil chemical properties and common nutrient (i.e., NH_4^+, NO_3^-, PO_4^{3-} and Ca^{2+}) release from the treated soil. We further analyzed the zeta potential changes of NBs in soil extract to analyze the adsorption mechanisms of soil species on NBs. Moreover, to understand the influence of different NBs on the soil, the chemical properties of soil extract and the released species were also analyzed by multiple factor correlation analysis and principal component analysis (PCA). The governing factors (e.g., the type or composition of NBs) were discussed to explain the difference between the NB-treated groups and to provide an insight into the inter-group clustering based on their similarities.

4.2 Materials and Methods

4.2.1 Production and characterization of bulk NBs in water

The water suspensions of NBs were generated by directly passing compressed O_2, air, CO_2, H_2 and N_2 gases respectively though a tubular ceramic membrane (100 nm, model WFA 0.1, Refractron, USA), which was immersed in deionized (DI) water as we previously reported (Ahmed, Sun, et al., 2018; Khaled Abdella Ahmed et al., 2018). The size and

concentration of NBs in the produced water suspension was 100-400 nm and $4\times10^8 - 6\times10^8$ #·ml^{-1} as reported previously (X. Shi et al., 2021). Major colloidal properties such as bubble size distribution and zeta potential of different bulk NBs in water were reported in our previous studies (Ahmed, Shi, et al., 2018; Ahmed, Sun, et al., 2018; Khaled Abdella Ahmed et al., 2018).

The soil extract was obtained by immersing the air-dried and pre-screened soil (<2 mm) with DI water in a solid–solution-ratio of 1:10 (w/v) under mild shaking for 3 h. The soil slurry passed through a filter paper (qualitative P5, Fisherband, USA) and a 0.2-μm polyethersulfone (PES) membrane (Basix Syringe Filters, USA). Then, the filtrate was placed in a centrifugal filter unit (Millipore, Amicon® Ultra-4, USA) and centrifuged (5430 R, Eppendorf Centrifuge, USA) for 30 min at a speed of 7500×g (25 °C) to remove any residuals larger than a diameter of 3 KDa. Finally, 2 mL different water suspensions of NBs were added to 2 mL of the soil extract. Zeta potential of NBs in the soil extract was determined by the Zetasizer instrument (Nano ZS, Malvern Instruments, USA). The results are derived from the average of three independent measurements.

4.2.2 Evaluation of the properties of soil

Garden soil (All purpose, Miracle Gro, USA) was purchased from Home Depot and stored in brown glass bottles sealed with cover to avoid light and evaporation at 4°C. Extractable P, K, Ca and Mg were measured by Mehlich 3 (ICP) (Sims & Wolf, 1995; Wolf & Beegle,

2011). Measurements of total sorbed Cu, Zn, Pb, Ni, Cd, and Cr followed the EPA Method 3050B+6010. This method (EPA, method 3050B) is a very strong acid digestion that will dissolve almost all elements that could become "environmentally available." Organic matter determinations were based on weight loss. Weight loss is on removal of the organic matter from the mineral fraction by Ignition (Schulte & Hoskins, 1995; Sims & Wolf, 1995). Cation exchange capacity (CEC) was determined by the summation of exchangeable Ca, Mg and K (Ross & Ketterings, 1995; Sims & Wolf, 1995). Nitrate N and ammonium N in soil were analyzed by Specific Ion Electrode (Griffin et al., 1995; Mulvaney, 1996; Sims & Wolf, 1995). Total nitrogen and total organic carbon were analyzed by high temperature combustion (Bremner, 1996; Nelson & Sommers, 1996). The Mehlich buffer method was used for determining exchangeable acidity. Soil pH was measured in a 1:1 ratio (w/v) of soil to water using pH electrode (PS-2102, PASCO) (Eckert & Sims, 1995). Calcium carbonate equivalency (CCE) was measured using ASTM Method C 25(ASTM, 2011). The electrical conductivity (EC) of the soil was measured at ratio of 1:5 (w/v) soil : water using conductivity sensor (PS-321, PASCO) (D. Corwin & S. Lesch, 2005; Sonmez, Buyuktas, Okturen, & Citak, 2008).

4.2.3 Evaluation of soil nutrient release

The soil samples were air-dried at room temperature and passed through a USS #10 sieve (2 mm mesh). The experimental groups consisted of 6 paralleled 250-ml glass flasks for

each condition. For each condition, 10 g of the air-dried and sieved soil were shaken with 100 mL NBs water (e.g., O_2, N_2, H_2, CO_2 and air NBs) in the flasks that were sealed and shaken under 25 oscillations·min^{-1} for 3 h at room temperature as shown in **Figure 4.1**. The soil immersed in DI water was used as a negative control group. Sixty mL of slurry were collected at different times (0.5, 1, 1.5, 2, 2.5, 3 h) and centrifuged at 7000×g for 10 min to separate the supernatant, which was filtered by a 0.45-µm filter paper (No. 42, Whatman, USA). For each batch, duplicates were prepared to derive standard deviation of the different nutrient species concentrations.
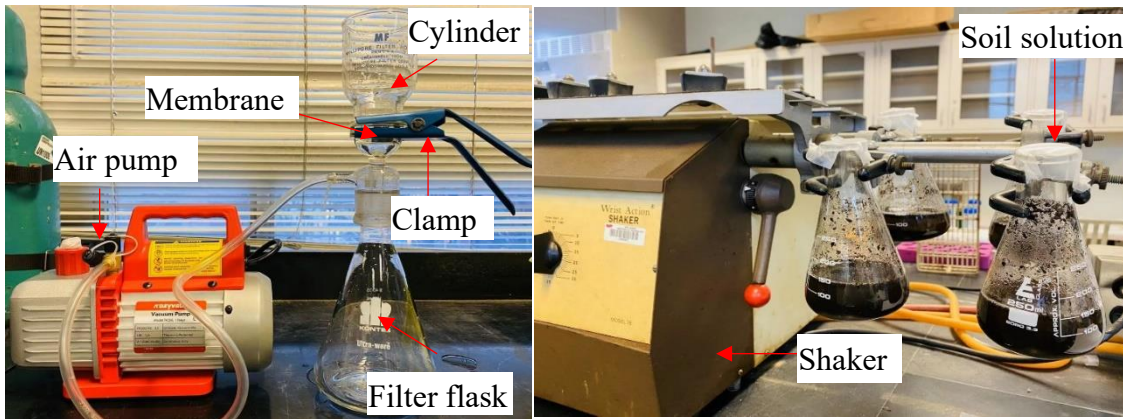
Figure 4.1 Photos of the lab-scale soil batch experiment.

4.2.4 Characterization of soil extract

4.2.4.1 Measurement of the water quality of the soil extract   A Xplorer GLX datalogger (PS 2002, PASCO, USA) with multiple sensors, such as the ORP sensor (CI-6716, PASCO, USA), the DO sensor (PS-2196, PASCO, USA), the pH sensor (PS-2102, PASCO, USA) and the conductivity sensor (PS-321, PASCO, USA), was used to measure

the major water quality parameters for the filtrate as shown in **Figure 4.2**. The pH and ORP

sensors were calibrated before experiments.
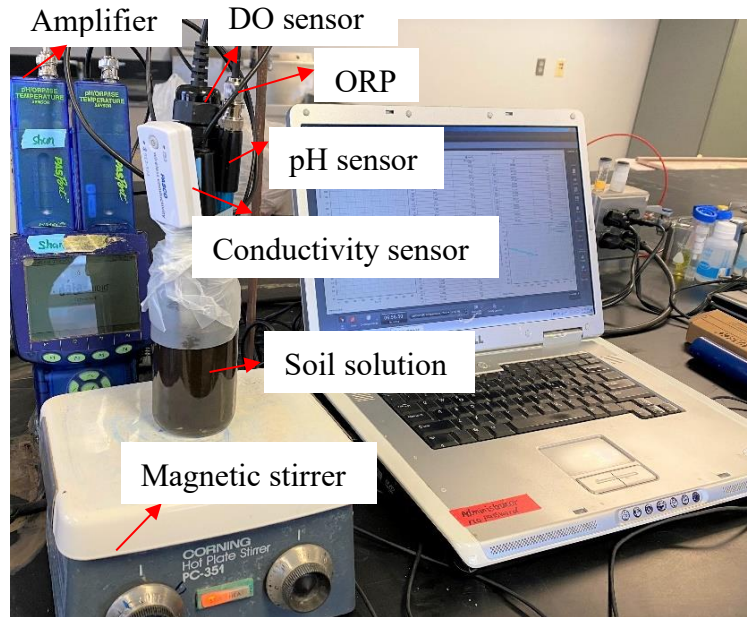
Figure 4.2 Photos of the batch experiment for pH, DO and redox potential measurement.

4.2.4.2 Measurement of anions and cations in the soil extract   Concentrations of

major cations and anions in the soil extract were measured by a Metrohm 881 Compact ion

chromatograph (IC) Pro with an 858 autosampler. For NH_4^+, Ca^{2+}, K^+, Mg^{2+}, and Na^+, a

cation exchange column Metrosep C4 150 column was used with a C4 eluent (1% HNO_3

and 0.120 g/L Diphenylamine). For NO_3^-, NO_2^-, Cl^-, SO_4^{2-}, F^-, and PO_4^{3-}, an anion exchange

column Metrosep A Supp 5-250 column was used with a Supp 5 eluent (0.32 mM Na_2CO_3

and 0.10 mM $NaHCO_3$). Water samples passed through a 0.45-µm pore size nylon filter

(Whatman, USA) and were properly diluted before IC analysis.

4.2.4.3 Measurement of dissolved organic matters (DOM) Chemical oxygen demand (COD) of the soil extract was measured according to the HACH method 8000 using high range vials (200–15000 $mg \cdot L^{-1}$). Excitation/emission matrix (EEM) spectra of the samples were measured using the 3D spectrum mode on a fluorescent spectrophotometer (Hitachi FL4500) for emission (Em) wavelengths 300-600 nm and excitation (Ex) wavelengths 200-500 nm at 8-nm intervals. To avoid the inner filter effects, the samples were diluted 10 times with DI water first when their maximum absorbance (254 nm in this study) was > 0.1. Water Raman scattering of sample spectra was eliminated by subtracting the DI water blank spectrum that was recorded under the same conditions (X.-q. Qin et al., 2020).

4.2.5 Statistical analysis

The data statistics were assessed using one-way ANOVA (*t*-test, two sided, a significance level $\alpha = 0.05$) to reveal significant differences between the control and experimental data. The violin plot was used to display the concentration data of ions released from soil treated by different NBs water. In addition to the full distribution of data, the violin plot also displays summary statistics such as mean, interquartile ranges and median.

The correlations between chemical properties (e.g., pH, DO, ORP and conductivity) of the soil extract and the released species (e.g., COD, NH_4^+-N, PO_4^{3-}-P, K^+, Ca^{2+}, Mg^{2+}, F^-, NO_2^--N and NO_3^-N) were tested using Pearson's correlation coefficients with statistical

significances of $p < 0.05$. PCA was conducted with all the measured parameters, which included chemical properties of the soil and the concentrations of all released species. To ensure that the experimental data had the same weight, all measured parameters were standardized to a Z score with a standard deviation of 1 and a mean value of 0. All statistical analysis and data plotting were done by Excel 2016 and Origin version 2020b.

4.3 Results and Discussions

4.3.1. Properties of soil

The major soil properties were tested by the Agricultural Analytical Services Laboratory at Pennsylvania State University and summarized in **Table 4.1**. Soil pH, available nutrients and cation exchange capacity (CEC), organic carbon (OC), and electrical conductivity (EC) are some key properties that govern the soil management decisions for crop production (Alliaume et al., 2010). The cation exchange capacity (CEC) of a soil determines the number of positively charged ions cations that the soil can hold. This, in turn, can have a significant effect on the fertility of the soil. The CEC concentration of soil sample was 28.9 ± 1.4 meq·$100g^{-1}$ which is in the normal range of CEC values for dark colored loams and silt loams (Mengel, 2011). The content of heavy metals (Cd, Cu, Cr, Pb, Ni and Zn) in soil are comparable to the content of heavy metals in agricultural soils worldwide (Baishya & Sarma, 2014). Soil organic matters (SOM) are considered as an important soil quality in

agricultural soils (Lal & Kimble, 1997; Marinissen, 1992) and is a key factor for

sustainable land use (Pulleman, Six, Uyl, Marinissen, & Jongmans, 2005; Reeves, 1997).

Surface soils are usually composed of approximately 1 to 6% organic matter, with SOM

decreasing with depth (Brandy & Weil, 2002). The total organic matter account in our soil

was 21% (w/w), which indicates our soil is rich in organics.

Table 4.1 Chemical Speciation and Elements of the Soil Sample

Cd (mg·kg^{-1})	Cu (mg·kg^{-1})	Cr (mg·kg^{-1})	Pb (mg·kg^{-1})	Ni (mg·kg^{-1})	Zn (mg·kg^{-1})	
0.33±0.02	65.44±3.27	28.69±1.43	14.60±0.73	21.54±1.08	137.80±6.89	
Total phosphate (mg·kg^{-1})	**Potassium** (meq·100g^{-1})	**Magnesium** (meq·100g^{-1})	**Calcium** (meq·100g^{-1})	**CEC** (meq·100g^{-1})	**Acidity** (meq·100g^{-1})	**pH**
205±10	7.4±0.37	6.6±0.33	28.0±1.4	28.9±1.4	0	7±0.35
Electrical conductivity (μs·cm^{-1})	**Nitrate-N** (mg·kg^{-1})	**Ammonium–N** (mg·kg^{-1})	**Total N** % (w/w)	**Total Carbon** %(w/w)	**Calcium Carbonate Equivalence * (CCE) %**	**Organic Matter** % (w/w)
8583.06±35.6	2500±125	14.9±0.75	1.35±0.02	17.07±0.85	9.1±0.46	21.4±1.07

4.3.2 The effect of different NBs on major water quality properties of the treated soil

Figure 4.3(a) shows that after immersion of the garden soil in the different NB water for 3

h, CO_2 NBs caused an immediate reduction of the soil pH to approximately 5.6, whereas

other NBs did not significantly alter the soil pH that was stable at around 7.1. The dissolved

CO_2 concentration in the soil water may reach or exceed the saturated level of 0.45 mg·L^{-1} under the partial pressure of CO_2 in ambient air (40 Pa) per the Henry's law.(Snell, Zhou,

Carpenter, & Randolph, 2016) This dissolved CO_2 is in a form of carbonic acid and reaches an equilibrium pH of 5.6, which explains the pH reduction. The CO_2-saturated soil progressively released the CO_2 vapor over time and thus raised the soil pH (red dot data). **Figure 4.3(b)** shows that O_2 NBs could significantly increase the DO level up to 22 $mg·L^{-1}$ compared to the control soil group immersed with DI water (8.5 $mg·L^{-1}$). By contrast, the DO levels were suppressed by other NBs, especially CO_2 NBs, which reduced the DO to approximately 2.8 $mg·L^{-1}$. Clearly, the presence of H_2, N_2 and CO_2 NBs decreased the partial pressure of O_2 in the treated soil and caused the DO decline. The O_2 NBs-treated soil exhibited a high initial level of DO that progressively declined to 11.45 $mg·L^{-1}$ after 3 h. Similarly, the soil DO levels under treatment of air, H_2, and N_2 NBs all declined due to the loss of soil O_2, whereas the CO_2 NB treated soil had a minor increase of the DO level due to the absorption of ambient O_2 back into the soil. Clearly, spiking O_2 NBs into soil not only increases the DO level but also sustains a longer retention time of soil O_2.
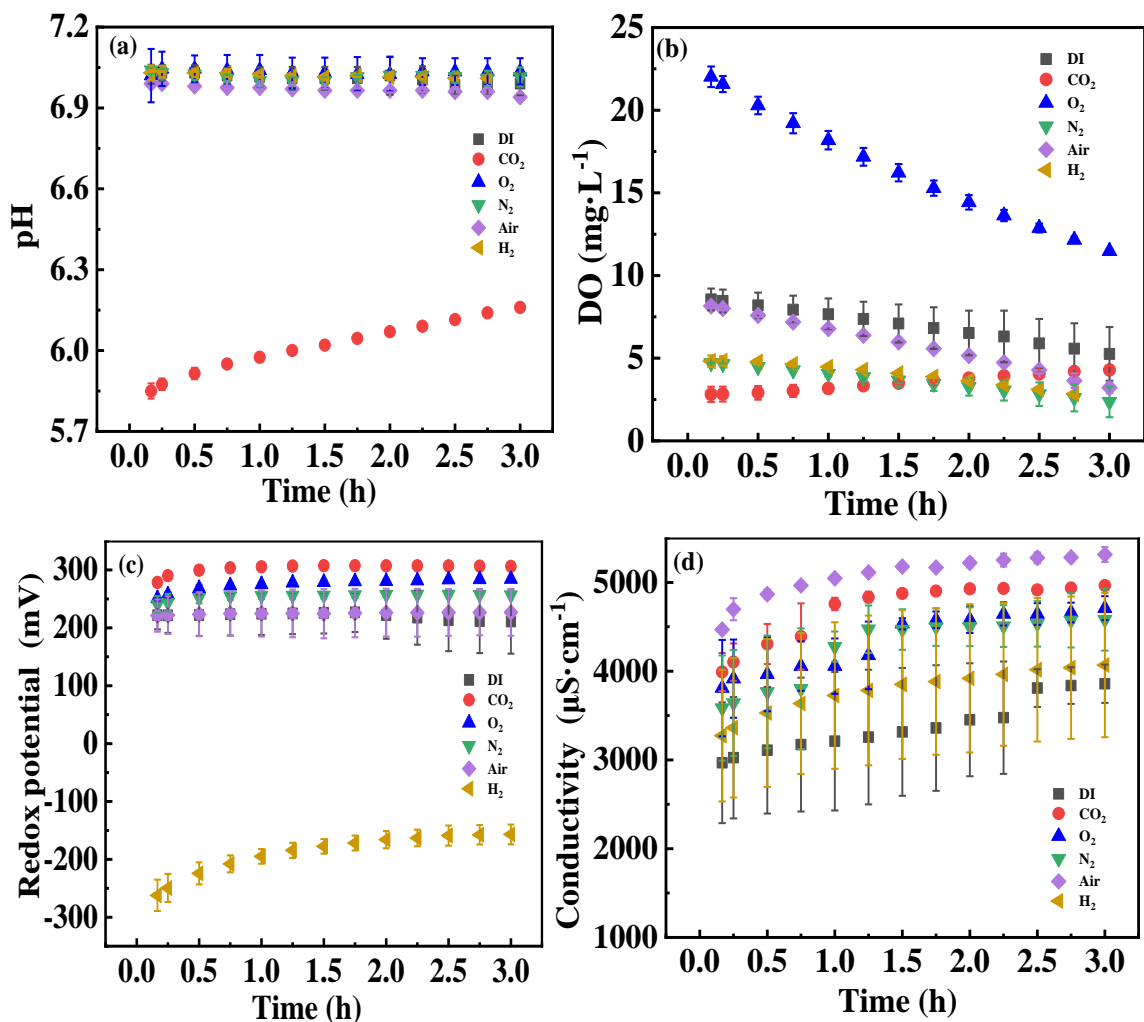
Figure 4.3 (a) pH, (b) DO concentration, (c) redox potential and (d) conductivity at different time in soil solution treated by different NBs.

Similar to the soil DO level, the soil's redox potential (Eh) is another important indicator for soil's reductive and oxidative properties. Soil's Eh generally fluctuates between −300 and +900 mV depending on the surround aqueous redox conditions (Husson, 2013). **Figure 4.3(c)** shows that after spiking the NB water into the soil, O_2, N_2, and CO_2 NBs caused a higher level of redox potentials between 200 and 300 mV, which could be rated as a moderately reduced soils or waterlogged soil. Soil treated by H_2 NBs was highly

reduced with an Eh value of -200 mV. It is worth noting that the air NBs-treated soil had a

similar redox potential with that treated by DI water, because DI water may have been

saturated with air. Interestingly, the CO_2 NBs-treated soil rendered a higher redox potential

than the O_2 NBs-treated soil, probably because CO_2 leads to soil acidification, which

increases the redox potential in soil water. To explain the above data and pH dependence

of redox potentials, the H_2/H_2O or O_2/H_2O redox potentials in H_2 or O_2 NBs water are

analyzed using the following reaction stoichiometry.

$$H_2O + e^- \rightleftharpoons \frac{1}{2}H_2 + OH^- \quad (E^0_{H2}\text{=}0.83 \text{ V}) \tag{4.1}$$

$$O_2 + 4H^+ + 4e^- \rightleftharpoons 2H_2O \quad (E^0_{O2}\text{=}1.229 \text{ V}) \tag{4.2}$$
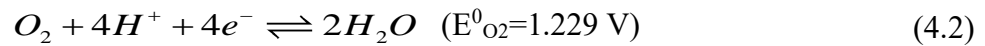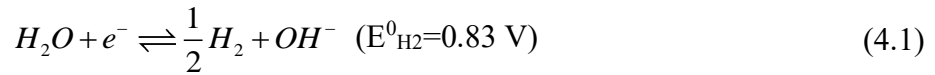
where the redox potential can be expressed by the Nernst Equation to relate to the

solution pH or partial pressure:

$$E_H = E^0_{H_2} - \frac{5}{169}\log P_{H_2} + \frac{1}{16.9}(14 - pH) \tag{4.3}$$

$$E_H = E^0_{O_2} + \frac{0.059}{4}\log P_{O_2} - 0.059\text{pH} \tag{4.4}$$

The redox potentials of H_2 or O_2 NB water depend on both the solution pH and the

partial pressure of H_2 or O_2 gases. **Figure 4.4(a)** indicates that E_H in the H_2 water will

decline with the increase of the partial pressure of H_2 or with the increasing pH, which

agrees with the experimental data. **Figure 4.4(b)** also reveals that E_H for O_2 water increases

with the increase of the partial pressure of O_2 gas or with the reduced pH, which is also

verified experimentally. The experimentally measured E_H in H_2 NBs-treated soil is located

between the prediction curves for pH 3 and pH 9, whereas the experimental data of E_H for

the O_2 NBs treated soil is significantly lower than the prediction or the calculated values with **Equation (4.4)**. The discrepancies between the experimental and calculated E_H levels could be caused by the actual partial pressures of H_2 or O_2 NBs that may be higher than we expect (e.g., 4 atm as we observed previously (X. Shi et al., 2021)) and thus yield different redox potentials compared to the dissolved H_2 or O_2 solutions. Moreover, the presence of other co-existing ions in the soil water such as sulfur (S), nitrogen (N), carbon (C), and Fe may also affect the actual redox levels besides the effects from H_2 or O_2 (Lin, He, Owens, & Chen, 2021).
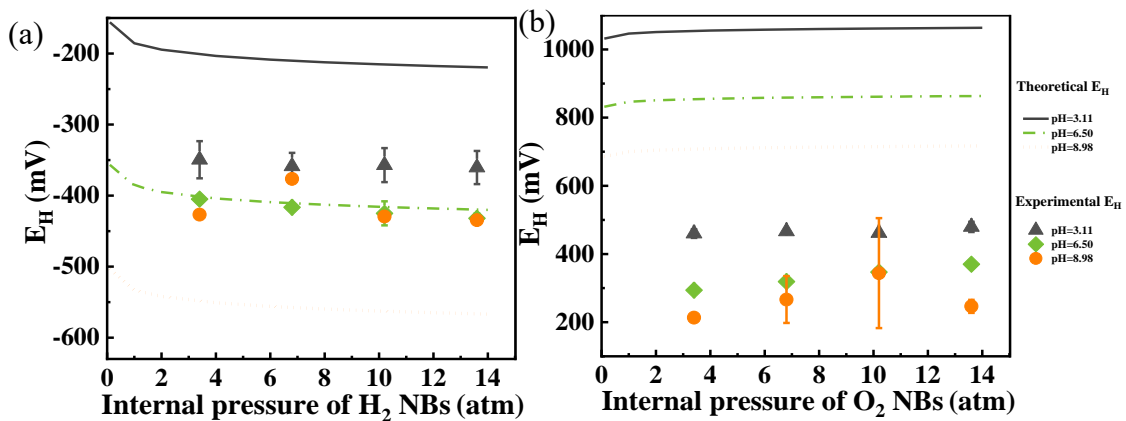
Figure 4.4 The redox potentials of the water solutions with H_2 (a) and O_2 NBs (b) with different internal pressures and solution pHs.

4.3.3 The effect of NB water washing on ions release from soil

4.3.3.1 Cation release   **Figure 4.3(d)** shows that except DI water, all other NB water resulted in the increased conductivity from 3000 to 5000 $\mu S \cdot cm^{-1}$, which indicates the increase of the mobile charged species. Violin plots (**Figure 4.5(a-e)**) show that the

variations of the released cation concentrations (Na^+, K^+, Ca^{2+}, Mg^{2+}, and NH_4^+) in the soil

extract after immersion in different NB water. Violin plot is a combination of a box plot

and density plot. A box indicates the interquartile range (IQR), which means 50% of the

data is contained in the box. The white dot and red bar represent median and mean of the

data. The whiskers (black lines) extended from the box display the lower (min) and upper

(max) adjacent values. The shape of the violin plot shows the frequency of values.

Compared to the result with DI water immersion, there is an evident impact from

CO_2 NBs on the Ca^{2+} or Mg^{2+} release ($p < 0.05$), as CO_2 NBs acidifies the soil and improves

the cation solubility (L. Zhang et al., 2018). H_2 NBs reduced all the cation release

significantly ($p < 0.05$) due to the resulting reducing condition, which may increase the

cation exchange capacity (CEC) of the treated soil (De-Campos, Mamedov, & Huang,

2009). In addition, N_2 NBs significantly improved the NH_4^+ concentration in soil extract

($p < 0.05$) probably due to the enhanced decay of organic nitrogen such as proteins, which

deserves additional research to clarify. However, the O_2 NBs water treatment did not affect

the release of any tested cations, which slightly differs from a study reporting the increased

the concentrations of NH_4^+-N as well as TN, NO_3^--N and NO_2^--N for the O_2 NBs-enriched

natural soil (Honggang Zhang et al., 2018). The difference might be caused by the different

soil conditions and the bubble application methods between the two studies. In our study,

the treated soil was open to the air and mixed with O_2 NB water, whereas Zhang's study

placed the O_2 NBs modified natural particles on the top of sediment layer to promote the

nutrient release due to the oxidation of organic detritus in the sediment that was sealed in a column and free from air (Honggang Zhang et al., 2018).
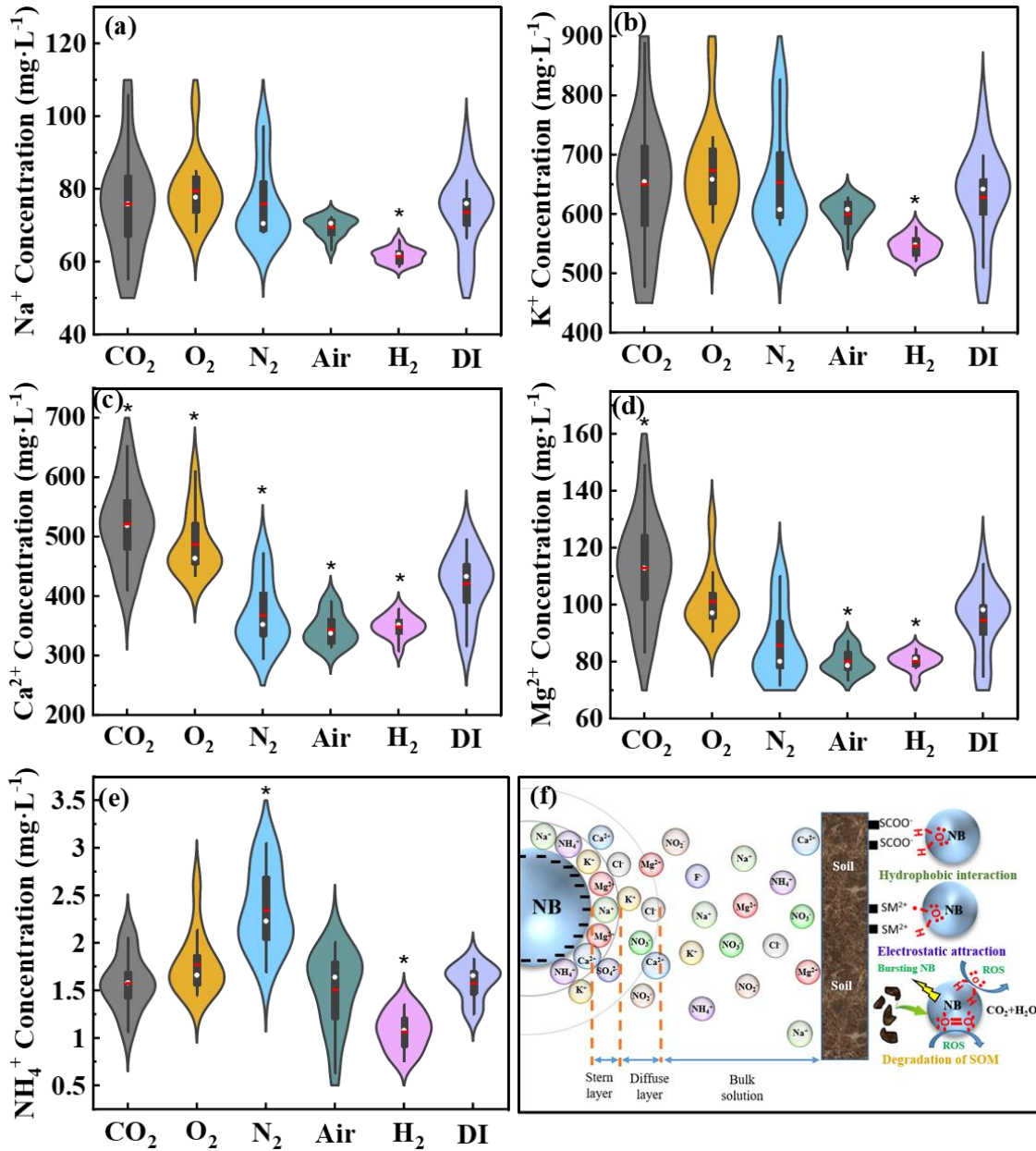
Figure 4.5 Violin graphs of the concentrations of the released cations (a) Na^+, (b) K^+, (c) Ca^{2+}, (d) Mg^{2+}, and (e) NH_4^+ under different NBs water and DI water treatment. (f) Schematics of the electric double layer of NBs in liquid and interaction mechanisms with SOM. * indicates the difference between NBs water and DI water treated group is significant ($p < 0.05$).

Figure 4.5(f) shows the electric double layer of NBs in liquid and their interactions with surrounding medium, ions and soil organic matter (SOM). Usually, NB has a stern layer of cations immediately connected to the surface of the NB and a diffuse layer which can exchange various ions with the bulk. Besides the water chemistry factor (e.g., pH or redox levels), all NBs in DI water or the soil extract are negatively charged (- 5 mV to -35 mV) as compared in **Figure 4.6**. Due to the relatively high salinity, the soil extract tends to reduce the negative surface charge of NBs as opposed to DI water because of the electrostatic double layer compression by the conductive species in the soil extract (Meegoda, Hewage, & Batagoda, 2019). **Figure 4.6(b)** shows that increasing the solution pH generally increased the zeta potential to a level of approximately -20 to -25 mV due to the increasing number of hydroxyl ions on the surface of NBs (Meegoda et al., 2018; Neelkanth Nirmalkar et al., 2018). The negatively charged NBs may attract those positively charged cations from the soil (N. Nirmalkar, A. W. Pacek, & M. Barigou, 2018). Moreover, in the presence of air NBs, the surface tension of water can be reduced by 15% (Ushida, Hasegawa, Narumi, & Nakajima, 2013), which makes NBs behave like surfactants and increase the leaching efficiency of soil substances.
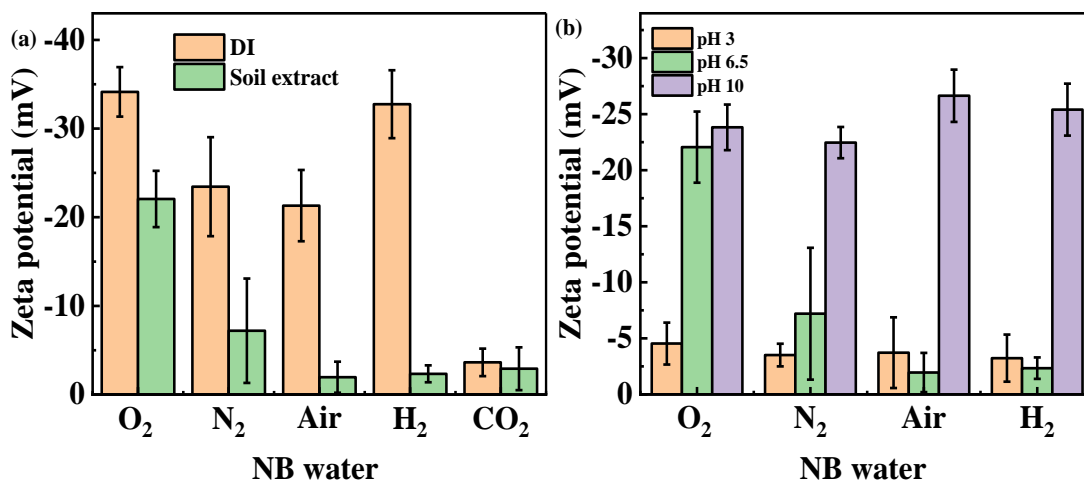
Figure 4.6 Zeta potential of different NB in DI water and soil extract (a) and at different pH (b) in soil extract.

4.3.3.2 Anion release   **Figure 4.7** compares the anions release from the treated soil under the exposure to different NBs water. Clearly, the release of NO_2^-, NO_3^-, and SO_4^{2-} was not significantly affected by NBs. Except O_2 NBs, other NBs exhibited remarkable effects on the release of Cl^-, F^-, and PO_4^{3-}. For example, CO_2 NBs apparently decreased the concentration of F^- and increased the concentration of PO_4^{3-} in soil extract compared to the control group ($p<0.05$). For the N_2 and air NBs treated soil, the release of F^- was promoted but the release of PO_4^{3-} was inhibited compared to control group ($p<0.05$). The resulting differences in the anion release from soil may be ascribed to the interactions between anions and NBs. For example, different anions may have differential and selective interactions on the interface of air/water, which are confirmed by the instrumental measurements using high pressure VUV photoelectron spectroscopy (da Silva Moura, Belmonte, Reddy, Gonslaves, & Weibel, 2018), second harmonic generation spectroscopy

(Ohno, Wang, & Geiger, 2017), X-ray photoelectron spectroscopy (Seidel, Winter, & Bradforth, 2016) and molecular dynamics (MD) simulation (N. F. Bunkin et al., 2016). The MD simulation and experimental measurement verified that the possibility of the adsorbing anions at the gas-water interface.

The enhanced PO_4^{3-} release might be attributed partially to the minor increase of the soil redox level by CO_2 NBs. The metal oxide–hydroxide complexes generally adsorbs inorganic phosphorus under oxic environment (W. Tang, Zhang, Zhang, Wang, & Shan, 2013). CO_2 NBs could reduce DO and pH, which potentially converts hydrous Fe oxides to Fe^{2+} ($Fe(OH)_3 + e^- + 3H^+ \rightleftarrows Fe^{2+} + 3H_2O$). The reductive dissolution of Fe-P minerals could leach out phosphate (Q. Chen et al., 2019; Ding et al., 2016). Conversely, (Yu et al., 2019) reported that O_2 NBs-modified minerals increased DO at the sediment/water interface, and then the release of PO_4^{3-} from sediment was inhibited.
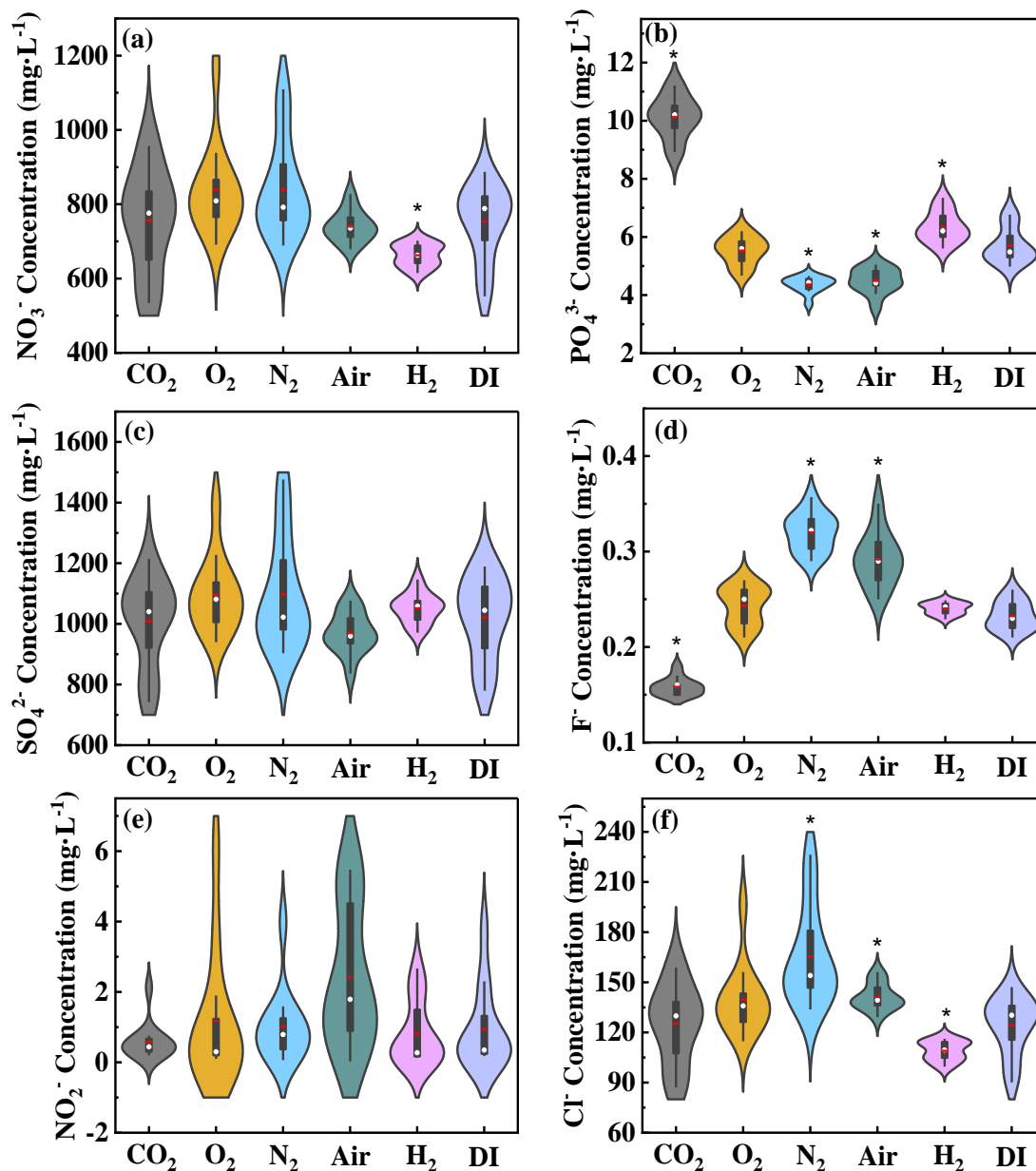
Figure 4.7 Violin graphs of the concentrations of released anions (a) NO_3^-, (b) PO_4^{3-}, (c) SO_4^{2-}, (d) F^-, (e) Cl^-, and (f) NO_2^- under different NBs water and DI water treatment. * indicates the difference between NBs water and DI water treated group is significant ($p<0.05$).

4.3.3.3 Leached dissolved organic matter (DOM) in the soil extract DOM in soil

derived from soil organic matter (SOM), which could leach out under the water washing

and affect soil fertility (Bolan et al., 2011). For example, fulvic acid (FA) and humic acid

(HA) are two major components of soil humic substances, and influence the elemental recycling and other soil functions (J. Hu, Wu, Sharaf, Sun, & Qu, 2019). To characterize the changes of DOM or those fluorescence emitting organic substances after immersion in NB water, the EEM spectra were acquired for soil extract and shown in **Figure 4.8**. Without the treatment by NBs (the DI water group), the EEMs yielded two main peaks, Peak A (Ex/Em: 308–312/422–434 nm) and Peak B (Ex/Em: 254–260/430–446 nm), respectively. According to (Guo et al., 2014), Peak A and Peak B are largely attributed to humic-like materials and fulvic-like materials. The intensity of peak A (HA) decreased or disappeared after the treatment of NBs. This result may be due to more electron withdrawing groups such as phenolic groups and carboxylic in the HA structure upon the more hydrophobic environment and the protonation inside the compact HA matrix (Xiaoli, Guixiang, Xin, Yongxia, & Youcai, 2012). **Figure 4.9** shows that the concentrations of COD in soil extract varied significantly with NBs (e.g., CO_2, H_2 and O_2). The leached organic matter concentration was much higher in those soil extract after exposure to CO_2 and O_2 NBs than that for DI water ($p<0.05$).
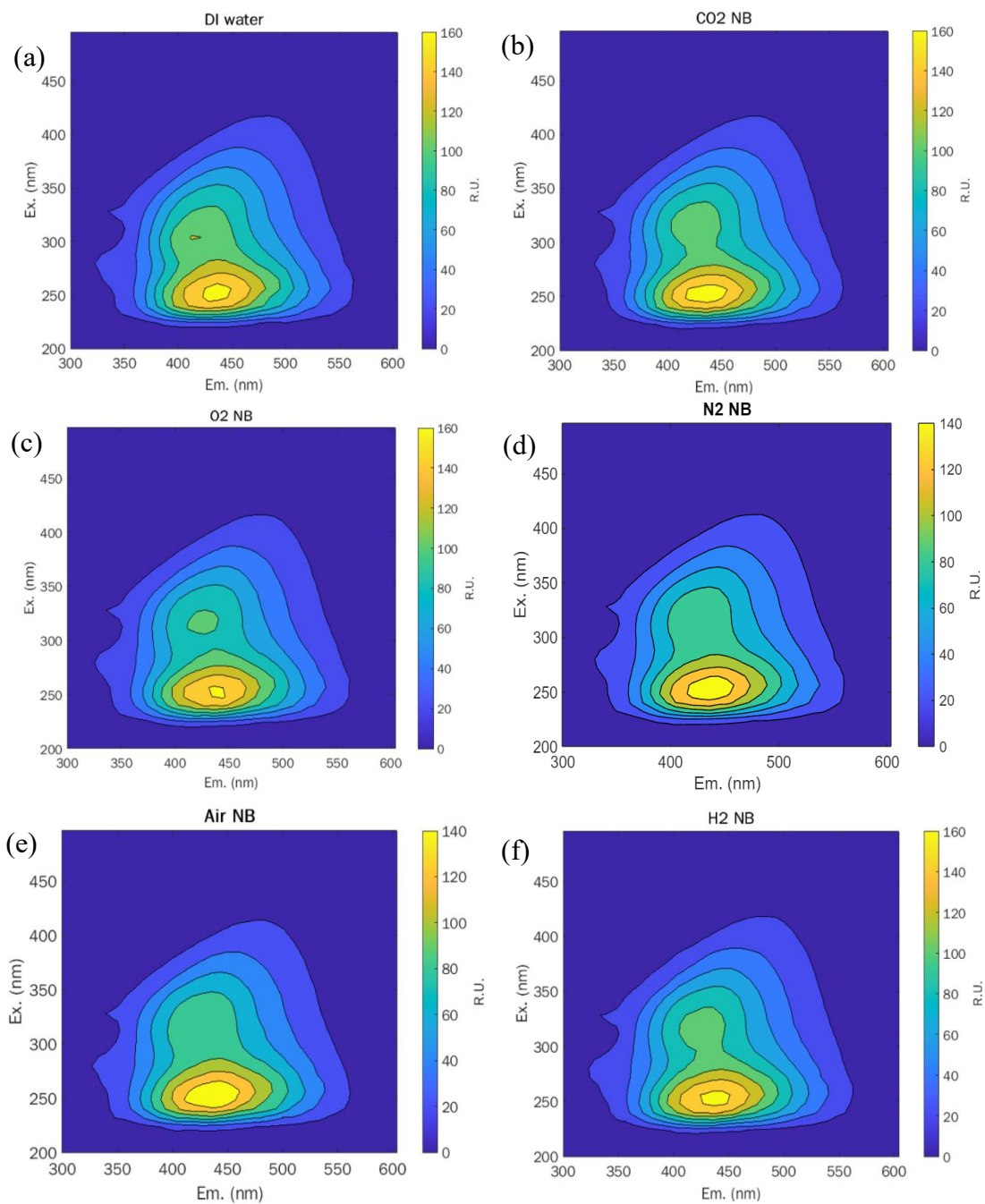
Figure 4.8 Excitation-emission matrix fluorescence spectra of soil extract after the application of (a) DI water, (b) CO_2 NBs water, (c) O_2 NBs water, (d) N_2 NBs water, (e) Air NBs water and (f) H_2 NBs water.

SOM contains a large number of reactive sites such as potentially cationic sulfhydryl (R-SH), anionic hydroxyls (R-OH), and aliphatic ($[-CH2-]_n$) moieties which are

the principally non-polar and un-charged regions of the soil (Thompson & Goyne, 2012). Non-polar and un-charged compounds do not combine with the polar water molecules effectively. However, when SOM contacts NBs, their hydrophobic interactions can be enhanced by the short-range van der Waals forces. Van der Waals forces are generated by resonating polarity fluctuations within the non-polar portions of sorbate and sorbent (Zaharia & Suteu, 2013). Frequent physical collisions from adsorption and desorption will result in the detachment of SOM from soil and partition into the aqueous phase with bubbles. For the SOM release in the presence of CO_2 NBs, the release could also be driven by other different mechanisms in addition to hydrophobic interactions. The CO_2 NBs treated soil was acidified to a low pH (5.5-5.6) and as the pH of the soil decreases, the carboxyl functional groups and SOM start to protonate and generate a positive surface charge ($Surf - H + H^+ \leftrightarrow Surf - H_2^+$). Thus, the negatively charged CO_2 NBs could attract the positively charged SOM from soil. For O_2 NBs, the enhanced release of organic matters might be attributed to the hydrophobic interactions, electrostatic attractions (with those positively charged moieties of SOM), and the additional minor oxidation of the soil organic matters with high levels of DO (~22 mg·L^{-1}).
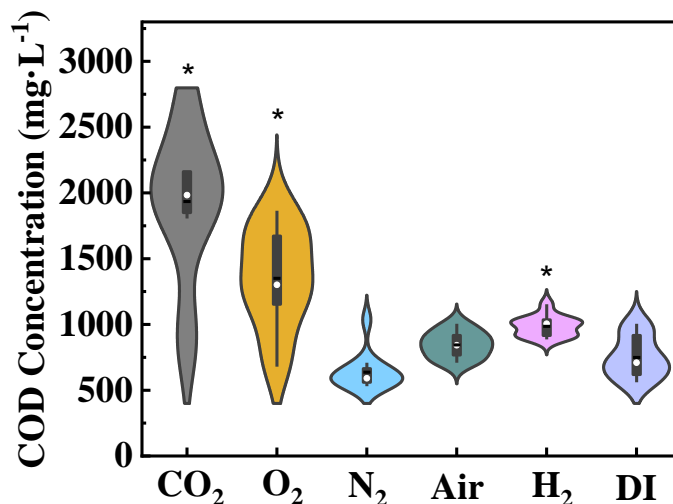
Figure 4.9 Comparison of COD concentration in soil extract. * indicates the difference between NBs water and DI water treated group is significant (p<0.05).

4.3.4 The relationships between the soil properties

Figure 4.10a plots the Pearson correlations between the measured chemical properties of soil. The color shifts from blue to red for data cells indicates the increased correlation strength. Eh and pH can affect the mobility of many nutrients in complex biological and chemical environments (Husson, 2013). For example, pH rendered significant negative correlations with Ca^{2+}, Mg^{2+}, PO_4^{3-} and COD ($p < 0.001$). Increased H^+ promoted Ca^{2+} and Mg^{2+} release from soil via a cation exchange (Cheng et al., 2010). Fe-P minerals could leach out free phosphate due to the reduction of Fe^{3+} as discussed above (Q. Chen et al., 2019). The release of Mg^{2+} has a significant positive correlation with the release of Ca^{2+} and K^+ ($p < 0.001$) as they always co-exist in soils (Khorshidi & Lu, 2017).
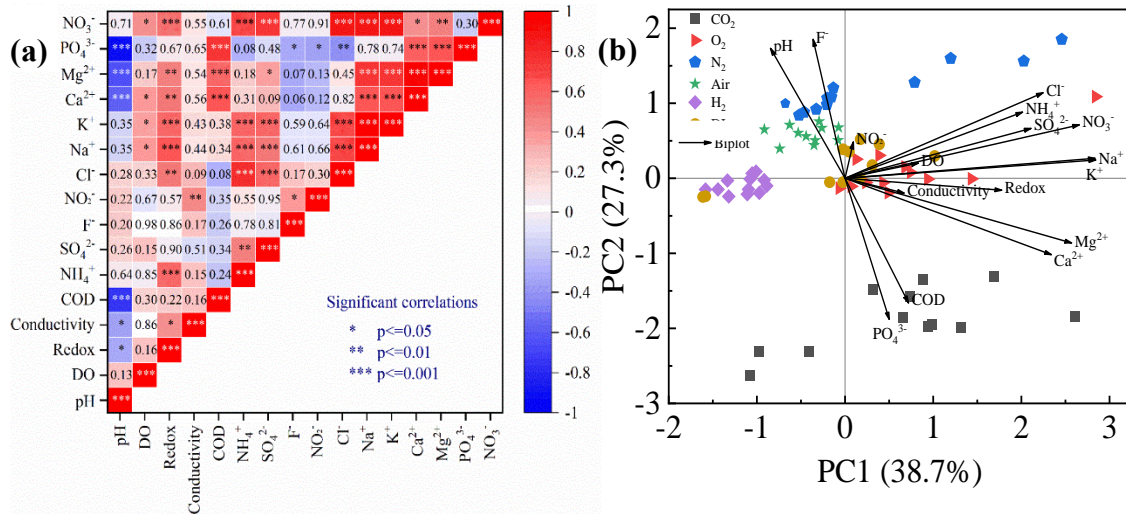
Figure 4.10 (a) Pearson correlations between water quality parameters (DO, ORP, pH and conductivity) and nutrient concentrations (K^+, Na^+, Mg^{2+}, Ca^{2+}, NH_4^+, Cl^-, NO_3^-, NO_2^-, SO_4^{2-}, PO_4^{3-}, F^- and COD) in soil extract. *p* values are shown in the square cells. (b) PCA of treatment performance patterns in five different NBs (CO_2, O_2, N_2, H_2, Air) and DI water treatment systems.

The redox level change shows significant positive correlations with the NH_4^+, NO_3^-, Na^+, K^+ ($p < 0.001$) and Ca^{2+}, Mg^{2+} and Cl^- ($p < 0.01$). In fact, K^+ and Na^+ solubility is not directly affected by Eh because these elements have only one possible redox number and they cannot exchange electrons (B. Wang et al., 2019). Thus, their release may be related to the sheering stress of NBs on soil. As both NO_3^- and NH_4^+ are soluble, Eh and pH variations can affect the dominant nitrogen forms that have different biological uptake for plants.

4.3.5 Discrimination of governing factors affecting nutrient release

PCA is an unsupervised clustering method that groups samples in a score plot based on the

similarities between samples (Huiling Zhang et al., 2018). There are 16 principal components (PCs) generated from the experimental data. **Table 4.2** shows the percentage of variance that each PC accounts for in the total variance around PCs and their cumulative percentages. The first two PCs, PC1 and PC2, account for 38.7% and 27.3% of variance, which represents up to 66% of the total variance. Thus, PC1 and PC2 could reflect most of the information of all original variables (e.g., pH, COD and Na^+) and were chosen for the discussions in PCA. **Figures 4.10(b)** shows the PCA plot that includes the loadings (arrows) and scores (dots) of the experimental data. An arrow with a greater projected length (large loading) on the axis of PC1 or PC2 indicates that the variable has a strong relationship to a particular PC. The dots represent samples taken from different treatment systems at different times.

Table 4.2 The Percentage of Variance and Cumulative Percentage of the 16 Identified PCs

	PC1	PC2	PC3	PC4	PC5	PC6	PC7	PC8
Variability (%)	38.68	27.25	10.52	7.51	6.18	3.18	1.86	1.81
Cumulative %	38.68	65.93	76.45	83.96	90.15	93.32	95.19	96.99
	PC9	PC10	PC11	PC12	PC13	PC14	PC15	PC16
Variability (%)	1.45	0.76	0.34	0.22	0.12	0.09	0.02	0.02
Cumulative %	98.44	99.20	99.54	99.76	99.88	99.97	99.98	100

The PCA plot shows the obvious group differences between the six NB-treated soils as indicated by the scattered distribution of data points of different colors, suggesting the ions release was dependent on the NBs type. The control group (dark yellow dots) are mainly located in the center of the coordinate. Some data from DI water and O_2 NBs treated

groups (red triangles) overlapped, which indicates that O_2 NBs treatment did not affect the ions release from soil. The data points (violet diamonds) for the H_2 NBs-treated soil are located on the negative side of PC1, whereas the variables of Cl^-, NH_4^+, SO_4^{2-}, NO_3^-, K^+, Ca^{2+}, Mg^{2+} and Na^+ have large positive loadings along the direction of PC1, which means these variables and PC1 are positively correlated. Thus, the H_2 NBs treated system and these variables are negatively related. In other words, H_2 NBs may inhibit these ions' release from soil because of the suppressed redox potential by H_2 as mentioned above. This is supported by that redox potential has a large positive loading on PC1 and thus is negatively correlated with the H_2 NBs treatment.

The air and N_2 NBs treated groups (green pentagrams and blue pentagons) are present on the positive direction of PC2. On the contrary, CO_2 NBs treatment system (black squares) are located in the negative direction of PC2. Moreover, the variable of F^- has a large positive loading on the PC2, whereas the variables of PO_4^{3-} and COD have large negative loadings on the PC2, which indicates the variables of PO_4^{3-} and COD are positively correlated with PC2 and negatively correlated with the variable of F^-. Such correlations agree with the above experimental observations that N_2 NBs and air NBs treatment systems led to high release of F- and low release of PO_4^{3-} and COD. Conversely, high CO_2 NBs caused high release of PO_4^{3-} and COD and low release of F^-. Because pH has a large positive loading along the direction of PC2, indicating that increasing the soil pH may increase the release of F^- and reduce the release of PO_4^{3-} and COD, which also are

in line with the results from subsections 4.3.3 and 4.3.4.

4.4 Conclusion

Spiking different types of gaseous NBs into soil induced complex interactions with soil substances and various impacts on soil characteristics. The changes of these soil properties may yield tremendous impacts or implications on soil fertility and plant growth, which deserves further investigations. In this study, the O_2 NBs did not affect the release of any tested cations and most anions. While, O_2 NBs could improve the organic fertilizer utilization by soil microbes that could indirectly supports the plant growth by increasing the plant-available N and P (Yuncheng Wu et al., 2019). Moreover, O_2 NBs could enhance O_2 delivery to soil and promote the aerobic respiration of plant and the ROS generations, which could activate plant proliferative pathways (S. Wang, Liu, Lyu, Pan, & Li, 2020). N_2 NBs seem to increase the soil nitrogen, which is the most limiting factor in the production of crop (Hassanein, Ahmed, & Zaki, 2018). Our study proved that N_2 NBs could promote the release of NH_4^+ and decrease the release of PO_4^{3-} from soil, which also agrees with a study showing nitrogen addition significantly decreased soil labile phosphorus (Jiang et al., 2019). CO_2 NBs could acidify the soil and may negatively affect plant growth. However, CO_2 NBs water irrigation may neutralize the alkaline soil such as Red mud (S. Patel, Pal, & Patel, 2018). Meanwhile, CO_2 NBs could improve the PO_4^{3-} release to enhance the plant growth as discussed above. H_2 could regulate the growth of plant root and increase the

plant resistance to abiotic stress, such as the Hg, Cd and Al (B. Wang et al., 2019), although H_2 NBs inhibited the release of common ions release from soil. Air NBs could increase some ions released from soil such as F^- and Cl^-, but the effect of air NBs on plant growth could be similar with O_2 and N_2 NBs. This study offers a new insight into the approach of NB water irrigation and its positive impacts on the soil properties and plant growth. Moreover, the results may also promote other novel engineering practices using NBs such as soil remediation or surface washing.

CHAPTER 5

UNVEILING THE POTENTIAL OF NANOBUBBLES IN WATER: IMPACTS ON TOMATO'S EARLY GROWTH AND SOIL PROPERTIES

5.1 Introduction

Recently, fine bubble water technologies demonstrated tremendously high potential in agricultural irrigation. Fine bubble water refers to the water that is suspended with microbubbles (MBs) and/or nanobubbles (NBs). MBs usually have diameters between 100 μm and 1 μm (Temesgen et al., 2017), while the diameters of NBs is less than 1 μm according to the Peclet number that describes the interplay of Brownian motion and buoyancy (Khaled Abdella Ahmed et al., 2018). NBs have unique properties that distinguish them from macro-bubble and MBs, including high mass transfer efficiency (Yasui et al., 2019a), high zeta potential, long stability in water (Neelkanth Nirmalkar et al., 2018) and ability to generate mild levels of hydroxyl radicals (•OH) when they collapse (S. Liu, S. Oshita, S. Kawabata, et al., 2016; Ushikubo et al., 2010). These characteristics offer many new possibilities in environmental and agricultural applications such as water treatment, remediation and irrigation.

It has been reported that the crop yields (Ying Wang, Wang, Sun, Dai, Zhang, Xiang, Hu, Li, et al., 2021), plant growth (Ahmed, Shi, et al., 2018; Yuncheng Wu et al., 2019) and seed germination (S. Liu, S. Oshita, Y. Makino, et al., 2016; M. Zhu et al., 2021) were increased by irrigation with water containing NBs. The mechanisms of plant growth

promotion can be attributed to several key factors. For example, when air or oxygen NB water is applied to the root zone of plants, the oxygen content within NBs will increase the soil oxygen and promote aerobic respiration in the roots, leading to increased energy production and enhanced metabolic activity. Improved oxygen supply stimulates root growth, active nutrient absorption, and the overall plant growth rate (Baram, Evans, Berezkin, & Ben-Hur, 2021; Y. Zhou, Li, et al., 2019b; Y. Zhou, Zhou, et al., 2019). Moreover, the presence of NBs can enhance nutrient availability and uptake by plants as a carrier that mobilizes soil nutrients and transports them to the root zone of plants. Our recent study also indicated that the negatively charged surface of NBs may immobilize the soil cations or anions via ion exchange with H^+ and OH^- and thus could strip off the surface nutrient ions (e.g., NH_4^+, K^+, and Mg^{2+}) from soil and increase bioavailability (Ying Wang, Wang, Sun, Dai, Zhang, Xiang, Hu, Li, et al., 2021; Yuncheng Wu et al., 2019; Xue, Marhaba, & Zhang, 2022). Other studies attributed the enhanced plant growth to the root zone modification, as the soil microbiome community and activities may be changed by NBs (Weijie Chen et al., 2023; Y. Zhou et al., 2020). Despite the advances in this field, there are still many elusive mechanisms associated with the effects of NBs on soil-based plant growth. For example, enzyme activity in soil that directly influences biochemical processes of soil nutrients and the NBs-produced reactive oxygen species (ROS) in plants are still poorly studied. Moreover, the soil chemical properties changes such as dissolved organic matter (DOM) which could assist in transferring nutrients from the soil to the plant

also deserves investigations. Thus, a systematic investigation of the interactions between NBs, soil, and plant is imperative for better understanding of the syncretistic effects of NBs in water irrigation.

This study investigated the impacts of irrigation water containing oxygen NBs (ONBs) and nitrogen NBs (NNBs) on seed germination and tomato's early stage growth, as ONBs could enhance oxygen delivery to soil and promote the aerobic respiration (S. Wang, Y. Liu, T. Lyu, et al., 2020) and NNBs was expected to increase the soil nitrogen and support plant growth (Hassanein et al., 2018). The influences of irrigation frequency and dissolved oxygen (DO) concentration were also studied. Furthermore, the key enzyme activities such as superoxidase dismutase (SOD), peroxidase and catalase were measured in the affected plant and soil samples. To probe the activities of the plant root, we employed an electrochemical impedance method to monitor the interfacial electric properties during the tomatoes root growth as we irrigated the soil with different kinds of NB water. Ultimately, this study provides insights into the mechanisms underlying the observed effects of NBs on plant growth as well as the potential benefits of using ONB and NNB for promoting plant growth and improving soil health.

5.2 Materials and Methods

5.2.1. NB water preparation

The water suspension of the two types of NBs was generated by our previously reported method of membrane bubbling (Ahmed, Sun, et al., 2018). Briefly, a ceramic tubular membrane with diameter of 10 mm and length of 250 mm (140 nm pore size, Sterlitech, USA) with hydrophobic coating was used to dispense the high-pressure (60 psi) gas (i.e., pure oxygen or nitrogen) into the tap water that flew through the membrane module using a water pump (model 75211-70, Cole Parmer, USA)   (Ahmed, Sun, et al., 2018; Khaled Abdella Ahmed et al., 2018). The tap water was placed at room temperature for 24 h to remove any free residual chlorine before using for the generation of NBs. The resulting concentration of NBs in water was $4{\sim}6{\times}10^8$ mL^{-1} as measured by NTA (NanoSight NS300, Malvern Panalytical Ltd, UK) (X. Shi et al., 2021). In differentiating the effects of DO and NBs, the prepared NB water was diluted about 50 times by tap water to reach the similar DO level (9 mg·L^{-1}) with tap water. The size distribution and zeta potential of NBs in tap water were measured by Zetasizer (Nano ZS, Malvern Panalytical Ltd, UK).

5.2.2 Plant growth conditions

The potting soil (Miracle-Gro) for plant growth was loamy sand (predominantly sand with some silt and clay). The large clumps were removed from the soil to minimize substrate

variability. The polypropylene plastic pots with size of 13 cm/13 cm/15 cm (length/width/height) were filled with soil (850 g dry weight) and the bulk density was 1.0 g·cm^{-3}, which is considered as appropriate for plant growth.(USDA, 2012) The bottom of the pot has 8 drainage holes (12 mm in diameter) for water drainage.

Following our published paper and others (Ahmed, Shi, et al., 2018; Yuncheng Wu et al., 2019; Y. Zhou, Li, et al., 2019b; Y. Zhou, Zhou, et al., 2019), tomato (Dwarf Heirloom) was chosen in this study as the test plant due to its relatively fast growth and simple assessment. The tomato seeds were first disinfected by 10% H_2O_2 solution for 15 min and rigorously rinsed with sterile deionized (DI) water (Peng et al., 2018; Peng et al., 2020). The sterile seeds were soaked in DI water for 6 h, and then sown in the plastic pot soil at a depth of 1 cm in a greenhouse as shown in **Figure 5.1**. These soil pots were placed on top of a seedling heat mat (model 39401, VIVOSUN, USA) to keep a steady temperature (20-25°C). During germination, the soil was irrigated with different NB water (80 mL per pot) every two days to keep it moist. After seeds germination, the plants were illuminated by simulated natural sunlight (380 nm~800 nm) with LED grow lights (ddn-120, H-AM, USA) for 12 hours every day (Peng et al., 2018). In addition, the relative humidity in the greenhouse was kept at 60-75%. The control group was irrigated with tap water, while the treatment groups were irrigated with different NB water (ONB and NNB). **Table 5.1** shows the experimental design, where a 2×2 factorial design was performed to evaluate the effects of DO or NBs concentration and irrigation frequency (i.e., once every 2 days and once

every 4 days) with a total of 4 groups per treatment. Twelve replicates of each treatment were included (4 plants per pot). Since the potting soil was rich with growth nutrients, no additional nutrients were added during the test period.
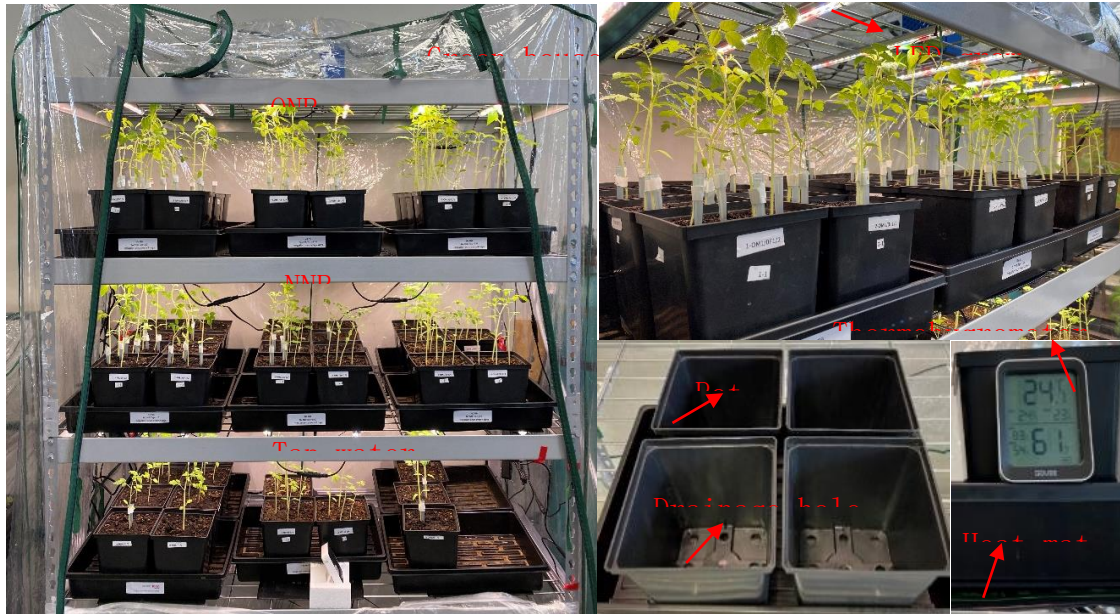
Figure 5.1 Photo of lab-scale plant culture experiment.

Table 5.1 Experimental Design of Irrigation Conditions

Mixing volumetric ratio (NB water : tap water)	Irrigation frequency (day)	Treatment name for NNBs	Treatment name for ONBs
1:0	2/4	NNB0	ONB0
1:50	2/4	NNB50	ONB50
0:1	2/4	Tap water	

5.2.3 Growth characteristics of tomato plants under influences of NBs

5.2.3.1 Plant stem and leaves   The diameter and height of individual plant stems and leaves number were measured every week from Day 11. The digital vernier caliper

(0.01-mm precision) was used for measuring the diameter of the stem (3 cm above the ground). After 32 days, seedlings were harvested, and all plants were taken out of the pot and their fresh weights were recorded after proper removal of the attached soil.

5.2.3.2 Determination of antioxidant enzymatic activity in plant leaves   To obtain a fine powder, 100 mg of freshly harvested plant leaves were pulverized with liquid nitrogen using a mortar and pestle. The powder was then transferred to 2 mL tubes, and 1 mL of cold phosphate buffer (0.1 M, pH 7.4) was also added. After vortexing for 1 minute, the tubes were centrifuged at 10000×g and 4°C for 20 minutes, with the resulting supernatant used for three enzyme measurements as outlined in detail below. Specifically, SOD activities were measured using a SOD Assay Kit-WST (Dojindo, Kumamoto, Japan), peroxidase activity was measured using a Peroxidase Activity Assay Kit (Sigma Aldrich, USA) (S. Liu et al., 2017) and soluble proteins were quantified with a Pierce™ BCA Protein Assay Kit (Thermo scientific, USA).

SOD assay: Briefly, add 20 µL of sample solution to each sample well (96-well microplate) and blank 2 well, and add 20 µL of DI water to each blank 1 and blank 3 well. Next, a WST working solution was made of (2-(4-Iodophenyl)-3-(4-nitrophenyl)-5-(2,4-disulfophenyl)-2H-tetrazolium, monosodium salt was added to each well and mixed gently by pipette. Then, add 20 µl of dilution buffer to each blank 2 and blank 3 well and add 20 µl of enzyme working solution to each sample and blank 1 well and mix thoroughly as shown in **Table 5.2**. Incubate the plate at 37°C for 20 min and read the absorbance at 450

nm using a microplate reader. To calculate the SOD activity, use the following formula

Equation (5.1):

$$SOD\ activity\ (\%) = \frac{(A_{blank1} - A_{blank3}) - (A_{sample} - A_{blank2})}{A_{blank1} - A_{blank3}} \times 100 \tag{5.1}$$

Table 5.2 Solution and Buffer Volumes in Each Well

	Sample	Blank 1	Blank 2	Blank 3
Sample solution	20 µL	-	20 µL	-
DI water	-	20 µL	-	20 µL
WST Working Solution	200 µL	200 µL	200 µL	200 µL
Dilution Buffer	-	-	20 µL	20 µL
Enzyme Working Solution	20 µL	20 µL	-	-

For the enzyme working solution, centrifuge the enzyme solution tube for 5 s, mix by pipetting, and dilute 15 µl of enzyme solution with 2.5 ml of dilution buffer. The WST working solution, enzyme working solution, buffer solution and dilution buffer were provided within the Assay Kit.

Peroxidase Activity Assay: To prepare the standard curve, first dilute the H_2O_2 substrate solution to 0.1 mM by adding 10 µL of the 12.5 mM H_2O_2 substrate solution to 1240 µL of assay buffer. Mix the solution well and add 0, 10, 20, 30, 40, and 50 µL into a series of wells (96-well microplate) in duplicate. Then, adjust the final volume to 50 µL with assay buffer to generate 0, 1, 2, 3, 4, and 5 nmol/well of H_2O_2 standard. To measure the standard curve, dilute the HRP positive control solution 1:199 in assay buffer and prepare a total of 50 µL reaction mix by mixing 2 µL of OxiRed Probe with 48 µL of HRP positive control solution. Mix the solution well and incubate it for 5 minutes before

128

measuring the OD at 570 nm in a microplate reader. To prepare the positive control, add 1 µL of the diluted positive control solution into the desired well(s) and adjust the final volume to 50 µL with Assay Buffer.

For each well, prepare a total 50 µL Reaction Mix: 46 µL Assay Buffer, 2 µL OxiRed Probe solution, 2 µL H_2O_2 substrate solution. Add 50 µL of the Reaction Mix to each test sample (50 µL), mix well, and incubate the mix for 3 minutes at 37°C. Measure OD at 570 nm (A0). Then, incubate the reaction mix for another 30 minutes to 2 hours at 37°C and measure OD at 570 nm (A1) again. To calculate the peroxidase activity of the test samples, use $\Delta A = A1 - A0$, and apply the ΔA to the H_2O_2 Standard Curve to determine B nmol of H_2O_2 generated by peroxidase in the given time. The peroxidase activity is calculated as $B/(T \times V) \times$ Sample Dilution Factor $= nmol \cdot min^{-1} \cdot mL^{-1} = mU \cdot mL^{-1}$, where T is the time incubated, V is the sample volume added into the reaction well, and one unit of peroxidase is defined as the amount of enzyme that will oxidize 1.0 µmol of H_2O_2 per minute at 37°C.

Soluble proteins: To perform the protein assay, pipette 25 µL of each standard or unknown sample replicate into a microplate well with a working range of 20–2000 $µg \cdot mL^{-1}$. Next, add 200 µL of the working reagent to each well and mix the plate thoroughly on a plate shaker for 30 seconds. Cover the plate and incubate it at 37°C for 30 minutes. After incubation, cool the plate to room temperature and measure the absorbance at or near 562 nm on a plate reader. Subtract the average 562 nm absorbance measurement of the Blank

standard replicates from the 562 nm measurements of all other individual standard and

unknown sample replicates. Then, prepare a standard curve by plotting the average Blank-

corrected 562 nm measurement for each BSA standard versus its concentration in $\mu g \cdot mL^{-1}$. Finally, use the standard curve to determine the protein concentration of each unknown

sample. The working reagent was prepared by mixing 50 parts of BCA Reagent A with 1

part of BCA Reagent B (50:1, Reagent A: B).

The following **Table 5.3** was used as a guide to prepare a set of protein standards.

The concentration of the albumin (BSA) stock solution is 2 $mg \cdot mL^{-1}$.

Table 5.3 Preparation of Diluted BSA Standards

Vial	Volume of Dilute (μL)	Volume and Source of BSA (μL)	Final BCA Concentration ($\mu g \cdot mL^{-1}$)
A	0	300 of Stock	2000
B	125	375 of Stock	1500
C	325	325 of Stock	1000
D	175	175 of vial B dilution	750
E	325	325 of vial C dilution	500
F	325	325 of vial E dilution	250
G	325	325 of vial F dilution	125
H	400	100 of vial G dilution	25
I	400	0	0=blank

5.2.3.3 Determination of total chlorophyll content   Fresh leaves weighing about 50

mg were cut into small pieces and soaked in 10 mL of 95% (v/v) ethanol to extract

chlorophyll. The samples were then placed in the dark and left to incubate for three days

before measuring the absorbance of the supernatant at 665 and 649 nm using a fluorescence

spectrophotometer (FL4500, Hitachi, Japan). Total chlorophyll was calculated by Chla =

13.36A665 − 5.19A649, Chlb = 27.43A649− 8.12A665, and total chlorophyll = Chla +

Chlb (Shang et al., 2021).

5.2.3.4 Analysis of root growth by impedance spectroscopy   The electrochemical

impedance spectrometry (EIS) measurement platform using a two-electrode configuration,

where a platinum (Pt) wire was inserted into the bottom of the plant's stem at 2 cm above

the root–soil junction and used as the working electrode to enable electric charge transfer

(**Figure 5.2**). The graphite column (15 cm in length, 2 mm in diameter) was inserted 12.5

cm deep into potting soil and used both as the counter electrode and the reference electrode.

Before the EIS test, the soil was irrigated thoroughly with the appropriate amount of tap or

NB water   (e.g., 80 mL per pot) and then measured at the open circuit potential (OCP)

using frequencies ranging from 10^4 to 0.1 Hz and a potential amplitude of 5 mV (Y. Liu et

al., 2021; Ozier-Lafontaine & Bajazet, 2005a). The increase in applied frequency in EIS

from 0.1 to 10^4 Hz resulted in the opening of all ion channels, enabling the passage of

current through the cell membranes (Y. Liu et al., 2021). As a consequence, the total

impedance produced could integrate and exhibit the electrochemical characteristics of the

extracellular fluid, apoplast, cytoplasm, and membrane (Ehosioke et al., 2020). The plant

electrode may cause cracks at the insertion point of the stem that resulted in unreliable

measurements, thus 5 plants per treantment condition were prepared at different

development stages (31, 41, and 49 days) as shown in **Table 5.4**, which were tested for the

EIS measurement.
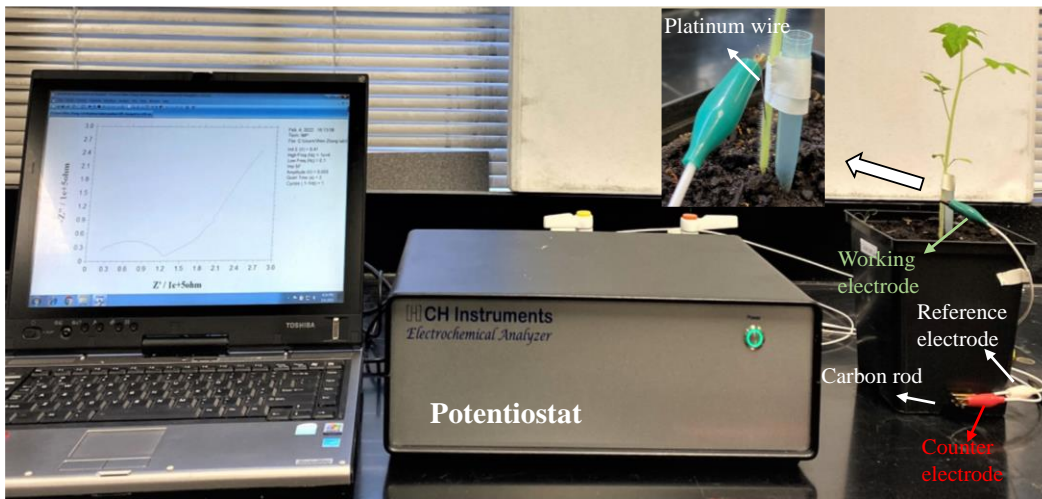
Figure 5.2 The photo of the EIS measurement of plant.

Table 5.4 EIS Experiment Arrangement

Growth days	Treatment name for NBs	Plant Number or quantity
	ONB0	5
	ONB50	5
31, 41, and 49 days	NNB0	5
	NNB50	5
	Tap	5

5.2.3.4 Surface functional groups of plant roots   To investigate NBs effects on the

functional groups of plant roots, the air-dried roots were analyzed by attenuated total

reflectance-Fourier transform infrared spectroscopy (ATR-FTIR) using an FTIR

spectrometer (Cary 670, Agilent Technologies, USA) equipped with an ATR diamond crystal (Lu et al., 2020). Prior to ATR-FTIR analysis, the whole roots of plants were evenly placed on the ATR diamond crystal. A spectral range of 400-4000 cm^{-1} was used with a resolution of 4 cm^{-1}, and 32 scans were performed. All spectra resulted from 16 scans (Savassa et al., 2021).

5.2.4 Soil chemical properties and enzymatic activity under influences of NBs

5.2.4.1 Soil chemical properties   After 32 days of irrigation, about 20 g of the soil near the roots were collected, air-dried, crushed and then passed through a 2-mm mesh (L. Chen et al., 2022). The soil electrical conductivity (water: air-dried soil = 5:1) (v/wt) was measured using a conductivity sensor (PS-321, PASCO, USA) (M. Zhu et al., 2021). The pH of the air-dried soil that was mixed in DI water in a 1:2.5 (v/wt) ratio was measured by a pH sensor (PS-2102, PASCO, USA) (L. Chen et al., 2022; D. Shen et al., 2018). DOM was extracted from 10 g air-dried soil using 100 ml DI water by continuously shaking for 24 h at room temperature (20°C). After centrifugation at 7000×g for 10 minutes, the extracts were immediately passed through a 0.45-μm filter membrane. The filtered solutions were stored in sterilized amber glasses at 4 °C prior to additional analysis (X.-q. Qin et al., 2020). The measurement of dissolved organic carbon (DOC) was conducted using a total organic carbon (TOC) analyzer (TOC-L, Shimadzu Corporation, Japan).

To analyze the impacts of NB water on DOMs, fluorescence regional integration

(FRI), a quantitative technique in excitation-emission regions in excitation/emission matrix (EEM), was used to quantitatively analyze the configuration and heterogeneity of DOM from the treated soil leachate after irrigation with proper filtration (0.45-µm pore size nylon membrane filter, Whatman, USA) to remove the soil dirt and retain DOM in the filtrate (Wen Chen, Westerhoff, Leenheer, & Booksh, 2003; Yulai Wang, Hu, Yang, Wang, & Jiang, 2019; Wenming et al., 2017). The fluorescent spectrophotometer (FL4500, Hitachi, Japan) was utilized to conduct EEM spectral measurements of the samples at intervals of 8 nm for emission (Em) wavelengths from 300-600 nm and excitation (Ex) wavelengths from 200-500 nm in 3D spectrum mode. To prevent inner filter effects, sample dilution with DI water at a ratio of 1:10 was done in instances where their maximum absorbance exceeded 0.1 nm. Elimination of water Raman scattering in sample spectra was achieved by subtracting the DI water spectrum (X.-q. Qin et al., 2020). Then, the EEM spectra were sorted into five distinct regions, labeled as Region I-V. Region I (Ex/Em: 200-250/250-330 nm) pertains to aromatic proteins, specifically those that resemble tyrosine-like materials. Region II (Ex/Em: 200-250/330-380 nm) relates to tryptophan-like materials. Regions III to V, on the other hand, are associated with different substances - fulvic-like materials (Region III; Ex/Em 200-250/380-550 nm), soluble microbial byproduct-like substances (Region IV; Ex/Em 250-450/250-380 nm), and humic-like materials (Region V; Ex/Em 250-450/380-550 nm) in that order (Wen Chen et al., 2003; F. Song et al., 2018).

5.2.4.2 Rhizosphere soil enzymatic activity   To assess soil enzymatic activity changes

upon treatment by nanobubbles, two selected soil enzymes, urease and catalase, were measured for the rhizosphere soils, which were collected, air-dried, crushed and then passed through a 2-mm mesh. Urease and catalase were measured with a Urease Activity Assay Kit (Sigma Aldrich, USA) and Johnson and Temple method (del Carmen Cuevas-Díaz et al., 2017a), which are detailed below.

Urease assay: The urease was tested with urease activity assay kit (Sigma Aldrich, USA). For the determination of soil urease activity, a 0.5 g soil sample was suspended in 10 mL sodium phosphate buffer (10 mM, pH 7.0). Supernatant containing urease was obtained by centrifugation at $14,000 \times g$ for 5 min. In this assay, urease catalyzed the hydrolysis of urea resulting in the production of ammonia. The ammonia was determined by the Berthelot method resulting in colorimetric product measure at 670 nm, proportionate to the urease activity present in the sample. One unit of urease is the amount of enzyme that catalyzes the formation of 1.0 μmol ammonia per minute at pH 7.0.

Soil catalase assay: 40 mL of DI water was added to 1 g of soil and shaken for 30 min, then 5 mL of 0.3% H_2O_2 in distilled water was added and shaken for 30 min at 20 °C, followed by the addition of 5 mL of 1.5 M H_2SO_4 to stop the enzymatic activity. The solution was filtered by Whatman no. 42 filter paper and a 25 mL aliquot was evaluated with 0.01 M $KMnO_4$. Control tests were processed in the same manner as the samples but the 5 mL of H_2O_2 was replaced by DI water. A blank was conducted with a mix of 40 mL of DI water, 5 mL of H_2O_2, and 5 mL of 1.5 M H_2SO_4, and 25 mL of this mixture was

evaluated with $KMnO_4$. The assay was carried out in triplicate for each sample. The CAT activity was expressed as μmol of H_2O_2 oxidized per hour per gram of dry soil (del Carmen Cuevas-Díaz et al., 2017b).

5.2.5 Viability of rhizobacteria in the plant root

The viability of rhizobacteria near the plant root was analyzed by nuclear staining with acridine orange (Bouranis, Chorianopoulou, Siyiannis, Protonotarios, & Hawkesford, 2003). Several plants were randomly chosen. The root-attached soil was washed with distilled water. Samples were pre-incubated in 0.1 M phosphate buffer (0.1 M, pH 6) for 5 min at room temperature, then incubated in acridine orange at a final concentration of 1.6 mM in the previously mentioned phosphate buffer for 20 min at 25 ^{o}C and rinsed by buffer (Bouranis et al., 2003). The observation was performed under a confocal laser scanning microscope (Leica, TCS SP8 MP) equipped with LAS X software, using water lens with 40X magnification. The roots were fixed between the slide and cover slip. The excitation wavelength (beam splitter) was 488 nm, and the emission wavelengths were between 500 and 530 nm for the green image (DNA-bound acridine orange) and higher than 600 nm for the red image (RNA-bound acridine orange) (van Aarle et al., 2007).

5.2.6 Assessment microbial community in rhizosphere soil

A total of 40 soil samples were collected (4 replicates per treatment). Each sample was a

composite sample containing soil directly collected from the rhizosphere of 3 plants. The original soil (before planting use or exposure to nanobubbles) was also prepared as the control group at time 0. Soil samples were preserved by DMSO-salt solution (i.e., 6 mL DMSO-salt solution for 2 g soil). The soil samples with ice packs were immediately shipped overnight from NJIT to the laboratory at the University of Michigan for microbial community analysis.

For the microbial DNA analysis, 16S rRNA gene sequencing was performed on the microbial DNA to examine changes in the soil microbial community composition and diversity. Data quality control was done using mothur (v. 1.48.0)(Schloss et al., 2009). Each sample had reads between 3825 and 8317, which were classified into 13,678 operational taxonomic units (OTUs) using SILVA (v. 138) for sequence alignment and with 97% sequence similarity. The data was filtered by removing OTUs that had fewer than 3 reads across all samples, then rarefied to achieve the same read depth across all samples. After filtering, each sample had 3693 reads spanning 7241 OTUs.

5.2.7 Statistical analysis

Each set of trials was done in triplicate to obtain the mean and standard deviation (SD) as the error bars. One-way ANOVA (*t*-test, two sided, a significance level $\alpha = 0.05$) was used to confirm the significant differences between different groups in plant growth or enzyme activities. Species richness (operational taxonomic units, or OTUs) and Shannon index (H')

were calculated to assess the within-sample biodiversity (alpha diversity) of the bacterial communities. The Shannon index was calculated by $H' = -\sum p_i \ln p_i$, where p_i is the proportion of clones in the ith OUT (Hill, Walsh, Harris, & Moffett, 2003). Differences in community structure between samples (beta diversity) were analyzed by Principal Coordinates Analysis (PCoA) and analysis of molecular variance (AMOVA) using mothur, an open-source, platform-independent, community-supported software for describing and comparing microbial communities (Schloss et al., 2009).

5.3 Results and Discussions

5.3.1 Characterization of NBs in tap water

Figure 5.3(a) shows the bubble size distribution of ONBs and NNBs dispersed in tap water. The size distribution for the ONBs (200–400 nm) and NNBs (200-600 nm) was slightly different probably due to their different surface charges or surface tension that stabilize the bubble/water interface (Khaled Abdella Ahmed et al., 2018). The bubble sizes became larger after diluting 50 times (or diluted to 2% of their original concentrations) with tap water. The size distribution of NNB became slightly broader after dilution, which could result from the dissolution of NBs, coalescence and the formation of larger bubbles (Xue, Zhang, et al., 2022). However, the ONBs had a similar broadened size distribution after dilution, which is less significant than NNBs. The size distribution of NBs in aqueous

solution largely depends on the dispersion and bubble formation or characteristics such as the water-gas interface surface tension. It is suspected that the potential coalescence and the formation of larger bubbles were more significant for NNBs than ONBs, which is why a larger broader bubble size range occurred to NNBs. The freshly prepared suspensions of ONB and NNB had concentrations around 4–6×10^8 bubbles·mL^{-1} under a room temperature. The concentrations of NBs in diluted suspensions were reduced to 0.8-1.2×10^7 bubbles·mL^{-1}, which is proportional to the dilution factor as we reported previously (X. Shi et al., 2021; Xue, Zhang, et al., 2022).

Figure 5.3(b) shows that ONBs significantly increase the DO level up to 25 mg·L^{-1} in tap water. By contrast, the DO levels were suppressed by NNBs to approximately 2 mg·L^{-1}. Meanwhile, the DO concentrations of these two diluted NB waters (ONB50 and NNB50) were around 9 mg·L^{-1} after dilution with tap water. Therefore, these two groups (ONB50 and NNB50) can be used as control groups to compare the effect of NBs only without the influence of DO differences. **Figure 5.3(b)** also shows the zeta potentials of any background colloidal particles and two kinds of NBs in tap water, which were from -0.5 to -0.8 mV. ONBs and NNBs were reported to have higher zeta potentials (-20 to -30 mV) in DI water (Khaled Abdella Ahmed et al., 2018). The reduced negative surface charge of NBs in tap water may be attributed to the presence of salinity or dissolved solid in tap water that may compress the electric double layer and neutralize surface charges (Meegoda et al., 2019).
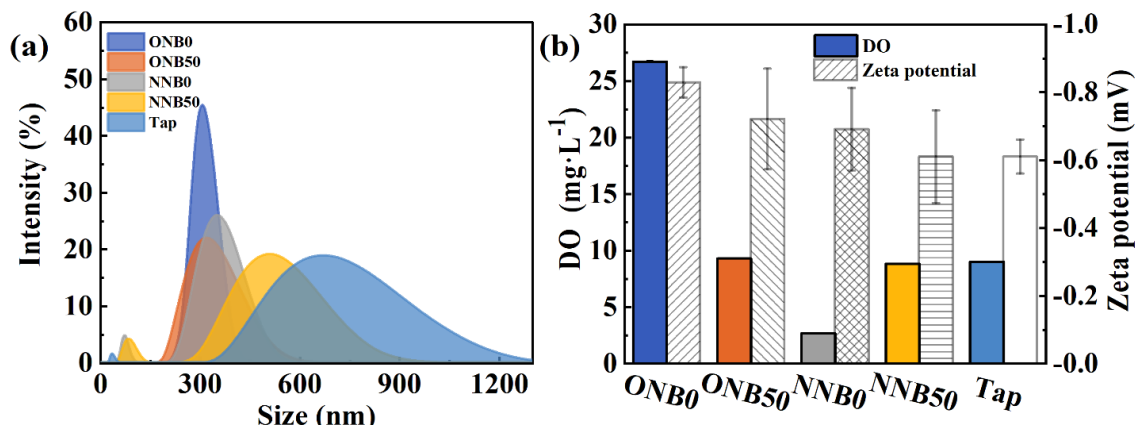
Figure 5.3 (a) The size distribution and (b) DO concentration and zeta potential of ONBs and NNBs in tap water.

5.3.2 Impacts of NBs on tomato growth and root properties

5.3.2.1 Assessment of the seed germination rates Figure 5.4(a) shows that the tomato seeds reached a germination rate of 14.7% and 5.9% on day 5 irrigated by NNB50 and ONB0 as indicated by the visible cotyledon and hypocotyl formation. The seeds in other treatment groups appeared to germinate at slightly lower rates. On day 7, the germination rates with ONB0, ONB50 and NNB50 irrigation were 53-59%, about 10% higher than that irrigated with tap water. The initial promotion of NBs on the tomato seed germination is largely attributed to the formation of ROS in seeds (Ahmed, Shi, et al., 2018; X. Sun, Chen, Fan, Liu, & Kamruzzaman, 2022). As reported by (S. Liu et al., 2017), the introduction of exogenous ROS, such as H_2O_2 and NBs, in the water can stimulate the endogenous production of ROS in barley seeds. However, after day 8, the groups treated by tap water demonstrated higher germination rates that eventually caught up with the rates of other NBs-treated groups. After 14 days, nearly 100% of the seeds germinated for all the

treatment groups. This is probably because the soil that was irrigated with tap water also garnered the optimal condition (e.g., moisture, nutrient, temperature, and oxygen) for seed germination. However, the sprouting parts of the tomato seeds irrigated by ONB water were considerably larger than those in the other groups as shown in **Figure 5.4(b)**. By contrast, NNB0 did not promote seed germination compared to tap water or NNB50, suggesting a high concentration of NNBs did not promote seed germination and instead a diluted NNB suspension seems to facilitate germination. That is because seed germination requires oxygen to carry out cellular respiration, which provides the energy needed for germination and growth. During germination, the embryo inside the seed begins to metabolize the stored nutrients and consumes oxygen (Corbineau & Come, 2017). High concentrations of NNBs in water (NNB0) suppressed the DO level ($2 \text{ mg} \cdot \text{L}^{-1}$) and thus inhibited seed germination.
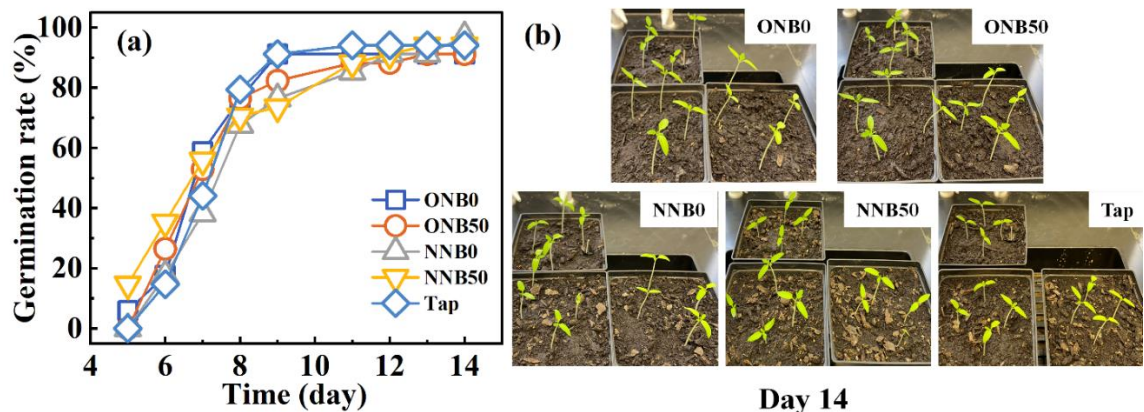
Figure 5.4 Effect of irrigation of different NB water on the germination of tomato. Note: There were 34 seeds in each treatment group.

5.3.2.2 Assessment of tomato growth   The tomato growth characteristics were

assessed after irrigation with NB water every 2 or 4 days. **Figure 5.5** and **Figure 5.6** show that the ONB significantly improved the tomato growth as indicated by the higher levels of leaves number, plant height, stem diameter and fresh weight on day 32. Compared to the tap water group, the growth rates for different plant parts increased by 30%-50% (e.g., height and stem diameter). However, NNB had less significant promotion on plant growth than ONB did. Because the quantity of •OH radicals generated by NNBs is less pronounced than that by ONBs (Ahmed, Shi, et al., 2018). Moreover, both ONB and NNB treatment groups yielded no significant improvements at the early stage of plant growth (before day 18). **Figure 5.5(d)** also indicates that the total chlorophyll content in tomato leaves were similar in all treatment groups, indicating that the chlorophyll content was not affected by NBs in irrigated water. In addition, the irrigation frequency (irrigated once every 2 or 4 days) in this research didn't influence the plant growth.

Although the initial concentration of DO in ONB50 was the same as that in tap water, the growth (e.g., height and diameter) of tomato plant under diluted ONB water irrigation was still better than the control groups (higher by 10% to 50% at different growth stage). This result rules out the influence of the initial DO concentration and highlights the importance of ONBs or bubble-related influences such as the ROS signaling effects on cell wall loosening and cell elongation (S. Liu et al., 2017). Many previous studies reported that ONBs promoted the growth of various plants (e.g., soybean, rice, tomato and maize) (Ahmed, Shi, et al., 2018; Ebina et al., 2013b; Ying Wang, Wang, Sun, Dai, Zhang, Xiang,

Hu, Li, et al., 2021; Y. Zhou, Li, et al., 2019b). The observed promotion is largely attributed to the slow release of oxygen from the ONBs and diffusion to the rhizosphere, which boosts up the activity of rhizosphere bacteria (Yuncheng Wu et al., 2019; Y. Zhou, Li, et al., 2019b; Y. Zhou, Zhou, et al., 2019), and thus enhances plant growth (Ying Wang, Wang, Sun, Dai, Zhang, Xiang, Hu, Hu, et al., 2021). However, our result indicates that high oxygen content when using the original ONB0 at 25 mg·L^{-1} was not beneficial for tomato growth, probably because excessive DO may elevate the ROS-induced stress and trigger plant senescence as reported elsewhere (S. Wang, Y. Liu, P. Li, et al., 2020).
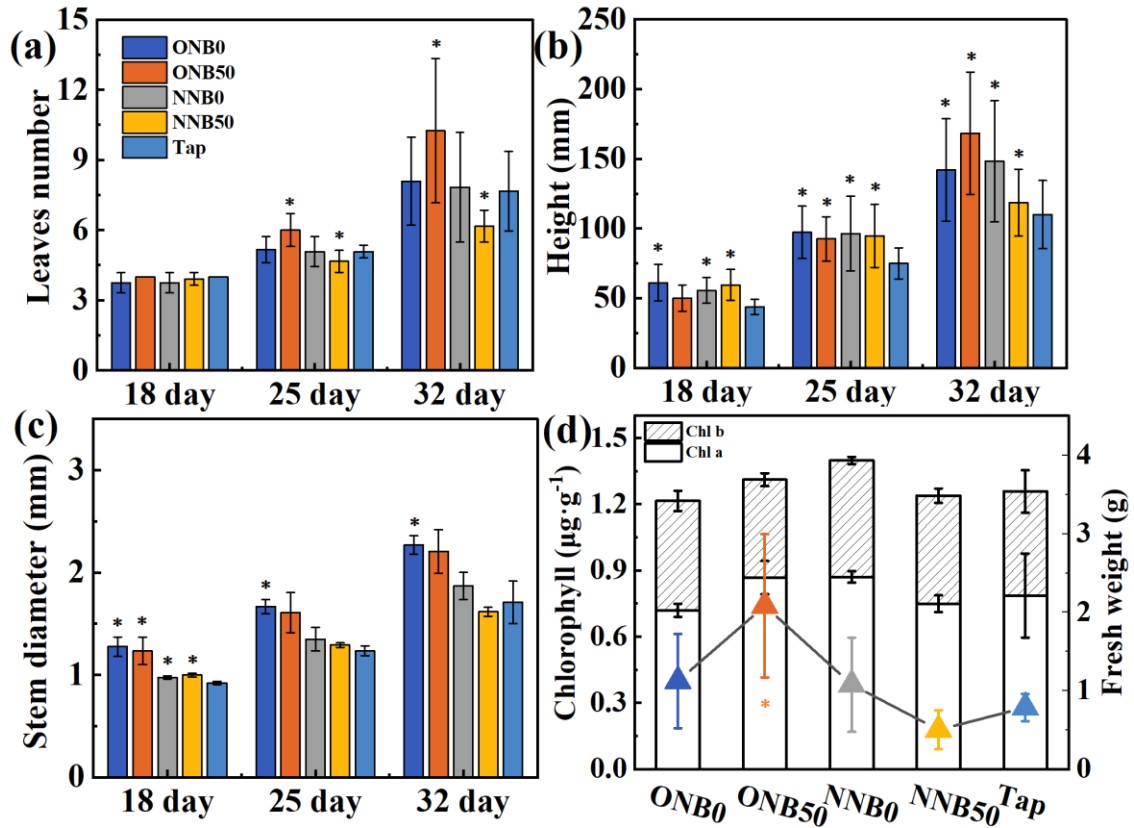
Figure 5.5 Growth characteristics of different tomato plant parts irrigated with different NB water (80 ml per pot every 2 days). (a) leaves number, (b) plant height, (c) steam diameter, (d) fresh weight and total chlorophyll content. The * indicates a significant difference between NB treatment group and tap water ($p < 0.05$).
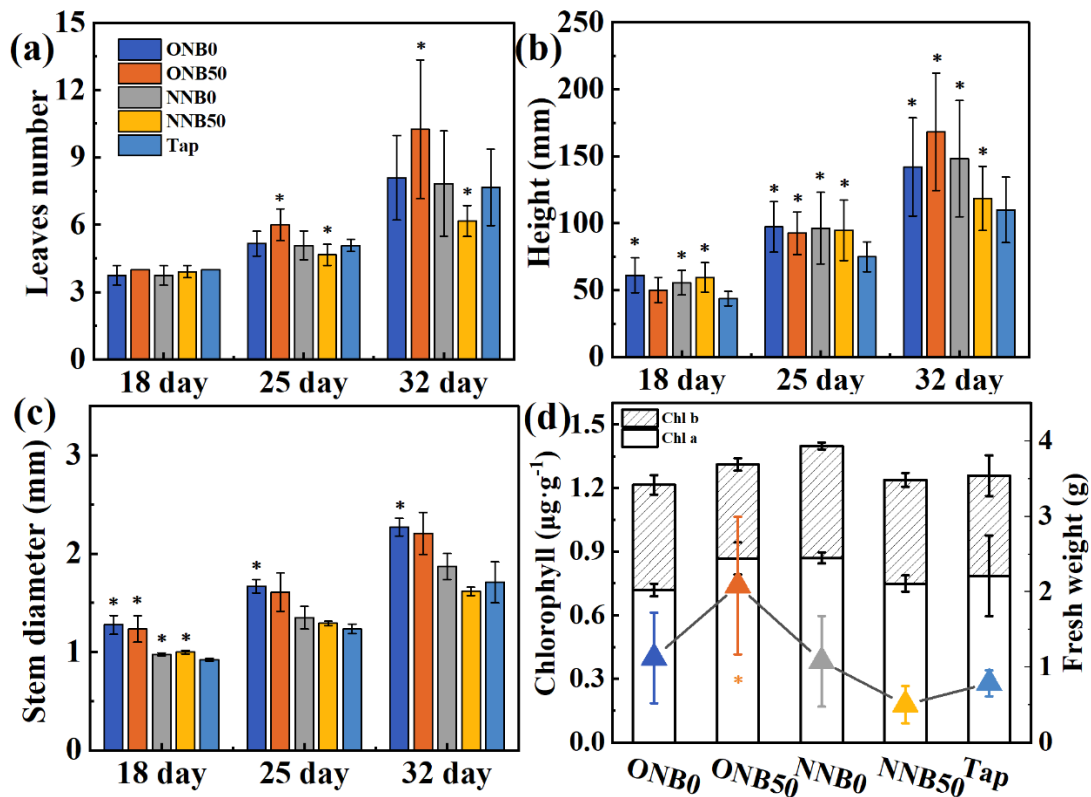
Figure 5.6 Growth characteristics of different tomato plant parts irrigated with different NB water (80 ml per pot every 4 days). (a) leaves number, (b) plant height, (c) steam diameter, (d) fresh weight and total chlorophyll content. The * indicates a significant difference between NB treatment group and tap water ($p < 0.05$).

5.3.2.3 Electrochemical properties of plant roots   This study employed EIS to probe the complex impedance response of the affected root in the soil to assess root growth under irrigation of NB water. According to relevant studies that used EIS to indicate the root activity (Jócsák, Végvári, & Vozáry, 2019; Weigand & Kemna, 2019), an equivalent circuit can be established for the soil–root-electrode continuum (Ozier-Lafontaine & Bajazet, 2005b), where the root capacitance could change with the quantity of root cells and membranes (Ozier-Lafontaine & Bajazet, 2005b). For example, EIS can be used to monitor the willows growth in hydroponic systems through impedance spectra changes (Cao, Repo,

Silvennoinen, Lehto, & Pelkonen, 2011). **Figure 5.7(a)** shows the schematics of our EIS

measurement process. The EIS test generated a Nyquist plot in **Figure 5.7(b)** for the plant

root that was irrigated with ONB0 water from day 31 to day 49. The interfacial impedance

of the root changed with the plant growth as indicated by the semicircular shape changes,

which suggests that the plant root may have changes of their interfacial charge-transfer

resistance (R_c) on the plant root due to the growth and responses to NBs. To clarify the

alteration in interfacial impedance, the EIS spectra data were analyzed by fitting them to a

hypothetical equivalent electric circuit model as illustrated in the inset of **Figure 5.7(b)**,

where R_s is the resistance of the solution (ohm·cm^{-2}), R_c represents the charge-transfer

resistance of the root system (ohm·cm^{-2}), and C is the electrode double-layer capacitance

(F·cm^{-2}) that formed at the root/soil/solution interface and W is the Warburg impedance

(Gao, Jiang, Ni, Qi, & Bi, 2020). The fitting data is summarized in **Table 5.5**. The variations

of R_s reflect the changes of electrical resistance or conductivity of the potting soil mix,

which was treated using the same irrigation intensity to avoid significant changes. The inset

of **Figure 5.7(c)** shows the R_c value was negatively correlated with the tomato height,

which means the growing root may have increased ion transfer channels on the root surface

and thus exhibited reduced the electrical impedance (N. Khan et al., 2021; Ozier-

Lafontaine & Bajazet, 2005a). The root growth is proportional to the height of the plant,

and thus, the root growth may result in a different distance from the graphite

counter/reference electrode, which also affects R_c. However, due to the vulnerability of

roots in the soil, no samples were taken for imaging analysis and confirmation.

Table 5.5 The Fitting Data of the EIS Equivalent Electric Circuit

Sample names	R_s (ohm)	C (F)	R_c (ohm)	W	Height (mm)	Diameter (mm)
ONB0-31	2236±130	7.83±0.31E-10	111700±2144	5.79±0.49E-06	220	2.638
ONB0-41	10570±508	1.78±0.06E-09	43060±805	7.69±0.58E-06	350	3.299
ONB0-49	3957±136	3.81±0.16E-09	7300±124	1.14±0.04E-05	500	3.85
ONB50-49	4987±209	3.43±0.19E-09	8566±193	9.75±0.48E-06	410	2.848
Tap-49	6751±295	3.04±0.12E-09	20950±404	1.33±0.11E-05	440	3.322
NNB0-49	9615±474	1.6±0.06E-09	36750±635	7.9±0.56E-07	430	3.576
NNB50-49	9016±410	1.68±0.06E-09	28030±459	1.16±0.07E-06	290	3.231

Furthermore, we compared the EIS results for the plants that were irrigated with ONB, NNB, and tap water in **Figure 5.7(d)**, which shows the root interfacial resistances are different, as indicated by the different arc radius in the Nyquist plot. The diameters of the semicircle arc of ONB water irrigated plants were significantly smaller than that of tap water and NNB water irrigated plants. A smaller semicircle arc diameter corresponds to faster interfacial charge transport on the root system. Similar to **Figure 5.7(b)**, increasing the growth time or irrigation with ONB water yielded lower interfacial impedance due to the capillary root development and active rhizosphere bacteria formation that could increase the active surface area of root and electrical conductivity.
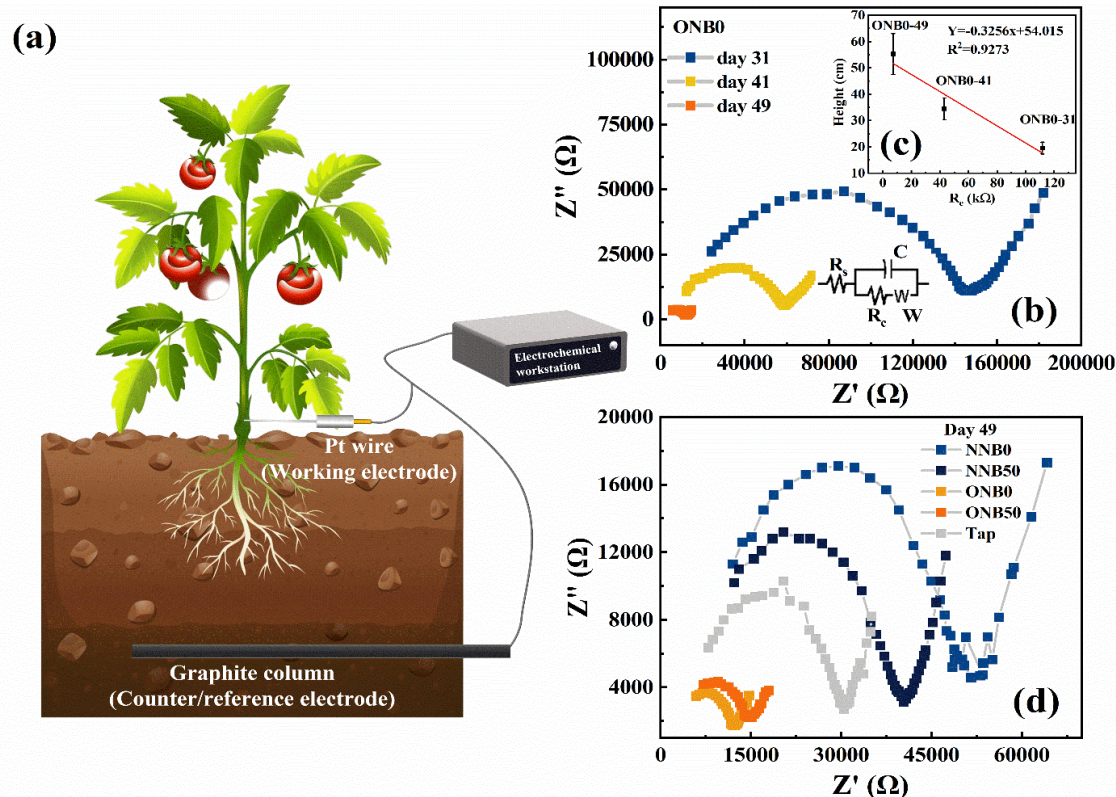
Figure 5.7 (a) Schematics of the EIS measurement process; (b) EIS spectra of the ONB0 at different time, (c) the relationship between R_c of the root system and the height of the plant, (d) EIS spectra of ONB0, ONB50, NNB0, NNB50 and Tap water on day 49.

5.3.3 Effect of NBs on the surface functional groups of plant roots

The plant root surface are usually enriched with surface functional groups (−COOH, −OH, −NH$_2$, and -H$_2$PO$_4$) due to the presence of bioactive molecules such as enzymes on cell walls and membranes (Z.-d. Liu, Wang, & Xu, 2016; Lu et al., 2020). **Figure 5.8** shows the absorption peaks at 1635, 1542, and 1249 cm^{-1} that could be attributed to the C=O stretching vibrations and N-H bending vibrations in amide I, N-H bending vibrations in amide II, and C-N stretching and N-H bending vibrations in amide III, respectively (Sharifi, Khoshgoftarmanesh, & Hadadzadeh, 2016). The absorption bands at 1417 and 1036 cm^{-1}

could be assigned to the symmetric -COO⁻ stretching (J. Wang, Evangelou, & Nielsen, 1992) and C-OH bending vibrations in carbohydrates, respectively (Singh & Lee, 2016). The peaks at 1371 and 1317 cm^{-1} could be assigned to cellulose CH_2 stretching (Lv et al., 2016). **Figure 5.8** compares the FTIR spectra of the root surfaces after treatment by NBs, which exhibit no significant differences in the location of absorption peaks among all treatments and thus surface-bound functional groups on roots were not altered by NBs. However, the intensity of absorption bands (e.g., -COO⁻, C-OH and N-H) of plants in NB treatment groups was higher than that in control group no matter irrigated every 2 or 4 days, suggesting that the concentration of functional groups on plant roots treated with NB was probably higher than that on plant roots treated with tap water, which means NB could increase the ability of root on nutrients   absorption.
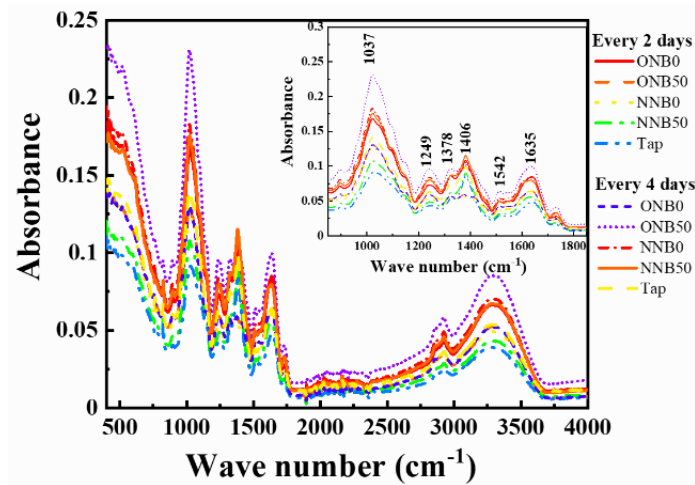
Figure 5.8 The ATR-FTIR spectra of the tomato root surfaces after treatment with NBs every 2 or 4 days for 32 days.

5.3.4 Effects of NBs on soil chemical properties

5.3.4.1 Soil conductivity and pH   **Figure 5.9(a)** shows the pH and conductivity of soil after treatment with different water for 32 days. The ONBs or NNBs did not significantly alter the soil pH that was stable at around 7.4. The conductivity of soil irrigated every 2 days (1600-2400 $\mu S \cdot cm^{-1}$) was lower than that irrigated every 4 days (2500-3200 $\mu S \cdot cm^{-1}$) as shown in **Figure 5.9(b)**. The high irrigation frequency probably resulted in the elution and loss of some mobile ions from the irrigated soil and thus the soil conductivity was reduced (Weiping Chen, Lu, Pan, & Jiao, 2013). Compared to the results for the NNB or DI water irrigation, irrigation of ONBs reduced the soil conductivity more significantly probably because of the slightly higher negative zeta potential of ONBs (**Figure 5.9**), which allows ONBs elicited stronger interactions with soil electrolyte and eluted more soil ions during irrigation than NNBs or DI water.
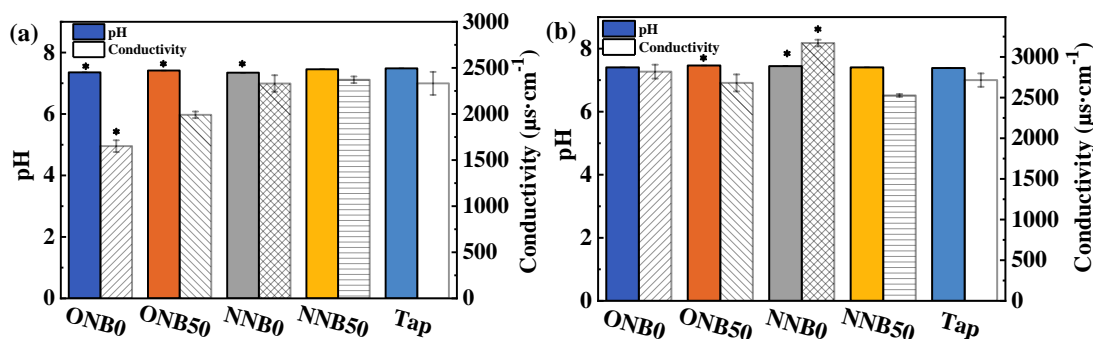
Figure 5.9 (a) The soil conductivity and pH of soil after plant harvest which was irrigated every 2 days (a) and 4 days (b) for 32 days.

5.3.4.2 Fluorescence components of DOM in soil The DOM of soil refers to the complex mixture of organic compounds that are dissolved in soil water, which are produced by the decomposition of plant and animal residues, as well as by the exudation of living plant roots. The composition of DOM in soil is highly variable and can be influenced by various biotic and abiotic factors, such as soil pH, temperature, moisture, vegetation type, and microbial activity. The DOM of soil plays a crucial role in a range of soil processes, including nutrient cycling, carbon sequestration, soil structure formation, and contaminant transport (Gmach, Cherubin, Kaiser, & Cerri, 2019). Therefore, understanding the nature and dynamics of DOM in soil is essential for predicting and managing soil functions and ecosystem services. **Figures 5.10-5.11** show the EEM spectra of soils under different NB water treatment and irrigation frequency, which both indicated two main peaks for all soil leachate samples. Peak A (Ex/Em: 240-260/430-460 nm) is located in Region III, thus corresponding to fulvic-like materials, while Peak B (Ex/Em: 300-350/400-450 nm), is located in Region V, corresponding to fulvic-like materials. **Figures 5.10(f)** and **5.11(f)** display the volumetric fluorescence distribution of the soil extract under different treatments was similar. The added volumetric distribution of regions of II, III and V is more than 80%, indicating that aromatic proteins, fulvic-like and humic-like were the main organic substances in the soil.
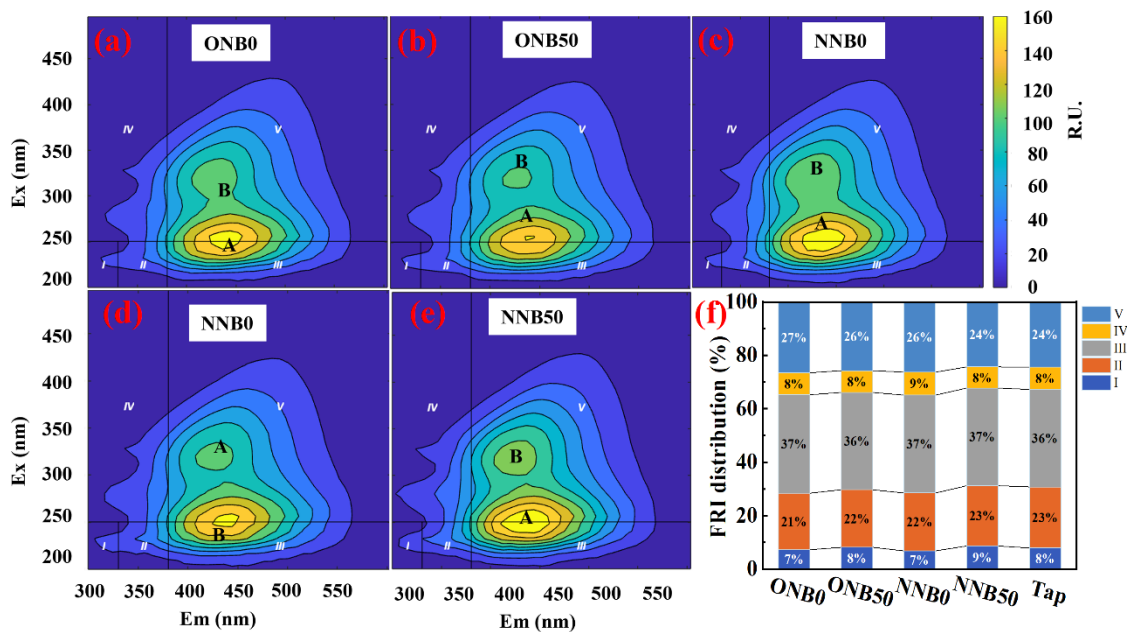
Figure 5.10 (a)-(e) 3D fluorescence spectra of DOM and (f) volumetric fluorescence distribution of soil irrigated every 2 days with different NB water and tap water.
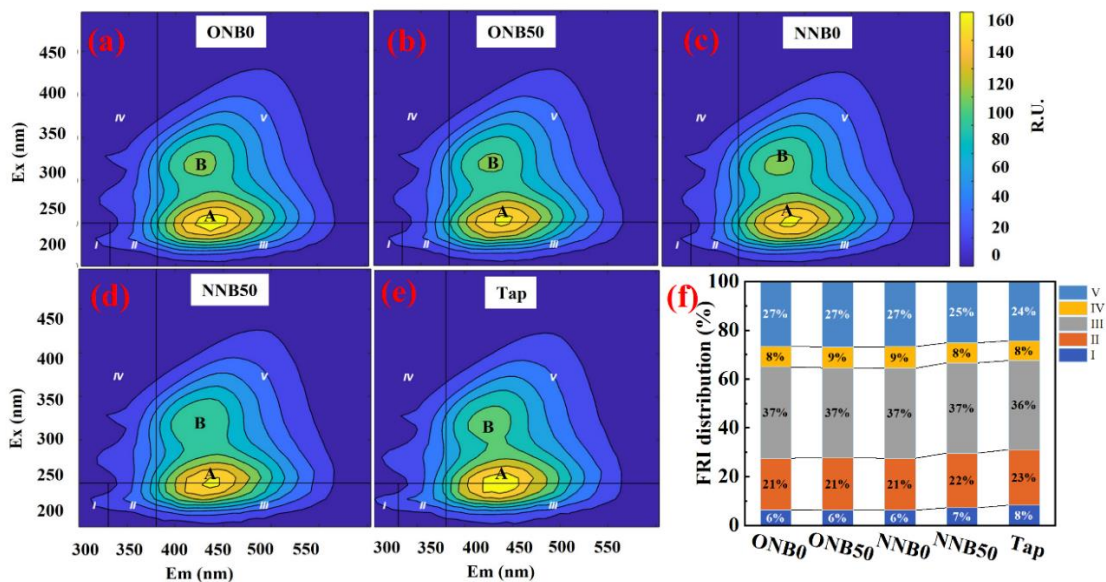
Figure 5.11 (a)-(e) 3D fluorescence spectra of DOM and (f) volumetric fluorescence distribution of soil irrigated every 4 days with different NB water and tap water.

Though the irrigation of NB water did not alter the fluorescence partners of DOM,

the relative fluorescence intensity was changed. **Figures 5.12(a)** and **5.13(a)** compare the

fluorescence intensities of Peak A and B, which shows that the fluorescence intensities of fulvic-like materials and humic-like materials in NB treatment groups were significantly lower than that in tap water. **Figures 5.12(b)** and **5.13(b)** show that the concentration of DOC in NB treated soil leachate was also lower than that in control group (especially in every 2 days). The reduced DOC and fluorescence intensities could be attributed to the improved bacterial degradation of DOM under stimulus effects from NBs (Smreczak & Ukalska-Jaruga, 2021).
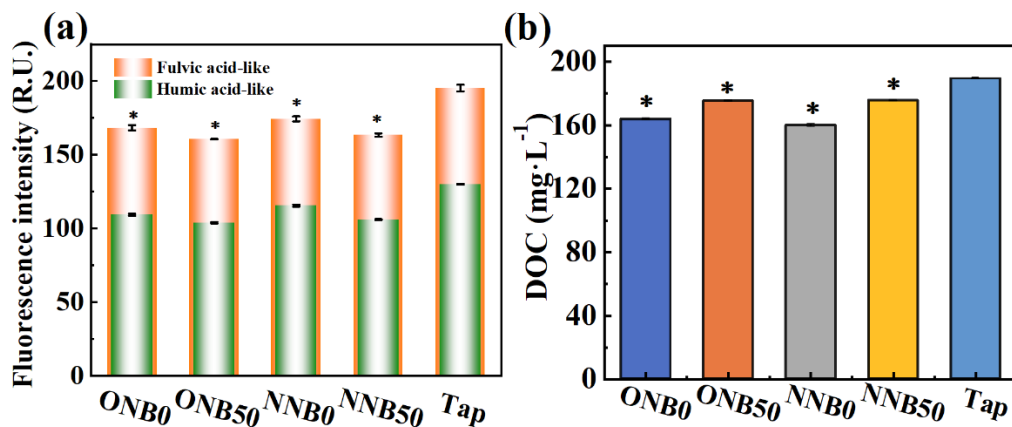
Figure 5.12 The results of the changes of fluorescence densities of fulvic acid-like and humic acid-like materials (a) and DOC (b) for soils that were irrigated every 2 days. * indicate a significant difference between NB treatment group and tap water ($p < 0.05$).
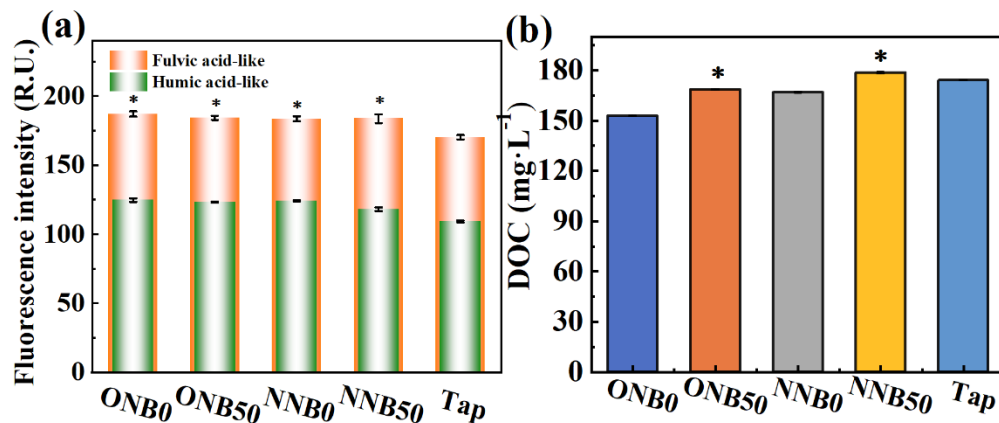
Figure 5.13 The results of the changes of fluorescence densities of fulvic acid-like and humic acid-like materials (a) and DOC (b) for soils that were irrigated every 4 days. * indicate a significant difference between NB treatment group and tap water ($p < 0.05$).

5.3.5 Effects of NBs on enzymatic activity

5.3.5.1 Rhizosphere soil enzymatic activity   Soil enzymes are important indicators of

soil quality, reflecting soil fertility and microbial activity (Acosta-Martinez, Cano, &

Johnson, 2018). Soil oxygenation is known to have an impact on enzyme activities,

improving the soil microhabitat(S. Liu, S. Oshita, S. Kawabata, et al., 2016).   In this

particular study, urease and catalase were monitored as indicators of soil enzyme activities,

since they originate from plant roots and rhizosphere bacteria. Catalase, a type of

oxidoreductase, is responsible for breaking down oxygen peroxide ($O_2^{\bullet-}$) and relieving its

toxic effects on plants and soils (Guangming et al., 2017). The results presented in

Figures 5.14(a) and **5.14(b)** indicate no significant difference in soil catalase activity

between the different treatment groups. It is worth noting that soil catalase activity can

increase with increased soil permeability, as this enzyme is closely related to soil

respiration intensity (Y. Zhou, Zhou, et al., 2019). However, no changes in catalase activity were observed in this study, likely due to the fact that the NB-treated soil did not exhibit significant changes in permeability compared to the soil irrigated with DI water.

Urease is a crucial hydrolase in soil, responsible for the hydrolysis of urea and the utilization of urea nitrogen in soil (Bending, Turner, Rayns, Marx, & Wood, 2004). In the study, **Figures 5.14(a)** and **5.14(b)** clearly demonstrate a decrease in soil urease activity under the irrigation of ONBs. However, no significant changes were observed in NNBs compared to the control group. These findings contradict a previous study (Y. Zhou, Zhou, et al., 2019), which reported an increase in urease content (ranging from 1.29% to 35.43%) in the rhizosphere soil of tomato plants during the fruiting stage. This increase was observed when the DO concentration was elevated from 15 mg·L^{-1} to 25 mg·L^{-1} via water irrigation with air mixed micro-nanobubbles (MNBs). Typically, high DO levels promote the decomposition of urea by providing oxygen to the microorganisms responsible for breaking down urea. Whereas our data suggest that ONBs may also yield a strong oxidative stress on microorganisms or disrupt the physical structure of the microbial community responsible for urease production. This oxidative stress or disruption may have hindered the activity of urease enzymes. Further research exploring the specific microbial community responses and the potential interactions between ONBs and microorganisms could better explain the changes of urease activity in soil upon exposure to ONBs.
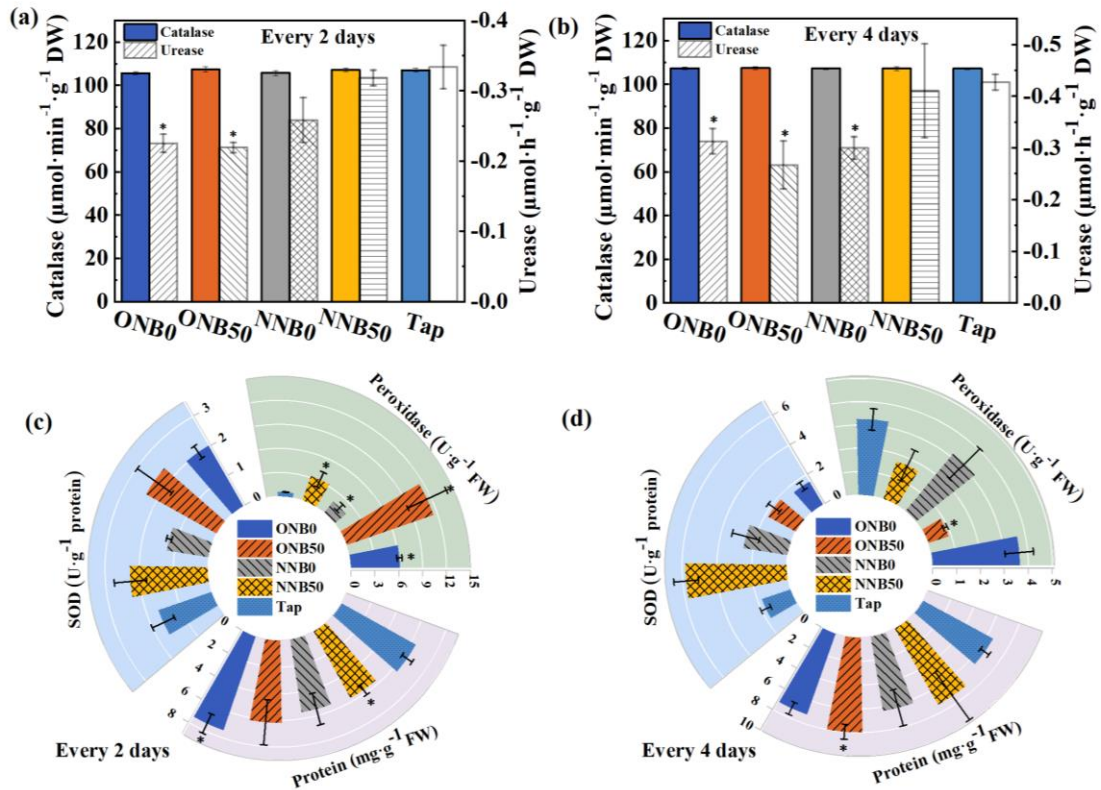
Figure 5.14 (a)-(b) The levels of catalase activity and urease activity under irrigation frequencies of every 2 or every 4 days. (c)-(d) Antioxidant levels of peroxidase, SOD and protein content. * indicates a significant difference between NB treatment group and tap water ($p < 0.05$).

5.3.5.2 Plant antioxidant enzymatic activity Accordingly, we examined the antioxidant enzyme activities in tomato plants by quantifying peroxidase, SOD and protein content. **Figure 5.14(c)** shows the peroxidase activities of tomato leaves increased appreciably (100%-1000%) under exposure to ONBs or NNBs compared with tap water when irrigated every 2 days. However, when irrigated every 4 days (**Figure 5.14(d)**), the changes of peroxidase were not significant. The increased peroxidase may be attributed to the formation of exogenous •OH by NBs that may affect the expression of genes for peroxidase (S. Liu, S. Oshita, S. Kawabata, et al., 2016).

Similar to peroxidase, SOD also plays a vital role in defending against ROS by catalyzing the dismutation of $O_2^{\bullet-}$ to H_2O_2 (Alscher, Erturk, & Heath, 2002). **Figures 5.14(c)-5.14(d)** shows no apparent differences in SOD activities among the control and NB treatment groups, except for ONB50, which caused a slightly higher SOD when irrigated every 4 days. This suggests that ONBs or NNBs did not promote the significant generation of $O_2^{\bullet-}$ (S. Liu et al., 2017). The high SOD level in the NNB50 group may derive from the experimental errors (e.g., enzyme extraction from the leaves). Finally, the total dissolved protein contents in tomato leaves were all similar in all treatment groups under two irrigation frequencies.

5.3.6 Effect of NBs on microbial community

5.3.6.1 Viability of rhizobacteria in the plant root   The tomato roots on day 49 were randomly selected from the treatment groups that irrigated every 2 days to examine the viability of rhizobacteria on their surface. Since the image brightness, contrast and saturation vary from image to image depending on the staining quality, microscope settings and sample itself, for each treatment group, 5 paralleled tests were conducted to select a typical image for comparisons in **Figure 5.15**. The root samples were stained with acridine orange to highlight the presence of DNA and RNA in red and green respectively. The right column in **Figure 5.15** shows the digitally combined images of DNA and RNA. There is a strong fluorescence intensity on the surface of root in ONB50 water group than other group

due to the higher abundance of bacteria on the plant root, which suggests that the activity of the rhizosphere microbial communities could be enriched after exposure to ONBs. By contrast, the NNB treatment did not yield significant differences compared to that under tap water irrigation.
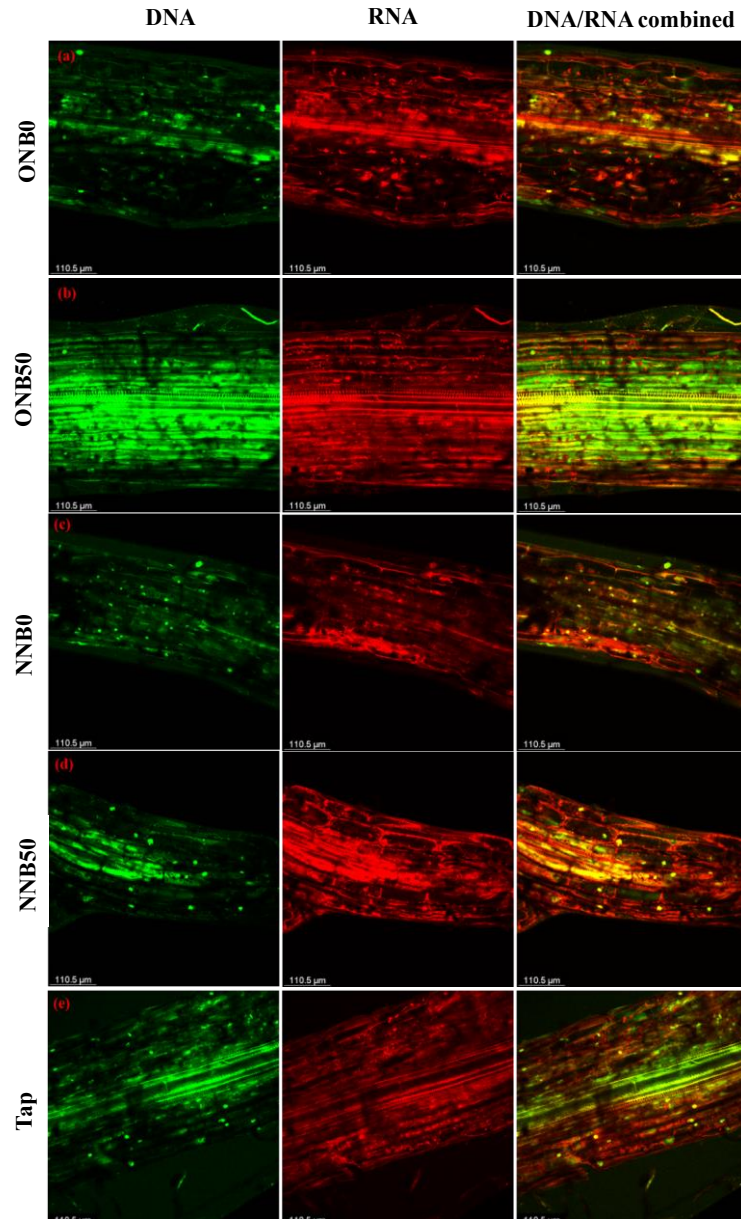
Figure 5.15 Confocal laser scanning images of DNA (left,), RNA (middle) and the merged image of DNA and RNA (right) of rhizobacteria in the plant root visualized with acridine orange staining. (a) ONB0, (b) ONB50, (c) NNB0, (d) NNB50 and (e) Tap water.

5.3.6.2 Alpha diversity of rhizosphere soil microbial communities Species richness (number of observed OTUs) and Shannon index are measures of within-sample biodiversity (alpha diversity). **Figure 16** shows that these two indexes were not changed

appreciably for samples when irrigated every 2 days. However, the two indexes decreased significantly after irrigation with NB water every 4 days in comparison to control group, which is consistent with the results of (Y. Zhou et al., 2020). The type of NBs and the NB concentrations did not have a significant impact on the species richness and Shannon index of the rhizosphere microbial communities. The irrigation every 4 days may only enable certain bacterial populations to proliferate and thus change the bacterial diversity. For example, previous studies have found that, the air environment and oxygen content in the plant rhizosphere were improved by water irrigation with NBs, which changed the abundance of aerobic microbial species and reduced the abundance of anaerobic microbes and altered bacterial diversity (Niu et al., 2016; Y. Sun et al., 2018). In addition, NB water irrigation could increase available nutrients and SOM (Xue, Marhaba, et al., 2022), which resulted in decrease in bacterial diversity (Kumar et al., 2018).
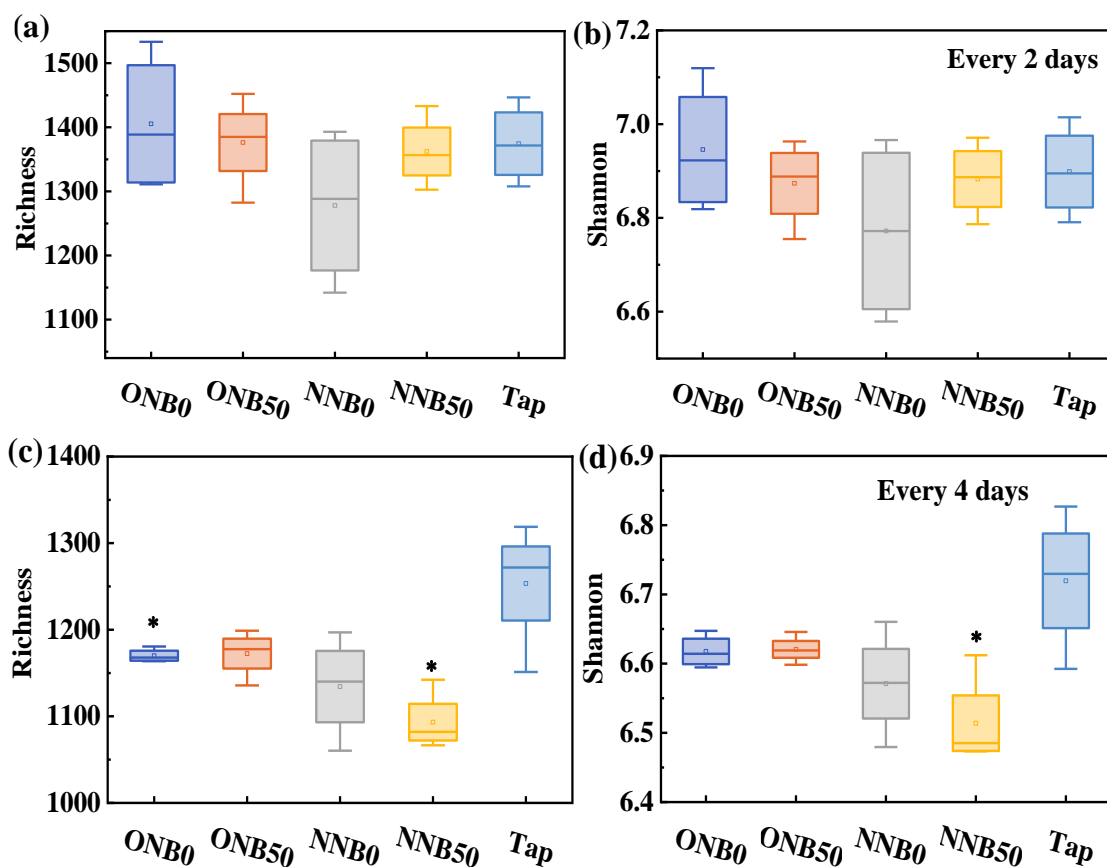
Figure 5.16 Species richness and Shannon index of samples irrigated (a)-(b) every 2 days and (c)-(d) every 4 days. The * indicates a significant difference between NB treatment group and tap water ($p < 0.05$).

5.3.6.3 Beta diversity of rhizosphere soil microbial communities   **Figure 5.17**

shows the relative abundance of each bacterial phylum in the rhizosphere samples. Overall,

the most abundant phyla were Proteobacteria (30%-36%), Bacteroidetes (8%-12%),

Chloroflexi (8%-13%), Acidobacteria (8%-14%) and Planctomycetes (7%-8%). Between

14% and 17% of the sequences in each sample could not be classified. The NB-treated

samples had 16.2% higher abundance of Bacteroidetes ($p = 0.0095$), 7.3% lower abundance

of Proteobacteria ($p = 0.0006$), and 7.3% lower abundance of Chloroflexi ($p = 0.036$) than

the control. In addition, the ONB-treated samples had a 12.7% increase in Planctomycetes compared to the control (p = 0.048).
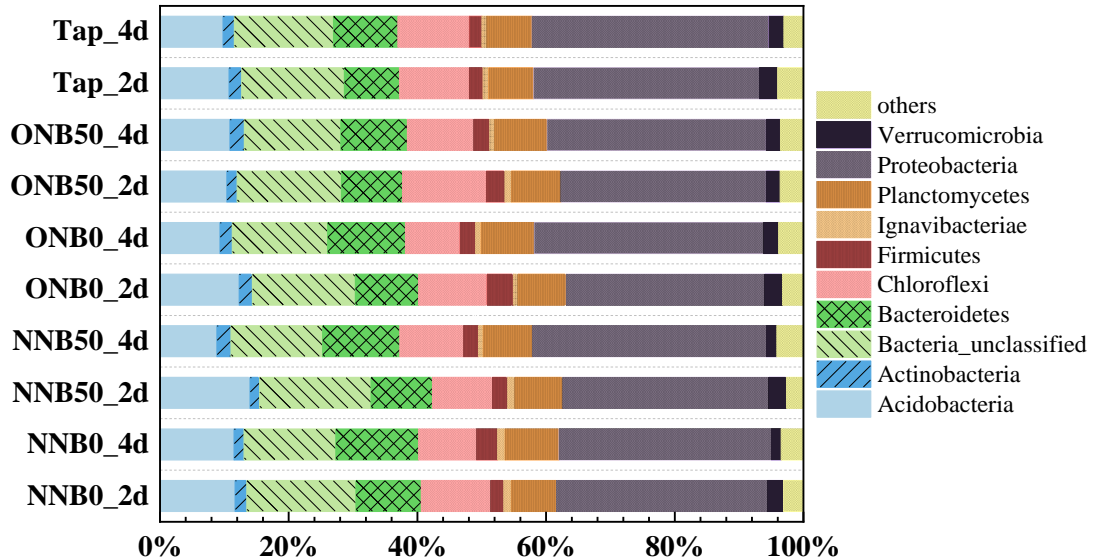
Figure 5.17 Microbial community composition of each rhizosphere soil sample by percentage of each phylum. The control groups were irrigated with tap water.

PCoA was applied to examine the changes of community structure in the rhizosphere microbial community structure associated with different types of NBs, NB concentrations, and irrigation frequencies. **Figure 5.18(a)** shows all the rhizosphere samples in relation to the first 2 PCoA axes, while **Figure 5.18(b)** and **Figure 5.18(c)** show the samples under different irrigation frequency (every 2 days and every 4 days, respectively). Some treatment groups such as ONB0 (every 2 days) and NNB0 (every 2 days) showed very large variation. There were also 3 outliers among the irrigated-every-2-day samples that contributed to the large variation in these groups, as seen in **Figure 5.18(b)** and **Figure 5.18(c)**. These outliers were likely due to uneven mixing of the soil and were

removed from further analyses. The remaining dataset was subsampled again to 3774 reads per sample and included 7060 OTUs.

Figure 5.18(a) shows that the differences between the every-4-days NB treatment groups and the control were more evident than the differences between the every-2-days NB treatment groups and the control, which was an unexpected outcome. Among samples with higher irrigation frequency (every 2 days), as shown in Figure 5.18(b), only the ONB0 group clustered separately from the control (tap water), while the ONB50, NNB0, and NNB50 all overlapped with the control. Among samples with lower irrigation frequency (every 4 days), as shown in Figure 5.18(c), the ONB0, NNB0, and NNB50 clusters were all clearly separated from the control. The ONB50 cluster was positioned between the ONB0 cluster and the control, suggesting that high-concentration ONB water (ONB0) had a stronger effect on the rhizosphere microbiome than diluted ONB water (ONB50), which could be attributed to differences in DO level as well as bubble-specific influences like ROS. In addition, it appeared that the effects of diluted ONB and NNB on microbial communities were similar while high-concentration ONB and NNB favored distinct microbial community structures, as seen from the clear separation between the ONB_0 and NNB_0 clusters. Overall, irrigation frequency, NB concentration, and the types of NBs all had some effects on the structure of rhizosphere microbiomes of tomato plants.
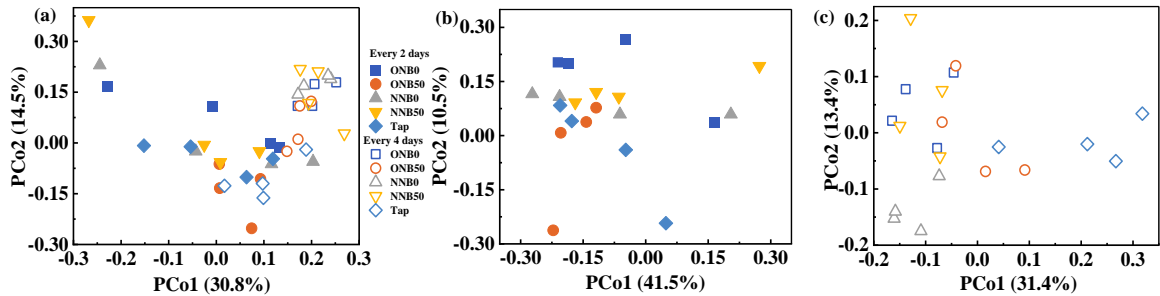
Figure 5.18 Principal Coordinates Analysis comparing the microbial compositions of rhizosphere soil samples after NB water irrigation: (a) all samples, (b) samples irrigated every 2 days, and (c) samples irrigated every 4 days.

Analysis of molecular variance (AMOVA) was carried out to test for statistically significant differences between different treatment groups. The resulting p-values of comparison pairs of interest are shown in **Table 5.6**. Overall, the NB-treated rhizosphere microbiomes showed statistically significant differences from the control ($p = 0.002$). Each type of NB also produced significantly different microbial communities than the control (p = 0.012 for ONB; p = 0.002 for NNB). In addition, while no significant differences were found when comparing all ONB samples and all NNB samples (p = 0.26), a subgroup comparison between the ONB0 and NNB0 (high concentration) treatments at every-4-day irrigation frequency showed significant differences (p = 0.015), which reflects their separate clustering in the PCoA plot. The samples with lower NB water irrigation frequency also tended to have significantly different microbial community structures from the samples with higher irrigation frequency.

Table 5.6 Result from AMOVA Test for Comparison Pairs of Interest

Comparison pairs	p-value
All NB samples – All tap samples	**0.002**
ONB samples – All tap samples	**0.012**
NNB samples – All tap samples	**0.002**
ONB samples – NNB samples	0.26
ONB_2d – Tap_2d	0.073
ONB_4d – Tap_4d	**0.003**
NNB_2d – Tap_2d	**0.028**
NNB_4d – Tap_4d	**< 0.001**
ONB0_2d – NNB0_2d	0.40
ONB50_2d – NNB50_2d	0.11
ONB0_4d – NNB0_4d	**0.015**
ONB50_4d – NNB50_4d	0.13
ONB0_2d – ONB0_4d	**0.029**
ONB50_2d – ONB50_4d	**0.028**
NNB0 _2d – NNB0_4d	**0.016**
NNB50_2d – NNB50_4d	**0.019**
Tap_2d – Tap_4d	0.085

Statistically significant p-values ($p < 0.05$) are shown in bold.

5.4 Conclusion

This study provides important insights into the effects of NBs in water irrigation on tomato seed germination, plant's early growth, and soil properties. The results suggest that the type of NB used can have a significant impact on plant growth, with ONBs promoting growth by 30%-50% compared to the control group without NBs. The findings also indicate that while NBs can faster seed germination by 10%, they do not affect chlorophyll content in tomato leaves. Although the irrigation of NB water did not change the fluorescence partners of DOM, it altered the relative fluorescence intensity. Moreover, tomato leaves' peroxidase

activities increased significantly (100%-1000%) under exposure to ONBs or NNBs when irrigated every 2 days. On the other hand, NBs did not affect SOD and total dissolved protein contents in tomato leaves. These findings suggest that the type of NB can influence plant growth and confirm that ONBs themselves promote plant growth rather than the increased DO concentration caused by their presence. In addition, the research demonstrates that EIS can be an effective technique for analyzing the impact of NBs on plant root growth. The species richness and Shannon index of the rhizosphere microbial communities were not significantly influenced by the type of NBs or the NB concentrations. However, the structure of rhizosphere microbiomes in tomato plants was found to be affected by irrigation frequency, NB concentration, and the types of NBs. Besides the plant growth, NBs could also affect other attributes of plants or products such as nutritional quality. The relevant mechanisms are more complex and deserve further study. Overall, the study provides valuable insights into the potential effects of NBs on plant growth and soil properties, contributing to our understanding of the environmental implications of nanobubble technology in water resources and agriculture.

CHAPTER 6

COMMERCIALIZATION

6.1 Commercialization Effort

Our team conducted a National Science Foundation's Innovation Corps (I-Corps) project on Reactive Nanobubbles Technology for Green and Sustainable Environmental and Agricultural Applications (NSF: I-Corps, #1912367), which enabled us to learn about business development, technology transfer and commercialization. Our commercial partner, BRISEA International Inc. (BRISEA), is a minority women owned small business that was founded in 1999 in New Jersey USA (www.brisea.com). BRISEA has been dedicated in providing environmental and energy professional services, technology and know-how transfer from USA to other nations. BRISEA holds the exclusive licensing agreements on patents owned by NJIT. In 2018, BRISEA was awarded for $100,000 EPA SBIR Phase I project with Zhang's team (Federal Contract #: 68HERD19C0014) to investigate the PFOA degradation via this microwave reactive membrane system. Besides this successful collaboration, BRISEA and NJIT's team also works on commercialization and field demonstration of a nanobubble-enabled algal removal boat for harmful algal bloom mitigation in New Jersey lakes under funding support from New Jersey Department of Environmental Protection (NJDEP, Award #1343716). In 2023, BRISEA registered a new startup company, Purenano Technology (PNT), to promote the commercialization of

the patented nanobubble technology that was developed by Zhang's team at NJIT.

6.2 Business Model

The business model can be defined as the framework that outlines the fundamental principles behind how an organization generates, delivers, and captures value. In this particular context, the business model is elucidated through a "canvas" consisting of nine essential building blocks that depict the rationale of how a company aims to attain profitability. These nine blocks encompass the key aspects of a business, namely customers, offerings, infrastructure, and financial viability as shown in **Figure 6.1**. Comparable to a blueprint, the business model serves as a strategic guide for the implementation of organizational structures, processes, and systems. This concept has undergone extensive application and evaluation worldwide and is already adopted by renowned organizations such as IBM, Ericsson, Deloitte, the Public Works and Government Services of Canada, among many others (Osterwalder, Pigneur, Oliveira, & Ferreira, 2011).

Key Partners	Key Activities	Value Propositions	Customer Relationships	Customer Segments
1. Pall Corporation 2. BRISEA Corporation	1. Customer support and technical consulting 2. Product website development for sale and demonstration. 3. Mobile treatment system production	1. Increase of water quality at relatively low cost; reduce hazardous chemical usage; increase of safety and human health; lower the exposure to toxic pollutants in water; reduce the operational cost of water treatment and impaired water remediation. 2. Solve the problem of high energy consumption and disinfection byproduct formation in traditional HABs control methods. 3. Provide an efficient and cost-effective approach for the cultivation of hydroponics vegetables; improve plants health, acceleration of crop growth rate, increase crop production and improvement of the crop quality.	1. Personal assistance 2. Co-creation.	Water / wastewater treatment companies Swimming pool owners Farmers Residents Lawn service providers
	Key Resources 1.NJIT lab facilities and research equipment 2.Grants from NSF, NJIT and industrial partners 3. KP's testing facilities		Channels 1.Direct sales through our website 2. Indirect sales (referral from our KPs and third-party website)	
Cost Structure Material cost; Fabrication; Labor fee; Long range delivery fee; Storage fee			Revenue Streams Asset sale; Product leasing and rental; Patent and licensing	

Figure 6.1 The business model canvas.

6.2.1 Value proposition

The value proposition serves as a solution to address customer problems and fulfill their needs. There were 3 original value propositions:

1. Increase of water quality at relatively low cost; reduce hazardous chemical usage; increase of safety and human health; lower the exposure to toxic pollutants in water; reduce the operational cost of water treatment and impaired water remediation.

2. Solve the problem of high energy consumption and disinfection byproduct formation in traditional harmful algal blooms (HABs) control methods.

3. Provide an efficient and cost-effective approach for the cultivation of hydroponics vegetables; improve plants health, acceleration of crop growth rate, increase crop production and improvement of crop quality.

6.2.2 Customer segment

Based on the value proposition, the market is divided by 9 different parts: (1) farms to raise cows/sheep to provide drink water with oxygenated water, (2) lake/contaminated water remediation/algal bloom mitigation for aeration, (3) agricultural applications (e.g., lawn grower, small farms for hypotonic cultures), (4) food and vegetable disinfection for household applications, (5) laboratory researchers to produce well defined bubbles with sizes and composition, (6) flue gas/CO_2 capture/treatment to increase reactivity and solubility for algal cultivation, (7) fuel cells for hydrogen and oxygen reactions, (8) hydrogen or ozone water as medicine supplement, and (9) dental cleaning to replace deionized or distilled water to enhance teeth cleaning.

6.2.3 Channels

When it comes to product commercialization, channels play a vital role as they encompass the diverse paths and platforms that a company employs to distribute, market, and sell its products to customers. Acting as the vital link between the company and its target market, these channels facilitate the seamless flow of products from their production phase to the hands of consumers. Channels can manifest in various shapes and forms, such as brick-and-mortar retail stores, online marketplaces, direct sales teams, distributors, wholesalers, resellers, and e-commerce platforms. The art of selecting and managing channels effectively holds immense significance as it directly impacts the company's ability to

connect with and captivate its intended audience, optimize product visibility, and stimulate

sales. Within the hypothesis, as the NB generation system is a tangible product, the

utilization of Physical Distribution Channels becomes relevant. These channels encompass

a range of methods, including direct sales via our own website, as well as indirect sales

facilitated by distributors, retailers, value-added resellers (VARs), and system integrators.

The interplay between these channels is visually represented in the distribution complexity

diagram, depicted as **Figure 6.2**.
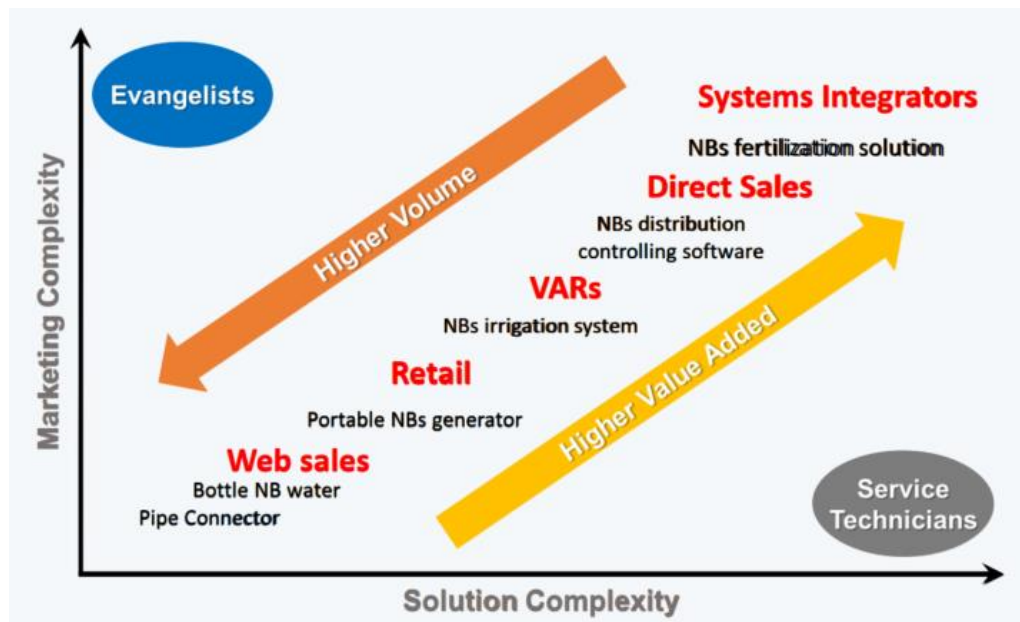
Figure 6.2 Distribution Complexity assumptions. The red texts are different types of
channels defined: Web, VARs, Direct Sales, and Integrators. In between that are product
types for the range of complexity from these types of channels.

6.2.4 Customer relationships

Customer relationships are a crucial aspect of engaging and nurturing each customer

segment. They are built and sustained through three key components: "Get," "Keep," and

"Grow" customers. These components can be visualized using a funnel diagram as shown

in **Figure 6.3**, effectively illustrating the progression and interdependence of each stage in

the customer relationship journey.
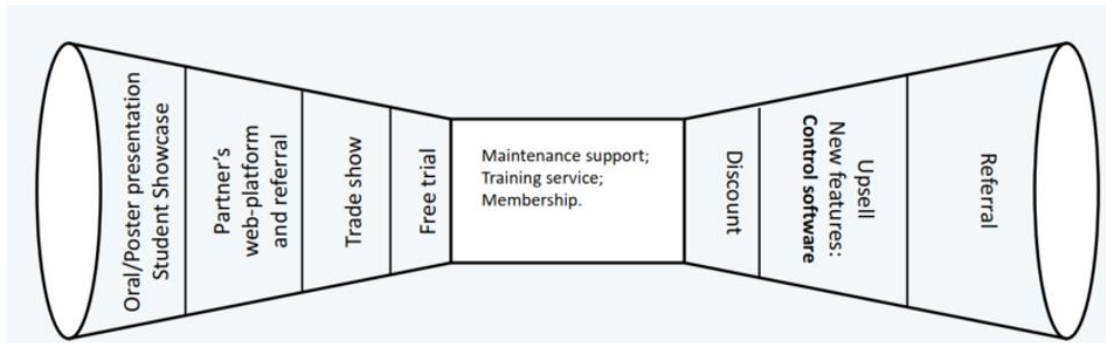
Figure 6.3 Funnel diagram of "Get/Keep/Grow" relationships. Left and right funnels
showed the "Get" and "Grow" processes while the square in the middle shows the
"Keep" processes.

6.2.5 Revenue streams

Revenue streams are the outcomes of effectively delivering value propositions to customers.

They represent the strategic approach to generating revenues for each Customer Segment.

In line with the funnel diagram, our revenue model strategy encompasses three distinct

parts:

1. Asset Sale: This involves the sale of the NB generation system itself, along with
its corresponding parts. Customers acquire the physical components of the system as a one-
time purchase.

2. Freemium: We offer customers the opportunity to use the NB generation system
for a specified duration, typically one month, free of charge. This serves as a way to
introduce the product and allow customers to experience its value before committing to a

purchase.

3. Licensing (Upsell): The control and simulation software associated with the NB generation system can be licensed separately. This provides customers with the option to enhance their system capabilities by acquiring software which offers additional control and simulation functionalities.

6.2.6 Key partners

Partnerships operate on a reciprocal basis, where both parties stand to benefit or face the

consequences together. We identified three types of partners, each with its unique dynamics:

1. Raw Material Suppliers: These partners hold significant importance as they provide and sell essential parts for the NB generation system. By collaborating with us, they not only contribute to our business but also reap benefits themselves. The cost associated with this partnership involves the raw materials and shipping fees, while the risk pertains to maintaining quality control.

2. Distributors: Positioned within the channel section, distributors play a vital role as our product addresses concerns for their customers. The partnership involves a profit-sharing arrangement within the distribution channel. However, potential risks may arise from saboteurs within other pool equipment manufacturers, as well as concerns about the reliability and performance of the distributor.

3. Membrane System Manufacturer: Collaborating with a membrane system manufacturer in a joint venture presents an opportunity for mutual benefit. Their involvement in manufacturing the system leads to shared profits, and cooperative research can generate novel ideas for their own R&D department. The costs associated with this partnership include manufacturing expenses, shipping, and time investments. Risks involved encompass the potential shift of a common customer becoming a competitor, intellectual property (IP) concerns, and the impact of key personnel changes on the alliance.

Navigating these partnerships requires careful consideration of costs, risks, and

potential challenges. By fostering strong relationships with our partners, we can maximize

shared successes while proactively addressing and mitigating potential failures or setbacks.

The potential customer/cooperator was shown in **Figure 6.4**.

Linde	Linde plc	Industrial, Process and Specialty Gases
EDIBLE GARDEN	Edible Garden	Leader of Sustainable Crop Produce
blueplanet GERMANY	Blue Planet Germany	Agriculture and Aquaculture, Wastewater Treatment
h2o innovation / GENESYS / PWT	H2O Innovation / GENESYS / PWT	Water and Wastewater Treatment Company
MOLEAER ADVANCING NANOBUBBLE TECHNOLOGY	Moleaer Inc.	Advancing Nanobubble Technology Company
HY-TEK Bio	HY-TEK Bio	Photosynthesis Flue Gas Capture

Figure 6.4 The potential customer/cooperator.

6.2.7 Key resources

Key resources include: (1) financial resources: federal grant and award, and the investment from key partners, such as USDA for irrigation and food disinfection, DOE's algal cultivation using flue gas, EPA for biofilm disinfection and mitigation   and NJDEP funding. (2) physical resources : university lab space and storage, key partners' facility, and (3) Intellectual property: a patent which has been already granted (*Generation of nanobubbles using a surface functionalized ceramic nanofiltration membrane*. # US 2019/0083945 A1), and (4) Human resources: mentors, advisors and qualified employees, which could be the above mentioned team or hire additional personnel.

6.2.8 Key activities

The team has initiated collaborations with membrane manufacturers, water treatment companies, farms, and water/wastewater industries, such as Suez, American Waters, and Moleaer, on the market of NB technology for impaired water remediation such as harmful algal bloom (HAB) affected waters in 2020-2021. Specifically, we performed the following research and customer discoveries/interviews:

Soil and plant quality improvement. Our hypothesis is that irrigation using NBs in water could trigger the grass growth by delivering nutrients and soil texture improvement, which reduces water usage and fertilizer use.

Our activities: We grow vegetable plants (e.g., tomato and lettuce) in our laboratory at NJIT with different NBs (e.g., CO_2, N_2, O_2) to evaluate and verify the claimed benefits and added values compared to regular fertilized water. Moreover, we interviewed 15 different lawn service companies (e.g., Z0 landscaping, landscaping Supply, Braen Supply, SiteOne Landscape Supply, Empire Supplies and Cedar Grove Garden Center) and local farmers as well as soil science professors such as Dr. James White at Rutgers.

The lessons learned: (1) longevity of NBs in water is critical for the aeration or nutrient delivery within soil water; (2) selling NB water as a commodity product may not be practical and instead producing NB water using a commercial generator of NBs is preferred. (3) chemical-free fertilization and irrigation using NBs is desirable, but soil replenishment may be needed in the long term as the nutrients such as nitrogen or

phosphate may run out after intensive irrigation. (4) Organic farming does require stringent regulation of fertilizer use and may find the NB irrigation more beneficial than other farming businesses.

Small decentralized water treatment facilities or plants. Our hypothesis is that the use of ozonation NBs to replace chlorination or traditional ozonation could reduce the cost of water treatment or disinfection and also increase the effectiveness of disinfection.

Our activities: (1) Studying the aquatic and chemical properties of ozone NBs in the laboratory and investigate the antimicrobial activity of ozone NBs in comparison with the traditional dissolved ozone water (bubbleless) in bacterial inactivation. (2) Performing 25 interviews with water treatment operators in water treatment facilities in private and project engineers of American Water, Moleaear's engineers and chief manager of sales, and other key consultants from Suez, Middlesex Water, CDM Smith, Praxair, Linde, Aquionics, Hach, 3M, Pall, Millipore, and Mott MacDonald.

The lessons learned: (1) The existing technologies of water treatment such as chlorination disinfection suffer toxic/hazardous chemical use and formation of disinfection by products that are carcinogenic. (2) ozonation suffers high cost for large scale water treatment. (3) ozone NBs are hard to quantify or detect due to the rapid decay and collapse. (4) No standardized methods for production and quantification for ozone NBs may add barriers for applications. (5) Current air nanobubbling or aeration technology fails to reduce low concentration ammonia from blackish water in post treatment, which is critical for

water reuse.

Medical and dental health applications. Our hypothesis is that the use of ozonation or oxygen NBs in dental rinsing could reduce periodontal diseases that are primarily driven by microbial biofilm growth. Current antiseptics or antimicrobials (subclinical doxycycline, chlorhexidine (CHX), minocycline, azithromycin, metronidazole, povidone-iodine, or hydrogen peroxide) increases a global concern that antibiotic overuse and antimicrobial resistance.

Our activities: (1) Zhang' team collaborates with biomedical researchers such as Dr. Kumar, Dr. Cugini, an oral microbiologist with extensive experience in the cultivation of oral microbes, biofilm formation, and anti-microbial testing and Dr. Strickland, DMD, MPH in a project for developing electric toothbrushes with suction for preventing aspiration. (2) Interviewed 5 dentists in New Jersey dentistry offices.

The lessons learned: (1) FDA requires limited use of reactive water or materials for direct exposure to patients. Thus, the potential irritation effects from exposure to NB water, especially ozone NBs must be evaluated prior to product sale. (2) biofilm removal from teeth could be difficult to achieve with non-reactive NB water such as oxygen or air NBs.

Nanobubble water as a surfactant-like water for soil remediation. Our hypothesis is that nanobubbles in water could reduce surface tension and increase the mobility of soil contaminants such as heavy metals, oil and organic compounds such as PAH, which may lead to greener soil remediation and cleaning processes (without the use

of surfactants or other chemical rising solutions).

Our activities: (1) The team collaborated with a soil remediation expert, Professor Kurt Pennel, at Brown University to study the use of nanobubbles to mitigate soil acidification and other pollutant removal processes. Moreover, the team elevated the nutrient release and soil characteristics changes upon exposure to different types of gases nanobubbles to understand the impacts on plant growth eventually. For instance, one of the recent collaborative research projects at NJIT revealed that the field experiments verified the laboratory observations that nanobubbles significantly increased rice yield by almost 8% and saved approximately 25% fertilizer. The underlying mechanisms are that nanobubbles influence growth hormone synthesis and plant growth/development genes.

The lessons learned: (1) The rinsing ability of pure NB water is not comparable with the surfactant chemical solutions and thus, the practical use of NBs could be an additive to reduce the surfactant consumption. (2) the longevity of NBs in water during storage or variation of ambient temperature could limit the industrial adoption or sale/delivery.

Nanobubble aeration for hypoxia abatement and algal bloom mitigation. Our hypothesis is that air or oxygen NBs can reduce algae-induced anoxia/hypoxia via boosting up aerobic microbial activity such that water quality in natural waters such lakes/ponds could be improved.

Our activities: (1) The NJIT team actively evaluated the antimicrobial activity of

oxygen NBs in the laboratory and garnered other federal grants such as EPA P3 phase I and II grants. (2) The NJIT team teamed up with BRISEA and Meadowland Environmental Research Institute (MERI) and secured a NJDEP grant to study the use of micro-nanobubble aeration to mitigate harmful algal bloom in two NJ lakes (Branch Brook and Deal lakes) from 2020-2021. (3) The team conducted over 30 interviews with the lake managers, non-profit organizations such as Jersey Care and equipment manufacturers (Geotech) to validate the market demand for ultrafine bubble aeration and availability of products for lake water replenishment.

The lessons learned: (1) NBs are too small to rise and yield air flotation effects, whereas the microbubbles as purged bubbles tend to perform better in air flotation; (2) NBs are also unable to interact with negatively charged species such as algal cells. Thus, usually cationic surfactants are needed to increase the heteroaggregation for bubbles and microbes in water. (3) Energy consumption for NBs could be prohibitive for large scale water treatment.

Recreational water quality and safety improvement. Our hypothesis is that for swimming pools and other recreational water treatment, injection of NBs could reduce hazardous disinfectant chemical usage (free chlorine or copper sulphate), which may reduce the safety concerns and human health effects (e.g., skin irrigation from synthetic chemical exposure).

Our activities: (1) The NJIT team had 30 interviews with pool managers and pool

engineers of hotels, schools and fitness in MO, NJ, NY, PA and CT states. (2) The NJIT

team had more than 20 interviews to professional pool service and equipment providers to

discuss the possibility of utilizing NBs technology in pool cleaning and disinfection.

The lessons learned: (1) swimming pool water treatment at hotels and gyms are

usually outsourced to contractors using commercial processes and chemicals that are

designed per state or federal regulations. (2) more research data are required to confirm the

claimed benefits such as reducing chlorine or other disinfectants, which requires official

approval to prevent health risks from the adjusted operation conditions.

6.2.9 Cost structure

The cost of $ 248,400 will cover the team labor cost, materials, and external services during

these activities as shown in **Table 6.1** and **Figure 6.5** shows the cost structure.

Table 6.1 The Cost of Commercialization Activities

Tasks	Labor	External service	Materials/ Suppliers
Modify demo system	$32,000	$10.000	
Install and test and analysis	$28,000	$15,000	$52,000
Plant growth test and analysis	$29,500	$18,000	
Market activity	$39,000		
IP patent prosecution		$24,900	
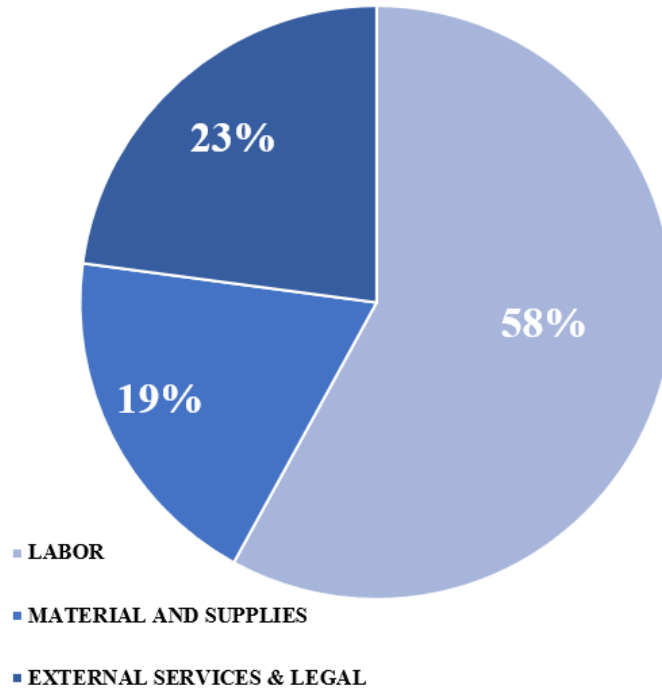
Figure 6.5 The cost structure.

6.3 Results

Our team developed a special functionalization method as well as operational strategies to produce NBs in liquid such as water, electrolyte, solvents or oil. The produce fine bubbles are tunable with respect to bubble sizes and bubble compositions. Compared to this technology, other existing nanobubble generators, such as hydrodynamic and sonication cavitation, are not able to control bubble sizes or bubble compositions. Bubble size or composition control is critical for enhanced mass transfer, gas delivery or storage in liquid. For instance, our technology could convert various compressed gases such as air, nitrogen, carbon dioxide, hydrogen, methane and ozone into bubble forms stored in liquid for long

periods of time (e.g., a few hours to days) depending on the storage conditions.

This technology, developed in 2016 at NJIT, has been extensively evaluated via different federal sponsored projects for different applications as shown below. For example, we have completed the assessment of the nanobubble generation mechanisms and stability. We evaluated the effects of operational parameters such as injection gas pressure, membrane properties (pore size and surface energy), and solution chemistries (e.g., pH, salinity, surfactant and temperature) on the produced nanobubble sizes, surface charges/surface tension and stability. We studied the synergistic effects of irrigation and NBs on various plants using different gas types under a USDA grant and confirmed the positive promotion of plant growth using the nanobubble water we generated. For environmental applications, we use the nanobubble water for biofilm and/or pathogen control under EPA funding support and verified that ozone NBs could enable longer residence times for beneficial reactions and disinfection and increase the efficacies of ozone-based pollution and pathogen removal. As shown in **Figure 6.6**, the commercial partner, BRISEA Inc., has fabricated a NB generator prototype for future validation and demonstration at different sites or application scenarios and the NB generator product is also produced.

Figure 6.6 The nanobubble generator prototype and product we built in partnership with BRISEA Inc..

Our commercial partner, BRISEA Group, Inc., has made initial contact with business different companies that are interested in NB technology from different industries. BRISEA has signed non-disclosure agreement with three of the interested parties. Meanwhile, BRISEA also found manufacturers partner for future large-scale manufacture. BRISEA is currently applying for a grant for further development from New Jersey Economic Development Authority (NJEDA) in partnership with our team at NJIT. Meanwhile, BRISEA is negotiating Linde PLC, one of the world's top 500 industrial enterprises, and Moleaer for intentional cooperation. Additionally, BRISEA is actively preparing for a new start-up forming based on this technology, including seeking third party investment.

Several projects were awarded, which allowed the team to evaluate the NBs for agriculture, antimicrobial and other environmental applications:

1. United State Department of Agriculture (USDA): Agriculture Systems and Technology: Nanotechnology for Agricultural and Food Systems: Project Title: Use of Novel Nanobubble Watering Processes for Enhanced Plant Growth and Pathogen Control. Award number: 2018-07549. Total: $469,999. Start date: 05/15/2019 and End date: 05/04/2022

2. NSF: I-Corp: Reactive Nanobubbles Technology for Green and Sustainable Environmental and Agricultural Applications, Total: $50,000, Award Number: 1912367. Duration: 01/25/2019-07/25/2021

3. EPA. P3 phase I and phase II: "Development of Reactive Nanobubble Systems for Efficient and Scalable Harmful Algae and Cyanotoxin Removal" with grant number 83945101-0 and 84001901. Total: $15,000/$75,000. Duration: 9/1/2018-06/30/2019, 07/01/2020 - 06/30/2021.

4. NJDEP: "Mechanical Removal of HABs in Lakes using Air Micro-Nano Bubbles from a Specialized Floating Platform" with grant number: 1343716. Total: $500,000. Duration: 01/2021-01/2024

5. New Jersey Water Resources Research Institute (NJWRRI) : "Effects of Microbubble Formation on Sediment Pollutant Resuspension" with grant number: 2020NJ027B. Total: $5,000. Duration: 06/01/2020-12/30/2021.

6. New Jersey Water Resources Research Institute (NJWRRI) : " A Green and Powerful Wash with Nanobubble Water for Soil Contamination Removal to Alleviate Groundwater Pollution " with grant number: 2020NJ027B. Total: $5,000. Duration: 09/01/2022-08/31/2023.

7. EPA. P2: "Ozone Nanobubble Water for Pathogen Control and Disinfection in Food Processing and Equipment Cleaning" with grant number: 96259122. Total: $320,000 Duration: 09/30/2022-09/29/2024.

Through conducting interviews with over 200 individuals across diverse sectors such as landscape, water treatment, agriculture, and food industries, we gained valuable

insights into the market's demands. Our research shed light on the specific needs of various segments, including landscapers, recreational water users (e.g., swimming pools), farmers, water utilities, as well as lake or natural park administrators. Notably, we discovered that NBs hold tremendous potential in a market that could be worth billions of dollars, with significant implications for the aquaculture, water treatment, and agriculture sectors. In the existing market, numerous commercial NB generators are available, catering to both laboratory and pilot-scale applications. These generators have the capacity to bring about transformative changes in the environmental, food, and wastewater treatment industries. Their applications span a wide range, including water purification and sterilization, drug delivery, agriculture and food production, as well as the oxygenation of fish and aquaculture dams in the aquaculture sector. The insights gathered from our extensive interviews highlight the immense opportunities presented by the utilization of NB technology across various industries, emphasizing its potential for addressing critical challenges and facilitating advancements in areas such as environmental sustainability, food production, and water treatment.

6.4 Future Work

The future research for NB in agriculture applications holds tremendous potential for enhancing various aspects of agricultural practices. Here are some potential areas of research:

1. Water Management and Irrigation: Exploring the potential of NBs in improving water management and irrigation efficiency can be crucial for water-stressed regions. Investigating how NBs affect water retention and penetration in soils can lead to more efficient water usage in agriculture.

2. Pest and Disease Control: Research on utilizing NBs to control pests and diseases in crops can be beneficial in reducing the reliance on conventional pesticides. Investigating the mechanisms of NBs action on pests and pathogens can help develop environmentally friendly and targeted pest management strategies.

3. Synergistic Effects with Fertilizers: NBs can potentially enhance the effectiveness of fertilizers. When applied in combination with fertilizers, NBs may facilitate the penetration and distribution of nutrients in the soil, leading to a more efficient and targeted nutrient application.

4. Nutrient Content in Plant: NBs can influence plant nutrient metabolism by affecting gene expression and enzyme activity related to nutrient assimilation and storage. Depending on the specific nutrients involved, NBs may promote higher nutrient content in plants.

APPENDIX

INTERVIEW INFORMATION

Table A.1 to Table A.5 are questionnaires designed for conducting customer interviews during the commercialization phase.

Table A.1 Question List for Swimming Pool/Aquarium Owners/Operators

Interview Questions	Answers
Who is your interviewee (name, contact phone or email, title, location, employer, etc)	
What technics you applied?	
What water treatment product are you selling to the customers? (Equipment? Service?)	
Who is the major customer?	
How do you introduce those products to distributors or the customers?	
What are the major problems or pain during the sale of current products and customer discovery? What strategies you undertake to mitigate the problems?	
Will you or do you apply technology from institutes and universities? How and Why?	
Are these products certified? Who of authorities issue the certification?	

Table A.2 Question List for Lake Managers, Nonprofit Organizations

Interview Questions	Answers
Who is your interviewee (name, contact phone or email, title, location, employer, etc)	
The capacity of a single algae control device? Mobile or fixed platform?	
Time interval? (When to start the system? Continuous or intermittent? How to control?)	
Power source?	
Power consumption? Maintenance cost? (Labor and material) Lifetime? Depreciation? Cost accounting?	
Effect of algae control? (Selective control? Resistance after multiple treatments? Safety to other life form including operator?)	

Table A.3 Question List for Farmers and Managers of Lawn

Interview Questions	Answers
Who is your interviewee (name, contact phone or email, title, location, etc)	
What are the current technical processes or systems for irrigation and fertilization?	
What is the major concern, problem, and pain of the current technic/process/system (e.g. crop rotation)?	
Do you use fertilization? If yes, what is the amount? What kind of fertilizer?	
Who is the supplier? Who provides service/maintenance (supplier, themselves or a third party)? Why chooses this supplier?	
How much does the system cost? the installation cost as well as the operational cost	
What is the daily/monthly cost of the entire process? Cost structure? (e.g., labor fee, electric and fertilizer consumption, …)	
How much would be acceptable for you to change the current system to new technology? How much do you expect the new technology to reduce the cost?	
Current crop production rate? (For farm)	
Could you recommend some other business around this area? Or do you know someone may be interested in our topic?	

Table A.4 Question List for Pool Water Treatment Manufacturers

Interview Questions	Answers
Who is your interviewee (name, contact phone or email, title, location, employer, etc)	
What technics you applied?	
What water treatment product are you selling to the customers? (Equipment? Service?)	
Who is the major customer?	
How do you introduce those products to distributors or the customers?	
What are the major problems or pain during the sale of current products and customer discovery? What strategies you undertake to mitigate the problems?	
Will you or do you apply technology from institutes and universities? How and Why?	
Are these products certified? Who of authorities issue the certification?	

Table A.5 Question List for Water Treatment Suppliers

Interview Questions	Answers
Who is your interviewee (name, contact phone or email, title, location, employer, etc)	
What water treatment product are you selling to the customers? (Filters? Chlorine pills? Equipment? Service?)	
Are these products certified? Who of authorities issue the certification?	
How do the manufactures introduce those products to you? What factors make you decide to purchase and sell them at your store?	
Who is the major customer? (Hotel? Fitness center? Private residential?)	
What are the major problems or pain during the sale of current products and customer discovery? What strategies you undertake to mitigate the problems?	

The information about some major interviewees is summarized in **Table A.6**.

Table A.6 Interviewee Information

Name	Contact (phone or email; address)	Company	Title	Industry
Rae Liening	farm@earthdancefarms.org	EarthDance Organic Farm School	Assistant Grower	Agriculture
Chris Saunders	3142613175	Saunders Lawn Care	Owner	Service
Anna Brown		Resident	Resident	Other
Jay Everatt	(314) 426-6100	Rottler Pest & Lawn Solutions	Lawn specialist	Service
Shontez Blue	3144214000	Holiday Inn St. Louis - Downtown Convention Center	Chief Engineer	Service
Bob Goeltz	robert.goeltz@amwater.com	American Water Missouri	Senior project engineer	Other
Craig D. Adams	craig.adams@slu.edu	Parks College of St Louis University	Endowed Chair; Professor	Education
Travis Calvert	Travis.Calvert@hilton.com	Hilton Garden Inn St. Louis Airport	Engineer	Service
Jeremy Walker	jeremy.walker@hilton.com	Manager	General	Service
Roger		Park Avenue - Soulard Farmers Market	Farm store owner	Retail
Donna Schroeter		Schroeter's Farm	Farm Owner	Agriculture
Steve Sides, JR.		Rottler Pest & Lawn Solutions	Lawn care manager	

Table A.6 (Continued) Interviewee Information

Benjamin Leonard	benjamin.leonard@sheratonclayton.com	Sheraton Clayton Plaza Hotel	Chief engineer, Certificated pool operator	Service
Paul Smith	egreen@sonesta.com	The Chase Park Plaza	Chief engineer	Service
Chris Meinert	Christopher.Meinert@Hilton.com	Embassy Suites St. Louis Downtown	Chief engineer	Service
Justine Kandra	3145779561	Missouri Botanical Garden	Home Gradening Consultant	Other
Marjavia	3145779440	Resident	Resident	Other
Victoria Scheultz	3145775137	Garden Gate Store of Missouri Botanical Garden	Garden Sales staff	Retail
Ryan Hirsch	rhirsch@city-green.org	City Green Growing Healthy Cites	Greenhouse Manager	Agriculture
Louis	(201) 955-7400	Kearny Farmer Market	Market Owner	Retail
Wanyi Fu	9736424858	Resident	Resident	Other
Ronnie	7325412333	RJW Rahway fitness & wellness center	Pool supervisor	Service
Paul Calicco	9737515089	CLI Landscape Service	Owner	Service

Table A.6 (Continued) Interviewee Information

lori	2018910278	Abma's Farm, Market, Greenhouse & Petting Zoo	manager	Agriculture
Tim Christ	tchrist@parks.essexcountynj.org	Essex County Department of Parks, Recreation and Cultural Affairs	Director of Golf Operation	Entertainment & Leisure
Jin Fan	9739543090	farm	farmer	Agriculture
He Dong	kd353@njit.edu	Resident	Resident	Other
Tunan Tang	nickdon2007@gmail.com	Resident	Resident	Other
Eric Jackson	ejackson@hartshornarboretum.org	Cora Hartshorn Arboretum	Environmental Educator	Service
John Dunn	webmaster@arboretumfriends.org	Frelinghuysen Arboretum	Consultant	Service
Jean Bader	9732270294	Bader Farms Home Grown Produce	owner	Agriculture
Yuhong Jiang	yhjiang@brisea.com	Brisea Group, Inc.	Vice President	Technology
Xiulin Ren		Resident	Resident	Other
Ye Yang	1164311916@qq.com	Resident	Resident	Other
Hani Faouri	hfaouri@hotmail.com	Resident	Resident	Other
Laith		Resident	Resident	
Joseph Williams		Resident	Resident	Other
Xivandell Emmanuel		Resident	Resident	Other
Christopher Bartell	7323881581	Bartell Farm & Garden Supply	Owner	Retail & Wholesale
Robert J.Amberg	Ramberg178@aol.com	Amberg Perennial Farm	Owner	Retail

Table A.6 (Continued) Interviewee Information

Althea Llewellyn	a.llewellyn@reeves-reedarboretum.org	Reeves-Reed Arboretum	Environmental Educator	Service
Alfred Michalik	Alfred.Michalik@brightview.com	BrightView Landscape Services	Operations Manager	Service
Bob Caffrey	Bob@caffreytree.com	Caffrey Tree & Landscape	owner	Service
Hui Liu		Resident	Resident	Other
Ning Wang	+86 02583329322	Resident	Resident	Other
Steven Rosenstark	steven.rosenstark@lps-students.org	Resident	Resident	Other
Qingquan Ma	qm32@njit.edu	Resident	Resident	Other
Stewart	Unionsquaregrassman@gmail.com	Union Square Grassman	Owner	Retail
John Adams	portbenfarm@mac.com	Hudson Valley Organic	Owner	Agriculture
Christy Checo		Resident	Resident	Other
Beatriz Cabral		Resident	Resident	Other
Dolma	windfallfarm@gmail.com	Windfall farms	Owner	Agriculture
Vince Butrico	9087699698	A-Tech Landscape Design	Owner	Service
Helayne	7327386660	Country Club Lawns	owner	Service
Jim Walker	7327381720	Forever Flowers	Owner	Retail
TJ Wydner	tjwydner@kempersports.com	Ash Brook Golf Course	General Manager	Sports

Table A.6 (Continued) Interviewee Information

Matthew Smith	9733981776	Resident	Resident	Other
Ross Komura	7322821776	Resident	Resident	Other
Nick Patel	(908) 315-6014	Resident	Resident	Other
Ripal Majmudar	(317) 294-1822	Resident	Resident	Other
Umberto Fusco	9736356282	Fusco Brothers Landscape Suppliers	Manager	Retail
Mavilyn Kitchell	9734259510	Great Swamp National Wildlife Refuge	Consultant / Biologist	Other
Karin Thorpe	gscshrubs@gmail.com	Great Swamp Greenhouses	Shrub Manager	Retail
Michael Beneduce	9086473725	Great Swamp Greenhouses	Owner	Retail
Alan	9734509140	Alpine Nursery & Garden Center	Owner	Retail
Christine Wargacki	chrissy@metroplantexchange.com	Metropolitan plant & flower exchange	Floral Manager	Retail
Gan Shi	9735664968	Resident	Resident	Other
Connor Ford	cford@storefredeny.com	Resident	Resident	Other
Daniel Massaro	2019525759	Resident	Resident	Other
Darren Nikolz	nikolz@gmail.com	Resident	Resident	Other
Nikki Rodriguez		Resident	Resident	Other

Table A.6 (Continued) Interviewee Information

Shane Sung	sung.shane@gmail.com	Resident	Resident	Other
Kim Shibata	7322837277	Resident	Resident	Other
Edwin Uy	Euy8195@yahoo.com	Resident	Resident	Other
Ernest Werner Jr.	7326685660	Resident	Resident	Other
David Shuback	8456458882	Resident	Resident	Other
Jimmy	stonebrook451@gmail.com	Stone Brook Garden Center & landscape supply	Manager	Retail
Tracie	sales@metropolitanwholesale.com	Metropolitan Wholesale	sales manager	Retail & Wholesale
Jamie Grahn	9736287375	Wayne Wholesale Fertilizer Co.	shop manager	Retail & Wholesale
Xing Wu	hdjwx@126.com	Resident	Resident	Other
Mei Zheng	+86 13665693207	Resident	Resident	Other
Yu Hua	453724148@qq.com	Resident	Resident	Other
Wei li	185058@qq.com	Resident	Resident	Other
Sherry Tang	yazi1990@126.com	Resident	Resident	Other
Newton Dilone	9736730025	Empire Supplies	Manager	Retail & Wholesale
George Berger	6094396915	Resident	Resident	Other
Myra Borsos	6095859883	Resident	Resident	Other
David Shoudy	dshoudy56@gmail.com	Resident	Resident	Other
Charles Liu	charles_liu@pall.com	Pall Corporation	Principles Engineer	Manufacturing
Winnie Shih	3108696977	Nanostone Water	Application Engineering Manager	Manufacturing

Table A.6 (Continued) Interviewee Information

Juan Tang	595868991@qq.com	Resident	Resident	Other
Fang Xie	1320916019@qq.com	Resident	Resident	Other
Anton Venediktov	av387@njit.edu	Resident	Resident	Other
Tom Wolf	7325033668	Resident	Resident	Other
Alberto Ventura	9733655529	Resident	Resident	Other
Xiaolu Wang		Resident	Resident	Other
Mark Moese	markmoese@brisea.com	Brisea Group, Inc.	President	Technology

REFERENCES

Abu-Shahba, M. S., Mansour, M. M., Mohamed, H. I., & Sofy, M. R. (2021). Comparative cultivation and biochemical analysis of iceberg lettuce grown in sand soil and hydroponics with or without microbubbles and macrobubbles. *Journal of Soil Science and Plant Nutrition, 21*(1), 389-403.

Acosta-Martinez, V., Cano, A., & Johnson, J. (2018). Simultaneous determination of multiple soil enzyme activities for soil health-biogeochemical indices. *Applied Soil Ecology, 126*, 121-128.

Agarwal, A., Ng, W. J., & Liu, Y. (2011). Principle and applications of microbubble and nanobubble technology for water treatment. *Chemosphere, 84*(9), 1175-1180.

Ahmadi, R., & Okawa, T. (2015). Influence of surface wettability on bubble behavior and void evolution in subcooled flow boiling. *International Journal of Thermal Sciences, 97*, 114-125.

Ahmed, A. K. A., Shi, X., Hua, L., Manzueta, L., Qing, W., Marhaba, T., & Zhang, W. (2018). Influences of air, oxygen, nitrogen, and carbon dioxide nanobubbles on seed germination and plant growth. *Journal of Agricultural and Food Chemistry, 66*(20), 5117-5124.

Ahmed, A. K. A., Sun, C., Hua, L., Zhang, Z., Zhang, Y., Zhang, W., & Marhaba, T. (2018). Generation of nanobubbles by ceramic membrane filters: The dependence of bubble size and zeta potential on surface coating, pore size and injected gas pressure. *Chemosphere, 203*, 327-335.

Alexander, J., Knopp, G., Dötsch, A., Wieland, A., & Schwartz, T. (2016). Ozone treatment of conditioned wastewater selects antibiotic resistance genes, opportunistic bacteria, and induce strong population shifts. *Science of The Total Environment, 559*, 103-112.

Alheshibri, M., Qian, J., Jehannin, M., & Craig, V. S. (2016). A history of nanobubbles. *Langmuir, 32*(43), 11086-11100.

Alliaume, F., Garcia, M., Rossing, W., Giller, K., Mancasola, V., & Dogliotti, S. (2010). Quantification of some soil properties as affected by land use, and its implication for vegetable farm systems. *Paper presented at the Proceedings 19th World Congress of Soil Science*. Soil Solutions for A Changing World, Brisbane, Australia, 1-6 august, 2010.

Alscher, R. G., Erturk, N., & Heath, L. S. (2002). Role of superoxide dismutases (SODs) in controlling oxidative stress in plants. *Journal of Experimental Botany, 53*(372), 1331-1341.

Antonietti, M., & Vorwerg, L. (1997). Examination of the atypical electrophoretic mobility behavior of charged colloids in the low salt region using the O'Brian-White theory. *Colloid and Polymer Science, 275*(9), 883-887.

Atkinson, A. J., Apul, O. G., Schneider, O., Garcia-Segura, S., & Westerhoff, P. (2019). Nanobubble technologies offer opportunities to improve water treatment. *Accounts of Chemical Research, 52*(5), 1196-1205.

Attard, P. (2013). The stability of nanobubbles. *The European Physical Journal Special Topics*, 1-22.

Bailly, C., El-Maarouf-Bouteau, H., & Corbineau, F. (2008). From intracellular signaling networks to cell death: the dual role of reactive oxygen species in seed physiology. *Comptes Rendus Biologies, 331*(10), 806-814.

Baishya, K., & Sarma, H. (2014). Effect of agrochemicals application on accumulation of heavy metals on soil of different land uses with respect to its nutrient status. *IOSR Journal of Environmental Science, Toxicology and Food Technology, 8*(7), 46-54.

Bando, Y., Yoshimatsu, T., Luo, W., Wang, Y., Yasuda, K., Nakamura, M., Oshima, M. (2008). Flow characteristics in cocurrent upflow bubble column dispersed with micro-bubbles. *Journal of Chemical Engineering of Japan, 41*(7), 562-567.

Baram, S., Evans, J. F., Berezkin, A., & Ben-Hur, M. (2021). Irrigation with treated wastewater containing nanobubbles to aerate soils and reduce nitrous oxide emissions. *Journal of Cleaner Production, 280*, 124509.

Behkish, A., Lemoine, R., Sehabiague, L., Oukaci, R., & Morsi, B. I. (2007). Gas holdup and bubble size behavior in a large-scale slurry bubble column reactor operating with an organic liquid under elevated pressures and temperatures. *Chemical Engineering Journal, 128*(2-3), 69-84.

Bénard, C., Gautier, H., Bourgaud, F., Grasselly, D., Navez, B., Caris-Veyrat, C., . . . Génard, M. (2009). Effects of Low Nitrogen Supply on Tomato (Solanum lycopersicum) Fruit Yield and Quality with Special Emphasis on Sugars, Acids, Ascorbate, Carotenoids, and Phenolic Compounds. *Journal of Agricultural and Food Chemistry, 57*(10), 4112-4123.

Bending, G. D., Turner, M. K., Rayns, F., Marx, M.-C., & Wood, M. (2004). Microbial and biochemical soil quality indicators and their potential for differentiating areas under contrasting agricultural management regimes. *Soil Biology and Biochemistry, 36*(11), 1785-1792.

Berkelaar, R. P., Seddon, J. R., Zandvliet, H. J., & Lohse, D. (2012). Temperature dependence of surface nanobubbles. *ChemPhysChem, 13*(8), 2213-2217.

Bhushan, B., Pan, Y., & Daniels, S. (2013). AFM characterization of nanobubble formation and slip condition in oxygenated and electrokinetically altered fluids. *Journal of Colloid and Interface Science, 392*, 105-116.

Bolan, N. S., Adriano, D. C., Kunhikrishnan, A., James, T., McDowell, R., & Senesi, N. (2011). Dissolved organic matter: biogeochemistry, dynamics, and environmental significance in soils. In *Advances in Agronomy*, 110, 1-75.

Boshenyatov, B., Kosharidze, S., & Levin, Y. K. (2019). On the stability of nanobubbles in water. *Russian Physics Journal, 61*(10), 1914-1921.

Bostrom, M., Williams, D., & Ninham, B. (2001). Specific ion effects: why DLVO theory fails for biology and colloid systems. *Physical Review Lletters, 87*(16), 168103-168103.

Bouaifi, M., Hebrard, G., Bastoul, D., & Roustan, M. (2001). A comparative study of gas hold-up, bubble size, interfacial area and mass transfer coefficients in stirred gas–liquid reactors and bubble columns. *Chemical Engineering and Processing: Process Intensification, 40*(2), 97-111.

Bouranis, D., Chorianopoulou, S., Siyiannis, V., Protonotarios, V., & Hawkesford, M. (2003). Aerenchyma formation in roots of maize during sulphate starvation. *Planta, 217*(3), 382-391.

Bowley, W. W., & Hammond, G. L. (1978). Controlling factors for oxygen transfer through bubbles. *Industrial & Engineering Chemistry Process Design and Development, 17*(1), 2-8.

Breitburg, D., Levin, L. A., Oschlies, A., Grégoire, M., Chavez, F. P., Conley, D. J., .Isensee, K. (2018). Declining oxygen in the global ocean and coastal waters. *Science, 359*(6371).

Brennen, C. E. (2013). *Cavitation and bubble dynamics*, Cambridge, England, Cambridge University Press.

Buhmann, M. T., Abt, D., Altenried, S., Rupper, P., Betschart, P., Zumstein, V., . . . Ren, Q. (2018). Extraction of Biofilms from Ureteral Stents for Quantification and Cultivation–Dependent and-Independent Analyses. *Frontiers in Microbiology, 9*, 1470.

Bui, T. T., Nguyen, D. C., & Han, M. (2019). Average size and zeta potential of nanobubbles in different reagent solutions. *Journal of Nanoparticle Research, 21*(8), 1-11.

Bunkin, N., Shkirin, A., Ignatiev, P., Chaikov, L., Burkhanov, I., & Starosvetskij, A. (2012). Nanobubble clusters of dissolved gas in aqueous solutions of electrolyte. I. Experimental proof. *The Journal of Chemical Physics, 137*(5), 054706.

Bunkin, N. F., Shkirin, A. V., Penkov, N. V., Goltayev, M. V., Ignatiev, P. S., Gudkov, S. V., & Izmailov, A. Y. (2021). Effect of gas type and its pressure on nanobubble generation. *Frontiers in Chemistry, 9*, 630074.

Bunkin, N. F., Shkirin, A. V., Suyazov, N. V., Babenko, V. A., Sychev, A. A., Penkov, N. V., . . . Gudkov, S. V. (2016). Formation and dynamics of ion-stabilized gas nanobubble phase in the bulk of aqueous NaCl solutions. *The Journal of Physical Chemistry B, 120*(7), 1291-1303.

Butt, H.-J. (1991). Measuring electrostatic, van der Waals, and hydration forces in electrolyte solutions with an atomic force microscope. *Biophysical Journal, 60*(6), 1438-1444.

Butt, H.-J., Cappella, B., & Kappl, M. (2005). Force measurements with the atomic force microscope: Technique, interpretation and applications. *Surface Science Reports, 59*(1-6), 1-152.

Calgaroto, S., Wilberg, K., & Rubio, J. (2014). On the nanobubbles interfacial properties and future applications in flotation. *Minerals Engineering, 60*, 33-40.

Cancelos, S., Villamizar, G., Saavedra-Ruiz, A., Garcia-Rodriguez, W., Filoni, P. T., & Marin, C. (2016). Experiments with nano-scaled helium bubbles in water subjected to standing acoustic fields. *Nuclear Engineering and Design, 310*, 587-591.

Cao, Y., Repo, T., Silvennoinen, R., Lehto, T., & Pelkonen, P. (2011). Analysis of the willow root system by electrical impedance spectroscopy. *Journal of Experimental Botany, 62*(1), 351-358.

Chan, C. U., Arora, M., & Ohl, C.-D. (2015). Coalescence, growth, and stability of surface-attached nanobubbles. *Langmuir, 31*(25), 7041-7046.

Chang, Y.-I., & Chang, P.-K. (2002). The role of hydration force on the stability of the suspension of Saccharomyces cerevisiae–application of the extended DLVO theory. *Colloids and Surfaces A: Physicochemical and Engineering Aspects, 211*(1), 67-77.

Chen, H., Mao, H., Wu, L., Zhang, J., Dong, Y., Wu, Z., & Hu, J. (2009). Defouling and cleaning using nanobubbles on stainless steel. *Biofouling, 25*(4), 353-357.

Chen, L., Han, L., Sun, K., Chen, G., Ma, C., Zhang, B., . . . Yang, Z. (2022). Molecular transformation of dissolved organic carbon of rhizosphere soil induced by flooding and copper pollution. *Geoderma, 407*, 115563.

Chen, Q., Chen, J., Wang, J., Guo, J., Jin, Z., Yu, P., & Ma, Z. (2019). In situ, high-resolution evidence of phosphorus release from sediments controlled by the reductive dissolution of iron-bound phosphorus in a deep reservoir, southwestern China. *Science of the Total Environment, 666*, 39-45.

Chen, W., Bastida, F., Liu, Y., Zhou, Y., He, J., Song, P., Li, Y. (2023). Nanobubble oxygenated increases crop production via soil structure improvement: The perspective of microbially mediated effects. *Agricultural Water Management, 282*, 108263.

Chen, W., Lu, S., Pan, N., & Jiao, W. (2013). Impacts of long-term reclaimed water irrigation on soil salinity accumulation in urban green land in Beijing. *Water Resources Research, 49*(11), 7401-7410.

Chen, W., Westerhoff, P., Leenheer, J. A., & Booksh, K. (2003). Fluorescence excitation− emission matrix regional integration to quantify spectra for dissolved organic matter. *Environmental Science & Technology, 37*(24), 5701-5710.

Chen, X., Dai, C., Zhang, T., Xu, P., Ke, W., Wu, J., . . . Fan, Y. (2022). Efficient construction of a robust PTFE/Al2O3 hydrophobic membrane for effective oil purification. *Chemical Engineering Journal, 435*, 134972.

Cheng, L., Zhu, J., Chen, G., Zheng, X., Oh, N. H., Rufty, T., . . . Hu, S. (2010). Atmospheric CO2 enrichment facilitates cation release from soil. *Ecology Letters, 13*(3), 284-291.

Choi, H., Li, C., & Peterson, G. (2021). Dynamic Processes of Nanobubbles: Growth, Collapse, and Coalescence. *Journal of Heat Transfer, 143*(10), 102501.

Chu, L.-B., Xing, X.-H., Yu, A.-F., Zhou, Y.-N., Sun, X.-L., & Jurcik, B. (2007). Enhanced ozonation of simulated dyestuff wastewater by microbubbles. *Chemosphere, 68*(10), 1854-1860.

Chu, L.-B., Yan, S.-T., Xing, X.-H., Yu, A.-F., Sun, X.-L., & Jurcik, B. (2008). Enhanced sludge solubilization by microbubble ozonation. *Chemosphere, 72*(2), 205-212.

Chu, Y.-S., Dufour, S., Thiery, J. P., Perez, E., & Pincet, F. (2005). Johnson-Kendall-Roberts theory applied to living cells. *Physical Review Letters, 94*(2), 028102.

Conley, D.J., Paerl, H.W., Howarth, R.W., Boesch, D.F., Seitzinger, S.P., Havens, K.E., Lancelot, C. and Likens, G.E. (2009). Controlling eutrophication: nitrogen and phosphorus. *Science*, 323(5917), 1014-1015.

Conley, D. J., Bonsdorff, E., Carstensen, J., Destouni, G., Gustafsson, B. G., Hansson, L. A., .Technology. (2009). Tackling Hypoxia in the Baltic Sea: Is Engineering a Solution? *Environmental Science and Technology*, *43*(10), 3407-3411.

Corbineau, F., & Come, D. (2017). Control of seed germination and dormancy by the gaseous environment. *Seed Development and Germination*, 397-424.

Corwin, D., & Lesch, S. (2005). Apparent soil electrical conductivity measurements in agriculture. *Computers and Electronics in Agriculture, 46*(1-3), 11-43.

Corwin, D. L., & Lesch, S. M. (2005). Apparent soil electrical conductivity measurements in agriculture. *Computers and Electronics in Agriculture, 46*(1), 11-43.

Craig, V. S., Ninham, B. W., & Pashley, R. M. (1993). The effect of electrolytes on bubble coalescence in water. *The Journal of Physical Chemistry, 97*(39), 10192-10197.

Cui, X., Shi, C., Xie, L., Liu, J., & Zeng, H. (2016). Probing interactions between air bubble and hydrophobic polymer surface: impact of solution salinity and interfacial nanobubbles. *Langmuir, 32*(43), 11236-11244.

D, B., Levin LA, A, O., M, G., FP, C., DJ, C., GS, J. (2018). Declining oxygen in the global ocean and coastal waters. *Science, 359*(6371).

da Silva Moura, C. A., Belmonte, G. K., Reddy, P. G., Gonslaves, K. E., & Weibel, D. E. (2018). EUV photofragmentation study of hybrid nonchemically amplified resists containing antimony as an absorption enhancer. *RSC advances, 8*(20), 10930-10938.

Daiber, E. J., DeMarini, D. M., Ravuri, S. A., Liberatore, H. K., Cuthbertson, A. A., Thompson-Klemish, A., Richardson, S. D. (2016). Progressive Increase in Disinfection Byproducts and Mutagenicity from Source to Tap to Swimming Pool and Spa Water: Impact of Human Inputs. *Environmental Science & Technology, 50*(13), 6652-6662.

De-Campos, A. B., Mamedov, A. I., & Huang, C.-h. (2009). Short-term reducing conditions decrease soil aggregation. *Soil Science Society of America Journal, 73*(2), 550-559.

del Carmen Cuevas-Díaz, M., Martínez-Toledo, Á., Guzmán-López, O., Torres-López, C. P., del C Ortega-Martínez, A., & Hermida-Mendoza, L. J. (2017a). Catalase and phosphatase activities during hydrocarbon removal from oil-contaminated soil amended with agro-industrial by-products and macronutrients. *Water, Air, & Soil Pollution, 228*, 1-11.

del Carmen Cuevas-Díaz, M., Martínez-Toledo, Á., Guzmán-López, O., Torres-López, C. P., del C Ortega-Martínez, A., & Hermida-Mendoza, L. J. (2017b). Catalase and phosphatase activities during hydrocarbon removal from oil-contaminated soil amended with agro-industrial by-products and macronutrients. *Water, Air, & Soil Pollution, 228*(4), 1-11.

Ding, S., Wang, Y., Wang, D., Li, Y. Y., Gong, M., & Zhang, C. (2016). In situ, high-resolution evidence for iron-coupled mobilization of phosphorus in sediments. *Scientific Reports, 6*(1), 1-11.

DODDS, W. K., BOUSKA, W. W., EITZMANN, J. L., PILGER, T. J., PITTS, K. L., RILEY, A. J., Technology. (2009). Eutrophication Of U.S. Freshwaters: Analysis Of Potential Economic Damages. *Environmental Science and Technology*, *43*(1), 12-19.

Duncan, P. B., & Needham, D. (2004). Test of the Epstein− Plesset Model for gas microparticle dissolution in aqueous media: effect of surface tension and gas undersaturation in solution. *Langmuir, 20*(7), 2567-2578.

Dzubiella, J. (2010). Explicit and implicit modeling of nanobubbles in hydrophobic confinement. *Anais da Academia Brasileira de Ciências, 82*(1), 3-12.

Ebina, K., Shi, K., Hirao, M., Hashimoto, J., Kawato, Y., Kaneshiro, S., . . . Yoshikawa, H. (2013b). Oxygen and air nanobubble water solution promote the growth of plants, fishes, and mice. *PLoS One, 8*(6), e65339.

Eckert, D., & Sims, J. T. (1995). Recommended soil pH and lime requirement tests. *Recommended soil testing procedures for the northeastern United States. Northeast Regional Bulletin, 493*, 11-16.

Fan, W., Zhang, Y., Liu, S., Li, X., & Li, J. (2020). Alleviation of copper toxicity in Daphnia magna by hydrogen nanobubble water. *Journal of Hazardous Materials, 389*, 122155.

Favvas, E. P., Kyzas, G. Z., Efthimiadou, E. K., & Mitropoulos, A. C. (2021). Bulk nanobubbles, generation methods and potential applications. *Current Opinion in Colloid & Interface Science, 54*, 101455.

Gao, J., Jiang, B., Ni, C., Qi, Y., & Bi, X. (2020). Enhanced reduction of nitrate by noble metal-free electrocatalysis on P doped three-dimensional Co3O4 cathode: Mechanism exploration from both experimental and DFT studies. *Chemical Engineering Journal, 382*, 123034.

Ge, S., Agbakpe, M., Wu, Z., Kuang, L., Zhang, W., & Wang, X. (2014). Influences of surface coating, UV irradiation and magnetic field on the algae removal using magnetite nanoparticles. *Environmental Science and Technology, 49*(2), 1190-1196.

Ge, S., Agbakpe, M., Zhang, W., & Kuang, L. (2015). Heteroaggregation between PEI-coated magnetic nanoparticles and algae: effect of particle size on algal harvesting efficiency. *ACS Applied Materials and Interfaces, 7*(11), 6102-6108.

German, S. R., Chen, Q., Edwards, M. A., & White, H. S. (2016). Electrochemical measurement of hydrogen and nitrogen nanobubble lifetimes at pt nanoelectrodes. *Journal of The Electrochemical Society, 163*(4), H3160.

German, S. R., Edwards, M. A., Chen, Q., Liu, Y., Luo, L., & White, H. S. (2016). Electrochemistry of single nanobubbles. Estimating the critical size of bubble-forming nuclei for gas-evolving electrode reactions. *Faraday Discussions, 193*, 223-240.

Ghadimkhani, A., Zhang, W., & Marhaba, T. (2016). Ceramic membrane defouling (cleaning) by air Nano Bubbles. *Chemosphere, 146*, 379-384.

Gmach, M. R., Cherubin, M. R., Kaiser, K., & Cerri, C. E. P. (2019). Processes that influence dissolved organic matter in the soil: a review. *Scientia Agricola, 77*.

Gogate, P. R., & Pandit, A. B. (2005). A review and assessment of hydrodynamic cavitation as a technology for the future. *Ultrasonics Sonochemistry, 12*(1), 21-27.

Gogate, P. R., Shirgaonkar, I. Z., Sivakumar, M., Senthilkumar, P., Vichare, N. P., & Pandit, A. B. (2001). Cavitation reactors: efficiency assessment using a model reaction. *AIChE Journal, 47*(11), 2526-2538.

Guangming, L., Xuechen, Z., Xiuping, W., Hongbo, S., Jingsong, Y., & Xiangping, W. (2017). Soil enzymes as indicators of saline soil fertility under various soil amendments. *Agriculture, Ecosystems & Environment, 237*, 274-279.

Guo, L., Lu, M., Li, Q., Zhang, J., Zong, Y., & She, Z. (2014). Three-dimensional fluorescence excitation–emission matrix (EEM) spectroscopy with regional integration analysis for assessing waste sludge hydrolysis treated with multi-enzyme and thermophilic bacteria. *Bioresource Technology, 171*, 22-28.

Hammer, D. A., & Tirrell, M. (1996). Biological adhesion at interfaces. *Annual Review of Materials Science, 26*(1), 651-691.

Hampton, M. A., & Nguyen, A. V. (2009). Accumulation of dissolved gases at hydrophobic surfaces in water and sodium chloride solutions: Implications for coal flotation. *Minerals Engineering, 22*(9-10), 786-792.

Han, Y., Yang, T., Yan, X., Li, L., & Liu, J. (2020). Effect of aeration mode on aerosol characteristics from the same wastewater treatment plant. *Water Research, 170*, 115324.

Hassanein, M., Ahmed, A. G., & Zaki, N. M. (2018). Effect of nitrogen fertilizer and bio-fertilizer on yield and yield components of two wheat cultivars under sandy soil. *Middle East Journal of Applied Sciences, 8*(1), 37-42.

He, H., Zheng, L., Li, Y., & Song, W. (2015). Research on the Feasibility of Spraying Micro/Nano Bubble Ozonated Water for Airborne Disease Prevention. *Ozone: Science and Engineering, 37*(1), 78-84.

Henglin, A. (1998). Contributions to various aspects of cavitation chemistry. *Advanced in Sonochemistry, 38*, 17-83.

Hill, T. C., Walsh, K. A., Harris, J. A., & Moffett, B. F. (2003). Using ecological diversity measures with bacterial communities. *FEMS Microbiology Ecology, 43*(1), 1-11.

Hou, D., Jassby, D., Nerenberg, R., & Ren, Z. J. (2019). Hydrophobic gas transfer membranes for wastewater treatment and resource recovery. *Environmental Science and Technology, 53*(20), 11618-11635.

Hu, J., Wu, J., Sharaf, A., Sun, J., & Qu, X. (2019). Effects of organic wastes on structural characterizations of fulvic acid in semiarid soil under plastic mulched drip irrigation. *Chemosphere, 234*, 830-836.

Hu, L., & Xia, Z. (2018). Application of ozone micro-nano-bubbles to groundwater remediation. *Journal of Hazardous Materials, 342*, 446-453.

Huisman, Jef, Codd, Geoffrey, A., Paerl, Ibelings. (2018). Cyanobacterial blooms. *Nature Reviews Microbiology, 16*(8), 471-483.

Husson, O. (2013). Redox potential (Eh) and pH as drivers of soil/plant/microorganism systems: a transdisciplinary overview pointing to integrative opportunities for agronomy. *Plant and Soil, 362*(1), 389-417.

Ikeda-Dantsuji, Y., Feril, L. B., Tachibana, K., Ogawa, K., Endo, H., Harada, Y., . . . Maruyama, K. (2011). Synergistic effect of ultrasound and antibiotics against Chlamydia trachomatis-infected human epithelial cells in vitro. *Ultrasonics Sonochemistry, 18*(1), 425-430.

Ikeura, H., Kobayashi, F., & Tamaki, M. (2011). Removal of residual pesticide, fenitrothion, in vegetables by using ozone microbubbles generated by different methods. *Journal of Food Engineering, 103*(3), 345-349.

Islam, M. S., & Tanaka, M. (2004). Impacts of pollution on coastal and marine ecosystems including coastal and marine fisheries and approach for management: a review and synthesis. *Marine Pollution Bulletin, 48*(7-8), 624-649.

Izawa, S., Inoue, Y., & Kimura, A. (1995). Oxidative stress response in yeast: effect of glutathione on adaptation to hydrogen peroxide stress in Saccharomyces cerevisiae. *FEBS Letters, 368*(1), 73-76.

Jasevičius, R., Baronas, R., & Kruggel-Emden, H. (2015). Numerical modelling of the normal adhesive elastic–plastic interaction of a bacterium. *Advanced Powder Technology, 26*(3), 742-752.

Jeong, C. H., Postigo, C., Richardson, S. D., Simmons, J. E., Kimura, S. Y., Mariñas, B. J., Plewa, M. J. (2015). Occurrence and Comparative Toxicity of Haloacetaldehyde Disinfection Byproducts in Drinking Water. *Environmental Science and Technology, 49*(23), 13749-13759.

Jiang, J., Wang, Y.-P., Yang, Y., Yu, M., Wang, C., & Yan, J. (2019). Interactive effects of nitrogen and phosphorus additions on plant growth vary with ecosystem type. *Plant and Soil, 440*(1), 523-537.

Jócsák, I., Végvári, G., & Vozáry, E. (2019). Electrical impedance measurement on plants: a review with some insights to other fields. *Theoretical and Experimental Plant Physiology, 31*, 359-375.

JohnáElliot, A. (1990). Estimation of rate constants for near-diffusion-controlled reactions in water at high temperatures. *Journal of the Chemical Society, Faraday Transactions, 86*(9), 1539-1547.

Jyoti, K., & Pandit, A. (2003). Hybrid cavitation methods for water disinfection: simultaneous use of chemicals with cavitation. *Ultrasonics Sonochemistry, 10*(4-5), 255-264.

Jyoti, K., & Pandit, A. B. (2001). Water disinfection by acoustic and hydrodynamic cavitation. *Biochemical Engineering Journal, 7*(3), 201-212.

Kapodistrias, G., & Dahl, P. H. (2012). Scattering measurements from a dissolving bubble. *The Journal of the Acoustical Society of America, 131*(6), 4243-4251.

Karraker, K. A., & Radke, C. J. (2002). Disjoining pressures, zeta potentials and surface tensions of aqueous non-ionic surfactant/electrolyte solutions: theory and comparison to experiment. *Advances in Colloid and Interface Science, 96*(1), 231-264.

Khaled Abdella Ahmed, A., Sun, C., Hua, L., Zhang, Z., Zhang, Y., Marhaba, T., & Zhang, W. (2018). Colloidal properties of air, oxygen, and nitrogen nanobubbles in water: Effects of ionic strength, natural organic matters, and surfactants. *Environmental Engineering Science, 35*(7), 720-727.

Khan, N., Ali, S., Shahid, M. A., Mustafa, A., Sayyed, R., & Curá, J. A. (2021). Insights into the interactions among roots, rhizosphere, and rhizobacteria for improving plant growth and tolerance to abiotic stresses: a review. *Cells, 10*(6), 1551.

Khan, P., Zhu, W., Huang, F., Gao, W., & Khan, N. A. (2020). Micro–nanobubble technology and water-related application. *Water Supply, 20*(6), 2021-2035.

Khorshidi, M., & Lu, N. (2017). Quantification of exchangeable cations using soil water retention curve. *Journal of Geotechnical and Geoenvironmental Engineering, 143*(9), 04017057.

Kim, J.-Y., Song, M.-G., & Kim, J.-D. (2000). Zeta potential of nanobubbles generated by ultrasonication in aqueous alkyl polyglycoside solutions. *Journal of Colloid and Interface Science, 223*(2), 285-291.

Kim, M., Song, S., Kim, W., & Han, J.-G. (2020). An Experimental Study on Bubble Collapsing Effect of Nanobubble Using Ultrasonic Wave. *Journal of Nanoscience and Nanotechnology, 20*(1), 636-642.

Kim, T., & Han, M. (2010). Analysis of bubble potential energy and its application to disinfection and oil washing. *Doctorate, Seoul National University*.

Knox, J. W., Kay, M. G., & Weatherhead, E. K. (2012). Water regulation, crop production, and agricultural water management—Understanding farmer perspectives on irrigation efficiency. *Agricultural Water Management, 108*, 3-8.

Kononov, L. (2015). Chemical reactivity and solution structure: on the way to a paradigm shift? *RSC Advances, 5*(58), 46718-46734.

Korayem, M., Rastegar, Z., & Taheri, M. (2012). Sensitivity analysis of nano-contact mechanics models in manipulation of biological cell. *Nanoscience and Nanotechnology, 2*(3), 49-56.

Korayem, M., & Taheri, M. (2014). Modeling of various contact theories for the manipulation of different biological micro/nanoparticles based on AFM. *Journal of Nanoparticle Research, 16*(1), 2156.

Koshoridze, S. (2020). Coalescence conditions for bulk nanobubbles. *Technical Physics Letters, 46*(7), 699-702.

Krasner, S. W., Weinberg, H. S., Richardson, S. D., Pastor, S. J., Chinn, R., Sclimenti, M. J., Thruston, A. D. (2006). Occurrence of a New Generation of Disinfection Byproducts†. *Environmental Science and Technology, 40*(23), 7175-7185.

Krishnan, J. S., Dwivedi, P., & Moholkar, V. S. (2006). Numerical investigation into the chemistry induced by hydrodynamic cavitation. *Industrial & Engineering Chemistry Research, 45*(4), 1493-1504.

Kukizaki, M., & Goto, M. (2006). Size control of nanobubbles generated from Shirasu-porous-glass (SPG) membranes. *Journal of Membrane Science, 281*(1-2), 386-396.

Kukizaki, M., & Wada, T. (2008). Effect of the membrane wettability on the size and size distribution of microbubbles formed from Shirasu-porous-glass (SPG) membranes. *Colloids and Surfaces A: Physicochemical and Engineering Aspects, 317*(1-3), 146-154.

Kumar, U., Nayak, A. K., Shahid, M., Gupta, V. V., Panneerselvam, P., Mohanty, S., Lal, B. (2018). Continuous application of inorganic and organic fertilizers over 47 years in paddy soil alters the bacterial community structure and its influence on rice production. *Agriculture, Ecosystems and Environment, 262*, 65-75.

Kurata, K., Taniguchi, H., Fukunaga, T., Matsuda, J. and Higaki, H. (2007). Development of a compact microbubble generator and its usefulness for three-dimensional osteoblastic cell culture. *Journal of Biomechanical Science and Engineering, 2*(4), 166-177.

Kurita, Y., Chiba, I., & Kijima, A. (2017). Physical eradication of small planktonic crustaceans from aquaculture tanks with cavitation treatment. *Aquaculture International, 25*(6), 2127-2133.

LaFrance, P., & Grasso, D. (1995). Trajectory modeling of non-brownian particle flotation using an extended Derjaguin-Landau-Verwey oberbeek approach. *Environmental Science and Technology, 29*(5), 1346-1352.

Lal, R., & Kimble, J. (1997). Conservation tillage for carbon sequestration. *Nutrient Cycling in Agroecosystems, 49*(1-3), 243-253.

Lavonen, E. E., Gonsior, M., Tranvik, L. J., Schmitt-Kopplin, P., & Köhler, S. J. (2013). Selective Chlorination of Natural Organic Matter: Identification of Previously Unknown Disinfection Byproducts. *Environmental Science and Technology, 47*(5), 2264-2271.

Lee, J. K., Lee, C., Fahy, K. F., Kim, P. J., Krause, K., LaManna, J. M., Bazylak, A. (2020). Accelerating bubble detachment in porous transport layers with patterned through-pores. *ACS Applied Energy Materials, 3*(10), 9676-9684.

Lee, W.-J., Lee, T. A., Suda, K. J., Calip, G. S., Briars, L., & Schumock, G. T. (2017). Risk of serious bacterial infection associated with tumour necrosis factor-alpha inhibitors in children with juvenile idiopathic arthritis. *Rheumatology, 57*, 273-282.

Li, H., Hu, L., Song, D., & Lin, F. (2014). Characteristics of micro-nano bubbles and potential application in groundwater bioremediation. *Water Environment Research, 86*(9), 844-851.

Li, H., Hu, L., & Xia, Z. (2013). Impact of groundwater salinity on bioremediation enhanced by micro-nano bubbles. *Materials, 6*(9), 3676-3687.

Li, M., Ma, X., Eisener, J., Pfeiffer, P., Ohl, C.-D., & Sun, C. (2021). How bulk nanobubbles are stable over a wide range of temperatures. *Journal of Colloid and Interface Science, 596*, 184-198.

Li, P., Song, Y., & Yu, S. (2014). Removal of Microcystis aeruginosa using hydrodynamic cavitation: performance and mechanisms. *Water Research, 62*, 241-248.

Li, P., Takahashi, M., & Chiba, K. (2009). Degradation of phenol by the collapse of microbubbles. *Chemosphere, 75*(10), 1371-1375.

Lin, J., He, F., Owens, G., & Chen, Z. (2021). How do phytogenic iron oxide nanoparticles drive redox reactions to reduce cadmium availability in a flooded paddy soil? *Journal of Hazardous Materials, 403*, 123736.

Liu, G., & Craig, V. S. (2009). Improved cleaning of hydrophilic protein-coated surfaces using the combination of nanobubbles and SDS. *ACS Applied Materials and Interfaces, 1*(2), 481-487.

Liu, G., Wu, Z., & Craig, V. S. (2008). Cleaning of protein-coated surfaces using nanobubbles: an investigation using a quartz crystal microbalance. *The Journal of Physical Chemistry C, 112*(43), 16748-16753.

Liu, S., Kawagoe, Y., Makino, Y., & Oshita, S. (2013). Effects of nanobubbles on the physicochemical properties of water: The basis for peculiar properties of water containing nanobubbles. *Chemical Engineering Science, 93*, 250-256.

Liu, S., Oshita, S., Kawabata, S., Makino, Y., & Yoshimoto, T. (2016). Identification of ROS produced by nanobubbles and their positive and negative effects on vegetable seed germination. *Langmuir, 32*(43), 11295-11302.

Liu, S., Oshita, S., Kawabata, S., & Thuyet, D. Q. (2017). Nanobubble Water's Promotion Effect of Barley (Hordeum vulgare L.) Sprouts Supported by RNA-Seq Analysis. *Langmuir, 33*(43), 12478-12486.

Liu, S., Oshita, S., Makino, Y., Wang, Q., Kawagoe, Y., & Uchida, T. (2015). Oxidative capacity of nanobubbles and its effect on seed germination. *ACS Sustainable Chemistry and Engineering, 4*(3), 1347-1353.

Liu, S., Oshita, S., Thuyet, D. Q., Saito, M., & Yoshimoto, T. (2018). Antioxidant activity of hydrogen nanobubbles in water with different reactive oxygen species both in vivo and in vitro. *Langmuir, 34*(39), 11878-11885.

Liu, S., Wang, Q., Ma, H., Huang, P., Li, J., & Kikuchi, T. (2010). Effect of micro-bubbles on coagulation flotation process of dyeing wastewater. *Separation and Purification Technology, 71*(3), 337-346.

Liu, Y., Li, D., Qian, J., Di, B., Zhang, G., & Ren, Z. (2021). Electrical impedance spectroscopy (EIS) in plant roots research: a review. *Plant Methods, 17*(1), 1-25.

Liu, Y., Zhang, H., Sun, J., Liu, J., Shen, X., Zhan, J., Li, P. (2018). Degradation of aniline in aqueous solution using non-thermal plasma generated in microbubbles. *Chemical Engineering Journal, 345*, 679-687.

Liu, Z.D., Wang, H.C. and Xu, R.K. (2016). The effects of root surface charge and nitrogen forms on the adsorption of aluminum ions by the roots of rice with different aluminum tolerances. *Plant and Soil, 408*(1), 43-53.

Lu, H.-l., Nkoh, J. N., Abdulaha-Al Baquy, M., Dong, G., Li, J.-y., & Xu, R.-k. (2020). Plants alter surface charge and functional groups of their roots to adapt to acidic soil conditions. *Environmental Pollution, 267*, 115590.

Lv, J., Zhang, W., Liu, S., Chen, R., Feng, J., Zhou, S., & Liu, Y. (2016). Analysis of 52 automotive coating samples for forensic purposes with Fourier transform infrared spectroscopy (FTIR) and Raman microscopy. *Environmental Forensics, 17*(1), 59-67.

Magaletti, F., Marino, L., & Casciola, C. M. (2015). Shock wave formation in the collapse of a vapor nanobubble. *Physical Review Letters, 114*(6), 064501.

Maoming, F., Daniel, T., Honaker, R., & Zhenfu, L. (2010). Nanobubble generation and its application in froth flotation (part I): nanobubble generation and its effects on properties of microbubble and millimeter scale bubble solutions. *Mining Science and Technology (China), 20*(1), 1-19.

Marenduzzo, D., Finan, K., & Cook, P. R. (2006). The depletion attraction: an underappreciated force driving cellular organization. *The Journal of Cell Biology, 175*(5), 681-686.

Marinissen, J. (1992). Population dynamics of earthworms in a silt loam soil under conventional and "integrated" arable farming during two years with different weather patterns. *Soil Biology and Biochemistry, 24*(12), 1647-1654.

Meegoda, J. N., Aluthgun Hewage, S., & Batagoda, J. H. (2018). Stability of nanobubbles. *Environmental Engineering Science, 35*(11), 1216-1227.

Meegoda, J. N., Hewage, S. A., & Batagoda, J. H. (2019). Application of the diffused double layer theory to nanobubbles. *Langmuir, 35*(37), 12100-12112.

Mezule, L., Tsyfansky, S., Yakushevich, V., & Juhna, T. (2009). A simple technique for water disinfection with hydrodynamic cavitation: effect on survival of Escherichia coli. *Desalination, 248*(1-3), 152-159.

Michailidi, E. D., Bomis, G., Varoutoglou, A., Kyzas, G. Z., Mitrikas, G., Mitropoulos, A. C., Favvas, E. P. (2020). Bulk nanobubbles: Production and investigation of their formation/stability mechanism. *Journal of Colloid and interface Science, 564*, 371-380.

Michelin, S., Guérin, E., & Lauga, E. (2018). Collective dissolution of microbubbles. *Physical Review Fluids, 3*(4), 043601.

Millare, J. C., & Basilia, B. A. (2018). Nanobubbles from Ethanol-Water Mixtures: Generation and Solute Effects via Solvent Replacement Method. *ChemistrySelect, 3*(32), 9268-9275.

Minamikawa, K., Takahashi, M., Makino, T., Tago, K., & Hayatsu, M. (2015). Irrigation with oxygen-nanobubble water can reduce methane emission and arsenic dissolution in a flooded rice paddy. *Environmental Research Letters, 10*(8), 084012.

Miyashita, K., Yasuda, M., Ota, T., & Suzuki, T. (1999). Antioxidative activity of a cathodic solution produced by the electrolysis of a dilute NaCl solution. *Bioscience, Biotechnology, and Biochemistry, 63*(2), 421-423.

Modi, K. K., Jana, A., Ghosh, S., Watson, R., & Pahan, K. (2014). A physically-modified saline suppresses neuronal apoptosis, attenuates tau phosphorylation and protects memory in an animal model of Alzheimer's disease. *PloS one, 9*(8).

Mohseni, E., Chiamulera, M. E., Reinecke, S., & Hampel, U. (2022). Bubble formation from sub-millimeter orifices: Experimental analysis and modeling. *Chemical Engineering and Processing-Process Intensification, 173*, 108809.

Mukumoto, M., Ohshima, T., Ozaki, M., Konishi, H., Maeda, N., & Nakamura, Y. (2012). Effect of microbubbled water on the removal of a biofilm attached to orthodontic appliances. *Dental Materials Journal, 31*(5), 821-827.

Mulvaney, R. (1996). Nitrogen—inorganic forms. *Methods of soil analysis: Part 3 Chemical methods, 5*, 1123-1184.

Nazari, S., Shafaei, S. Z., Hassanzadeh, A., Azizi, A., Gharabaghi, M., Ahmadi, R., & Shahbazi, B. (2020). Study of effective parameters on generating submicron (nano)-bubbles using the hydrodynamic cavitation. *Physicochem. Physicochemical Problems of Mineral Processing, 56*(5), 884-904.

Nelson, D. W., & Sommers, L. E. (1996). Total carbon, organic carbon, and organic matter. *Methods of soil analysis: Part 3 Chemical Methods, 5*, 961-1010.

Newton, A., Icely, J., Cristina, S., Brito, A., Cardoso, A. C., Colijn, F.,Holmer, M. (2014). An overview of ecological status, vulnerability and future perspectives of European large shallow, semi-enclosed coastal systems, lagoons and transitional waters. *Estuarine, Coastal and Shelf Science, 140*, 95-122.

Ngai, T., Xing, X., & Jin, F. (2008). Depletion attraction between a polystyrene particle and a hydrophilic surface in a pluronic aqueous solution. *Langmuir, 24*(24), 13912-13917.

Nirmalkar, N., Pacek, A., & Barigou, M. (2018). On the existence and stability of bulk nanobubbles. *Langmuir, 34*(37), 10964-10973.

Nirmalkar, N., Pacek, A. W., & Barigou, M. (2018). Interpreting the interfacial and colloidal stability of bulk nanobubbles. *Soft Matter, 14*(47), 9643-9656.

Niu, T., Zhou, Z., Shen, X., Qiao, W., Jiang, L.-M., Pan, W., & Zhou, J. (2016). Effects of dissolved oxygen on performance and microbial community structure in a micro-aerobic hydrolysis sludge in situ reduction process. *Water Research, 90*, 369-377.

Oguz, H. N., & Prosperetti, A. (1993). Dynamics of bubble growth and detachment from a needle. *Journal of Fluid Mechanics, 257*, 111-145.

Oh, S. H., & Kim, J.-M. (2017). Generation and stability of bulk nanobubbles. *Langmuir, 33*(15), 3818-3823.

Ohgaki, K., Khanh, N. Q., Joden, Y., Tsuji, A., & Nakagawa, T. (2010). Physicochemical approach to nanobubble solutions. *Chemical Engineering Science, 65*(3), 1296-1300.

Ohno, P. E., Wang, H.-f., & Geiger, F. M. (2017). Second-order spectral lineshapes from charged interfaces. *Nature Communications, 8*(1), 1-9.

Ohshima, H. (1995). Electrophoresis of soft particles. *Advances in Colloid and Interface Science, 62*(2), 189-235.

Ong, Y.-L., Razatos, A., Georgiou, G., & Sharma, M. M. (1999). Adhesion Forces between E. c oli bacteria and biomaterial surfaces. *Langmuir, 15*(8), 2719-2725.

Osterwalder, A., Pigneur, Y., Oliveira, M. A.-Y., & Ferreira, J. J. P. (2011). Business Model Generation: A handbook for visionaries, game changers and challengers. *African Journal of Business Management, 5*(7), 22-30.

Ozier-Lafontaine, H., & Bajazet, T. (2005a). Analysis of root growth by impedance spectroscopy (EIS). *Plant and Soil, 277*(1), 299-313.

Park, J.-S., & Kurata, K. (2009). Application of microbubbles to hydroponics solution promotes lettuce growth. *HortTechnology, 19*(1), 212-215.

Park, J., Ohashi, K., Kurata, K., & Lee, J. (2010). Promotion of lettuce growth by application of microbubbles in nutrient solution using different rates of electrical conductivity and under periodic intermittent generation in a deep flow technique culture system. *European Journal of Horticultural Science*, 198-203.

Park, M. J., Gonzales, R. R., Abdel-Wahab, A., Phuntsho, S., & Shon, H. K. (2018). Hydrophilic polyvinyl alcohol coating on hydrophobic electrospun nanofiber membrane for high performance thin film composite forward osmosis membrane. *Desalination, 426*, 50-59.

Parker, J. L., Claesson, P. M., & Attard, P. (1994). Bubbles, cavities, and the long-ranged attraction between hydrophobic surfaces. *The Journal of Physical Chemistry, 98*(34), 8468-8480.

Patel, A. K., Singhania, R. R., Chen, C.-W., Tseng, Y.-S., Kuo, C.-H., Wu, C.-H., & Di Dong, C. (2021). Advances in micro-and nano bubbles technology for application in biochemical processes. *Environmental Technology and Innovation, 23*, 101729.

Patel, S., Pal, B. K., & Patel, R. K. (2018). A novel approach in red mud neutralization using cow dung. *Environmental Science and Pollution Research, 25*(13), 12841-12848.

Peñas-López, P., Soto, Á. M., Parrales, M. A., Van Der Meer, D., Lohse, D., & Rodríguez-Rodríguez, J. (2017). The history effect on bubble growth and dissolution. Part 2. Experiments and simulations of a spherical bubble attached to a horizontal flat plate. *Journal of Fluid Mechanics, 820*, 479-510.

Peng, C., Chen, S., Shen, C., He, M., Zhang, Y., Ye, J., Shi, J. (2018). Iron plaque: A barrier layer to the uptake and translocation of copper oxide nanoparticles by rice plants. *Environmental Science and Technology, 52*(21), 12244-12254.

Peng, C., Tong, H., Shen, C., Sun, L., Yuan, P., He, M., & Shi, J. (2020). Bioavailability and translocation of metal oxide nanoparticles in the soil-rice plant system. *Science of the Total Environment, 713*, 136662.

Perez Sirkin, Y. A., Gadea, E. D., Scherlis, D. A., & Molinero, V. (2019). Mechanisms of nucleation and stationary states of electrochemically generated nanobubbles. *Journal of the American Chemical Society, 141*(27), 10801-10811.

Plascencia, G., Díaz–Damacillo, L., & Robles-Agudo, M. (2020). On the estimation of the friction factor: A review of recent approaches. *SN Applied Sciences, 2*(2), 163.

Postnikov, A. V., Uvarov, I. V., Penkov, N. V., & Svetovoy, V. B. (2018). Collective behavior of bulk nanobubbles produced by alternating polarity electrolysis. *Nanoscale, 10*(1), 428-435.

Pulleman, M., Six, J., Uyl, A., Marinissen, J., & Jongmans, A. (2005). Earthworms and management affect organic matter incorporation and microaggregate formation in agricultural soils. *Applied Soil Ecology, 29*(1), 1-15.

Qin, X.-q., Yao, B., Jin, L., Zheng, X.-z., Ma, J., Benedetti, M. F., . . . Ren, Z.-l. (2020). Characterizing soil dissolved organic matter in typical soils from China using fluorescence EEM–PARAFAC and UV–visible absorption. *Aquatic Geochemistry, 26*(1), 71-88.

Qiu, J., Zou, Z., Wang, S., Wang, X., Wang, L., Dong, Y., Hu, J. (2017). Formation and Stability of Bulk Nanobubbles Generated by Ethanol–Water Exchange. *ChemPhysChem, 18*(10), 1345-1350.

Rak, D., Ovadová, M., & Sedlák, M. (2019). (Non) existence of bulk nanobubbles: the role of ultrasonic cavitation and organic solutes in water. *The Journal of Physical Chemistry Letters, 10*(15), 4215-4221.

Ranaweera, R., & Luo, L. (2020). Electrochemistry of nanobubbles. *Current Opinion in Electrochemistry, 22*, 102-109.

Reeves, D. (1997). The role of soil organic matter in maintaining soil quality in continuous cropping systems. *Soil and Tillage Research, 43*(1-2), 131-167.

Rijnaarts, H. H., Norde, W., Lyklema, J., & Zehnder, A. J. (1999). DLVO and steric contributions to bacterial deposition in media of different ionic strengths. *Colloids and Surfaces B: Biointerfaces, 14*(1), 179-195.

Rodrigues, M. Â., Ladeira, L. C., & Arrobas, M. (2018). Azotobacter-enriched organic manures to increase nitrogen fixation and crop productivity. *European Journal of Agronomy, 93*, 88-94.

Rongwong, W., & Goh, K. (2020). Resource recovery from industrial wastewaters by hydrophobic membrane contactors: A review. *Journal of Environmental Chemical Engineering, 8*(5), 104242.

Ross, D. S., & Ketterings, Q. (1995). Recommended methods for determining soil cation exchange capacity. *Recommended soil testing procedures for the northeastern United States, 2*, 62-70.

Roy, S. M., Machavaram, R., Pareek, C., & Mal, B. (2021). Diversified aeration facilities for effective aquaculture systems—a comprehensive review. *Aquaculture International, 29*(3), 1181-1217.

Ryan, W. L., & Hemmingsen, E. A. (1993). Bubble Formation in Water at Smooth Hydrophobic Surfaces. *Journal of Colloid and Interface Science, 157*(2), 312-317.

Safonov, V. L., & Khitrin, A. K. (2013). Hydrogen nanobubbles in a water solution of dietary supplement. *Colloids and Surfaces A: Physicochemical and Engineering Aspects, 436*, 333-336.

Saijai, S., Thonglek, V., & Yoshikawa, K. (2019). Sterilization effects of ozone fine (micro/nano) bubble water. *International Plasma Environmental Science and Technology, 12*(2), 55-58.

Sander, S., Behnisch, J., & Wagner, M. (2017). Energy, cost and design aspects of coarse-and fine-bubble aeration systems in the MBBR IFAS process. *Water Science and Technology, 75*(4), 890-897.

Sardeing, R., Painmanakul, P., & Hébrard, G. (2006). Effect of surfactants on liquid-side mass transfer coefficients in gas–liquid systems: a first step to modeling. *Chemical Engineering Science, 61*(19), 6249-6260.

Savassa, S. M., Castillo-Michel, H., del Real, A. E. P., Reyes-Herrera, J., Marques, J. P. R., & de Carvalho, H. W. (2021). Ag nanoparticles enhancing Phaseolus vulgaris seedling development: understanding nanoparticle migration and chemical transformation across the seed coat. *Environmental Science: Nano, 8*(2), 493-501.

Schloss, P. D., Westcott, S. L., Ryabin, T., Hall, J. R., Hartmann, M., Hollister, E. B., . . . Robinson, C. J. (2009). Introducing mothur: open-source, platform-independent, community-supported software for describing and comparing microbial communities. *Applied and Environmental Microbiology, 75*(23), 7537-7541.

Schröder, V., & Schubert, H. (1999). Production of emulsions using microporous, ceramic membranes. *Colloids and Surfaces A: Physicochemical and Engineering Aspects, 152*(1-2), 103-109.

Schulte, E., & Hoskins, B. (1995). Recommended soil organic matter tests. *Recommended Soil Testing Procedures for the North Eastern USA. Northeastern Regional Publication, 493*, 52-60.

Seidel, R., Winter, B., & Bradforth, S. E. (2016). Valence electronic structure of aqueous solutions: Insights from photoelectron spectroscopy. *Annual Review of Physical Chemistry, 67*, 283-305.

Seo, H.-B., & Lee, S.-Y. (2023). High-concentration nanobubble generation by megasonic cavitation and atomization. *Colloid and Interface Science Communications, 52*, 100687.

Shahzad, Z., Canut, M., Tournaire-Roux, C., Martinière, A., Boursiac, Y., Loudet, O., & Maurel, C. (2016). A potassium-dependent oxygen sensing pathway regulates plant root hydraulics. *Cell, 167*(1), 87-98. e14.

Shang, H., Ma, C., Li, C., Zhao, J., Elmer, W., White, J. C., & Xing, B. (2021). Copper oxide nanoparticle-embedded hydrogels enhance nutrient supply and growth of lettuce (lactuca sativa) infected with Fusarium oxysporum f. sp. lactucae. *Environmental Science and Technology, 55*(20), 13432-13442.

Sharifi, M., Khoshgoftarmanesh, A., & Hadadzadeh, H. (2016). Changes in the chemical properties and swelling coefficient of alfalfa root cell walls in the presence of toluene as a toxic agent. *Environmental Science and Pollution Research, 23*(7), 7022-7031.

Shen, D., Ye, C., Hu, Z., Chen, X., Guo, H., Li, J., Liu, M. (2018). Increased chemical stability but decreased physical protection of soil organic carbon in response to nutrient amendment in a Tibetan alpine meadow. *Soil Biology and `Biochemistry, 126*, 11-21.

SHEN, Xs., SHEN, Cy., & LI, G. (2008). Bubble formation from large submerged single orifice at high gas velocity *Journal of Chemical Industry and Engineering, 9*, 2220-2225.

Shi, W., Pan, G., Chen, Q., Song, L., Zhu, L., & Ji, X. (2018). Hypoxia remediation and methane emission manipulation using surface oxygen nanobubbles. *Environmental Science and Technology, 52*(15), 8712-8717.

Shi, X., Xue, S., Marhaba, T., & Zhang, W. (2021). Probing Internal Pressures and Long-Term Stability of Nanobubbles in Water. *Langmuir, 37*(7), 2514-2522.

Shi, Y.-R., Ye, M.-P., Du, L.-C., & Weng, Y.-X. (2018). Experimental determination of particle size-dependent surface charge density for silica nanospheres. *The Journal of Physical Chemistry C, 122*(41), 23764-23771.

Shin, D., Park, J. B., Kim, Y.-J., Kim, S. J., Kang, J. H., Lee, B., Novoselov, K. S. (2015). Growth dynamics and gas transport mechanism of nanobubbles in graphene liquid cells. *Nature Communications, 6*(1), 1-6.

Sims, J., & Wolf, A. (1995). Recommended soil testing procedures for the Northeastern United States. *Northeast Regional Bulletin, 493*, 4756.

Singh, J., & Lee, B.-K. (2016). Influence of nano-TiO2 particles on the bioaccumulation of Cd in soybean plants (Glycine max): A possible mechanism for the removal of Cd from the contaminated soil. *Journal of Environmental Management, 170*, 88-96.

Smreczak, B., & Ukalska-Jaruga, A. (2021). Dissolved organic matter in agricultural soils. *Soil Science Annual, 72*(1), 132234.

Snell, J. R., Zhou, C., Carpenter, J. F., & Randolph, T. W. (2016). Particle formation and aggregation of a therapeutic protein in nanobubble suspensions. *Journal of Pharmaceutical Sciences, 105*(10), 3057-3063.

Solano-Altamirano, J., Malcolm, J. D., & Goldman, S. (2015). Gas bubble dynamics in soft materials. *Soft Matter, 11*(1), 202-210.

Somerlot, C., & Davis, D. (2015). Overview of Pathogens and Wastewater Disinfectants. *Clear Waters, 45*(1), 18.

Song, F., Wu, F., Feng, W., Tang, Z., Giesy, J. P., Guo, F., . . . Xing, B. (2018). Fluorescence regional integration and differential fluorescence spectroscopy for analysis of structural characteristics and proton binding properties of fulvic acid sub-fractions. *Journal of Environmental Sciences, 74*, 116-125.

Song, L., Wang, G., Hou, X., Kala, S., Qiu, Z., Wong, K. F., . . . Sun, L. (2020). Biogenic nanobubbles for effective oxygen delivery and enhanced photodynamic therapy of cancer. *Acta Biomaterialia, 108*, 313-325.

Sonmez, S., Buyuktas, D., Okturen, F., & Citak, S. (2008). Assessment of different soil to water ratios (1: 1, 1: 2.5, 1: 5) in soil salinity studies. *Geoderma, 144*(1-2), 361-369.

Srinivas, A., & Ghosh, P. (2011). Coalescence of bubbles in aqueous alcohol solutions. *Industrial & Engineering Chemistry Research, 51*(2), 795-806.

Suleymani, M., Ghotbi, C., Ashoori, S., Moghadasi, J., & Kharrat, R. (2020). Theoretical and experimental study of foam stability mechanism by nanoparticles: Interfacial, bulk, and porous media behavior. *Journal of Molecular Liquids, 304*, 112739.

Sumikura, M., Hidaka, M., Murakami, H., Nobutomo, Y., & Murakami, T. (2007). Ozone micro-bubble disinfection method for wastewater reuse system. *Water Science and Technology, 56*(5), 53-61.

Sun, Y., Wang, S., & Niu, J. (2018). Microbial community evolution of black and stinking rivers during in situ remediation through micro-nano bubble and submerged resin floating bed technology. *Bioresource Technology, 258*, 187-194.

Suwartha, N., Syamzida, D., Priadi, C. R., Moersidik, S. S., & Ali, F. (2020). Effect of size variation on microbubble mass transfer coefficient in flotation and aeration processes. *Heliyon, 6*(4), e03748.

Tada, K., Maeda, M., Nishiuchi, Y., Nagahara, J., Hata, T., Zhuowei, Z., . . . Ohmori, M. (2014). ESR measurement of hydroxyl radicals in micro-nanobubble water. *Chemistry Letters, 43*(12), 1907-1908.

Takahashi, M. (2009). Base and technological application of micro-bubble and nanobubble. *Materials Integration, 22*(5), 2-19.

Takahashi, M., Chiba, K., & Li, P. (2007a). Formation of hydroxyl radicals by collapsing ozone microbubbles under strongly acidic conditions. *The Journal of Physical Chemistry B, 111*(39), 11443-11446.

Takahashi, M., Chiba, K., & Li, P. (2007b). Free-radical generation from collapsing microbubbles in the absence of a dynamic stimulus. *The Journal of Physical Chemistry B, 111*(6), 1343-1347.

Tan, B. H., An, H., & Ohl, C.-D. (2020). How bulk nanobubbles might survive. *Physical Review Letters, 124*(13), 134503.

Tanaka, S., Kastens, S., Fujioka, S., Schlüter, M., & Terasaka, K. (2020). Mass transfer from freely rising microbubbles in aqueous solutions of surfactant or salt. *Chemical Engineering Journal, 387*, 121246.

Tang, J., Zhang, Y., Yao, Y., Dai, N., Ge, Z., & Wu, D. (2021). High-performance ultrafine bubble aeration on janus aluminum foil prepared by laser microfabrication. *Langmuir, 37*(23), 6947-6952.

Tang, W., Zhang, H., Zhang, W., Wang, C., & Shan, B. (2013). Biological invasions induced phosphorus release from sediments in freshwater ecosystems. *Colloids and Surfaces A: Physicochemical and Engineering Aspects, 436*, 873-880.

Tavarini, S., Sgherri, C., Ranieri, A. M., & Angelini, L. G. (2015). Effect of Nitrogen Fertilization and Harvest Time on Steviol Glycosides, Flavonoid Composition, and Antioxidant Properties in Stevia rebaudiana Bertoni. *Journal of Agricultural and Food Chemistry, 63*(31), 7041-7050.

Tcholakova, S., Mustan, F., Pagureva, N., Golemanov, K., Denkov, N. D., Pelan, E. G., & Stoyanov, S. D. (2017). Role of surface properties for the kinetics of bubble Ostwald ripening in saponin-stabilized foams. *Colloids and Surfaces A: Physicochemical and Engineering Aspects, 534*, 16-25.

Tekile, A., Kim, I., & Lee, J.-Y. (2016). Extent and persistence of dissolved oxygen enhancement using nanobubbles. *Environmental Engineering Research, 21*(4), 427-435.

Temesgen, T., Bui, T. T., Han, M., Kim, T.-i., & Park, H. (2017). Micro and nanobubble technologies as a new horizon for water-treatment techniques: A review. *Advances in Colloid and Interface Science, 246*, 40-51.

Terasaka, K., Hirabayashi, A., Nishino, T., Fujioka, S., & Kobayashi, D. (2011). Development of microbubble aerator for waste water treatment using aerobic activated sludge. *Chemical Engineering Science, 66*(14), 3172-3179.

Thomas, B., Ohde, D., Matthes, S., Engelmann, C., Bubenheim, P., Terasaka, K., . . . Liese, A. (2021). Comparative investigation of fine bubble and macrobubble aeration on gas utility and biotransformation productivity. *Biotechnology and Bioengineering, 118*(1), 130-141.

Thomas, O. C., Cavicchi, R. E., & Tarlov, M. J. (2003). Effect of surface wettability on fast transient microboiling behavior. *Langmuir, 19*(15), 6168-6177.

Thompson, A., & Goyne, K. (2012). Introduction to the sorption of chemical constituents in soils. *Nature Education Knowledge, 4*(4), 7.

Tomisaki, M., Natsui, K., Fujioka, S., Terasaka, K., & Einaga, Y. (2021). Unique properties of fine bubbles in the electrochemical reduction of carbon dioxide using boron-doped diamond electrodes. *Electrochimica Acta, 389*, 138769.

Touhami, A., Othmane, A., Ouerghi, O., Ouada, H. B., Fretigny, C., & Jaffrezic-Renault, N. (2002). Red blood cells imaging and antigen–antibody interaction measurement. *Biomolecular Engineering, 19*(2-6), 189-193.

Tuziuti, T., Yasui, K., & Kanematsu, W. (2018). Influence of addition of degassed water on bulk nanobubbles. *Ultrasonics Sonochemistry, 43*, 272-274.

Uchida, T., Oshita, S., Ohmori, M., Tsuno, T., Soejima, K., Shinozaki, S., Mitsuda, K. (2011). Transmission electron microscopic observations of nanobubbles and their capture of impurities in wastewater. *Nanoscale Research Letters, 6*(1), 1.

Ulatowski, K., Sobieszuk, P., Mróz, A., & Ciach, T. (2019). Stability of nanobubbles generated in water using porous membrane system. *Chemical Engineering and Processing-Process Intensification, 136*, 62-71.

USDA, N. (2012). Soil bulk density/moisture/aeration. *Nutrition & Food Science, 42*(4), 11-14.

Ushida, A., Hasegawa, T., Narumi, T., & Nakajima, T. (2013). Flow properties of nanobubble mixtures passing through micro-orifices. *International Journal of Heat and Fluid Flow, 40*, 106-115.

Ushikubo, F. Y., Furukawa, T., Nakagawa, R., Enari, M., Makino, Y., Kawagoe, Y., . . . Oshita, S. (2010). Evidence of the existence and the stability of nano-bubbles in water. *Colloids and Surfaces A: Physicochemical and Engineering Aspects, 361*(1), 31-37.

van Aarle, I. M., Viennois, G., Amenc, L. K., Tatry, M.-V., Luu, D. T., & Plassard, C. (2007). Fluorescent in situ RT-PCR to visualise the expression of a phosphate transporter gene from an ectomycorrhizal fungus. *Mycorrhiza, 17*(6), 487-494.

Vandamme, D., Foubert, I., & Muylaert, K. (2013). Flocculation as a low-cost method for harvesting microalgae for bulk biomass production. *Trends in Biotechnology, 31*(4), 233-239.

Verma, K., Gupta, D., & Gupta, A. (2016). Optimization of ozone disinfection and its effect on trihalomethanes. *Journal of Environmental Chemical Engineering, 4*(3), 3021-3032.

Wan, J., & Wilson, J. L. (1994). Visualization of the role of the gas-water interface on the fate and transport of colloids in porous media. *Water Resources Research, 30*(1), 11-23.

Wang, B., Bian, B., Wang, C., Li, C., Fang, H., Zhang, J., Liao, W. (2019). Hydrogen gas promotes the adventitious rooting in cucumber under cadmium stress. *PLoS One, 14*(2), e0212639.

Wang, C., Li, N., Huang, X., & Weng, C. (2022). Investigation of the effect of nozzle on underwater detonation shock wave and bubble pulsation. *Energies, 15*(9), 3194.

Wang, J., Evangelou, B. P., & Nielsen, M. T. (1992). Surface chemical properties of purified root cell walls from two tobacco genotypes exhibiting different tolerance to manganese toxicity. *Plant Physiology, 100*(1), 496-501.

Wang, K., Hou, D., Wang, J., Wang, Z., Tian, B., & Liang, P. (2018). Hydrophilic surface coating on hydrophobic PTFE membrane for robust anti-oil-fouling membrane distillation. *Applied Surface Science, 450*, 57-65.

Wang, L., Ali, J., Wang, Z., Oladoja, N., Cheng, R., Zhang, C., Pan, G. (2020). Oxygen nanobubbles enhanced photodegradation of oxytetracycline under visible light: Synergistic effect and mechanism. *Chemical Engineering Journal, 388*, 124227.

Wang, L., Miao, X., Lyu, T., & Pan, G. (2018). Quantification of Oxygen Nanobubbles in Particulate Matters and Potential Applications in Remediation of Anaerobic Environment. *ACS Omega, 3*(9), 10624-10630.

Wang, S., Liu, M., & Dong, Y. (2013). Understanding the stability of surface nanobubbles. *Journal of Physics: Condensed Matter, 25*(18), 184007.

Wang, S., Liu, Y., Li, P., Wang, Y., Yang, J., & Zhang, W. (2020). Micro-nanobubble aeration promotes senescence of submerged macrophytes with low total antioxidant capacity in urban landscape water. *Environmental Science: Water Research and Technology, 6*(3), 523-531.

Wang, S., Liu, Y., Lyu, T., Pan, G., & Li, P. (2020). Aquatic macrophytes in morphological and physiological responses to the nanobubble technology application for water restoration. *ACS Environmental Science and Technology Water, 1*(2), 376-387.

Wang, Y., & Bhushan, B. (2010). Boundary slip and nanobubble study in micro/nanofluidics using atomic force microscopy. *Soft Matter, 6*(1), 29-66.

Wang, Y., Hu, Y., Yang, C., Wang, Q., & Jiang, D. (2019). Variations of DOM quantity and compositions along WWTPs-river-lake continuum: Implications for watershed environmental management. *Chemosphere, 218*, 468-476.

Wang, Y., Wang, S., Sun, J., Dai, H., Zhang, B., Xiang, W., Yang, J. (2021). Nanobubbles promote nutrient utilization and plant growth in rice by upregulating nutrient uptake genes and stimulating growth hormone production. *Science of The Total Environment*, 149627.

Wang, Y., Wang, S., Sun, J., Dai, H., Zhang, B., Xiang, W., Zhang, W. (2021). Nanobubbles promote nutrient utilization and plant growth in rice by upregulating nutrient uptake genes and stimulating growth hormone production. *Science of The Total Environment, 800*, 149627.

Wang, Z., Guo, K., Liu, H., Liu, C., Geng, Y., Lu, Z., Chen, D. (2020). Effects of bubble size on the gas–liquid mass transfer of bubble swarms with Sauter mean diameters of 0.38–4.88 mm in a co-current upflow bubble column. *Journal of Chemical Technology & Biotechnology, 95*(11), 2853-2867.

Weigand, M., & Kemna, A. (2019). Imaging and functional characterization of crop root systems using spectroscopic electrical impedance measurements. *Plant and Soil, 435*, 201-224.

Wenming, X., Zhang, S., Lin, R., Mingyue, Y., Weiming, S., Zhang, H., & Weihua, L. (2017). Evaluating soil dissolved organic matter extraction using three-dimensional excitation-emission matrix fluorescence spectroscopy. *Pedosphere, 27*(5), 968-973.

Wilkinson, P. M., & Dierendonck, L. L. v. (1990). Pressure and gas density effects on bubble break-up and gas hold-up in bubble columns. *Chemical Engineering Science, 45*(8), 2309-2315.

Wu, Y., Lin, H., Yin, W., Shao, S., Lv, S., & Hu, Y. (2019). Water quality and microbial community changes in an urban river after micro-nano bubble technology in situ treatment. *Water, 11*(1), 66.

Wu, Y., Lyu, T., Yue, B., Tonoli, E., Verderio, E. A., Ma, Y., & Pan, G. (2019). Enhancement of tomato plant growth and productivity in organic farming by agri-nanotechnology using nanobubble oxygation. *Journal of Agricultural and Food Chemistry, 67*(39), 10823-10831.

Wu, Z., Chen, H., Dong, Y., Mao, H., Sun, J., Chen, S., . . . Hu, J. (2008). Cleaning using nanobubbles: defouling by electrochemical generation of bubbles. *Journal of Colloid and Interface Science, 328*(1), 10-14.

Wu, Z., Ferreira, D. F., Crudo, D., Bosco, V., Stevanato, L., Costale, A., & Cravotto, G. (2019). Plant and biomass extraction and valorisation under hydrodynamic cavitation. *Processes, 7*(12), 965.

Wu, Z., Zhang, X., Zhang, X., Li, G., Sun, J., Zhang, Y., Hu, J. (2006). Nanobubbles influence on BSA adsorption on mica surface. *Surface and Interface Analysis, 38*(6), 990-995.

Wu, Z., Zhang, X., Zhang, X., Sun, J., Dong, Y., & Hu, J. (2007). In situ AFM observation of BSA adsorption on HOPG with nanobubble. *Chinese Science Bulletin, 52*(14), 1913-1919.

Xiao, L., Sun, S., Li, K., Lei, Z., Shimizu, K., Zhang, Z., & Adachi, Y. (2020). Effects of nanobubble water supplementation on biomass accumulation during mycelium cultivation of Cordyceps militaris and the antioxidant activities of extracted polysaccharides. *Bioresource Technology Reports, 12*, 100600.

Xiao, W., & Xu, G. (2020). Mass transfer of nanobubble aeration and its effect on biofilm growth: Microbial activity and structural properties. *Science of the Total Environment, 703*, 134976.

Xiao, Z., Aftab, T. B., & Li, D. (2019). Applications of micro–nano bubble technology in environmental pollution control. *Micro and Nano Letters, 14*(7), 782-787.

Xiao, Z., Li, D., Wang, F., Sun, Z., & Lin, Z. (2020). Simultaneous removal of NO and SO2 with a new recycling micro-nano bubble oxidation-absorption process based on HA-Na. *Separation and Purification Technology, 242*, 116788.

Xiao, Z., Li, D., Zhu, Q., & Sun, Z. (2020). Simultaneous removal of NO and SO2 through a new wet recycling oxidation–reduction process utilizing micro-nano bubble gas–liquid dispersion system based on Na2SO3. *Fuel, 263*, 116682.

Xiaoli, C., Guixiang, L., Xin, Z., Yongxia, H., & Youcai, Z. (2012). Fluorescence excitation–emission matrix combined with regional integration analysis to characterize the composition and transformation of humic and fulvic acids from landfill at different stabilization stages. *Waste Management, 32*(3), 438-447.

Xu, P., Jin, Z., Zhang, T., Chen, X., Qiu, M., & Fan, Y. (2021). Fabrication of a Ceramic Membrane with Antifouling PTFE Coating for Gas-Absorption Desulfurization. *Industrial & Engineering Chemistry Research, 60*(6), 2492-2500.

Xu, Q., Nakajima, M., Ichikawa, S., Nakamura, N., & Shiina, T. (2008). A comparative study of microbubble generation by mechanical agitation and sonication. *Innovative Food Science and Emerging Technologies, 9*(4), 489-494.

Xue, S., Marhaba, T., & Zhang, W. (2022). Nanobubble watering affects nutrient release and soil characteristics. *ACS Agricultural Science and Technology, 2*(3), 453-461.

Xue, S., Zhang, Y., Marhaba, T., & Zhang, W. (2022). Aeration and dissolution behavior of oxygen nanobubbles in water. *Journal of Colloid and Interface Science, 609*, 584-591.

Yaminsky, V. V., Ohnishi, S., Vogler, E. A., & Horn, R. G. (2010). Stability of aqueous films between bubbles. Part 1. The effect of speed on bubble coalescence in purified water and simple electrolyte solutions. *Langmuir, 26*(11), 8061-8074.

Yang, H. C., Hou, J., Wan, L. S., Chen, V., & Xu, Z. K. (2016). Janus membranes with asymmetric wettability for fine bubble aeration. *Advanced Materials Interfaces, 3*(9), 1500774.

Yasui, K., Tuziuti, T., & Kanematsu, W. (2016). Extreme conditions in a dissolving air nanobubble. *Physical Review E, 94*(1), 013106.

Yasui, K., Tuziuti, T., & Kanematsu, W. (2018). Mysteries of bulk nanobubbles (ultrafine bubbles); stability and radical formation. *Ultrasonics Sonochemistry, 48*, 259-266.

Yasui, K., Tuziuti, T., & Kanematsu, W. (2019a). High temperature and pressure inside a dissolving oxygen nanobubble. *Ultrasonics Sonochemistry, 55*, 308-312.

Yasui, K., Tuziuti, T., & Kanematsu, W. (2019b). Mechanism of OH radical production from ozone bubbles in water after stopping cavitation. *Ultrasonics Sonochemistry, 58*, 104707.

Yasui, K., Tuziuti, T., Kozuka, T., Towata, A., & Iida, Y. (2007). Relationship between the bubble temperature and main oxidant created inside an air bubble under ultrasound. *The Journal of Chemical Physics, 127*(15), 154502.

Yodh, A., Lin, K., Crocker, J. C., Dinsmore, A., Verma, R., & Kaplan, P. (2001). Entropically driven self–assembly and interaction in suspension. *Philosophical Transactions of the Royal Society of London. Series A: Mathematical, Physical and Engineering Sciences, 359*(1782), 921-937.

Yost, M. A., Kitchen, N. R., Sudduth, K. A., Sadler, E. J., Drummond, S. T., & Volkmann, M. R. (2017). Long-term impact of a precision agriculture system on grain crop production. *Precision Agriculture, 18*(5), 823-842.

Yu, P., Wang, J., Chen, J., Guo, J., Yang, H., & Chen, Q. (2019). Successful control of phosphorus release from sediments using oxygen nano-bubble-modified minerals. *Science of the Total Environment, 663*, 654-661.

Zaharia, C., & Suteu, D. (2013). *Industrial wasted materials as 'low cost' sorbents for effluent treatmentCurrent Topics, Concepts and Research Priorities in Environmental Chemistry*,2, 189-212.

Żbik, M., & Horn, R. G. (2003). Hydrophobic attraction may contribute to aqueous flocculation of clays. *Colloids and Surfaces A: Physicochemical and Engineering Aspects, 222*(1), 323-328.

Zhai, H., Zhang, X., Zhu, X., Liu, J., & Ji, M. (2014). Formation of Brominated Disinfection Byproducts during Chloramination of Drinking Water: New Polar Species and Overall Kinetics. *Environmental Science and Technology, 48*(5), 2579-2588.

Zhang, D., Guan, J., Shen, C., Tang, S., & Zhou, J. (2022). Dynamic behavior of near-surface nanobubbles formation and development. *Journal of Molecular Liquids, 358*, 119190.

Zhang, H., Du, W., Peralta-Videa, J. R., Gardea-Torresdey, J. L., White, J. C., Keller, A., . . . Zhao, L. (2018). Metabolomics reveals how cucumber (Cucumis sativus) reprograms metabolites to cope with silver ions and silver nanoparticle-induced oxidative stress. *Environmental Science and Technology, 52*(14), 8016-8026.

Zhang, H., Lyu, T., Bi, L., Tempero, G., Hamilton, D. P., & Pan, G. (2018). Combating hypoxia/anoxia at sediment-water interfaces: A preliminary study of oxygen nanobubble modified clay materials. *Science of The Total Environment, 637*, 550-560.

Zhang, J., Chen, Y., Deng, C., Zhang, L., Sun, Z., Wang, J., Xie, M. (2019). The optimized fabrication of a novel nanobubble for tumor imaging. *Frontiers in Pharmacology, 10*, 610.

Zhang, L., Qiu, Y., Cheng, L., Wang, Y., Liu, L., Tu, C.,.Zhang, W. (2018). Atmospheric CO2 enrichment and reactive nitrogen inputs interactively stimulate soil cation losses and acidification. *Environmental Science and Technology, 52*(12), 6895-6902.

Zhang, L., Zhang, Y., Zhang, X., Li, Z., Shen, G., Ye, M., Hu, J. (2006). Electrochemically controlled formation and growth of hydrogen nanobubbles. *Langmuir, 22*(19), 8109-8113.

Zhang, W., Rittmann, B., & Chen, Y. (2011). Size Effects on Adsorption of Hematite Nanoparticles on E. coli cells. *Environmental Science and Technology, 45*(6), 2172-2178.

Zhang, W., Stack, A. G., & Chen, Y. (2011). Interaction force measurement between E. coli cells and nanoparticles immobilized surfaces by using AFM. *Colloids and Surfaces B: Biointerfaces, 82*(2), 316-324.

Zhang, W., Yao, Y., Sullivan, N., & Chen, Y. (2011). Modeling the primary size effects of citrate-coated silver nanoparticles on their ion release kinetics. *Environmental Science and Technology, 45*(10), 4422-4428.

Zhang, X., Chan, D. Y., Wang, D., & Maeda, N. (2013). Stability of interfacial nanobubbles. *Langmuir, 29*(4), 1017-1023.

Zhang, X. H., Quinn, A., & Ducker, W. A. (2008). Nanobubbles at the interface between water and a hydrophobic solid. *Langmuir, 24*(9), 4756-4764.

Zheng, J., Su, C., Zhou, J., Xu, L., Qian, Y., & Chen, H. (2017). Effects and mechanisms of ultraviolet, chlorination, and ozone disinfection on antibiotic resistance genes in secondary effluents of municipal wastewater treatment plants. *Chemical Engineering Journal, 317*, 309-316.

Zheng, T., Zhang, T., Wang, Q., Tian, Y., Shi, Z., Smale, N., & Xu, B. (2015). Advanced treatment of acrylic fiber manufacturing wastewater with a combined microbubble-ozonation/ultraviolet irradiation process. *RSC Advances, 5*(95), 77601-77609.

Zhou, S., Liu, M., Chen, B., Sun, L., & Lu, H. (2022). Microbubble-and nanobubble-aeration for upgrading conventional activated sludge process: A review. *Bioresource Technology*, 127826.

Zhou, Y., Bastida, F., Zhou, B., Sun, Y., Gu, T., Li, S., & Li, Y. (2020). Soil fertility and crop production are fostered by micro-nano bubble irrigation with associated changes in soil bacterial community. *Soil Biology and Biochemistry, 141*, 107663.

Zhou, Y., Li, Y., Liu, X., Wang, K., & Muhammad, T. (2019a). Synergistic improvement in spring maize yield and quality with micro/nanobubbles water oxygation. *Scientific Reports, 9*(1), 5226.

Zhou, Y., Li, Y., Liu, X., Wang, K., & Muhammad, T. (2019b). Synergistic improvement in spring maize yield and quality with micro/nanobubbles water oxygation. *Scientific Reports, 9*(1), 1-10.

Zhou, Y., Zhou, B., Xu, F., Muhammad, T., & Li, Y. (2019). Appropriate dissolved oxygen concentration and application stage of micro-nano bubble water oxygation in greenhouse crop plantation. *Agricultural Water Management, 223*, 105713.

Zhu, J., An, H., Alheshibri, M., Liu, L., Terpstra, P. M., Liu, G., & Craig, V. S. (2016). Cleaning with bulk nanobubbles. *Langmuir, 32*(43), 11203-11211.

Zhu, M., Wang, Q., Sun, Y., & Zhang, J. (2021). Effects of oxygenated brackish water on germination and growth characteristics of wheat. *Agricultural Water Management, 245*, 106520.